

STUDY ON SOIL BEHAVIOR UNDER MULTIPLE WETTING
AND DRYING CYCLES

A Dissertation

by

JUMANAH AHMAD MOHAMMAD HAJJAT

Submitted to the Office of Graduate and Professional Studies of
Texas A&M University
in partial fulfillment of the requirements for the degree of

DOCTOR OF PHILOSOPHY

Chair of Committee,	Marcelo Sanchez
Committee Members,	Charles Aubeny
	Minsu Cha
	Sara Abedi
Head of Department,	Robin Autenrieth

August 2018

Major Subject: Civil Engineering

Copyright 2018 Jumanah Ahmad Mohammad Hajjat

ABSTRACT

During thermal seasonal variations, expansive soils may exhibit increase in volume upon wetting (swell) and decrease in volume during drying (shrinkage). In this regard, it is essential to understand the variations in hydro-mechanical behavior of soils during wetting/drying cycles for evaluating the stability and sustainability of natural soils and engineering structures as well.

Crack formation is a widespread natural phenomenon raised during evaporation process of water from fully or partially-saturated soils during dry seasons. Fundamental to understanding crack development in soils is twofold; first to determine the tensile strength under circumstances mimicking those in the field and second to track the motion of soil particles during multiple wetting and drying cycles. In most of the previous studies, the tensile strength was measured when external applied tensile loads produced failure in a soil tested under constant water content and matric suction. However, very little attention has been directed to study the impact of wetting/drying cycles on tensile strength incorporated with the evolution and propagation of cracks.

The research herein has stemmed from the observation of crack propagation in some geotechnical structures when soils undergo successive drying and wetting cycles. Accordingly, this study was motivated by the assumption that crack propagation is owing to the decrease in tensile strength of soil over cycles. A novel approach was employed using a new innovative device for measuring the tensile strength of the soil subjected to multiple wetting/drying cycles similar to the field conditions. The determination of tensile strength was incorporated with tracking the motion of soil particles during cycles by utilizing the Digital Image Correlation (DIC) technique.

The reduction of tensile strength was determined, and crack propagation was quantitatively described and analyzed over cycles.

The influences of soil interfaces and initial saturation conditions on shear strength and crack behavior of soil were also studied. It was revealed through this research that crack formation in soil is strongly related to the variations in the configurations of soil particles and stress state that occur during alternative shrinkage and swelling when exposed to drying and wetting, respectively. The findings generated by this study can be used to improve our understanding of crack mechanism in soils during cyclic wetting/drying processes.

ACKNOWLEDGMENTS

In the name of Allah, the Most Beneficent, the Most Merciful. All praise is due to almighty Allah, the Lord of the universe. He alone worship; alone we ask for guidance and help. At the very beginning, I thank almighty Allah, who showered me with innumerable blessings and enable me to complete this work.

I would like to thank my supervisor Dr Marcelo Sanchez and my committee members, Dr. Charles Aubeny, Dr. Sara Abedi, and Dr. Minsu Cha for their support and guidance throughout my research. Also, I would like to thank my colleagues, friends, and Zachry department of civil engineering in Texas A & M university. Great thanks goes to Hashemite University/Jordan who supported and funded me throughout my Ph.D study.

My heartfelt thanks go to my husband Suleiman for his endless support, encouragement and for being in my life as well. Thanks go to my awesome son Layth for being proud of me, my pretty daughter Noor for her support, my little mermaids Jena and Alaa, and my little boy Mohammad for showering me with love and fun.

A lot of thanks go to my parents, Ahmad and Huda for their love, endless encouragement, and prayer for me throughout my life. Their personal sacrifices have been enormous and I will always appreciate their contributions in helping me to achieve studies and much more.

Finally, my sincere thanks go to my compassionate sisters Madleen for her love and support, Arwa, Gada, Reem, and Muna and my brothers Mohammad, Maher, Yousef, Ali, Thear and Sultan for their love and encouragement.

CONTRIBUTORS AND FUNDING SOURCES

This work was supported by a dissertation committee consisting of Professor Marcelo Sanchez, Professor Charles Aubeny and Professor Minsu Cha of the Department of Civil Engineering and Professor Sara Abedi of the Department of Petroleum Engineering.

All work for the dissertation was completed independently by the student, under the advisement of Dr. Marcelo Sanchez of the Department of Civil Engineering.

This work was made possible using funding provided by Hashemite University/Jordan. Also, the laboratory equipment was provided by Dr. Marcelo Sanchez.

The author's graduate study was also supported by the Graduate Teaching Fellowship from Texas A&M University.

The contents in this dissertation are solely the responsibility of the authors and do not necessarily represent the official views of the Civil Engineering Department, Texas A&M University.

TABLE OF CONTENTS

	Page
ABSTRACT.....	ii
ACKNOWLEDGMENTS	iv
CONTRIBUTORS AND FUNDING SOURCES	v
TABLE OF CONTENTS.....	vi
LIST OF FIGURES	ix
LIST OF TABLES.....	xx
CHAPTER I INTRODUCTION.....	1
1.1 Background and relevance	1
1.2 Objectives of the research	3
1.3 Methodology and activities	5
1.4 Thesis structure	6
CHAPTER II LITERATURE REVIEW	8
2.1 Desiccation cracking	8
2.2 Tensile Strength.....	14
2.2.1 Tensile Strength Testing	15
2.3 Effect of cyclic wetting and drying on the mechanical behavior of soils	20
CHAPTER III INTERFACE DIRECT SHEAR TESTS ON SATURATED AND UNSATURATED COMPACTED SOILS	24
3.1 Introduction	24
3.2 Basic soil characteristics	25
3.3 Compaction behavior	27
3.4 Water retention behavior.....	29
3.4.1 Water retention curve of fully-saturated soil.....	30
3.4.2 Water retention curve of unsaturated-compacted specimen.....	37
3.5 Compression behavior under wetting/drying cycles	41
3.6 Direct interface shear tests	42
3.6.1 Direct shear testing procedure	45

3.6.2	Results and discussion	46
3.7	Summary and conclusions.....	52
CHAPTER IV DESICCATION PLATE TESTS AND DIGITAL IMAGE CORRELATION ANALYSIS (DIC)		53
4.1	Introduction	53
4.2	Characteristic of cracking in soil.....	54
4.3	Desiccation plate tests	55
4.3.1	Objectives	55
4.3.2	Experimental test methodology	56
4.3.3	Experimental results of desiccation plate tests	62
4.3.4	Summary of constrained and free desiccation tests results.....	72
4.4	Constrained desiccation tests under osmotic suction condition.....	75
4.4.1	Experimental methodology	76
4.4.2	Materials and methods	77
4.4.3	Results and discussion	81
4.5	Digital Image Correlation analysis (DIC) for soil cracking.....	82
4.5.1	DIC experimental set up and materials.....	85
4.5.2	Results of DIC analysis.....	87
4.6	Concluding remarks	105
CHAPTER V A NEW INNOVATIVE DEVICE FOR MEASURING TENSILE STRENGTH OF SOILS DURING WETTING/DRYING CYCLES.....		106
5.1	Introduction	106
5.2	Objectives.....	107
5.3	Methodology	108
5.3.1	Design of experiment and test principle	108
5.3.2	Materials and methods	110
5.3.3	Quantitative analysis by using image technique.....	114
5.4	Results and discussion.....	116
5.4.1	Results of unlocked- gap test	118
5.4.2	Results of locked-gap test	130
5.4.3	Comparison between the unlocked and locked-gap tests	139
5.5	Digital Image Correlation (DIC) analysis	143
5.5.1	Image processing for DIC analysis	145
5.5.2	Results of tensile tests.....	146
5.5.3	Digital Image Correlation (DIC) results	152
5.6	Concluding remarks	161

CHAPTER VI TENSILE BEHAVIOR OF SOILS UNDER PARTIALLY RESTRICTED CONDITION DURING WETTING/DRYING CYCLES.....	163
6.1 Introduction	163
6.2 Objectives.....	163
6.3 Experimental methodology	164
6.4 Results and discussion.....	171
6.4.1 Reference case/ unsaturated-compacted soil specimen (MC1)	171
6.4.2 Specimen's thickness /Unsaturated-compacted specimen (MC2).....	181
6.4.3 Specimen's size and directional restriction/ MC3	190
6.4.4 Directional restriction/unsaturated-compacted specimen (MC4).....	198
6.4.5 Soil structure/fully-saturated specimen (MS)	203
6.4.6 Effect of specimen's thickness, size, restraining condition and soil structure on tensile and cracking behavior.....	213
6.5 Concluding remarks	220
CHAPTER VII CONCLUSIONS AND RECOMMENDATIONS	222
7.1 Introduction	222
7.2 Shear strength of unsaturated and saturated soil interfaces.....	223
7.2.1 Contributions and future recommendations.....	224
7.3 Desiccation plate tests	224
7.3.1 Contributions and future recommendations.....	226
7.4 A novel tensile device for the accurate determination of tensile strength	226
7.4.1 Contributions and recommendations for future work.....	228
REFERENCES	230

LIST OF FIGURES

	Page
Figure 3.1 Proctor compaction curve of the soil mixture consisted of 75% kaolin and 25% bentonite.....	28
Figure 3.4 Test set-up for determining the SWRC of fully-saturated specimen	32
Figure 3.5 (a) Free drying path of SWRC of the fully-saturated specimen (slurry), (b) water content vs. suction.....	35
Figure 3.6 Continued. free drying path of SWRC of the fully-saturated specimen (slurry), (a) void ratio vs. suction, (b) void ratio vs. water content.....	36
Figure 3.7 Specimens prepared for determining the drying and wetting paths of the soil water retention curve of unsaturated-compacted soil	37
Figure 3.8 (a) Free drying & wetting paths of SWRC of the unsaturated-compacted specimen, (b) water content vs. suction	39
Figure 3.9 Continued. free drying & wetting paths of SWRC of the unsaturated-compacted specimen, (a) void ratio vs. suction, (b) void ratio vs. water content	40
Figure 3.10 Compression behavior under wetting/drying cycles on compacted specimens prepared at $w = 42.6\%$, and $\gamma_d = 11.4 \text{ kN/m}^3$, under free loading and under vertical stress of 10 kPa; W: Wetting, D: Drying	42
Figure 3.11 Modified direct shear box for testing soil-shear interface: a) front view, b) top view.....	44
Figure 3.12 Different types of plate surfaces: a) spiral grooves, b) grooves oriented orthogonal with respect to the shear direction, c) grooves oriented parallel to the shear direction, and d) smooth surface.....	45
Figure 3.13 Shear stress vs horizontal displacements for perpendicular grooves at 0, and 15.5 kPa.....	47
Figure 3.14 Shear failure envelopes for saturated compacted specimens	48

Figure 3.15 Shear failure envelopes for unsaturated-compacted specimens	48
Figure 3.16 Comparison results from shear failure envelopes; (a) interfaces friction angles, (b) adhesion/cohesion for all tested sets	49
Figure 4.1 (a) The plate with smooth base for free desiccation tests, (b) a drawing of the smooth base	58
Figure 4.2 (a) The circular-spiral grooved base for constrained desiccation tests (b) a drawing of the grooved base.....	59
Figure 4.3 The experimental set up of desiccation tests	61
Figure 4.4 Image processing: a) a TrueColor (RGB) image, b) converting the RGB image to a grayscale (8-bit), c) subtracting background, d) converting to a binary image, and e) outline operation.....	61
Figure 4.5 Desiccation plates with two different base-surfaces a) circular patterns for constrained tests, b) smooth surface for free tests	62
Figure 4.6 Variations of water content over time during drying cycles, constrained samples	64
Figure 4.7 Crack patterns of constrained saturated samples (Groove-plate) at the end of each cycle (GSC).....	65
Figure 4.8 Crack patterns of constrained unsaturated samples (Groove-plate) at the end of each cycle (GUC).....	66
Figure 4.9 Variations of CIF's of constrained- saturated and unsaturated samples under wetting/drying cycles	68
Figure 4.10 Variations of water content over time during drying cycles, free samples	68
Figure 4.11 Crack patterns of free saturated specimens (Smooth-plate) at the end of each cycle (SSC).....	70
Figure 4.12 Crack patterns of free unsaturated samples (Smooth-plate) at the end of each cycle (SUC)	71
Figure 4.13 Variations of CIF's of free-saturated and unsaturated samples under wetting/drying cycles	72

Figure 4.14 Variations of CIF's of free and constrained-saturated and unsaturated samples under wetting/drying cycles	73
Figure 4.15 a) The plate with grooves and holes, b) schematic drawing of the base	78
Figure 4.16 The rectangular Perspex mold; (a) top view, (b) front view, (c) Top view after gluing the rectangular pieces, (d) schematic drawing of the groove patterns (using MgCl ₂ .6H ₂ O).....	79
Figure 4.17 (a) & (b) Crack patterns of a fully saturated soil sample consisted of 75% kaolin and 25% bentonite submerged in Ca(NO ₃) ₂ .4H ₂ O (w = 90.19%, $\rho_d=7.848 \text{ kN/m}^3$).....	80
Figure 4.18 (a) & (b) Crack patterns of a fully saturated natural soil submerged in MgCl ₂ .6H ₂ O (w = 66 %, $\rho_d=7.848 \text{ kN/m}^3$).....	80
Figure 4.19 (a) & (b) Crack patterns of a fully saturated natural soil submerged in Ca(NO ₃) ₂ .4H ₂ O (w = 66 %, $\rho_d=7.848 \text{ kN/m}^3$)	81
Figure 4.20 Digital Image Correlation principle.....	84
Figure 4.21 Speckle patterns on the surface of the specimen for DIC analysis.....	86
Figure 4.22 Experimental set up for DIC analysis.....	87
Figure 4.23 Image processing for DIC analysis; (a) TrueColor/RGB image, (b) grayscale (8 bit), (c) subtract background, (d) binary	88
Figure 4.24 Compacted specimen during 1 st drying at t= 30 hrs; (a) a true color photo; (b) specimen with displacement vectors; (c) displacement fields in x & y (pixels); (d) vorticity contours	91
Figure 4.25 Compacted specimen during 1 st drying; at t= 133.5 hrs; (a) a true color	92
Figure 4.26 Immediately after 1 st wetting; (a) a true color photo; (b) specimen with displacement vectors; (c) displacement fields in x, y (pixels) (d) vorticity contours	93

Figure 4.27 After 6 hours from 2 nd drying; (a) a true color photo; (b) specimen with displacement vectors; (c) displacement fields in x, y (in pixels); (d) vorticity contours	94
Figure 4.28 At failure-2 nd drying: (a) a true color photo; (b) specimen with displacement vectors; (c) displacement fields; (d) vorticity contours	95
Figure 4.29 Immediately after 2 nd wetting; (a) true color photo; (b) specimen with displacement vectors, at end of 2 nd wetting; (c) true color photo; (d) specimen with displacement vectors	96
Figure 4.30 At initial crack-(5 hours)-1 st drying: (a) a true color photo; (b) specimen with displacement vectors; (c) displacement fields; (d) displacement fields after smoothing	98
Figure 4.31 After 16 hours 1 st drying: (a) a true color photo; (b) specimen with displacement vectors; (c) displacement fields; (d) Vorticity	99
Figure 4.32 After 24 hours 1 st drying: (a) a true color photo; (b) specimen with displacement vectors; (c) displacement fields; (d) Vorticity	100
Figure 4.33 After 22 minutes 1 st wetting: (a) a true color photo; (b) specimen with displacement vectors; (c) displacement fields; (d) Vorticity	101
Figure 4.34 After 24 hours 2 nd drying: (a) a true color photo; (b) specimen with displacement vectors; (c) displacement fields; (d) Vorticity	102
Figure 4.35 Immediately after 2 nd wetting: (a) a true color photo; (b) specimen with displacement vectors; (c) displacement fields; (d) displacement field after smoothing	103
Figure 4.36 After 24 hours 3 rd drying: (a) a true color photo; (b) specimen with displacement vectors; (c) displacement fields; (d) vorticity	104
Figure 5.1 (a) the new tensile device; (b) & (c) schematic drawings for the device	110
Figure 5.2 The new tensile device during preparation of the soil sample; the first layer of the soil sample	112
Figure 5.3 Testing Set-up of the new tensile procedure	113

Figure 5.4 Image processing: a) A TrueColor (RGB) image; b) converting the RGB image to a grayscale (8-bit); c) subtracting background and converting to a binary image; and d) outline operation	115
Figure 5.5 Y-direction crack corresponded to the tensile failure.....	117
Figure 5.6 Variation of water content over time for the compacted specimen (MC-U) during drying processes; D: Drying	118
Figure 5.7 (a) Variation of void ratio vs. water content during drying cycles, (b) variation of soil's volume over time.....	120
Figure 5.8 Variation of tensile forces over time for MC-U during five drying cycles; D: Drying, U: Unlocked-gap after failure.....	122
Figure 5.9 Variation of lateral-induced expansion force (LIEF) over time for MC-U during four wetting cycles; W: Wetting, U: Unlocked-gap after failure.....	122
Figure 5.10 Variation of tensile forces as a function of (a) degree of saturation, (b) water content for MC-U; D: Drying, U: Unlocked-gap after failure.....	124
Figure 5.11 Variation of maximum tensile and lateral-induced expansion forces over cycles for (MC-U); D: Drying, W: Wetting, U: Unlocked-gap after failure.....	125
Figure 5.12 Variation of tensile strengths of the compacted specimen (MC-U); D: Drying, U: Unlocked-gap after failure.....	126
Figure 5.13 Crack patterns of MC-U specimen subjected to the new tensile test in cyclic wetting/drying	128
Figure 5.14 Variation of CIF and average crack aperture over wetting/drying cycles of unlocked-gap specimen	130
Figure 5.15 Variation of water content over time for the compacted specimen (MC-L) during drying processes; D: Drying	131
Figure 5.16 Variation of (a) void ratio vs. water content, and (b) soil's volume over time	132
Figure 5.17 Variations of tensile forces over time for the compacted specimen (MC-L) during five drying cycles; D: Drying, L: Locked-gap after failure	134

Figure 5.18 Variation of lateral-induced expansion forces over time for the compacted specimen (MC-L) during wetting cycles; W: Wetting, Locked-gap.....	134
Figure 5.19 Variations of tensile forces with changes of (a) degree of saturation and (b) water content for MC-L during drying cycles; D: Drying,.....	135
Figure 5.20 Variation of max. tensile and lateral-induced expansion forces over cycles for MC-L; D: Drying, W: Wetting, L: Locked-gap after failure	136
Figure 5.21 Variation of tensile strengths over cycles for MC-L; D: Drying, L: Locked-gap after failure	136
Figure 5.22 Crack patterns of the compacted sample (MC-L) subjected to cyclic wetting/drying in the new tensile test,.....	137
Figure 5.23 Continued: crack patterns of the compacted sample (MC-L) subjected to cyclic wetting/drying in the new tensile test.....	138
Figure 5.24 Variation of CIF and average crack aperture over wetting/drying cycles of locked-gap specimen	139
Figure 5.25 Variations of tensile strength of unlocked and locked-gap compacted specimens subjected to several wetting/drying cycles	141
Figure 5.26 Reduction in tensile strength of unlocked and locked-gap specimens for all drying cycles.....	142
Figure 5.27 Variations of CIF's of unlocked and locked-gap compacted specimens subjected to several wetting/drying cycles	143
Figure 5.28 Speckle pattern on the surface of the soil specimen for tensile-DIC test.....	144
Figure 5.29 The new tension-DIC test set up	145
Figure 5.30 Image processing for PIV analysis; (a) TrueColor/RGB image, (b) grayscale (8 bit), (c) subtract background, (d) binary	146
Figure 5.31 Variations of water content over time for the compacted specimen (MC3-DIC) during drying processes; D: Drying	147

Figure 5.32 Variation of tensile forces over time for the compacted specimen (MC3-DIC) during drying cycles; D: Drying.....	148
Figure 5.33 Variation of compression forces over time for the compacted specimen (MC3-DIC) during wetting processes; W: Wetting	149
Figure 5.34 Variations of tensile forces as a function of water content for the MC3-DIC during drying processes; D: Drying, locked-gap after failure	150
Figure 5.35 Effect of wetting/drying cycles on tensile strength of the compacted specimen (MC3-DIC)	151
Figure 5.36 The tensile specimen when cracks initiated after 6 hours during 1 st drying; (a) a true color photo; (b) specimen with displacement vectors; (c) displacement fields in x & y(pixels); (d) vorticity contours.....	154
Figure 5.37 After t = 10 hours during 1 st drying; (a) a true color photo; (b) specimen with displacement vectors; (c) displacement fields in x & y (pixels); (d) vorticity contours	155
Figure 5.38 At the peak, after t = 20 hours during 1 st drying; (a) a true color photo; (b) specimen with displacement vectors; (c) displacement fields in x & y (pixels); (d) vorticity contours.....	156
Figure 5.39 Crack widening after t = 21 hours from 1 st drying; (a) a true color photo; (b) specimen with displacement vectors; (c) displacement fields in x & y (pixels); (d) vorticity contours	157
Figure 5.40 Fully crack propagated at the end of 1st drying; (a) a true color photo; (b) specimen with displacement vectors; (c) displacement fields in x & y (pixels); (d) vorticity contours	158
Figure 5.41 Immediately after 1 st wetting; (a) a true color photo; (b) specimen with displacement vectors; (c) displacement fields in x & y (pixels); (d) displacement fields after smoothing	159
Figure 5.42 At the peak, 2nd drying; (a) a true color photo; (b) specimen with displacement vectors; (c) displacement fields in x & y (pixels); (d) vorticity	160
Figure 6.1 (a) & (b) The new tensile testing device with a high positioned micro-load sensor .	165

Figure 6.2 Experimental set-up of the testing procedure	166
Figure 6.3 Selected points for tensile tests from compaction curve of the soil mixture of 75 % kaolin and 25 % bentonite	167
Figure 6.4 the tensile device with high-positioned load sensor (a) perpendicular grooves for MC1, MC2; (b) parallel grooves for smaller size (MC3); (c) parallel grooves for MC4; (d) sectional view with perpendicular grooves.....	170
Figure 6.5 Variation of water content over time for MC1 specimen.....	172
Figure 6.6 Variations of (a) void ratio vs. water content, and (b) soil's volume over time for MC1	173
Figure 6.7 Variations of tensile forces over time for MC1; D: drying	174
Figure 6.8 Variations of lateral-induced expansion forces over time for MC1; W: wetting	175
Figure 6.9 Variations of lateral displacement over time for MC1; D: drying	175
Figure 6.10 Variations of tensile forces as a function of (a) degree of saturation, and (b) water content for MC1; D: drying	176
Figure 6.11 Lateral displacements vs. tensile forces for MC1 during five drying cycles	177
Figure 6.12 Crack patterns at the end of the cycle for the unsaturated-compacted specimen (MC1)	179
Figure 6.13 Continued crack patterns at the end of the cycle for MC1	180
Figure 6.14 Crack Intensity Factor (CIF) and average crack aperture at the end the cycle for MC1; W: Wetting, D: Drying.....	181
Figure 6.15 Variations of water content over time for MC2; soil thickness of 25.4 mm	182
Figure 6.16 (a) Variations of void ratio vs. water content, (b) volume change over time for MC2; soil thickness of 25.4 mm	183
Figure 6.17 Variation of tensile forces over time for MC2 subjected to five drying processes; soil thickness of 25.4 mm.....	184

Figure 6.18 Variation of lateral-induced expansion forces over time for MC2.....	185
Figure 6.19 Variation of lateral displacement over time for MC2	185
Figure 6.20 Variations of tensile forces for MC2 as a function of (a) degree of saturation, (b) water content	186
Figure 6.21 Lateral displacement vs. tensile forces over drying cycles for MC2	187
Figure 6.22 Crack patterns at the end of the cycle for the unsaturated-compacted specimen (MC2)	188
Figure 6.23 Continued crack patterns at the end of the cycle for MC2	189
Figure 6.24 Variations of CIF and crack aperture for MC2 at the end of the cycle	190
Figure 6.25 (a) A plane view of the reduced-dimensioned tensile device, (b) experimental set-up of the test	191
Figure 6.26 Variation of water content over time for MC3 during cycles	191
Figure 6.27 (a) Variation of void ratio with water content change, (b) Volume change over time for MC3	192
Figure 6.28 Variation of tensile forces over time for MC3 during drying cycles	194
Figure 6.29 Variation of lateral-induced expansion forces over time for MC3; W: Wetting.....	194
Figure 6.30 (a) Variation of tensile forces as a function of degree of saturation (b) tensile force vs water content for MC3; D: Drying	195
Figure 6.31 Side view of the MC3 at the end of first drying, (b) a curled edge with invisible crack beneath the surface	196
Figure 6.32 Crack patterns at the end of each cycle for the MC3	197
Figure 6.33 Variation of crack intensity factors (CIF) and average crack aperture for the MC3 over cycles.....	198
Figure 6.34 A photo of the new tensile device with parallel restraining condition	199

Figure 6.35 Variation of water content over time during the first drying process for the specimen MC4.....	199
Figure 6.36 Variation of tensile force over time during the first drying process for the specimen MC4.....	201
Figure 6.37 Variation of tensile force as a function of water content during the first drying process for the specimen MC4	201
Figure 6.38 Crack patterns at some time intervals for the specimen MC4 during the first drying process.....	202
Figure 6.39 Variations of water content over time for the fully-saturated specimen (MS) during four wetting-drying cycles; D: Drying.....	204
Figure 6.40 (a) Void ratio vs. water content, (b) volume change over time for fully-saturated specimen	205
Figure 6.41 Variations of tensile forces over time for the fully-saturated specimen (MS) during four drying cycles; D: Drying, with locking after failure	207
Figure 6.42 Variations of lateral-induced expansion forces over time for MS specimen	207
Figure 6.43 Lateral displacements over time for the fully-saturated specimen (MS) during drying; D: drying, with locking after failure	208
Figure 6.44 (a) Variations of tensile forces as a function of degree of saturation, (b) tensile force vs. water content for the fully-saturated specimen (MS)	209
Figure 6.45 Crack patterns of a fully saturated sample (slurry) (MS) subjected to the new tensile test in cyclic wetting/drying, with locked-gap scenario after failure.....	211
Figure 6.46 Continue. crack patterns of a fully saturated sample (slurry) (MS) subjected to the new tensile test in cyclic wetting/drying, with locked-gap scenario after failure.....	212
Figure 6.47 Crack Intensity Factor (CIF) and average crack aperture at the end of every wetting/drying process for the fully-saturated specimen (MS); Locked-gap after failure.....	212

Figure 6.48 Variation of tensile and lateral-induced expansion forces over cycles for MC1, MC2, MC3, MC4, & MS; W: Wetting, D: Drying	213
Figure 6.49 (a) Variation of Crack Intensity Factor (CIF); (b) variation of average crack aperture over cycles for MC1, MC2, MC3, MC4, & MS; W: Wetting, D: Drying	214
Figure 6.50 Variation of cracking water content over drying cycles for MC1, MC2, MC3, MC4, & MS; D: Drying	215
Figure 6.51 Comparison between MC1 and MC4 for the first drying cycle; (a) tensile forces over time, (b) tensile forces as a function of water content	218
Figure 6.52 Comparison between crack patterns for MC1 and MC4; (a) constraining case; (b) at the peak; (c) at the end of the first drying	219

LIST OF TABLES

	Page
Table 3.1 Basic properties of Kaolin provided from the manufacturer	26
Table 3.2 Basic properties of sodium bentonite.....	27
Table 3.3 Summary results of direct shear tests of soil and four interfaces	50
Table 4.1 CIF values of constrained- saturated and unsaturated specimens.....	67
Table 4.2 CIF values of constrained- saturated and unsaturated samples	72
Table 4.3 Common hypothesis opted for conceptual cracking mechanism.....	76
Table 5.1 Physical properties and initial conditions of 75% kaolin & 25% bentonite mixture...111	
Table 6.1 Test reference for tensile tests	169

CHAPTER I

INTRODUCTION

1.1 Background and relevance

One of the most significant characteristics of expansive clays is their susceptibility to volume changes when exposed to wetting or drying processes due to thermal seasonal variations. Upon wetting, the water content of soil increases resulting in an increase in the volume of the voids (swelling). While during drying, the soil-water content decreases and this gives rise to a reduction in the volume of the voids (shrinkage). The changes in soil-water content during the evaporations and precipitation periods cause volume changes of the active mineral clays below a structure. This causes ground movements which results in destructive damage to the engineering structures such as buffers, clay liners, embankments, landfills, and slopes. In this regard, it is essential to understand the hydro-mechanical behavior of soils during wetting/drying cycles for evaluating the stability and sustainability of natural soils and engineering structures as well.

During the dry spells, soils, especially, fine-grained, may undergo volumetric shrinkage accompanied with desiccation cracks. Formation of desiccation induced-cracks is a widespread natural phenomenon brought about by the evaporation process of water from the soil into the atmosphere during arid seasons. Desiccation cracks in soils may occur in naturally deposited soils as well as engineered soils (e.g., roadway embankments, compacted fills, slopes, hydraulic barriers, clay liners and buffers, etc). In fact, the presence of cracks may cause problematic impact on the mechanical behavior of the soil, and this may be destructive for a number of geotechnical, geo-environmental, and geological applications, such as clay liners, landfill covers, industry waste

(Omidi, et al., 1996, Albrecht and Benson, 2001, Tang, et al., 2011). Furthermore, cracks may become a preferential pathway for contaminates transport and water flow in the soil structure (McBrayer. et al., 1997, Albrecht and Benson, 2001, Greve et al., 2010). Hence, this may substantially increase the permeability of the soil, besides to detrimental variations and distortions in the structure of the soil (micro and macro structures) resulting in, some cases, physical failure. Moreover, the presence of cracks may likely cause a significant reduction in the compressibility which adversely influences on the performance of earthen structures (e. g., clay liners, landfill covers, foundations, slopes, and embankments). For example, at the same initial conditions (e.g., moisture content), a cracked soil may exhibit more compressibility and permeability than an uncracked soil (Morris et al., 1992), and as a result, a significant reduction in the mechanical strength of the cracked soil is obtained compared to the intact one.

Various concepts and frameworks have been adopted to interpret the inception and propagation of desiccation cracks in soils, for example, the frameworks of net-stress (e.g. Morris et al., 1992, Rodríguez, et al., 2007), total stress (e.g., Péron et al., 2009, Amarasiri et al., 2011), effective stress (Shin and Santamarina, 2011), and the combination of total and effective stress (Abu-Hejleh and Znidarcic, 1995). Majority researchers reported that the crack formation is owing to the tensile fracture mechanism, where the crack initiates in a soil when the developed stresses exceed the soil tensile strength (Rodríguez et al., 2007, Amarasiri et al., 2011, Lakshmikantha et al., 2009). While few researchers have supported the notion that desiccation cracks generate under compressive effective stress state conditions (Shin and Santamarina, 2011).

Although considerable research has been conducted for investigating the failure criteria behind crack formation in soils, the mechanism is still not well understood and more research efforts are still needed for better comprehension.

Basis to understanding desiccation crack formation in soils is twofold; the determination of tensile strength under circumstances imitated to those in the field, and the accurate tracking of the soil particles during crack evolution. Very few studies have examined the tensile strength during crack formation. In most of these studies, the tensile strength was determined when external applied tensile loads produce failure in a soil tested under constant water content and constant matric suction. However, very little attention has been directed to study the influence of wetting/drying cycles on tensile strength coupled with the evolution and propagation of cracks. The study described herein was motivated by the assumption that desiccation crack propagation is owing to the decrease in tensile strength of soil over wetting/drying cycles. Research in this thesis presents a new approach by using a novel device for determining tensile strength of a soil subjected to multiple wetting/drying cycles similar to the circumstances in field. The study of cracking mechanism was coupled with the determination of tensile strength and tracking soil particle during wetting/drying cycles.

1.2 Objectives of the research

The underlying objective of this study is to investigate the hydro-mechanical behavior of soils subjected to multiple drying and wetting cycles. This has been stemmed from the observation of crack propagation of soil when exposed to successive drying/wetting cycles. Most researchers come in to an agreement that accumulated irreversible deformations, such as swelling and shrinkage, may take place upon multiple wetting and drying cycles. Consequently, the soil

structure may undergo significant variations which may influence on the hydro-mechanical response of soil. Under drying, soil may develop irreversible deformations in fabric resulting in crack formation, while upon wetting, soil may undergo softening/weakening which provides healing and closing to the present cracks that formed in the previous drying. However, these cracks remain weak region and under alternate drying the cracks re-open and propagate increasingly. After a certain number of drying/wetting cycles, the cracks remain unchanged without any propagation.

Of particular significant in understanding of cracking mechanism, a new approach of tensile testing was utilized in this work to examine tensile strength of a soil subjected to sequential wetting and drying cycles. Previous laboratory tensile studies have been hindered a numerous of difficulties comprising; the soil sampling, detachment between the soil sample and tensile mold during the test, and the very high-water content of the soil sample. Consequently, my research had promoted more crucial improvements on tensile testing which simulates the natural conditions of soils as in field.

The main objectives of this research can be highlighted below:

- To study the influence of soil-interface associated with different initial conditions on shearing behavior of soil.
- To investigate the impact of soil-interface coupled with the effect of different initial conditions of soils on the inception and propagation of cracks.
- To develop a new approach using a novel device for measuring the tensile strength of soil subjected to circumstances similar to those in field, with an adequate recognition of the limitations of this approach, if any.

- To understand the effect of drying and wetting cycles on the tensile strength of soils.
- To employ image analysis technique to capture the crack patterns of tested soils in multiple drying and wetting cycles.
- To track the displacement fields of soils subjected to cyclic wetting/drying processes by using Digital Image Correlation analysis (DIC).

1.3 Methodology and activities

Research presented in this thesis focuses on the knowledge that obtained from the experimental tests. Laboratory tests provide better understanding of the actual soil behavior under controlled and natural environmental conditions. This thesis encompasses the main following activities:

- Laboratory tests to determine the engineering properties of the soil using the standard classification tests, such as, index properties, compaction curve, and soil-water retention curve using different techniques.
- Direct shear tests using different soil-interfaces and different initial conditions to study the shearing behavior of soils.
- Cyclic wetting/drying cracking plate tests to investigate the inception and propagation of soil cracks under free and constrained soil-interface with different initial conditions.
- New-developed tensile tests to investigate the influence of alternative wetting/drying cycles on the tensile strength of soils by using a novel device and new approach.

- Image analysis technique to quantitatively characterization of the crack morphology of the soil subjected to cyclic wetting/drying processes. Crack Intensity Factor (CIF) is the most significant parameter that obtained from the image analysis.
- Digital image Correlation (DIC) method to tracking the displacement fields of the soil undergoes to deformations during drying/wetting cycles.

1.4 Thesis structure

A brief outline of the dissertation structure is provided. The main contents of the thesis are presented as follows:

- Chapter II presents the literature review of relevant previous research on desiccation crack formation, the impact of cyclic wetting/drying processes on crack formation, soil-interface impact on the hydro-mechanical behavior of soils, previous and current soil-tensile testing methods.
- Chapter III explores the influence of different soil-interfaces and initial conditions on the shearing behavior of soil. Interface-direct shear tests were performed using four counterfaces; including perpendicular, circular, parallel, and smooth. The soil characterization has been presented in this chapter as well.
- Chapter IV consists of a series of laboratory drying/wetting tests performed on thin soil layers using circular plates. Constrained and free tests were performed under different initial conditions. The effect of alternative wetting/drying cycles on the propagation of cracks was investigated as well. Image analysis method was employed to characterize crack patterns on the surface of the soil specimen in each cycle. Also, DIC analysis was employed to interpret some emerging phenomena.

- Chapter V introduces a novel approach for studying the tensile strength of soils under sequential wetting/drying cycles, with an adequate recognition of the limitations of this approach, if any. A new innovative tensile device was fabricated, more details are presented in this chapter. Image analysis technique was employed to quantitate soil cracking at the end of each cycle. The impact of alternative wetting/drying cycles on the tensile strength is clearly presented and discussed in this chapter. A fundamental to understanding crack evolution in soils during tensile test by employing Digital Image Correlation analysis (DIC).
- Chapter VI presents additional tensile tests performed by using the new device that presented in chapter V. However, these tests were conducted under partially restrained condition in which the free part of the device was allowed to response with soil movement during drying and wetting.
- Chapter VII presents the primary conclusions, contributions, and some recommendations for the future work.

CHAPTER II

LITERATURE REVIEW

2.1 Desiccation cracking

This chapter presents literature review of relevant previous studies involving: desiccation cracks in soils, interface shear behavior, reviews on direct and indirect techniques employed to measuring the tensile strength of soils, the effect of wetting/drying cycles on the hydro-mechanical characteristics of soils. The literature review in this chapter is mainly focused in the engineering applications; reviews of methodologies (experimental) will be presented wherever needed.

Cracking in soils may commonly occur in naturally deposited soils as well as engineered soils (e.g., roadway embankments, compacted fills, slopes, hydraulic barriers and buffers, etc). Soils, especially, fine-grained, may undergo drying resulting in crack formation. Formation of cracks in soil can be due to several processes comprising; desiccation and shrinkage, freezing and thawing, differential settlement, syneresis, and penetrated plant roots (Yesiller. et. al., 2000). The evolution of desiccation cracks is considered a common phenomenon due to evaporation process (expulsion) of water from the soil into the atmosphere during the summer season. The presence of cracks may cause problematic impact on the hydro-mechanical behavior of the soil, and this likely leads to severe problems in the soil mass. For example, at the same initial condition (e.g., moisture content), a cracked soil has more compressibility than an uncracked soil, and as a result, less mechanical strength than the intact soil (Morris et. al., 1992). In addition, cracks may increase the permeability of the soil, besides to exhibit severe changes in the soil structure (fabric and inter-particles forces) that may cause physical failure in the soil structure. Furthermore, these cracks

may become a preferential pathway for contaminates transport and water flow (McBrayer. et. al., 1997, Albrecht and Benson, 2001, Greve et. al., 2010). Consequently, the performance of several engineering applications, such as, geotechnical, environmental, and geological applications (e.g., industry waste, clay liners, covers of landfills) may adversely affected by cracks (Omidi, et. al., 1996, Albrecht and Benson, 2001, Tang, et. al., 2011).

Over the last decades, laboratory and field experimental works had been performed to investigate desiccation cracking in various types of soils (Boynton and Daniel, 1985, Omidi et al., 1996, Ayad et. al., 1997, Yesiller et al. 2000, Rayhani et. al., 2008, Peron et. al, 2009a). Current experimental and numerical studies have mainly focused on investigating desiccation cracks of fully saturated soils (slurries) prepared either in rectangular bars (e.g., Nahlawi and Kodikara, 2006, Peron et al., 2009b) or circular plates (e.g., Rodríguez et al, 2007, Tang et al, 2011, Trabelsi et al., 2012). Most of these experimental studies were implemented under controlled laboratory circumstances (i.e., temperature and humidity). However, some researchers studied crack development at different ambient environmental conditions (e.g., temperature and humidity), besides to other different conditions related to the dimensions and types of the tested soils (Uday and Singh, 2013). Digital image technique had been opted to a fundamental understanding of the morphology of crack network. Depending on image technique, crack characteristics of soil were investigated through a number of related parameters (e.g., crack intensity factor, average length and width of cracks, etc), and so employed for quantifying of crack network. Basically, Crack Intensity Factor (CIF) is often utilized to quantify the cracks on the surface of the soil specimen, where CIF defines as the ratio of the crack area to the total area of the soil sample.

Majority studies reported that desiccation cracks may probably occur when the soil undergoes to any restrictions during evaporation or shrinkage process, and (or) to tensile stresses which exceeded the tensile strength of the soil (Corte and Higashi, 1960). These restrictions may arise at the contact surfaces of soil and structure (i.e., soil-plate interface) that may cause evolution of cracks during drying. Some of these restraints are involving (Hueckel 1992; Peron et al. 2009b):

- 1) any displacement boundary conditions, or any frictional stresses due to restraining structure (e.g., due to grooves at the soil-structure interface).
- 2) variations in the water content in the soil which may cause stress concentration.
- 3) distortion and/or heterogeneity in the soil structure of the specimen.

The initial compaction conditions comprising water content, dry density, and compaction energy have a significant impact on the hydro-mechanical behavior, especially, for fine-grained compacted soils. Some studies revealed that crack formation in compacted soil owing to the high fine contents, where the compacted soils with high fine fractions experienced higher cracking than those of compacted soils with lower fine fractions (Yesiller. et. al., 2000). In arid areas, it is recommended to compact the soil at low moisture content (dry of optimum, OMC) with high compactive energy to minimize any potential desiccation cracking during the dehydration process (Daniel and Wu ,1993). In this case, the soil experiences flocculated structure of high strength and stability. However, the soil may prone to swell when wetted, and then to shrink excessively when subjected to drying. On the other case, compacting the clayey soils at wet of optimum moisture content and low dry densities may decrease any potential wetting induced swelling. However, the soils may tend to shrink upon subsequent evaporation process resulting in crack formation.

Accordingly, the compacted soils may undergo either shrinkage when compacted at wet of optimum or swelling when compacted at dry of optimum (Yesiller. et al., 2000).

Various experimental studies were carried out to investigate desiccation cracking of different compacted soils (Boynton, 1983, Boynton and Daniel, 1985, Kleppe and Olson, 1985). Kleppe and Olson (1985) studied desiccation cracking of two highly expansive clays and sand/bentonite mixtures. Soils were compacted in rectangular slabs and then allowed to dry, while their edges were restrained. At the same water contents, the clayey soils developed higher shrinkage strains than those of sand/ bentonite mixtures. Also, the sand mixture with higher sand ratio exhibited lower shrinkage strains. For this study, it was revealed that the soils with high fine contents undergo more shrinkage accompanied with crack formation than those with low fine contents.

In response to performing very low permeable geotechnical structures, such as, clay barriers and buffers, previous research had studied the influence of desiccation cracking on the hydraulic conductivity of cracked soils during wetting/drying cycles. This issue has been taken into more consideration because of the necessity in various significant applications, such as nuclear waste isolation, covers and liners for landfills, etc (Tang et al., 2011). A study conducted by Albrecht and Benson, 2001 showed an increase in the permeability of clay liner with cracks by about three orders of magnitude (Albrecht and Benson, 2001). Subsequently, cracked soils experienced high permeability than that of intact soils. Boynton and Daniel (1985) conducted hydraulic conductivity tests on compacted clays (kaolinite and fire clay). Soil specimens were compacted in desiccation slabs with the thickness of about 2.5 inch at three different moisture contents, and then allowed to dry for three days at laboratory conditions. Specimens with four-

inch of diameters were cautiously trimmed and then subjected to hydraulic conductivity tests using flexible-wall permeameters. At low effective stresses, desiccated specimen exhibited larger permeability than that of undesiccated specimen by about one-half to one order of magnitude. Also, it was observed that the permeability of desiccated specimens reduced quickly with increase the effective stress (up to 56 kPa), and this likely due to closing of crack openings. This indicates that the overburden stresses subjected on the soil can be critical for closing cracks and preventing formation new ones in some of engineering applications that exposed to crack (Boynton and Daniel, 1985).

Another experimental study was performed by Omidi et al., (1996) to examine the influence of desiccation cracks on the hydraulic conductivity of compacted soils during two successive wetting-drying cycles (Omidi et. al., 1996). Two different permeameters were used, with the diameters of about 10 cm and 60 cm, to measure the hydraulic conductivity in small and large-scale specimens. Smectite and illite soils were used, in addition to mixtures of these soils with 30% of sand. The small-scale specimens exhibited lower hydraulic conductivity values than those of the large-scale specimens. This indicates that the hydraulic conductivity measured in the field is greater than that measured from laboratory tests. Generally, it was observed that the hydraulic conductivity of compacted soils increased due to evolution of cracks and continued to raise at the end of the second wetting-drying cycle. Consequently, the outflow rates increased through the soil samples. On the other hand, soil mixtures of smectite or illite plus 30% of sand exhibited constant hydraulic conductivity measurements at the end of the first and second desiccation cycles, as a result, the outflow rates remained constant. It was noticed that no significant cracks progressed in the mixtures after the end of the first wetting-drying cycle.

Similarly, Albrecht (1996) reported increase in the hydraulic conductivity of high plasticity soils up to the end of the second wetting-drying cycle, while low plasticity soils exhibited increase in the hydraulic conductivity at the end of the first wetting-drying cycle (Albrecht, 1996).

A previous study conducted by Yesiller et al. (2000) on large-scale specimens of three different compacted liner soils obtained from landfills to investigate desiccation cracking during wetting/ drying cycles. All specimens were low plasticity with a wide broad range of fine fractions. Suction measurements and crack characteristics (e.g., CIF; crack intensity factor) of the samples were taken during drying/wetting cycles. All samples were compacted at $\pm 2\%$ of optimum water content (as determined from the standard Proctor compaction test). All specimens were allowed to dehydrate at the initial compaction moisture content then subjected to one wetting-drying cycle. Only one test was conducted on a soil sample subjected initially to dry at the initial compaction water content then to three subsequent wetting-drying cycles. The study revealed that the soil of high fine content developed more cracks than that of low fine content even though they have the same plasticity index (PI). At the end of the compaction-drying process (first drying), the soils exhibited lower CIF values than those of wetting-drying cycle, even though the soils experienced higher suctions in the first drying than those in the wet-dry cycle. It seems that at the first drying, the soil strength is much greater than the developed tensile stresses that associated with high suctions. Therefore, the soil resisted the tensile stresses with tending to shrink with insignificant cracks. At the end of the first drying, it appears that the soil structure (fabric and inter-particle forces) was subjected to some changes during shrinkage process. These changes can be irreversible deformations and different configurations of particles. Upon wetting, the soil specimen was exposed to soften and weakened and then reduction in the tensile strength. Subsequent drying

process caused formation of cracks in the weakened positions that experienced reduced soil tensile strength. It was reported that the cracks developed at low suction values (e.g., less than 1000 kPa) with no more significant cracks progressed at very high suction value (e.g., suction of 6000 kPa). No significant cracks were observed after the second wetting-drying cycle of the soil sample. The maximum CIF value recorded of the three compacted soil samples was about 7 %.

2.2 Tensile Strength

Tensile strength of soil is a vital mechanical characteristic that can be employed to predict the stability and sustainability of geotechnical and geo-environmental structures, such as, earthen dams, embankments, landfill covers, clay liners. This property of soil has been taken in to consideration to understand the failure and fracture mechanism of desiccation-induced cracks (Rodríguez et al., 2007, Péron et al., 2009a, Miller et al., 2016, Varsei et al., 2016).

During evaporation process, the soil undergoes volumetric shrinkage that might be subjected to restraints due to non-uniform water gradients or any frictional or traction or displacement boundary effect at soil-interface or restraining in the soil structure (Hueckel 1992; Péron et al. 2009b). These restraints generate tensile stresses at soil-interface. When these stresses exceed the tensile strength of the soil, desiccation cracking develops (Corte and Higashi, 1960). This failure approach has been widely adopted in a number of studies in interpreting the phenomenon of crack formation during drying process (Rodríguez et al., 2007, Lakshmikantha et al., 2009, Amarasiri et al., 2011).

Testing techniques employed for measuring the tensile strength of soils split up into two main categories comprising indirect and direct testing methods. Indirect testing methods have been utilized to measure the tensile strength of the soils using a non-tensile loading (e.g., compression

loading). Indirect testing methods encompass Brazilian tensile test (Frydman, 1964), fracture toughness measurements using ring test (Harrison et al. 1994), beam flexure tests (Konard and Ayad, 1997), and an unconfined penetration device (Kim et al., 2012). While direct testing techniques are conducted by subjecting the soil specimen into a direct tension loading. For example, modulations had been made in the direct shear test device to perform the direct tensile test (e.g. Nahlawi et al. 2004, Tamrakar et al. 2005, Vesga 2009, Trabelsi et al., 2012, Tang et al., 2015, Stirling et al., 2015).

2.2.1 Tensile Strength Testing

Direct and indirect tensile testing techniques are employed for determining the tensile strength of soils. These techniques are categorized based on the loading fashion, where a direct tension loading is used in the direct testing methods and a non-tension loading fashion (e.g., compression loading) is used in the indirect methods. Different principles of these techniques were illustrated in Vanicek, 2013 (Vanicek, 2013) based on the loading manners.

Most of the experimental and numerical studies focused on studying the compression behavior of soils. Limited consideration has been taken to examine the tensile strength of the soils even though the crack-formation mechanism has been adapted, by a large number of researchers, as a failure criterion-based on tensile strength. Different testing methods were opted to investigate the tensile strength of the soils under undrained conditions. However, limited studies were performed to determine the tensile strength under drained condition, for example, Bishop and Gara (1969) (Bishop and Gara, 1969) modified a triaxial cell with a controlled strain rate to examine the tensile strength of drained clays.

Generally, for the tensile testing procedure, a uniaxial-tension loading fashion has been performed either by catching up the cylindrical soil specimen vertically from one side or by laterally constraining the specimen through two loading jaws. Recently, the second technique has been adapted more than the other one with variations in the geometrical design and dimensions of the loading tensile molds.

2.2.1.1 Indirect Tensile Testing Techniques

For indirect tensile tests, indirect measurements are obtained, while the soil specimen is subjected to a compression loading, and then, at the end of the test, the obtained parameters are employed for tensile strength determination. Examples of indirect tensile tests are comprising the Brazilian tensile test (Frydman, 1964, Ghosh and Subbarao, 2006), fracture toughness measurements using the ring test (Harrison et al. 1994), beam flexure test (Konard and Ayad, 1997), and an unconfined penetration test (Kim et al., 2012). In these tests, the soil samples are fractured under either point or linear compression loading. The developed tensile stresses are considered distributed uniformly on the failure plane of the sample, in which the tensile strength

is readily calculated. However, these techniques are more appropriate for investigating the tensile strength of brittle and elastic geomaterials (e.g., rock, stiff soils) than ductile materials (e.g., soft, wet clayey soils). Due to a number of limitations and assumptions of indirect tensile techniques, direct tensile methods are more preferable for soils.

2.2.1.2 Direct Tensile Testing Techniques

For the direct tensile tests, the soil specimen is commonly subjected to externally direct uniaxial-tension loads, where the tensile strength can be directly determined at the failure plane. Based on the tensile test device, the tensile strain and loading rates are both can be readily controlled. However, the main problem in conducting the direct tensile tests is twofold; the difficulty in preparation of the soil specimen, and the other one presence of a gap at soil-device interface during the shrinkage process. Consequently, new methodologies have been progressed to improve the direct tensile test of soils (Tamrakar et al. 2005, Lakshmikantha et al. 2012).

Nahlawi et al., (2004) investigated the tensile strength of the soils using the direct shear device with the modification of tensile box. The modified apparatus included two rectangular jaws with the dimensions of the whole enclosure of 200 x 100 x100 mm. The reduced central area was opted in this research. The notion behind reducing the central cross-sectional area of the soil specimen was to localize the maximum tensile stresses at that plane, as consequence, the tensile failure takes place (e.g., Trabelsi et al., 2010). Embedded shear keys were fabricated along way of the longitudinal sides of the tensile jaws to provide restraints against the tensile loads and to prevent the detachment at soil-device interface during the test. The central area (neck area) was tested under free condition to develop uniformly distributed tensile stresses at that plane. It was reported that the soil specimen with low water content experienced an increase in the tensile

strength and a decrease in the tensile strain (Nahlawi et al., 2004). In addition, the study revealed the difficulty in conducting the direct tensile test on specimens with very high moisture content (e.g., slurries) (Nahlawi et al., 2004).

Numerical and experimental studies were conducted by Trabelsi et al., (2010 and 2012) (Trabelsi et al., 2010, 2012) to measure the tensile strength of remolded and compacted clays at a broad range of water contents. External tensile forces were applied either by using the motor of the direct shear device (Trabelsi et al., 2010) to provide controlled tensile loads and strains or by using a traction system to apply incremental tension loads (Trabelsi et al., 2012). In both studies, similar tensile mold was employed comprising of two convergent halves in the form of bow-tie.

This mold includes one fixed-half and one movable-half setting on ball bearing for inducing free movement during the test without any frictions. Similar apparatus was used by Rodriguez et al. (2007) in which a traction device employed to apply incremental tension loads (see Rodriguez et al. 2007).

In Trabelsi et al., (2010, 2012), both slurry and compacted soil specimens were prepared directly in the tensile testing mold. Similar to Nahlawi et al., (2004) and Rodriguez et al., (2007), a central bridging area was introduced between the two halves to localize the maximum tensile stress at that plane. A LVDT was used to measure the displacement of the free half (Trabelsi et al., 2010) and a dial gauge in Trabelsi et al., 2012. However, it was difficult to measure the displacement at the central area, especially for the fully saturated specimens (slurries). A set of experimental tensile tests was performed at a wide range of water contents associated with the corresponding values of suction which were examined at the end each test using the psychrometric method (e.g., Dew point Method: Model WP4). The results of the tensile tests showed an increase

in the tensile strength with increase the suction or decrease in the corresponding water content. The variations in the tensile strength at a wide range of water contents/or suctions were presented as an exponential function.

One of the most testing problems taken into considerations for measuring tensile stresses is that the separation or detachment between the tensile mold and the soil specimen during the test. Previous studies used different approaches to maintain the attachment between soil sample and tensile device, during evaporation process. Some researcher used a number of shear keys embedded in the soil specimen to prevent a potential detachment at soil-interface (i.e., Nahlawi et al., 2004) where these keys assisted in catching the soil when subjected to drying with time. Kim and Hwang (2003) utilized four triangular wedges attached on their sides with sandpaper. These wedges were mounted in the way where the soil sample forming bowtie shape. The primary function of these wedges was to prevent any potential separation or slip-condition between the specimen and the tensile mold when tensile stresses develop (Kim and Hwang, 2003). Another study employed two groups of screws fixed in two desiccation halves; each group was mounted along the long wall of one jaw to maintain attachment between soil specimen and the convergent halves, and provide constraints for developing tensile stresses, as well (Varsei et al., 2016).

Most of previous numerical and experimental studies employed external tension loads either by using a direct shear device or traction apparatus. However, a unique study conducted by Varsei et al., (2016) (Varsei et al., 2016) used a rectangular desiccation box to measure the tensile strength of different types of soils during drying process. This desiccation box consisted of two identical halves; one half is fixed and the other one is free to move on the top of ball bearings with minimal friction. A small gap was introduced where the two halves combine. The tensile stresses

were measured via two large load cells mounted where the two halves join. A number of screws mounted along the side walls of the two halves were used to provide restraints at one direction in which the tensile stresses may develop to induce crack evolution during drying process. In Varsei et al., (2016) study, all soil samples were subjected only to a unique drying. The notion of Varsei et al., (2016) research is that to subject the soil sample to natural conditions, as in field, during drying process in which the tensile stresses may develop due to increase of suction and decrease of water content accompanied with crack formation.

Recently, many experimental and modeling studies have focused on investigating the influence of several factors on the tensile strength of compacted soils, such as, water content, dry density, and characteristics of clay particles (Rodríguez et al., 2007, Tang et al., 2015, Zhang et al., 2015). Majority studies revealed that compacted soil exhibits softening at failure when subjected to tensile loading where a clear post peak is obtained. It was observed a nonlinear relationship between the tensile strength of soil and water content. The soil may exhibit at the same dry density an increment in tensile strength with an increase of water content up to a certain water content where the tensile strength reaches the maximum, and then the tensile strength starts to decrease with increase of water content. However, the effect of water content on tensile strength is different than dry density in which soil may exhibit more resistance of tensile stresses with increase of dry densities at the same water content.

2.3 Effect of cyclic wetting and drying on the mechanical behavior of soils

The mechanism of desiccation cracking is a very complex. It is relevant to chemical, physical and mechanical characteristics of soil involving; initial water content, compaction condition, mineral composition and clay contents, etc (Morris et al. 1992, Albrecht and Benson

2001). Moreover, the variation in the surrounding climatic conditions is a very significant factor affecting the soil cracking behavior. In the field, soil periodically is exposed to cyclic wetting and drying due to seasonal variations. This leads to changes in the hydro-mechanical characteristics of soils. Various studies have been conducted on investigating the impact of wetting and drying cycles on the mechanical behavior of soils. However, very few research has studied the effect of wetting-drying cycles on evolution and propagation of cracks

Expansive soils are prone to volume changes due to intrinsic factors including; the initial water content, void ratio/or dry density, and the type of clay minerals (Mitchell and Van Genuchten 1992, Fredlund and Rahardjo 1993, Estabragh et al, 2015). Many researchers have studied the impact of wetting-drying cycles on the mechanical behavior of expansive clays in a variety of contexts. Majority researchers studied the effect of wetting-drying cycles on the compression behavior of soils using several suction control techniques (Wheeler et al. 2003, Alonso et al. 2005, and Nowamooz and Masrouri 2008, Liu et al, 2012), while some examined shear strength of soil subjected to wetting-drying cycles (Gallage & Uchimura, 2016). Wheeler et al. 2003 studied the behavior of soil subjected to one cycle of wetting-drying processes under isotropic loading fashion. They proposed a model for the coupling of compression behavior and hydraulic hysteresis. Alonso et al, 2005 explored the influence of wetting/drying cycles on expansive bentonite-sand mixtures. The vapor equilibrium technique was utilized for controlling the suction values with the range of 4 MPa to 130 MPa during a number of sequential wetting/drying cycles in the oedometer cell. They revealed that the soil developed a progressive shrinkage until a reversible elastic response occurred. This resulted in an increase in the over-consolidation ratio (OCR). Another research was conducted by Nowamooz and Masrouri 2008 to examine the effect of successive wetting/drying

cycles on the compression characteristics of an expansive bentonite/silt mixture by using an oedometer testing method. The Osmotic technique was employed to control the suction of four different values; including 0, 2, 3, and 8 MPa. It was found that the wetting/drying cycles influence on the compression properties of the soil involving; virgin compression index, elastic compression index, and preconsolidation stress.

Other researchers studied the variations of axial deformations of an expansive soil subjected to a number of wetting/drying cycles (i.e, Estabragh et al, 2015). A modified oedometer apparatus was used with different suction values and surcharge pressures. The water content and the deformations were obtained at different stages. The results showed that the swelling-shrinkage was irreversible until the soil approached to the equilibrium condition while a reversible elastic response with constant deformations occurred. Also, it was observed that the soil specimens with lower initial water content experienced higher swelling potential than those with higher initial water content.

A recent research was conducted by Wang et al., 2016 for investigating the effect of three wetting-drying cycles on the soil strength of a silty soil by employing micro-penetrometer tests. The study revealed the significant impact of wetting-drying cycles on the soil strength which decreases with increasing the cycles. This was owing to the presence of defects in soil microstructure and heterogeneity of the strength profile of the soil (Wang et al., 2016).

Very few studies have examined the impact of wetting-drying cycles on desiccation cracking behavior of soils. Tang et al., (2016) investigated the effect of five sequential wetting-drying cycles on fully saturated soil specimens. In this study, desiccation cracks were quantitatively characterized by using image analysis technique. The results revealed the significant impact of

wetting-drying cycles on the cracking morphology of the soil. Over cycles, the crack patterns approached to equilibrium state after the third cycle where no more cracks were obtained.

Desiccation cracking is a major concern in designing of some geostructures, such as, barriers for nuclear waste, clay buffers, and clay liners. In response to that, more research related to the effect of wetting-drying cycles on cracking behavior of soils is still needed. The main objective of the research in this thesis is to determine how much wetting-drying cycles influence the desiccation cracking of a high expansive soil.

CHAPTER III
INTERFACE DIRECT SHEAR TESTS ON SATURATED AND UNSATURATED
COMPACTED SOILS

3.1 Introduction

The interaction between soil and structure is an essential design and safety parameter in geotechnical applications, such as retaining wall, soil-pile interaction, slopes, buried pipes, and foundations. A reciprocal transmission of the developed stresses takes place between the soil and structure (Miller and Hamid, 2007, Hamid and Miller, 2009) where may give rise some problems for many geotechnical structures. The shear strength of a soil-structure interface depends on many factors involving; drainage and loading conditions, soil structure (i.e., compacted, slurry), surface roughness, and shear direction. Several studies have been conducted on a variety of soil types for different soil-structure interfaces (i.e., Yoshimi & Kishida, 1981, Miller & Hamid, 2007, Borana et al., 2016). Majority research has investigated the shear behavior of soil-structure interface in the context of surface roughness, loading and drainage conditions, and physical soil properties (Hossain & Yin, 2013, Chai & Saito, 2016, Boukpeti & White, 2017). Few studies have explored the influence of shear direction on the interface shear strength (Manzoli et al. 2017, Chen et al., 2017).

Any structural surface's geometry has likely a certain degree of anisotropy due to the natural characteristic of the material and the contributed skills for manufacturing the geotechnical structures. This leads to anisotropic distribution of the loads on the surface. Substantially, the shearing behavior varies with the variation of the shear direction. Accordingly, research

described herein was motivated to reveal how much the impact of shear direction on the shear strength of a soil-structure interface taken into consideration unsaturated and saturated conditions as well.

Fundamental to understanding the interaction between the soil and structure is the determination of interface shear strength considering several conditions for simulating the circumstances as in the field. The study herein investigates the influence of many factors on shear strength of the soil-structure interface including; surface roughness, shear direction, and saturation conditions. This integration improves our understanding of the shear behavior of soil-structure interface in geotechnical applications. The experimental campaign herein was conducted on a high-expansive soil mixture of 75% of kaolin and 25% of bentonite. Four different interfaces were employed involving circular-spiral, perpendicular, parallel, and smooth surfaces. Drained and undrained conditions were also considered for acquiring better understanding of the variation of the interface shear strength under different surface roughness and shear directions. A basis to understand the soil behavior, mechanical and hydraulic soil characteristics related to soil suction are required to be explored. Moreover, mineralogical composition, compaction, soil water retention behavior, and swell-shrink behavior are presented and described whenever they are required.

3.2 Basic soil characteristics

A high expansive soil mixture consisted of 75% kaolin and 25% bentonite was used in this research. The mineralogical composition of the clay minerals of kaolin (EdgarMineral, 2018) and the sodium bentonite (Kiviranta & Kumpulainen, 2011, BYK Additives & Instruments. 2015) are obtained from the manufacturers and presented in Table 3.1, Table 3.2, respectively. Based on

Table 3.1, kaolin is classified as low plastic clay with low linear shrinkage of 5.8%. While bentonite H is one of the clay minerals which has the most dramatic swell-shrink capability when exposed to wetting-drying processes. The expansive properties of bentonite are presented in Table 3.2, such as; liquid limit $\geq 250\%$, swelling index ≥ 20 ml/ 2g, 10^{-12} m/s of hydraulic conductivity, and other properties.

The soil mixture was subjected to classification and physical property tests according to ASTM standards (ASTM 2005): Atterberg limits (ASTM D4318). The Casagrande method was opted for determining the liquid limit, and the thread rolling method for the plastic limit. Atterberg limits are determined as follows; liquid limit is 88% and plastic limit is 48%. Accordingly, the soil is classified as high expansive soil (CH).

Table 3.1 Basic properties of Kaolin provided from the manufacturer

Product identifier	Kaolinite	
Molecular Formula	$(Al_2O_3, 2SiO_2, 2H_2O)$ - 97%	
Plasticity limit %	26	
Linear dry shrinkage %	5.8	
Cation Exchange Capacity (Methylene Blue Index):	4.5 meq/100 g	
Chemical components (%):	Kaolinite 99%-99.9% & Quartz 0.1%-1%	
	SiO ₂	45.73
	AL ₂ O ₃	37.36
	MgO	0.098
	Fe ₂ O ₃	0.79
	CaO	0.18
	Na ₂ O	0.059
	K ₂ O	0.33
	TiO ₂	0.37
	P ₂ O ₅	0.236
	LOI	13.91

Table 3.2 Basic properties of sodium bentonite

Product identifier	BENTONITE H	
Molecular Formula	Al ₂ O ₃ 4SiO ₂ xH ₂ O	
Density (g/cm ³)	2.6	
Estimated Specific gravity	2.6	
Swelling index	≥ 20 ml/ 2g ^a	
Swelling pressure (MPa)	≥ 2 ^a	
Liquid limit %	≥ 250 ^a	
Cation Exchange Capacity (CEC)	≥ 70 meq/100 g ^a	
Hydraulic conductivity m/s	10 ⁻¹² a	
Chemical components (%): bentonite	99-100% & Quartz < 1%	
	SiO ₂	68.1
	AL ₂ O ₃	13.5
	MgO	2.9
	Fe ₂ O ₃	0.7
	CaO	0.9
	Na ₂ O	3.5
	K ₂ O	0.1
	TiO ₂	0.2

a: values taken from (Kiviranta & Kumpulainen, 2011)

3.3 Compaction behavior

Soil compaction is a technique employed for placing the soil particles into a dense state. This can be performed by reducing the air pores in the soils with no reduction of the water content. Compaction is a very popular method used to improve the engineering characteristics of soil. The primary objective of soil compaction is to decrease the compressibility, while in the meantime increase shear strength and decrease the permeability of soil. A unique relationship can be established between the water content and dry density by conducting the standard Proctor test. The standard Proctor compaction test (ASTM D698) was performed to determine the compaction curve

of the soil mixture using the compaction effort ($600\text{kN}\cdot\text{m}/\text{m}^3$). Eight soil specimens were prepared at a wide range of water contents and then kept to promote moisture equilibrium. After that, each soil specimen was compacted into three layers in the standard compaction mold of 10.16 cm diameter and total volume of 944 cm^3 . The compaction curve of the soil mixture is plotted in the plane of water content and dry unit weight (Figure 3.1) In the same curve, the zero-air void curve is also plotted which represents the fully saturated condition of the soil. The optimum moisture content (OMC) of 36% is obtained from the compaction curve at the maximum dry unit weight of $12.16\text{ kN}/\text{m}^3$.

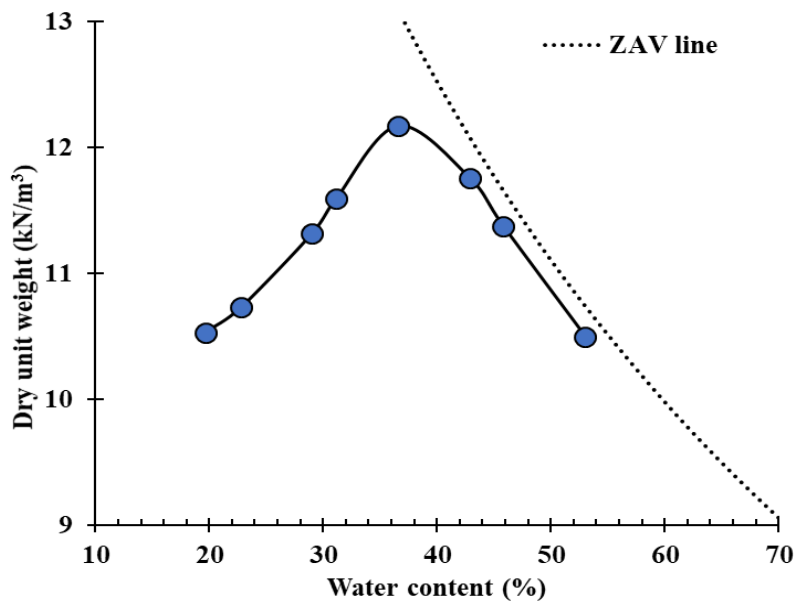


Figure 3.1 Proctor compaction curve of the soil mixture consisted of 75% kaolin and 25% bentonite

3.4 Water retention behavior

The unique relationship between suction and degree of saturation is known as the soil water retention curve (SWRC) or soil water characteristic curve (SWCC). This curve is very useful to interpret some soil characteristics, such as, strength, volume changes, permeability (Fredlund et al., 1994). In this study, the tensiometer (UMS, 2009) and chilled-mirror dew-point (WPT4) (Decagon 1998-2003) techniques were employed for determining the soil water retention curve of fully-saturated and unsaturated-compacted specimens prepared from the soil mixture of 75% kaolin and 25% bentonite.

Soil water retention curve (SWRC) was determined; while specimens were allowed to freely drying/shrinkage (no load) under controlled laboratory temperature and relative humidity (22.1 ± 1 C°, RH= 59 ± 1). More details regarding of SWRC determination are provided in the following sections.

Chilled-mirror dew-point technique provides quick and reliable suction measurements in the range of 1 to 100 MPa. The basis behind chilled-mirror dew-point method (WPT4) is based on measuring the relative humidity of a soil specimen in a sealed chamber. At equilibrium, the relative humidity in the chamber will be similar to the relative humidity of the soil specimen. Based on psychrometric law, the total suction can be then determined. The following equation shows the relationship between relative humidity and total suction.

$$s_t = -\frac{RT}{M_w} \ln\left(\frac{P}{P_0}\right) \quad (3.1)$$

s_t is defined as the total suction; R is the universal gas constant (8.314 J/Kmol), T is the absolute temperature (K), $\frac{P}{P_0}$ is the relative humidity in the air, M_w is the molecular mass of water, (see after Cardoso et al., 2007).

In addition, a low capacity tensiometer was employed for continuous and direct measuring of the matric suction of a soil specimen during drying process. More information related to the schematic drawing of the tensiometer is provided in UMS GmbH, 2009 (UMS GmbH, 2009). Reliable determination of matric suction need an adequate saturation of the porous ceramic cup. The saturation procedure of the porous tip is described in the manufacturer manual of (UMS GmbH, 2009).

3.4.1 Water retention curve of fully-saturated soil

The SWRC of fully-saturated (slurry) specimen was determined by using two different techniques. These techniques consisted of low suction tensiometer, type T5 (UMS, 2009) for measuring continuously matric suctions in the low range from 0 to around 275 kPa, while the chilled mirror dew-point psychrometer (WP4-T) utilized for discrete measurements of high suction values (Decagon 1998-2003).

For low suctions, two identical specimens were prepared at the initial water content of about 90.19% and dry unit weight of about 7.848 kN/m³. The soil was placed in three layers in a small stainless-steel ring of 75.6 mm diameter and 25.4 mm height; using light tapping to remove air bubbles from the specimen at the desired dry unit weight. The inside perimeter of stainless steel ring was previously lubricated to avoid any disturbance for the specimen when was extracted. Then the specimen was carefully extracted on a lubricated smooth acrylic plate. One specimen was

placed on an electronic balance connected to a data acquisition system for continuous measurements of mass (i.e. water loss). The other one was used for suction measurements using tensiometer. The tensiometer was inserted vertically in a small hole which was previously made at the center of the specimen. A small amount from the remaining specimen was used to close all around the tensiometer (at the contact surface of tensiometer and the sample) to prevent atmospheric pressure from getting into the sample and resulting in incorrect suction values (as observed in many fruitless attempts). The tensiometer was then fixed and supported to a stand. The test was terminated when the tensiometer cavitated. For volume measurements, two series of photographs were captured by using two cameras; one was fixed directly above the soil specimen (perpendicularly) for measuring the changes in the specimen's diameter, and the other one was mounted in the side view for thickness measurements. Figure 3.2 presents the test set-up of the experiment.

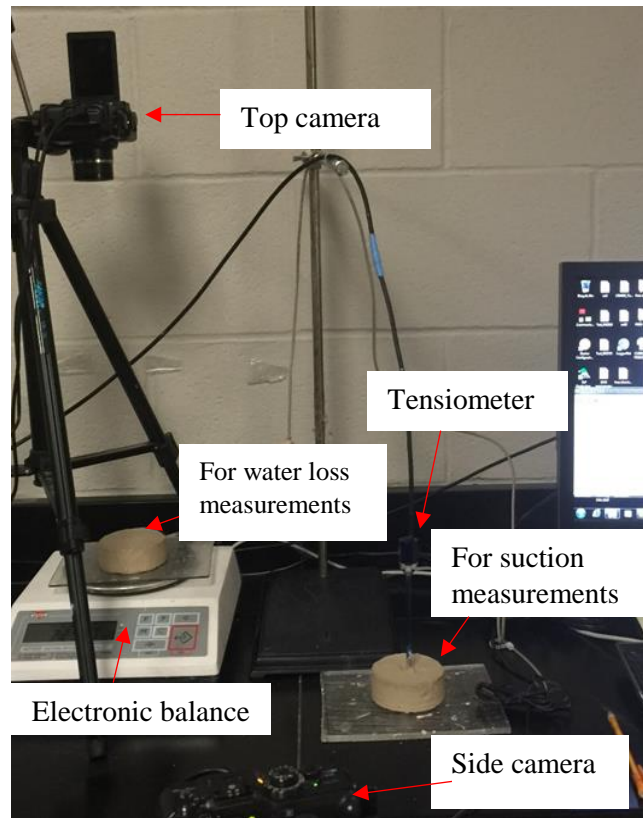


Figure 3.2 Test set-up for determining the SWRC of fully-saturated specimen

After a number of fruitless attempts, it was observed that the stiffness of tensiometer's cable influenced largely on the mass measurements during free shrinkage. Although a study performed by Liu et al (2015) showed a slight effect of the cable stiffness on the apparent mass (0.25 g). During shrinkage, the tensiometer was dragged by the soil in the direction of the electronic balance causing flocculated mass readings and thus, inauthentic mass measurements were obtained. Accordingly, the concept of having two identical specimens; one for water loss and another for suction measurements was adapted in this experiment.

Additional identical six specimens were prepared and then allowed to dry under controlled lab temperature and relative humidity (22.1 ± 1 C°, RH = 59 ± 1). The specimens were allowed to freely dry at different water contents corresponded to suction values. In this way, the SWRC was established over a wide range of suctions and volumetric changes. The volume was determined by using a digital caliper. Afterward, the specimen was divided into two portions; one was used for water content measurement, and the other one was placed in the drawer of the WP4-T for suction measurement.

Soil water retention curve (SWRC) was defined in the plane of the suction and effective degree of saturation (Figure 3.3). The effective degree of saturation was calculated based on the following equation:

$$S_r = \frac{S_l - S_{min}}{S_{max} - S_{min}} \quad (3.2)$$

Where S_r is the relative degree of saturation ($0 \leq S_r \leq 1$); S_l is the liquid degree of saturation; S_{min} is the minimum degree of saturation; S_{max} is the maximum degree of saturation. The experimental data are compared with the Villar et al., 2008 (Villar et al., 2008) which has the following formulas:

$$S_1 = \left(1 + \left(\frac{s}{P_0} \right)^{\frac{1}{1-\lambda}} \right)^{-\lambda_0} \quad fd \quad (3.3a)$$

$$fd = \left(1 - \frac{s}{P_d} \right)^{\lambda d} \quad (3.3b)$$

Where s is the suction, P_0 is a parameter related to the air entry value (AEV) and λ_0 is a parameter to control the shape of the curve (Van Genuchten, 1978). For more adequate values at

high suctions, f_d is added to the formula. P_d is a parameter related to the suction at 0 degree of saturation and λ_d is a model parameter, more details are provided in Villar et al, 2008 (Villar et al, 2008). Figure 3.3 and Figure 3.4 show the soil water retention results of the fully-saturated specimen. The opted parameters used herein are: $P_0 = 0.01$ kPa, $\lambda_0 = 0.075$, $P_d = 100$ kPa, and $\lambda_d = 2$. The experimental data shows reasonable agreement with the model.

Based on our calculations, it was observed that the fully saturated specimen exhibited a degree of saturation greater than 1.0, which was obtained in near the fully saturation. A number of previous research reported similar observation, in fact that for highly plastic soils, the degree of saturation can be higher than 1.0 (e.g. Villar, 2002, Jacinto, et al., 2011). This may attribute to the natural mineralogy of bentonite in which the properties of the water molecules inside interlays of clay are different than that of the free water. Therefore, in this case, the effective degree of saturation was adequate to define the SWRC.

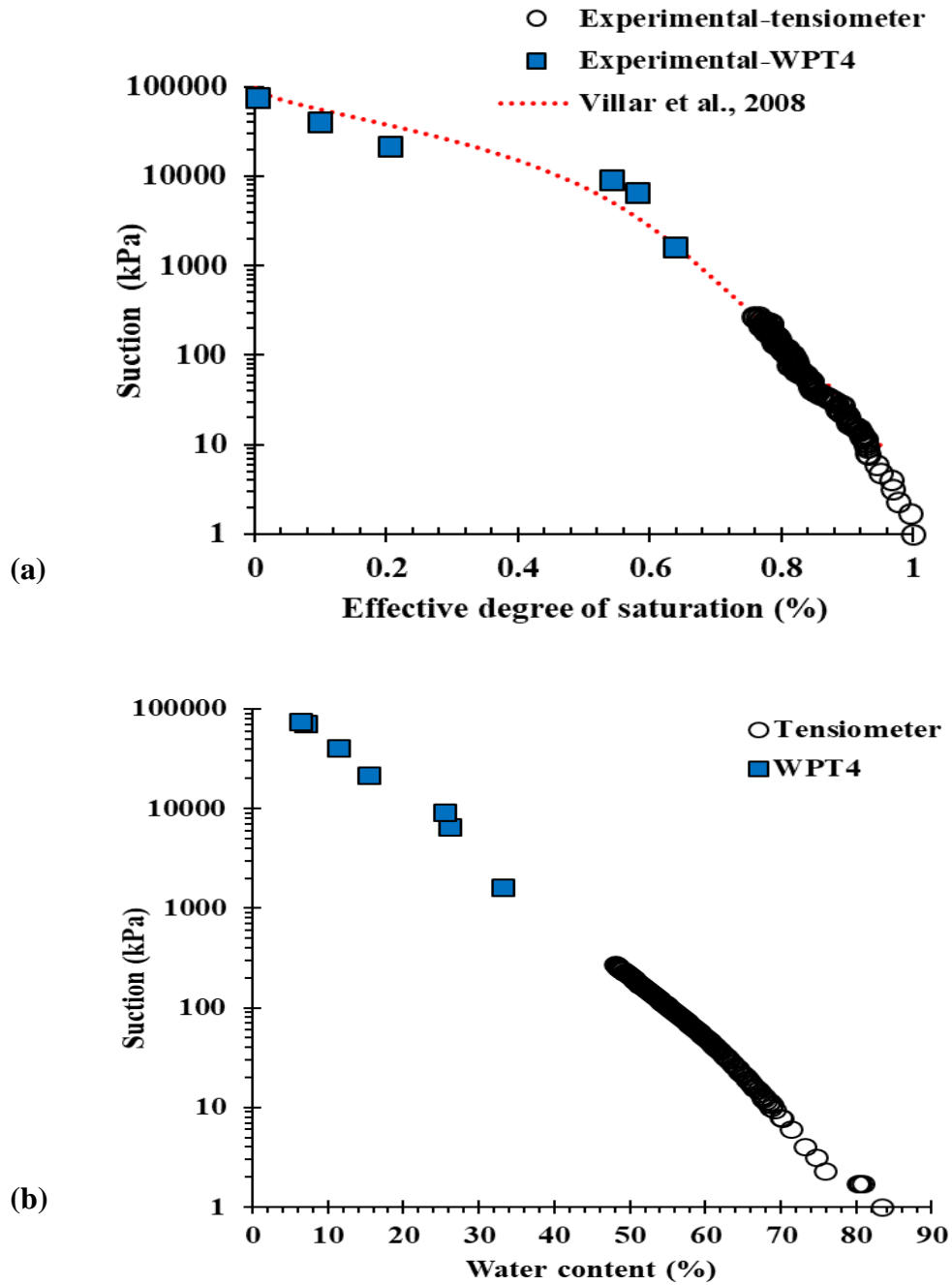


Figure 3.3 (a) Free drying path of SWRC of the fully-saturated specimen (slurry), (b) water content vs. suction

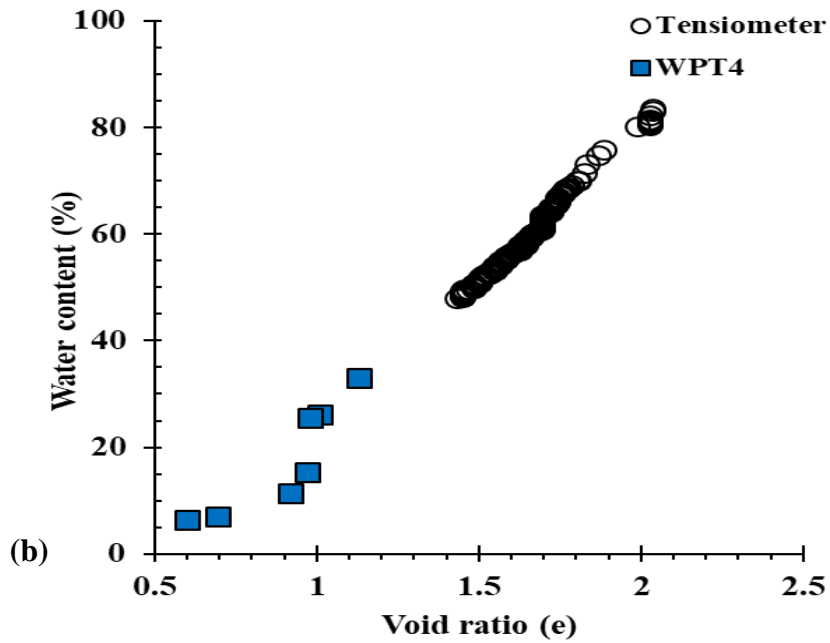
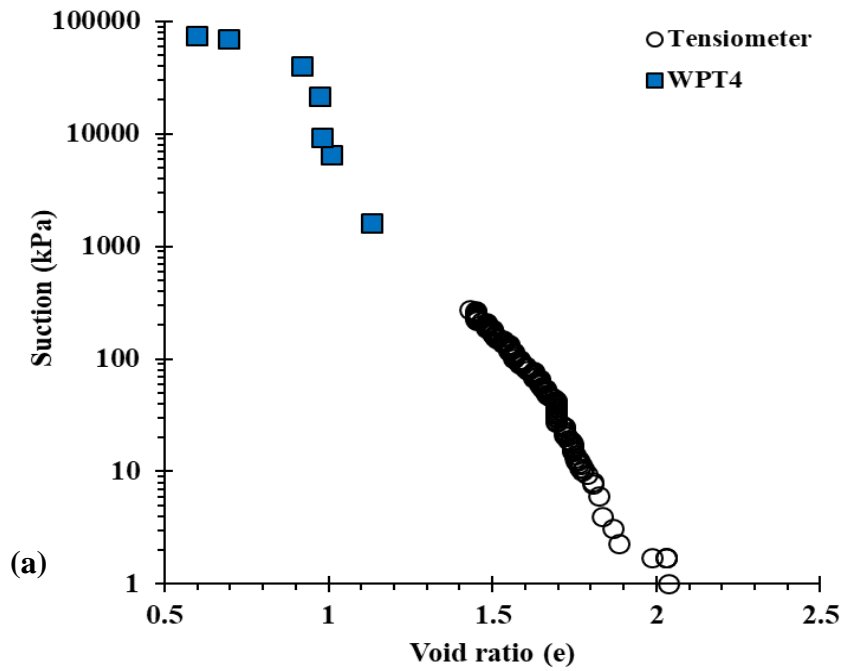


Figure 3.4 Continued. free drying path of SWRC of the fully-saturated specimen (slurry), (a) void ratio vs. suction, (b) void ratio vs. water content

3.4.2 Water retention curve of unsaturated-compacted specimen

The soil water retention curve (SWRC) was determined by using the chilled mirror dew-point psychrometer (WP4-T) for discrete measurements at high suction values (Decagon 1998-2003). Twenty soil specimens were prepared identically at initial water content of $42.67\% \pm 0.5$, and dry unit weight of 11.4 kN/m^3 similar to the initial conditions used for direct shear interface tests and desiccation tests (chapter IV), as shown in

Figure 3.5. The soil was compacted at the desired dry unit weight in three layers in a small stainless-steel ring of 75.6 mm diameter and 25.4 mm height. The inside perimeter of stainless steel ring was previously lubricated to avoid any disturbance for the specimen when was extracted. Then the specimen was then carefully extracted on a lubricated smooth acrylic plate.

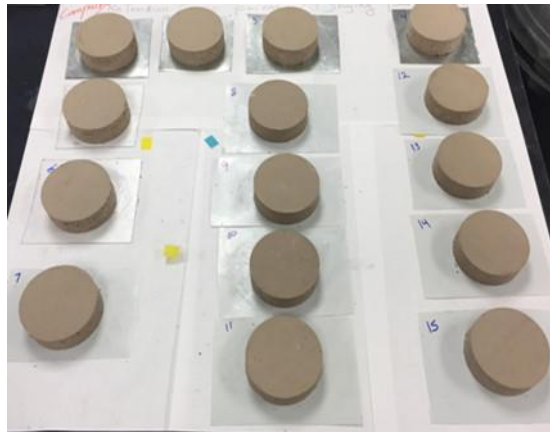


Figure 3.5 Specimens prepared for determining the drying and wetting paths of the soil water retention curve of unsaturated-compacted soil

Ten specimens were prepared for determining the drying path of the soil water retention curve; they were allowed to dry at different water contents corresponded to various suctions in which SWRC can be plotted over a wide range of suctions and degrees of saturation. For wetting

path, additional ten specimens were allowed to dry till approached equilibrium, or no significant changes were obtained. After that, every specimen was wetted by distilled water to a certain degree of saturation; suction and volume changes were obtained. For each specimen, the volume measurement was determined by using a digital caliper. Afterward, the sample was divided into two portions. One was used for water content measurement, and the other portion was placed in the drawer of the WP4-T for suction measurement.

Soil water retention curve (SWRC) of unsaturated-compacted soil prepared at initial water content of 42.67% and dry unit weight of 11.4 kN/m³ was defined in the plane of the suction and effective degree of saturation, as shown in Figure 3.6 and Figure 3.7 presents more results related to drying and wetting paths of the soil specimen. The experimental results are compared with the Van Genuchten, (1978) model (Van Genuchten, 1978) which has the below formula:

$$S_r = \frac{S_l - S_{min}}{S_{max} - S_{min}} = \left(1 + \left(\frac{P_g - P_l}{P_0} \right)^{1/(1-\lambda)} \right)^{-\lambda} \quad (3.4)$$

Where P_0 is a parameter related to the air entry value (AEV); λ is a parameter to control the shape of the curve; P_g is the gas pressure; and P_l is the liquid pressure. $P_g - P_l$ is the capillary pressure (or suction); S_{min} is the minimum degree of saturation; S_{max} is the maximum degree of saturation; S_l is the liquid degree of saturation. The following parameters of Van Genuchten's model are opted for drying and wetting curves, as follows; $P_0 = 10$ MPa, $\lambda = 0.6$, and $P_0 = 3.2$ MPa, $\lambda = 0.65$, respectively.

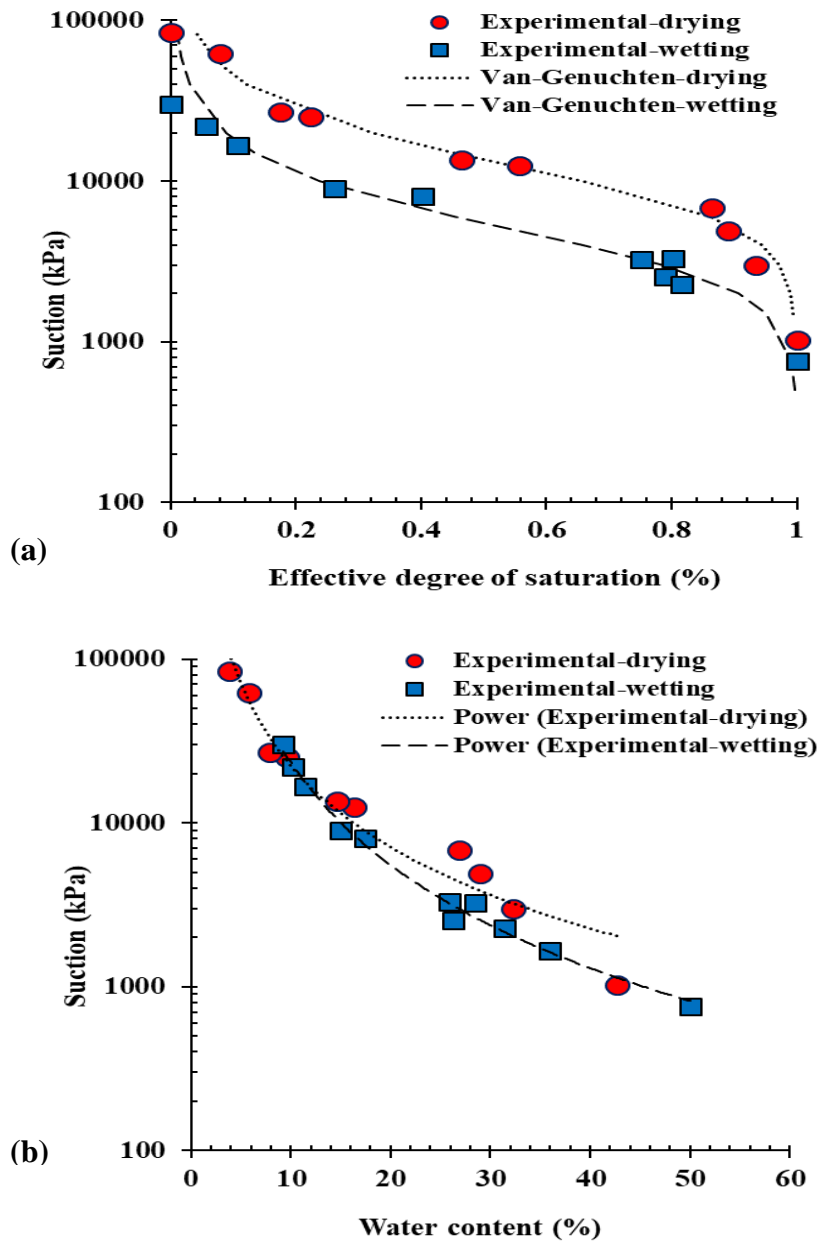


Figure 3.6 (a) Free drying & wetting paths of SWRC of the unsaturated-compacted specimen, (b) water content vs. suction

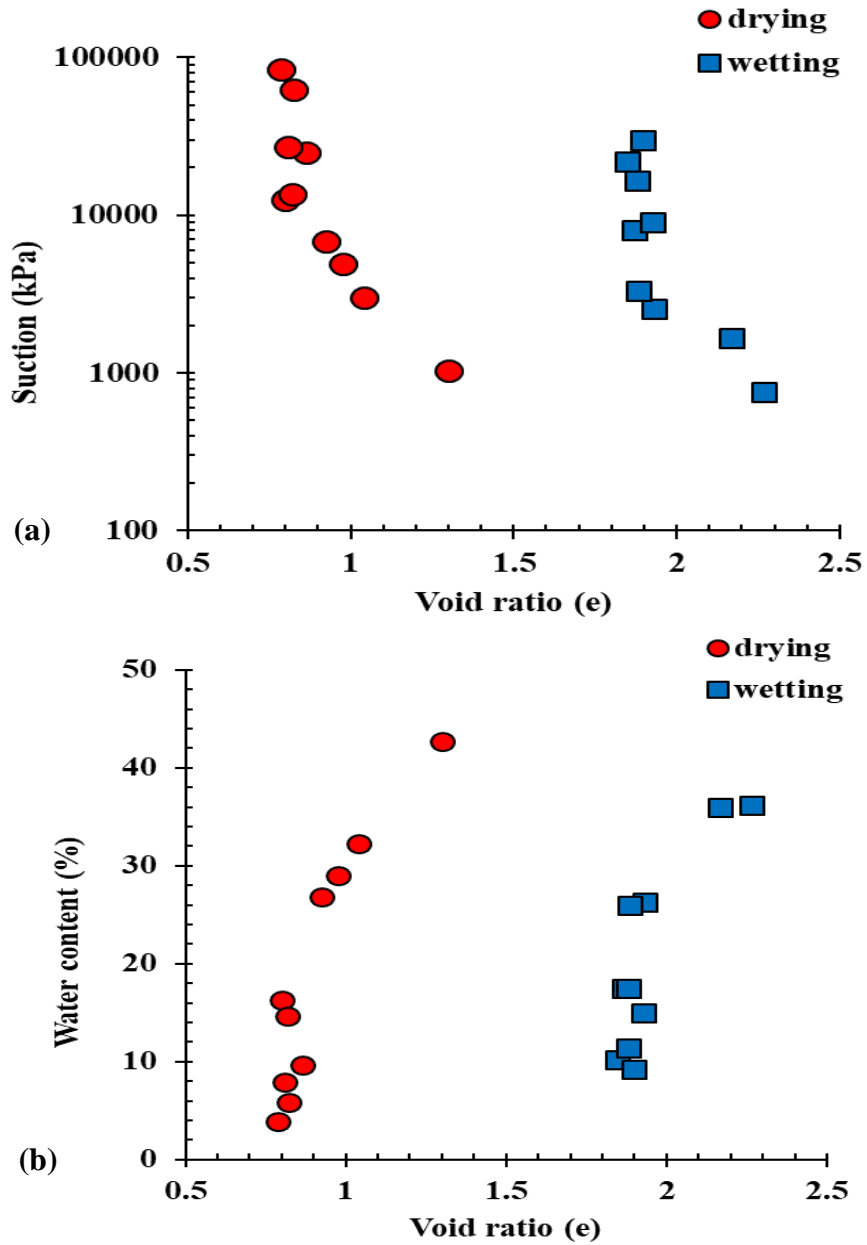


Figure 3.7 Continued. free drying & wetting paths of SWRC of the unsaturated-compact specimen, (a) void ratio vs. suction, (b) void ratio vs. water content

3.5 Compression behavior under wetting/drying cycles

The soil is exposed periodically to precipitation and dry weather cycles in which causing accumulated and irreversible deformations in the soil mass. This gives rise commonly in expansive soils, resulting in problematic behavior of soils. Accordingly, it was beneficial herein to investigate the impact of wetting and drying cycles on the compression behavior of soil. Two specimens were prepared at similar initial water content of about 42.6% and compacted at dry unit weight of 11.4 kN/m³ and then subjected to cyclic wetting/drying processes at different conditions. The two specimens were initially subjected to the first drying process, however under different loading conditions; the first one was subjected to free loading and the second one was subjected to a constant vertical stress, for example 10 kPa.

The wetting and drying cycles were conducted in the same procedure of that one of conventional oedometer test. At the end of each cycle, the final height was obtained using deformation sensors. The results of both cases in Figure 3.8 show that the vertical deformation upon the first wetting cycle is the greatest one over the other subsequent cycles. Different results were obtained after the first cycle for the two cases of free loading and under 10 kPa vertical load. For free load case, the specimen experienced irrecoverable strains over cycles, while no vertical strains were obtained for the specimen that subjected to a constant load. For free load case, the amount of swelling and shrinkage decreased over cycles till approached to an equilibrium state after the third cycle in which no any significant deformations were obtained.

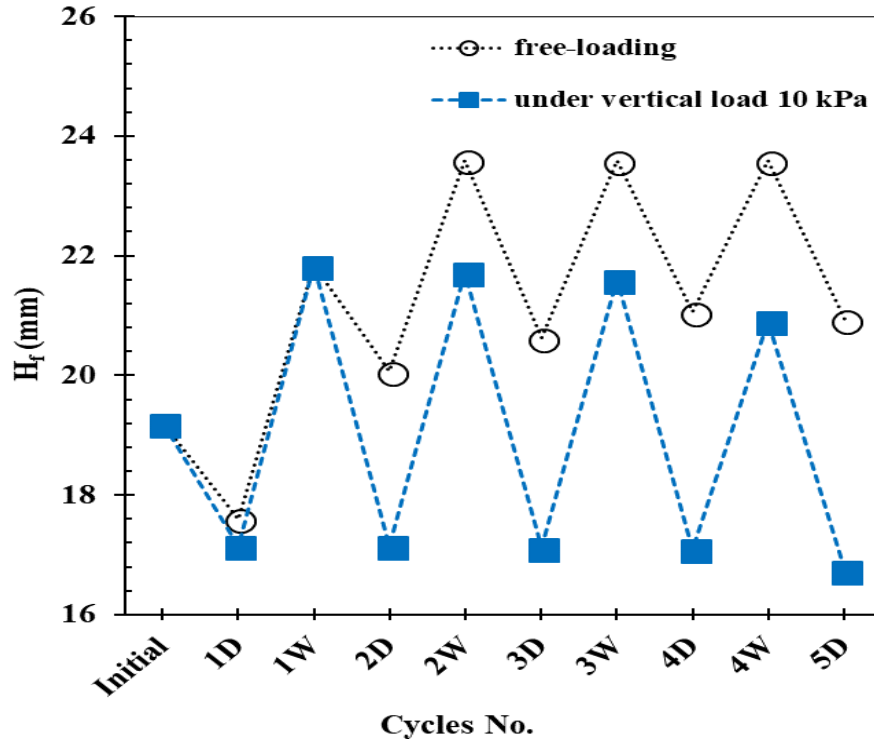


Figure 3.8 Compression behavior under wetting/drying cycles on compacted specimens prepared at $w = 42.6\%$, and $\gamma_d = 11.4 \text{ kN/m}^3$, under free loading and under vertical stress of 10 kPa; W: Wetting, D: Drying

3.6 Direct interface shear tests

Two series of shear tests were performed under unsaturated and saturated conditions. The unsaturated-compacted specimen was prepared by mixing thoroughly the mixture with distilled water at the target water content of 42.67% (4.67% wet of OMC from the standard Proctor test, ASTM D698), and then stored for 24 hours to promote moisture equilibrium. The soil was then compacted in the shear box in three layers to achieve the required dry density of about 11.40 kN/m^3 (94.4% of γ_{dmax} as determined from the standard Proctor test, ASTM D698). Laboratory compaction composed of tamping to achieve approximately uniform application of compaction

energy to the top of each layer. The initial degree of saturation was determined 0.87 and the matric suction was measured 1000 kPa by using the chilled mirror dew-point psychrometer (WP4-T) (Decagon 1998-2003).

The saturated-compacted specimen was initially prepared at the same initial conditions (i.e., $w = 42.67\%$, and $\gamma_d=11.40 \text{ kN/m}^3$) of those of unsaturated-compacted specimen. Then the specimen was inundated with water and kept for fully saturation or until no significant swelling where the free swelling index was obtained to be 2.68%. The degree of saturation of the specimen was calculated to check whether the samples reach to fully saturation or not, if not, the specimen was re-inundated.

In this study, 15 compacted specimens were subjected to direct shear testing under saturated conditions. These tests were referred as saturated direct shear and interface specimens. In addition, 15 unsaturated-compacted specimens were sheared under unsaturated conditions referred as unsaturated direct shear and interface specimens. For unsaturated specimen, the weight of the specimen was maintained constant during the whole period of the test by wrapping the specimen's surface with plastic wrap. Consequently, the initial water content and corresponded matric suction were maintained constant during the entire time of the test. The suction was determined at the end of each test by using WP4-T.

The conventional direct shear device was employed, the top half of the shear box was utilized, and the lower half consists of an acrylic square plate was sandwiched between the top and the bottom halves of the shear box, as shown in Figure 3.9. Two identical acrylic square bases were manufactured with the length of 88.9 mm and 6 mm of height. Triangular indentations of 1 mm deep and spaced every 1.5 mm grooved each plate; one with circular spiral and the other one

with straight patterns. The direct shear-interface tests were performed by using the two plates: (1) using circular indentations (Figure 3.10a); (2) orienting the straight grooves perpendicular to the shearing direction (Figure 3.10b); and (3) orienting the straight grooves parallel with respect to the shear direction (Figure 3.10c); and smooth surface (Figure 3.10d) (Manzoli et al., 2017). The orientation of the coordinate system (s , l) based on the grooves's direction. Accordingly, four counterfaces were utilized herein, including circular-spiral, orthogonal, parallel, and smooth surfaces, for studying the directional interface strengths under unsaturated and saturated conditions. Four series of direct shear interface tests were conducted for each condition. An additional series of direct shear tests were performed for each saturation condition without using any interface, where soil-soil shear strength can be determined. The soil-soil direct shear tests were performed for acquiring integral comprehension of the interface effect on the shearing behavior of soils at different saturation conditions.

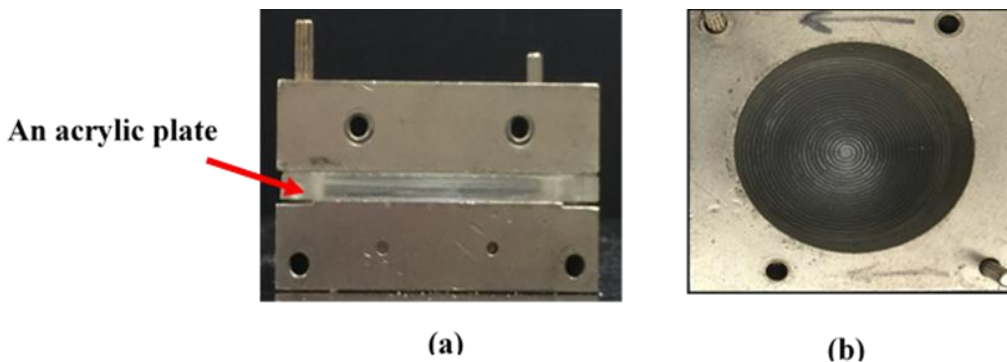


Figure 3.9 Modified direct shear box for testing soil-shear interface: a) front view, b) top view

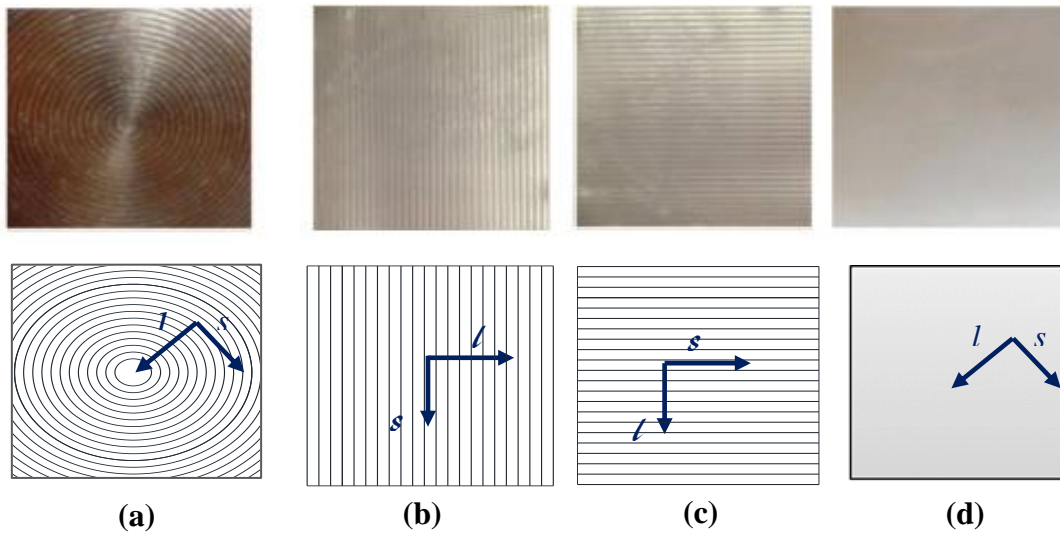


Figure 3.10 Different types of plate surfaces: a) spiral grooves, b) grooves oriented orthogonal with respect to the shear direction, c) grooves oriented parallel to the shear direction, and d) smooth surface

3.6.1 Direct shear testing procedure

The direct shear test was performed followed the standard one (ASTM D3080, 2011). The experimental campaign of the shear tests was conducted on the ten series (circular grooves, straight grooves parallel, perpendicular to the shear direction, smooth interface and soil-soil) at three different vertical stresses, including 0 kPa, 6.2 kPa, and 15.5 kPa which had been selected to define the shear failure envelopes of all tested specimens. All specimens were sheared at very low shear rate (i.e., 0.018 mm/min). The main purpose of selecting a slow shear rate was twofold; one to avoid overestimated shear strength parameters (e.g., friction angle, cohesion, and adhesion), second to prevent any changes in pore pressure during shearing for unsaturated specimens (Hamid and Miller, 2009). The test was terminated when the peak shear force value was obtained or until

no significant change observed. For the saturated shear test, the specimen was initially allowed to saturate and freely swell at zero normal stress. The specimen was then consolidated at the target normal stress. After completion of the primary consolidation, the specimen was sheared. Shearing process was continued until the peak value of the shear force was clearly obtained or until the shear force stabilized at constant value. In case of unsaturated shear test, the surface of specimen was completely covered with plastic wrap to maintain constant water content and suction values during the test.

3.6.2 Results and discussion

The effect of shear direction on the interface strength was examined by using four counterfaces, as follows: circular-spiral grooves, perpendicular grooves, parallel grooves, and smooth surface. The soil-soil strength was also determined for comparison with shear interface strength. Figure 3.11 presents the evolution of shear stress against horizontal displacements for the experiments conducted under the vertical stresses of 0 kPa, and 15.5 kPa, and under unsaturated condition. For two cases, grooves were placed perpendicular to the shear direction. The shear stress gradually increased until the peak value then decreased after failure. The maximum shear stress was determined for the maximum vertical stress of 15.5 kPa.

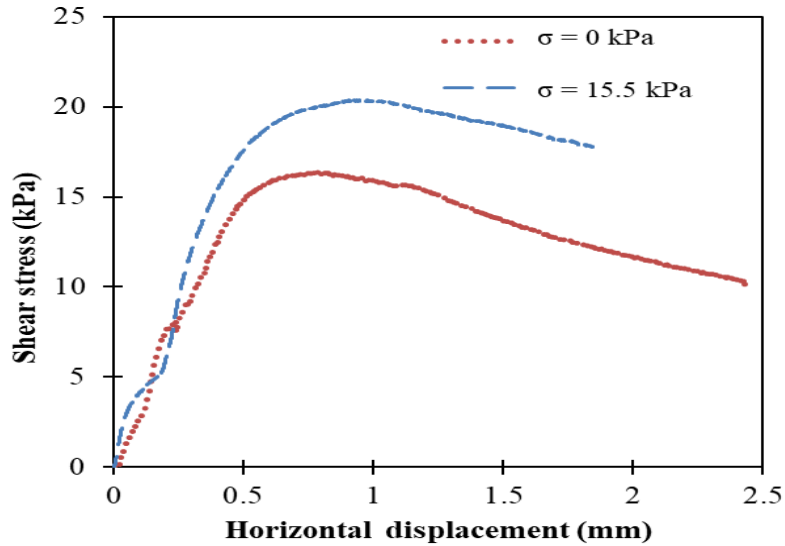


Figure 3.11 Shear stress vs horizontal displacements for perpendicular grooves at 0, and 15.5 kPa

For all direct shear tests (soil-soil and interfaces), the shear failure envelopes in the normal stress (σ_n) and maximum shear stress (τ_{max}) plane are presented in Figure 3.12 and Figure 3.13 for saturated and unsaturated conditions, respectively. A comparison between all shear strength parameters is presented in Figure 3.14. Summary results of shear strength parameters are tabulated in Table 3.3.

For direct shear saturated specimens (soil-soil), ϕ' and c' refer to the effective friction angle and cohesion intercept, respectively, that determined from direct shear tests under saturated conditions (drained conditions). For unsaturated specimens (soil-soil), ϕ^b and c^b indicate to the friction angle and cohesion intercept, respectively, with respect to matric suction effect. From saturated interface direct shear tests, δ' and ca' refer to the interface friction angle and adhesion intercept. Also, for unsaturated specimens, δ^b and ca^b indicate to the unsaturated interface friction angle and interface adhesion, respectively, with respect to the effect of matric suction.

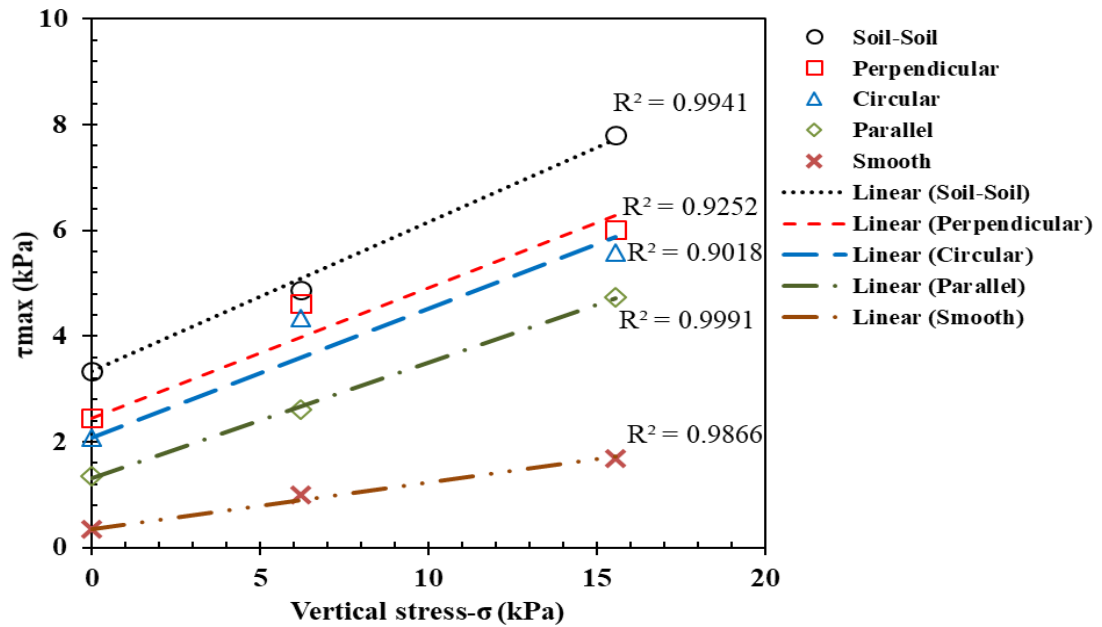


Figure 3.12 Shear failure envelopes for saturated compacted specimens

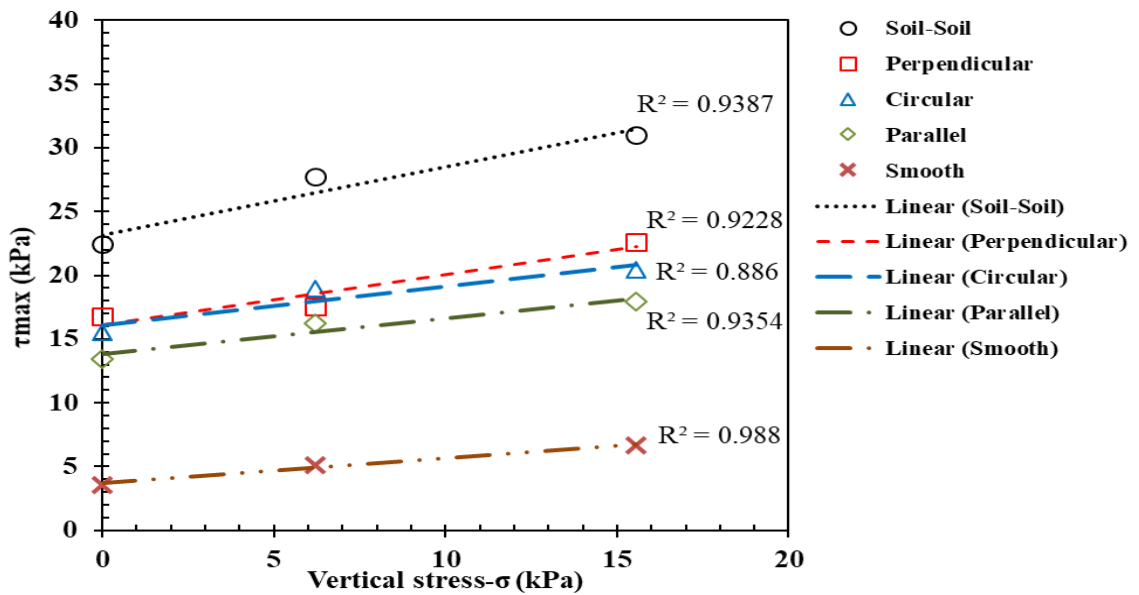


Figure 3.13 Shear failure envelopes for unsaturated-compact specimens

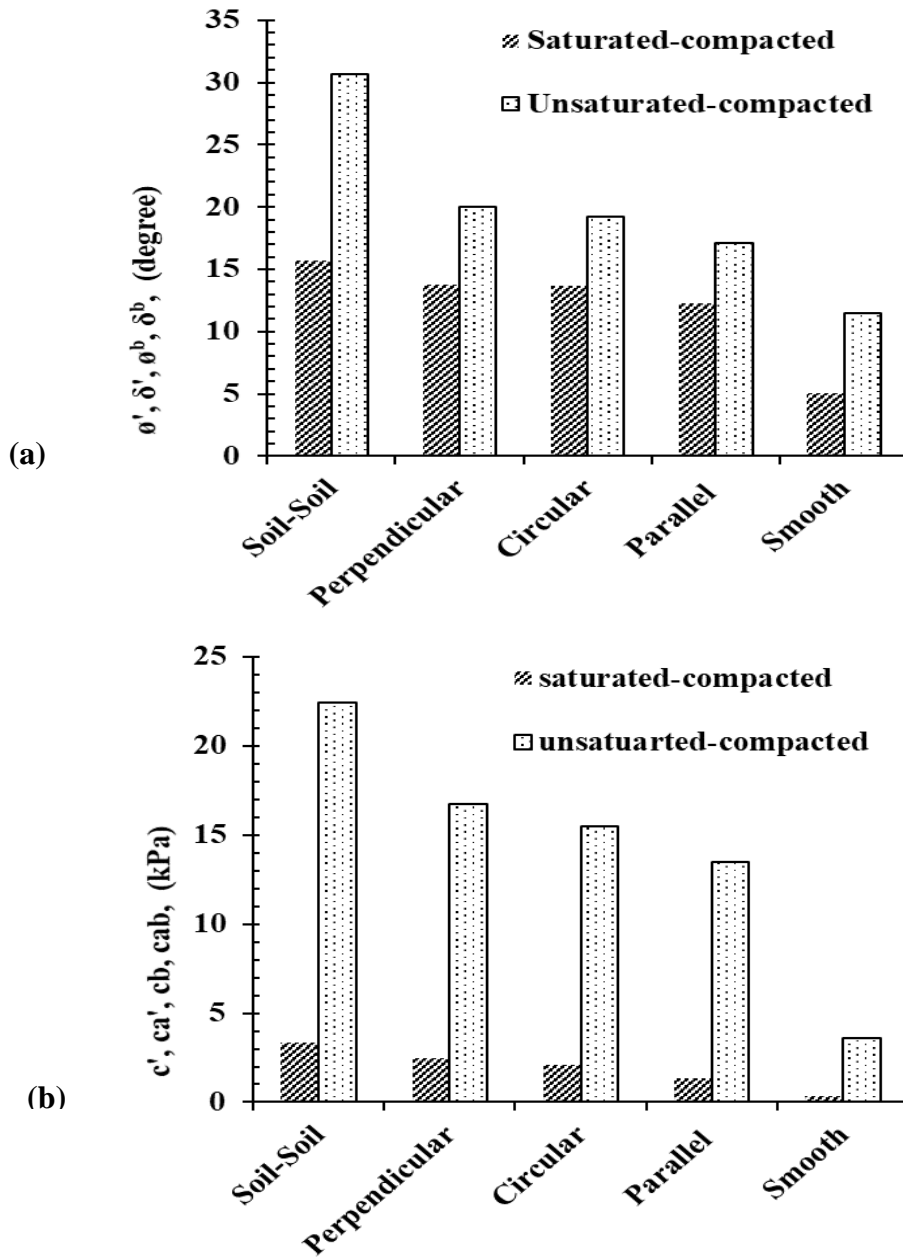


Figure 3.14 Comparison results from shear failure envelopes; (a) interfaces friction angles, (b) adhesion/cohesion for all tested sets

Table 3.3 Summary results of direct shear tests of soil and four interfaces

Interface type	c', c^b, c_a', c_a^b / (kPa)		$\phi', \phi^b, \delta', \delta^b$	
	Saturated-Compacted	Unsaturated-as Compacted	Saturated-Compacted	Unsaturated-as Compacted
Soil-Soil	3.34	22.44	15.70	30.62
Perpendicular	2.45	16.76	13.80	20.01
Circular	2.09	15.50	13.70	19.22
Parallel	1.35	13.46	12.30	17.13
Smooth	0.35	3.59	5.10	11.48

Note: c' & c_a' : Saturated cohesion and adhesion intercepts, respectively.
 c^b & c_a^b : Unsaturated soil cohesion and adhesion intercepts, respectively
 ϕ' & δ' : Saturated friction angle and interface friction angle, respectively.
 ϕ^b & δ^b : Unsaturated friction angle and interface friction angle, respectively.

Based on the results, some noteworthy findings were obtained:

1. In the case of saturated-compacted tests, the shearing resistance of soil-to-soil dominated on those of perpendicular, circular, parallel, and smooth interfaces. For example, the values of c' (3.34 kPa) and ϕ' (15.7°) of soil-to-soil are higher than the values of c_a' (2.45 kPa) and δ' (13.8°) of perpendicular-interface. Perpendicular and circular-interfaces experienced the same shearing resistance with slight differences in the values of δ' and c_a' ($\Delta\delta'= 0.1^\circ$ and $\Delta c_a'=0.36$ kPa). In the case of perpendicular and parallel-interfaces, they exhibited different shearing behavior at failure planes, even though the two interfaces had the same surface roughness. This is likely due to the combination effect of shearing direction and surface roughness that resulted in different shearing strength parameters. Therefore, it is important to notice that the direction of sliding of the soil particles against interface during shearing is very considerable factor

- should be accounted in stability analyses besides to the surface roughness. While in case of smooth-interface, the soil exhibited the lowest shear strength parameters.
2. Results of unsaturated-compacted direct shear tests showed that the selected value of suction (i.e., $S = 1\text{MPa}$) did reveal a considerable impact on the shearing behavior of soil. Before saturation stage, both saturated and unsaturated compacted samples exhibited similar structures (i.e., fabrics and internal bonding), however, under different saturation conditions, different shear strength parameters were obtained. This is largely due to the significant effect of air-water meniscus at shear plane for the case of unsaturated sample. It is known that the matric suction contributes in an increase in the effective stress of the soil, and as the effective stress increases the shear resistance increases, resulting in an increase in the shear strength at the failure plane. Consequently, as shearing process takes place, the unsaturated compacted sample gained more shear strength compared to saturated one. As mentioned before, the shear strength parameters of unsaturated-compacted tests of soil-to-soil dominated on those of saturated-compacted with values of ϕ_b (30.62°) and c_b (22.4 kPa) (Table 3.3).
 3. In fact, the most interface impact was apparently obtained in unsaturated-compacted samples. For soil-to-soil tests, the value of ϕ' (30.62°) is higher than the values of δ' of interfaces with significant differences of about 10° , 11.4° , 13.5° , and 19.1° for perpendicular, circular, parallel, and smooth-interfaces, respectively. In addition, the corresponding values of c' (22.4 kPa) decreased by about 5.7 , 6.9 , 9 , 18.9 kPa for perpendicular, circular, parallel, and smooth-interfaces, respectively. While, for saturated samples, the highest reduction of the value of ϕ' of soil-to-soil was

- determined of about 3.6° for parallel-interface, except, smooth interface that showed the lowest values in all tested samples.
4. Generally, for soil-interfaces tests, the values of δ' , δ^b and c_a' , c_a^b of the perpendicular interface are systematically higher compared to circular, parallel, and smooth-interfaces, except for saturated-compacted samples where negligible differences were observed between perpendicular and circular interfaces ($\Delta\delta' = 0.13^\circ$, $\Delta c_a' = 0.36$ kPa).
 5. The lowest values of δ' and c_a' (5.5° , 0kPa) were determined for smooth interface. The saturated-compacted sample experienced high reduction in the friction angle compared to unsaturated specimen. This may relate to potential distortion at the shear plane when inundating with water, resulting in a decrease in the shear strength.

3.7 Summary and conclusions

In this chapter a series of laboratory tests were conducted on a high expansive soil mixture consisted of 75% kaolin and 25% bentonite. The directional shear strengths were examined between the soil and four different interfaces involving; perpendicular, circular, parallel and smooth surfaces. The results have revealed that the shearing behavior of the soil is strongly affected by the interface patterns. The strength of unsaturated compacted soil is highly influenced more than that of saturated one. The highest strength is determined for the soil-soil and the lowest one was obtained for those experiments involving smooth interface. The strength for the case of perpendicular grooves is higher compared to the ones of circular, parallel, and smooth cases. The strengths of circular patterns are determined between the ones for perpendicular and parallel interfaces. The influence of different interfaces is mainly observed in the linear envelopes that used to define the shear strength parameters; the friction angles and the cohesion values.

CHAPTER IV

DESICCATION PLATE TESTS AND DIGITAL IMAGE CORRELATION ANALYSIS (DIC)

4.1 Introduction

Formation of desiccation cracking is a natural phenomenon which occurs due to loss of water. Presence of cracks produces zone of weakness in soils, results in an increase in the compressibility and permeability, also, a reduction in the overall strength and stability. This may be destructive for geotechnical and geo-environmental structures. Cracks in soil can develop due to several processes comprising; desiccation and shrinkage, freezing and thawing, differential settlement, syneresis, and penetrated plant roots (Yesiller. et. al., 2000).

So far, a number of experimental, modeling, and numerical studies has been performed to investigate the inception and propagation of desiccation cracks in soils (Morris et al., 1992, Albrecht and Benson 2001, Yoshida and Adachi 2004, Lakshmikantha et al., 2009, Atique et al., 2009, Lu et al., 2013, Tang et al., 2011, Tang et al., 2016, Lopez-Bellido et al., 2016). However, the prediction of the initiation and propagation of cracking in soils still faces many challenges and needs more interpretation for a better understanding of this natural phenomenon.

Desiccation cracking in soils is a very complex to predict due to the interactions that occur during the drying process among the soil grains, the boundary conditions, and the surrounding-environmental conditions of the soil mass. Moreover, coupled hydro-mechanical and sometime the thermal processes occur when soil exposed to drying (Rodriguez 2006). There are no direct and accurate measurement techniques to quantify and analyze the morphology of cracks during

drying process. However, image analysis method has been recently adopted by some researchers to characterize the crack patterns on the surface (Baer et al., 2009, Lakshmikantha et al., 2009).

This chapter investigates the potential desiccation cracks in a high expansive artificial soil mixture consisted of 75% kaolin and 25% bentonite. The desiccation plate-tests were conducted on thin layers of the soil mixture using two different soil-interfaces subjected to unsaturated and saturated conditions. Two different counter-faces; including smooth and circular groove, were used to study the effect of soil-interface on the cracking patterns. The effect of alternative wetting/drying cycles on the crack patterns had been investigated as well. The morphology of crack patterns was determined using the image analysis technique to analyzed and interpreted the effects on test outcome. Moreover, the Digital Image Correlation (DIC) technique was employed to understanding the emerging phenomenon behind soil cracking, particularly, during wetting process.

4.2 Characteristic of cracking in soil

The parameter of **Crack Intensity Factor (CIF)** was adopted by many researchers to quantify the magnitude of cracking in soils. CIF (Crack Intensity Factor) was initially opted as a descriptor to evaluate the crack patterns on the surface of soil specimen by Miller et al (1998). CIF is defined as the ratio of surface area of cracks to the total surface area of the drying soil sample. To determine the CIF, image analysis technique was employed as an efficient and accurate method to analyze the crack patterns of the soil from a number of images taken during cyclic processes. Recently, different software programs have been used to process the images, such as, MATLAB and *image j* software. In this study, all the images were processed by using the *image j* software, and then the CIF's were calculated

4.3 Desiccation plate tests

4.3.1 Objectives

Desiccation plate tests were conducted on a high expansive artificial soil mixture consisted of 75% kaolin and 25 % bentonite. This chapter presents several desiccation tests performed on thin clay layers with thickness of about 12.7 mm. The research herein was conducted to understand the effect of wetting/drying cycles on the initiation and propagation of cracks in soil under different initial conditions. These tests included the following:

- i) free desiccation tests (smooth-plate) subjected on saturated and unsaturated-compacted samples.
- ii) constrained desiccation tests (circular-spiral groove plate) subjected on saturated and unsaturated-compacted samples.
- iii) constrained desiccation tests subjected on a fully-saturated samples (slurry) inundated with salt solution.
- iv) a DIC analysis was used to understand the emerging phenomenon behind the initiation and propagation of cracks during cyclic wetting/drying processes.

Two identical circular plates made from acrylic were fabricated with 150 mm of diameter and 12.7 mm of height. However, the beds of the plates were manufactured with different roughness, as follows; one with smooth surface and the other one with circular-spiral grooved surface. More details are explained in the following sections.

The main objectives of these experimental tests are highlighted below:

- to investigate the effect of two different soil-interfaces; including smooth and circular grooved interfaces, on the inception and propagation of cracks.

- to study the impact of the initial saturation conditions on cracking behavior of soils.
- to investigate the influence of cyclic wetting-drying processes on the crack propagation.
- to advance our understanding of the mechanism behind the initiation of crack, particularly during wetting process.

The impact of sequential wetting-drying cycles on the initiation and propagation of cracks have been described and analyzed in this chapter. Significant findings behind the cracking mechanism were presented and highlighted.

4.3.2 Experimental test methodology

In this research, the impact of initial saturation conditions and the type of soil-interface were taken into our consideration in investigating the initiation and propagation of cracks. Three different desiccation tests were presented and described; including free and constrained desiccation tests on compacted soil samples.

The compacted specimens were prepared at similar initial water contents and dry densities of those used for the ones subjected to the shear tests in the previous chapter. For both free and constrained desiccation tests, two groups of soil specimens were prepared under two different initial saturation conditions; consisted of unsaturated-compacted, and saturated-compacted samples. Each set consisted of two compacted soil samples; one sample was tested in a plate with smooth bed and the other one in a plate with circular-indentations.

The unsaturated-compacted sample was prepared by mixing thoroughly the mixture with distilled water at the target water content of about 42.67% (+ 4.67% of OMC from the standard Proctor test, ASTM D698). Then the soil was stored for 24 hours to promote moisture equilibrium. The soil was then compacted in the plate in two layers to achieve the required dry density of about

11.40 kN/m³ (94.4% of γ_{dmax} as determined from the standard Proctor test, ASTM D698). Laboratory compaction composed of tamping was used to achieve approximately uniform application of compaction energy to the top of each layer. The initial degree of saturation and the matric suction obtained from WPT4 device were about 0.87 and 1000 kPa, respectively.

The saturated-compacted sample was initially prepared at the same initial conditions (i.e., $w = 42.67\%$, and $\gamma_d = 11.40 \text{ kN/m}^3$) of those of unsaturated-compacted sample. Then the sample was inundated with water and kept for fully saturation or until no significant swelling observed. The degree of saturation of the sample was calculated to check whether the samples reached to fully saturation or not, if not, the sample was re-inundated. At the end of saturation process, it was found that the sample exhibited degree of saturations greater than 1.0. This is consistent with results that have been reported in the literature review (e.g., Villar 2002, Jacinto et al., 2011).

4.3.2.1 Free desiccation tests (Smooth Plate Tests)

Free desiccation tests (or smooth plate tests) were performed by using a circular plate with the diameter of about 15 cm and thickness of about 1.27 cm, where the ratio of the thickness to diameter is about 0.08. This plate was fabricated with a smooth base to prevent any mechanical-restraints at the boundaries during drying-shrinkage process (Figure 4.1).

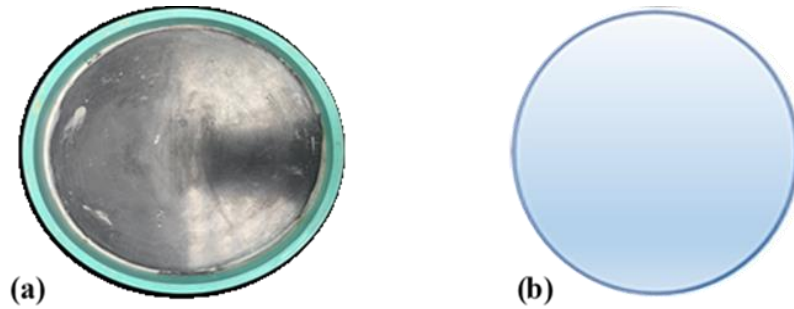


Figure 4.1 (a) The plate with smooth base for free desiccation tests, (b) a drawing of the smooth base

The smooth plate was also lubricated with grease all around the boundaries to prevent any potential restrictions during shrinkage. Two soil specimens were prepared; including unsaturated-compacted and saturated-compacted samples. In this study, the unsaturated-compacted and saturated-compacted samples prepared in smooth plates (free tests) are referred to “Smooth-Unsaturated-Compacted” (SUC) and “Smooth-Saturated-Compacted” (SSC), respectively.

4.3.2.2 Constrained desiccation tests (Circular-Spiral Plate Tests)

A circular plate was fabricated with similar dimensions to those of smooth one. The base of this plate was grooved with triangular grooves 1 mm deep and spaced every 1.5 mm to have the circular-spiral patterns at the soil bed. The main notion of the constrained desiccation tests (circular plate tests) was to develop mechanical-restraints at the boundaries of the specimens during drying process, and thus, resulting in crack formation (Figure 4.2).

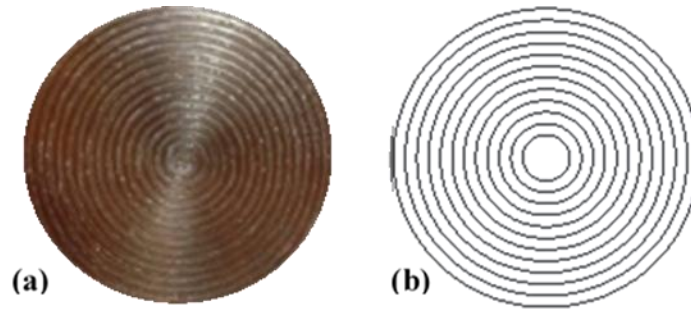


Figure 4.2 (a) The circular-spiral grooved base for constrained desiccation tests (b) a drawing of the grooved base

Two soil samples were prepared with the same procedure as that of the free tests. The unsaturated and saturated-compacted samples are referred to “Groove-Unsaturated-Compacted” (GUC) and “Groove-Saturated-Compacted” (GSC), respectively.

All free and constrained specimens were prepared and allowed to dry under controlled laboratory temperature and relative humidity (24 ± 1 C°, $RH = 52\pm 2\%$) until the weights of the specimens were constant. An electronic balance with an accuracy of 0.01 gram was used to monitor the water loss over time where the water contents can be calculated. A digital camera was fixed directly above the soil specimen (perpendicularly) to capture the crack patterns during wetting-drying cycles. The drying process was terminated when the weight of the specimen stabilized, or no more any significant change in the weight.

4.3.2.3 Quantitative crack networks analysis by using image technique

Digital image analysis technique (by using *image j software*) was employed to study the morphology of crack patterns on the surface of the samples at the end of each wetting-drying cycle. The procedure of digital image analysis was illustrated by (Atique A, Sánchez, 2009).

Figure 4.3 presents the experimental set-up of desiccation tests. The procedure that opted herein for image analysis technique is presented in Figure 4.4. Firstly, the digital image (TrueColor/RGB) of soil sample was converted to a grayscale image. In the conversion process, the grayscale image was obtained by converting the image to the type of 8-bit. Afterward, the background of the image had been subtracted from the image. Then, the grayscale image was converted to a binary black-and-white (B & W) image by thresholding technique. In this stage, the binary image has replaced all pixels in the grayscale image with luminance greater than a threshold value of 1(white) and the other pixels with the value 0 (black). So that, the binary image consists of only 1's and 0's, which represents the un-cracked and cracks areas respectively. Finally, an outline operation had been performed where the cracks and un-cracked areas can be obtained. Then the ratio of crack areas to the total area of the soil sample at the end of drying or wetting process can be determined as the crack intensity factor (CIF).



Figure 4.3 The experimental set up of desiccation tests

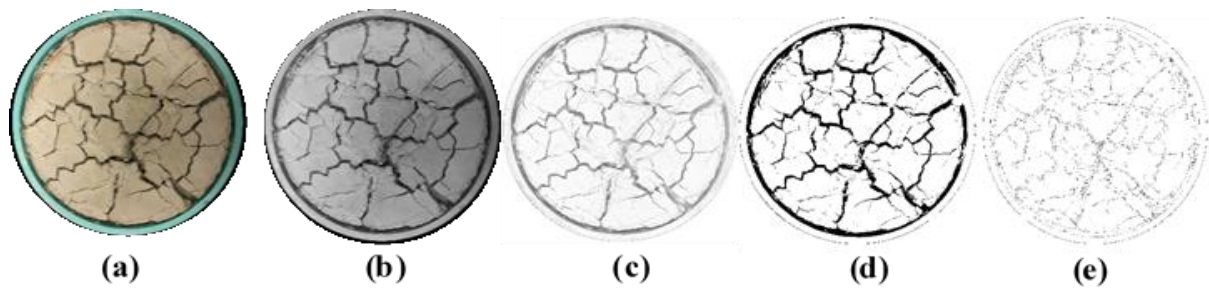


Figure 4.4 Image processing: a) a TrueColor (RGB) image, b) converting the RGB image to a grayscale (8-bit), c) subtracting background, d) converting to a binary image, and e) outline operation

4.3.3 Experimental results of desiccation plate tests

In this chapter, the initial saturation condition and the soil-interface type were taken into our consideration to investigate the formation and propagation of cracks in compacted soil. Results of desiccation plate tests are presented and described herein. The image j software was employed to characterize 2D cracking network. Cracking network of each soil specimen was characterized at the end of each cycle by using the Crack Intensity Factor (CIF).

Unsaturated and saturated-compacted soil specimens were tested under constrained and free and subjected to a number of wetting/drying processes. The constrained condition was achieved at the soil bed by fabricating circular-spiral indentations, while the free condition was provided at the boundary condition using very smooth base of the plate (see Figure 4.5).

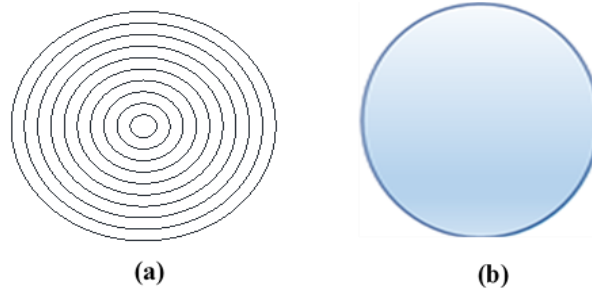


Figure 4.5 Desiccation plates with two different base-surfaces a) circular patterns for constrained tests, b) smooth surface for free tests

The notion of these tests is to investigate the cracking response of compacted soils at different initial conditions and soil-interfaces. The constrained saturated and unsaturated

compacted samples are referred to GSC and GUC respectively. Also, the free or smooth saturated and unsaturated compacted samples are referred to SSC and SUC respectively.

4.3.3.1 Effect of wetting/drying cycles constrained specimens

Cracking is a very intricate phenomenon to understand. This is mainly related to the complex hydro-mechanical behavior of soils during wetting and drying cycles. Hydro-mechanical behavior of soil is strongly relevant to the inter-aggregate and intra-aggregate pore size distributions resulting from different clod sizes and the moisture conditions (suctions) within and between clods (Cerato e. al., 2009). The initial conditions besides to soil structures (fabrics and inter-particle forces) are very considerable factors that should be accounted for understanding the hydro-mechanical behavior of a soil. The effect of wetting/drying cycles had been mainly taken into our consideration for studying cracking in addition to the coupled effect of initial saturation condition and soil-interface. Figure 4.6 shows the variations of water content over time during the drying cycles for the constrained saturated and unsaturated specimens (GSC & GUC), respectively. Figure 4.7 and Figure 4.8 present crack patterns of the GUC and GSC samples with the initial water contents of 42.7 % and 62 %, respectively. Three wetting/drying cycles were subjected on the saturated and unsaturated samples and one more drying cycle for the latter one.

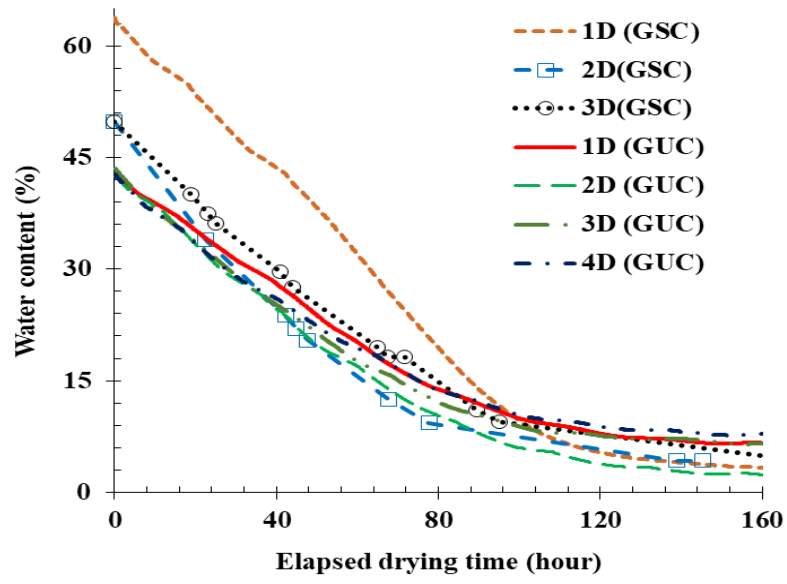


Figure 4.6 Variations of water content over time during drying cycles, constrained samples

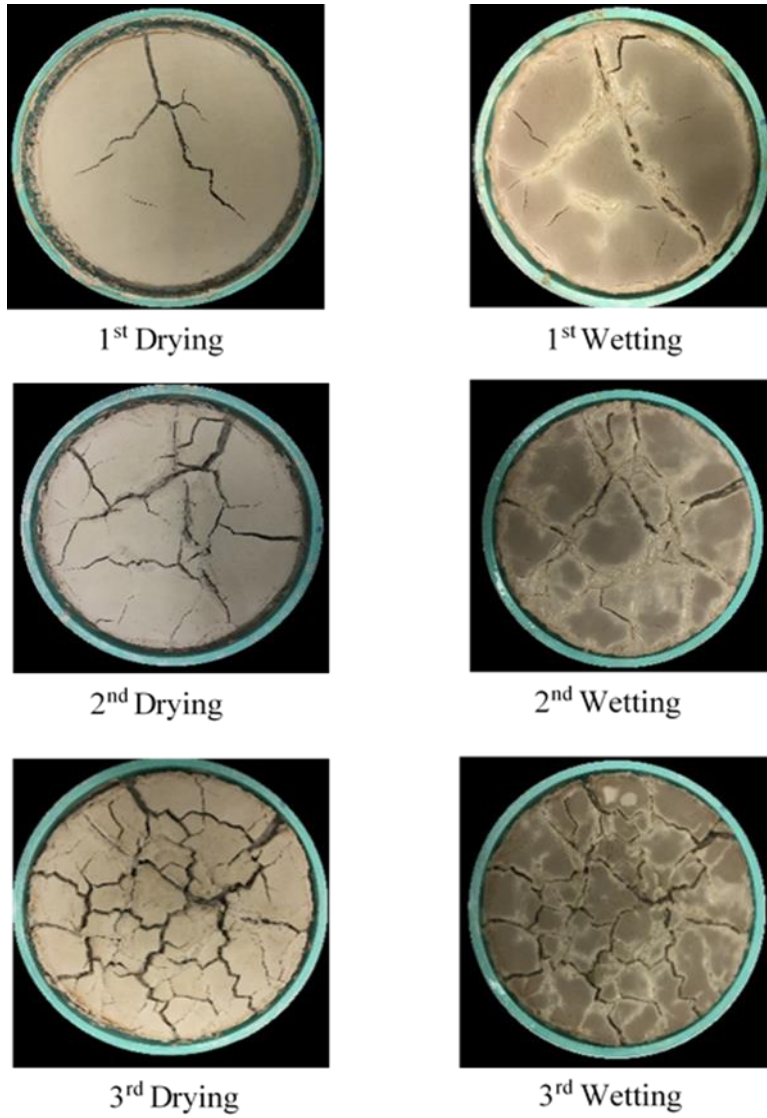


Figure 4.7 Crack patterns of constrained saturated samples (Groove-plate) at the end of each cycle (GSC)

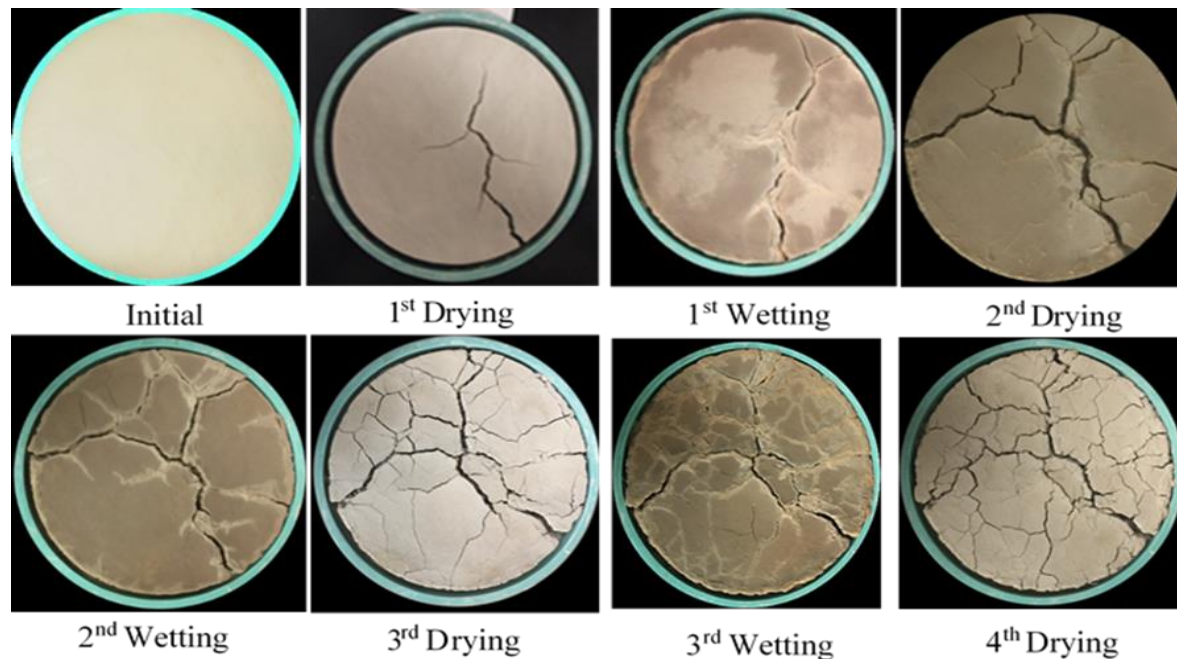


Figure 4.8 Crack patterns of constrained unsaturated samples (Groove-plate) at the end of each cycle (GUC)

In general, few cracks were developed in GSC and GUC specimens after the first drying with very low crack intensity factors (CIF's), as follows; 1.16% for saturated specimen (GSC), and 0.65% for unsaturated one (GUC). Upon the first wetting, the saturated specimen experienced healing for the current cracks and developing news cracks at the end of the process (i.e., CIF = 1.2 %). The unsaturated specimen (GUC) experienced some crack healing, where the CIF decreased from 0.65% to 0.46%, (see Table 4.1 and Figure 4.9). Formation of few cracks in the first cycle indicates that the specimens underwent small irreversible deformation and negligible changes in the void ratios. Over wetting-drying cycles, more cracks propagated in both specimens. The saturated specimen (GSC) developed more cracks compared to the unsaturated one (GUC). This

may attribute to the initial water content which caused large irreversible deformations and decrease in the tensile strength of the saturated specimen (GSC) compared to unsaturated specimen (GUC). The results of drying cycles have revealed significant variations in the CIF's of the saturated specimen (GSC) much more than those of the unsaturated specimen (GUC). Over wetting cycles, both specimens experienced swelling which resulted in healing and closure of some cracks that formed in the drying process. This is mainly related to that the soil mixture consisted of high swelling clay mineral of the montmorillonites, particularly, sodium bentonite (see Table 3.2) which is prone to expand largely when exposed to water. More wetting/drying cycles are required to investigate at what cycle the crack propagations may terminate.

Table 4.1 CIF values of constrained- saturated and unsaturated specimens

Sample	1 st drying	1 st wetting	2 nd drying	2 nd wetting	3 rd drying	3 rd wetting	4 th drying
GSC	1.16	1.2	7.34	5.13	13.7	11.33	N/A
GUC	0.65	0.46	4.86	2.40	6.07	3.07	7.87

Note: GSC & GUC: Constrained saturated and unsaturated, respectively

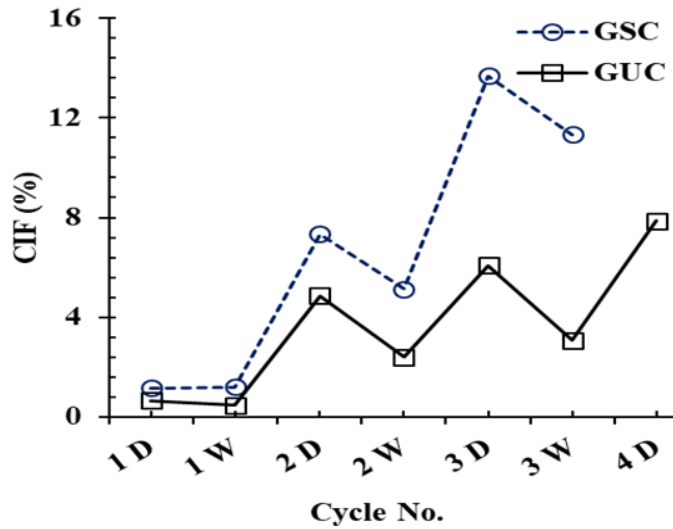


Figure 4.9 Variations of CIF's of constrained- saturated and unsaturated samples under wetting/drying cycles

4.3.3.2 Effect of wetting/drying cycles on free specimens

Figure 4.10 shows the variations of water content over time for the free saturated and unsaturated samples (SSC & SUC) during three drying cycles.

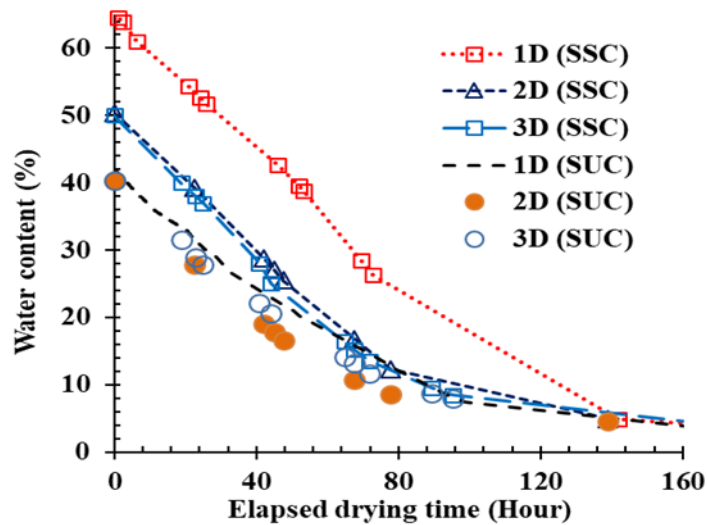


Figure 4.10 Variations of water content over time during drying cycles, free samples

Crack patterns of the free-unsaturated and saturated specimens subjected to wetting/drying cycles are shown in Figure 4.11 and Figure 4.12, respectively. As expected, neither saturated nor unsaturated samples developed cracks in the first drying. The smooth plate provided negligible friction at the soil bed, so that when the samples subjected to evaporation process, they freely shrank with no restrictions at the soil boundaries. In this case, due to low adhesion between the soil and the plate, no tensile stresses developed at interface, and that resulting in no crack formation. However, the free specimens developed few cracks upon wetting, and more cracks propagated over cycles. This may be attributed to the large deformations that experienced by the samples when soil wetted. As mentioned previously, the soil mixture used consisted of sodium bentonite which has very high capability to absorb water. It seems that during the first wetting, the sample absorbed a lot of water-molecules which caused in high swelling with large irreversible deformation, as a consequence, cracks developed.

Another interpretation is that the samples exhibited large deformation and change in stress state during cycles. Initially the soil particles were oriented in a way due to the compaction process. When the sample subjected to drying, the sample shrank in different orientations than those in the initial state (different soil fabric and interparticle forces), for example, from parallel to flocculated arrangements. This may cause roughness between the contacts of the soil particles. This roughness may become constrains at the contact surfaces of the soil particles, as a result tensile stresses generated. When the developed tensile stresses exceed the tensile strength of the sample, cracks developed. Accordingly, a unique free desiccation test was performed to understand the emerging phenomenon behind crack formation in one hand during wetting, and in the other hand why cracks develop under free condition. More details are provided later.

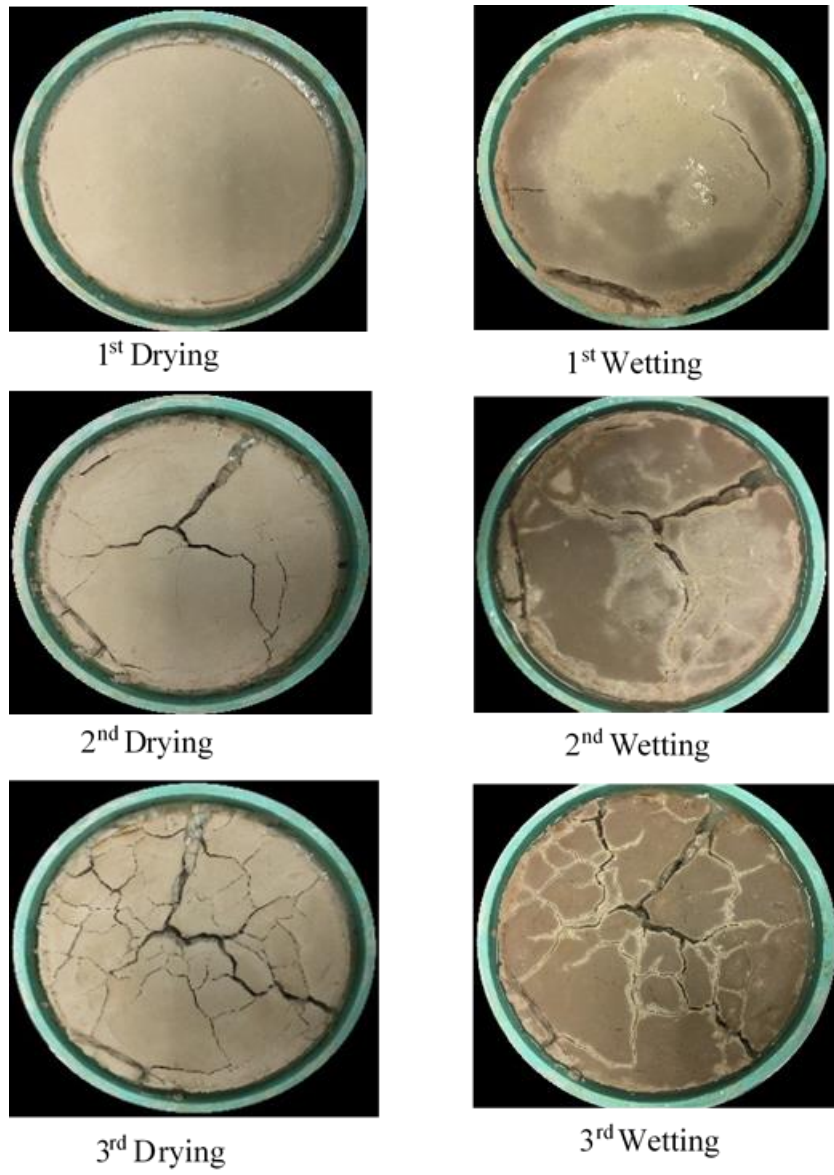


Figure 4.11 Crack patterns of free saturated specimens (Smooth-plate) at the end of each cycle (SSC)

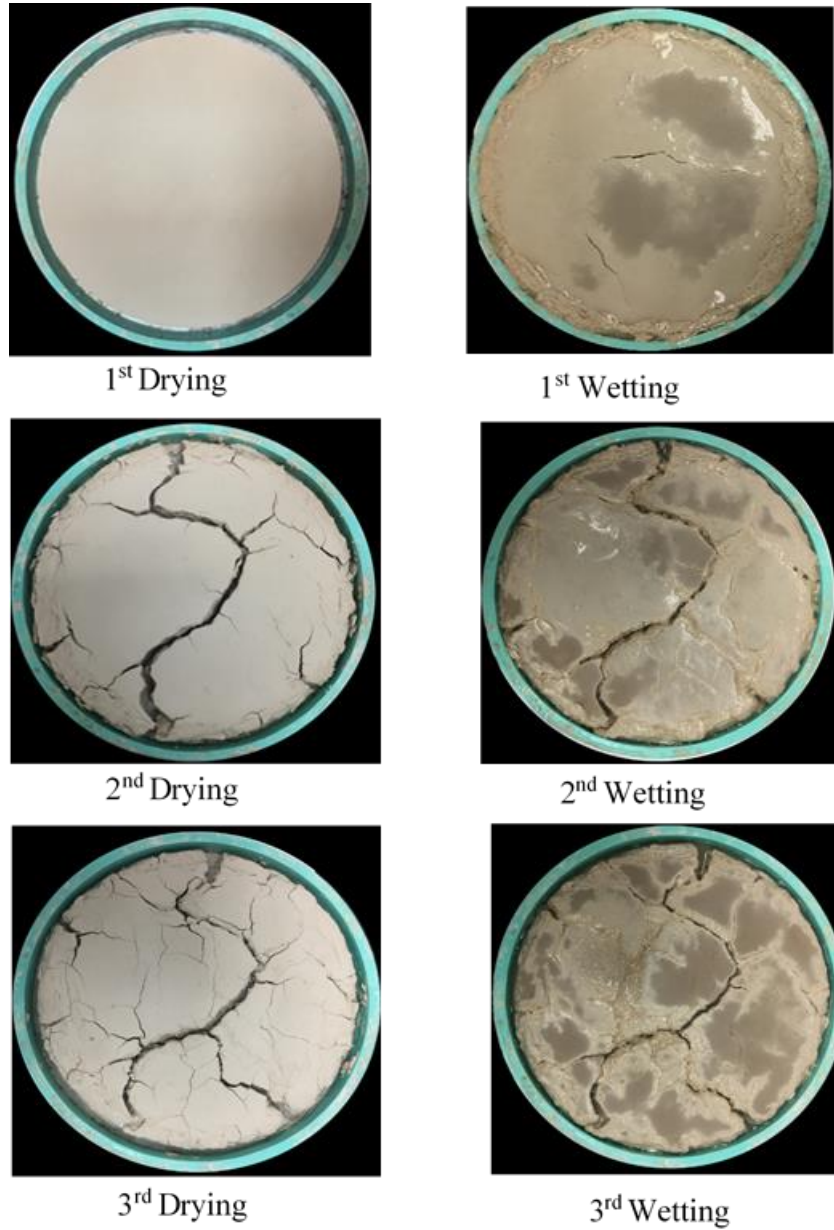


Figure 4.12 Crack patterns of free unsaturated samples (Smooth-plate) at the end of each cycle (SUC)

It was observed that the saturated and unsaturated samples have almost similar CIF's in the first and the second cycles (see Table 4.1 and Figure 4.13). However, after the second cycle, the saturated sample developed more cracks than the unsaturated one.

Table 4.2 CIF values of constrained- saturated and unsaturated samples

Sample	1 st drying	1 st wetting	2 nd drying	2 nd wetting	3 rd drying	3 rd wetting
SSC	0	0.87	3.57	3.48	7.6	6.5
SUC	0	0.28	3.39	1.88	4.77	3.23

Note: SSC & SUC: Free saturated and unsaturated, respectively

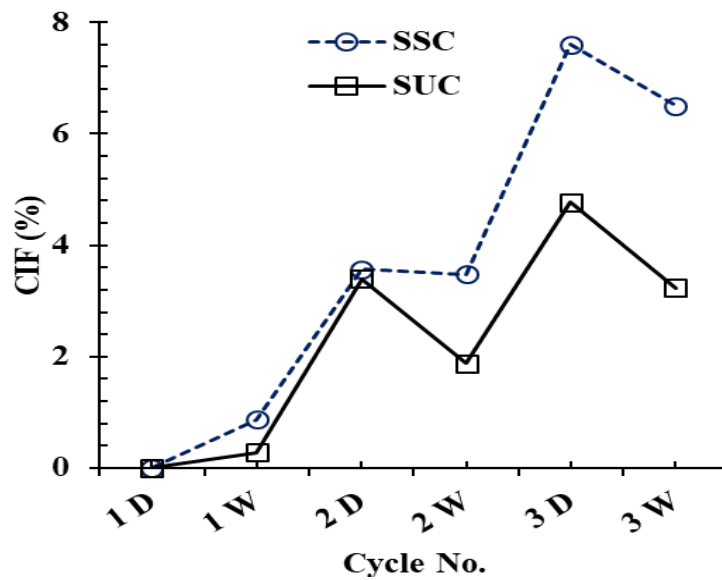


Figure 4.13 Variations of CIF's of free-saturated and unsaturated samples under wetting/drying cycles

4.3.4 Summary of constrained and free desiccation tests results

Figure 4.14 presents the variations of CIF's of all tested specimens involving: GSC, SSC, GUC, and SUC. Some significant observations may be made from the desiccation tests:

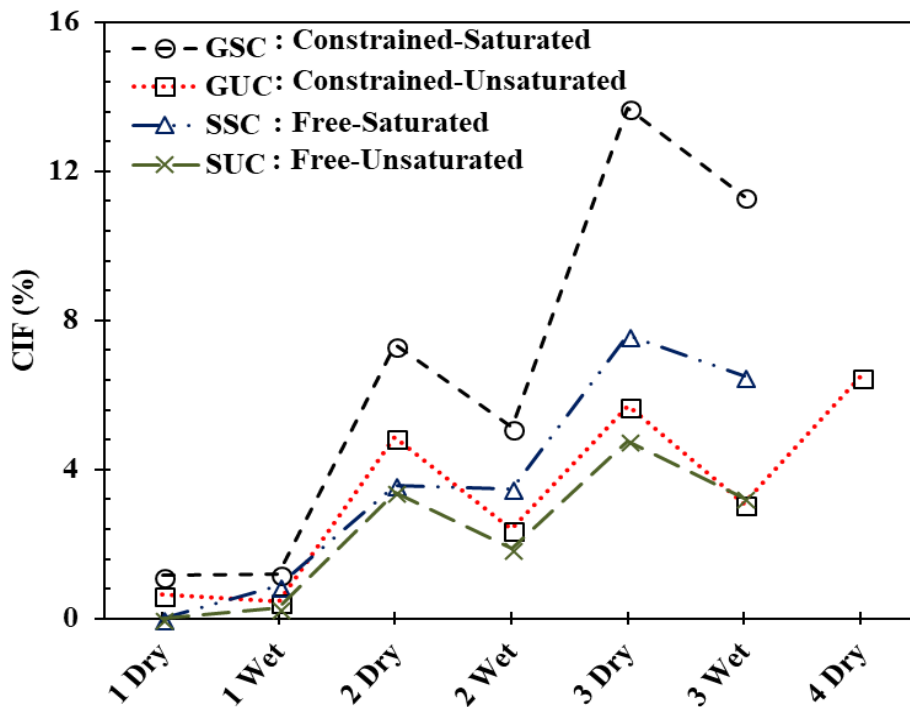


Figure 4.14 Variations of CIF's of free and constrained-saturated and unsaturated samples under wetting/drying cycles

- In general, it can be noticed from
- that the initial water content influences on cracking behavior of soil, where GSC and SSC exhibited higher CIF's compared to those of GUC and SUC.
- For the saturated specimens, the interface type influenced on the cracking behavior, where the GSC exhibited higher CIF's than those of SSC; more tensile stresses developed in the constrained tests.
- Even though negligible constrains were provided between the soil and the smooth interface, the free samples (SSC and SUC) exhibited evolution and propagation of cracks

during the wetting/drying cycles. This indicates that the interface factor can't be taken as the only factor in interpreting the cracking mechanism in soils.

- The significant effect of the cyclic wetting/drying processes on the evolution and propagation of cracks in soils can be highlighted in this study. More cracks developed each cycle till reach to an equilibrium state of no significant cracks observed.
- Although all unsaturated and saturated samples were compacted at high compaction energy, where this degree is highly recommended to compact some geotechnical structures, such as embankments (i.e., 94.4% of γ_{dmax} as determined from the standard Proctor test, ASTM D698), they all experienced cracks when subjected to alternatives wetting/drying cycles regardless to the restriction conditions at the soil boundaries (i.e., soil-interface) and the initial saturation conditions.
- The high expansive soil mixture used in this study consisted of bentonite which is mainly consisted of the montmorillonite (sodium bentonite). The montmorillonite has a very strong hydrophilic property, which can form a thick film of water molecules around the clay particles, and this can provide greater swelling and shrinkage during wetting and drying processes, respectively. Upon wetting, the water molecules coat the clay particles to form a thick film, this create large spaces between the particles. During the drying process, the free water in the soil is gradually vaporized, and then the spaces between the particles become smaller, proceeding drying results in much thinner film. Consequently, the soil structure is completely changed in which the pores decrease and the clay particles tend to move toward each other in different orientations than those in the initial state, and then cracks will generate when the tensile stresses exceed the tensile strength of the soil.

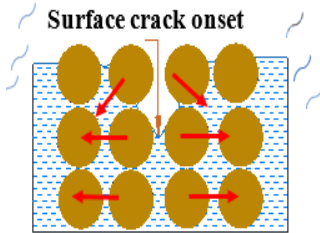
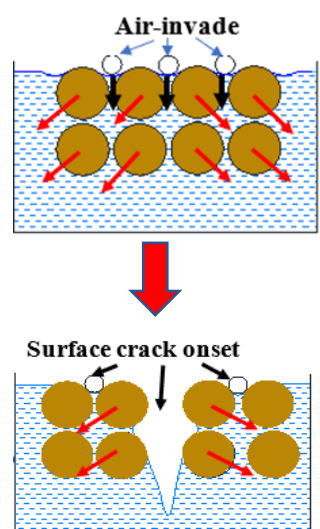
It can be concluded that the volumetric deformation (swelling/shrinkage) of soils is the originator factor of evolution and propagation of cracks. The volumetric deformation is strongly relevant to the type of clay minerals of soils.

4.4 Constrained desiccation tests under osmotic suction condition

Various frameworks have been adopted to interpret the initiation and propagation of desiccation cracks in soils; net-stresses and suction (e.g. Morris et al., 1992, Rodríguez, et al., 2007); total stress concept (e.g., Péron et al., 2009, Amarasiri et al., 2011); the effective stress concept (Shin and Santamarina, 2011), and the combination of both total and effective stress concepts (Abu-Hejleh and Znidarcic, 1995).

On one hand, some investigations state that the inception of cracks is associated with the increment of tensile stress during drying process, and hence the formation of the soil cracks occurs when the stresses surpass the soil tensile strength (Rodríguez et al., 2007, Amarasiri et al., 2011,). On the other hand, other studies support the notion that desiccation cracks generate under compressive effective stress state conditions (Shin and Santamarina, 2011). The two common conceptual frameworks of cracking mechanism, including tensile failure and air-invasion, are presented in Table 4.3.

Table 4.3 Common hypothesis opted for conceptual cracking mechanism

Name	Conceptual framework	Description	References
Tensile failure		If a fully saturated soil subjected to drying, the water-air interface meniscus develops on the surface of the soil, then the cracks generates at the surface due to distortion and shrinkage and/or because the tensile stresses exceed the tensile strength of the soil	Sánchez et al., 2014, Tang et al., 2011, Rodríguez et al., 2007, Konard and Ayad, 1997, Morris et al., 1992
Air-invasion		When air invades the water-air interface meniscus, the crack initiates	Shin and Santamarina, 2011

4.4.1 Experimental methodology

Some researchers have supported the tensile failure criteria in interpreting the cracking mechanism of soils; the crack initiates when the tensile stresses exceed the tensile strength of soil (Morris et al., 1992, Konard and Ayad, 1997, Tang et al., 2011, Rodríguez et al., 2007, Sánchez et al., 2014). On the other hand, others have adopted the hypothesis that the crack initiates when air

invades the interfacial membrane of the soil under compressive effective stress state conditions (Shin and Santamarina, 2011). In response to that, desiccation tests were implemented herein on fully saturated specimens subjected to osmotic suction, while inundating with salt solution.

The main concept of this testing is that the fully saturated soil specimen (slurry) was exposed to osmotic suction through inundating the soil with a saturated salt solution. Liquid transfer method was employed to impose suction inside the soil. In this case, the soil was not allowed to dry under atmospheric; and hence the air was prevented to invade the surface of the soil and results in cracks, according to Shin and Santamarina, 2011. In my study, constrained condition was provided to induce the tensile stresses at the soil-interface when the soil tends to dry due to the effect of osmotic suction. Two high expansive soils were used; one is an artificial soil mixture of 75% kaolin and 25 % bentonite, and the other one is a natural soil collected from the railroad in Texas. More details of materials and methods are provided in the following sections.

4.4.2 Materials and methods

Two high expansive soils were used including soil mixture of 75% kaolin and 25% bentonite, and a natural soil collected from Texas railroad. The desiccation tests herein were performed using two different desiccation molds with different groove patterns, and salt solutions. A circular plate and a rectangular perspex mold were grooved with different patterns in the bases. The circular plate was fabricated and grooved similarly to the plates that utilized in the previous constrained desiccation plate tests. In addition, very small holes were manufactured at the base to allow the soil-water drains when the salt solution occupy the voids in the soil sample. Another ring with the same diameter of 15 cm was fixed on the top of the first plate in order to provide more space for adding the salt solution on the surface of the sample (see Figure 4.15).

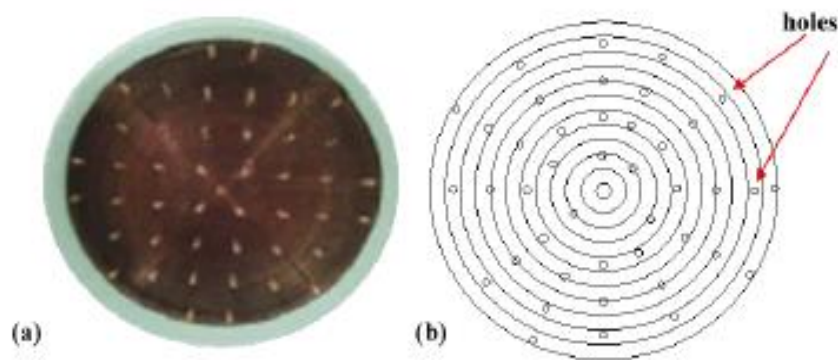


Figure 4.15 a) The plate with grooves and holes, b) schematic drawing of the base

The rectangular Perspex mold was used with the length of 15.9 cm, width of 2.9 cm and 1.42 cm of thickness. Three small rectangular pieces fabricated from polycarbonate sheet with height of 2.4 mm and length of about 15 cm were glued in the base of the mold to provide restrictions during desiccation process (see Figure 4.16).

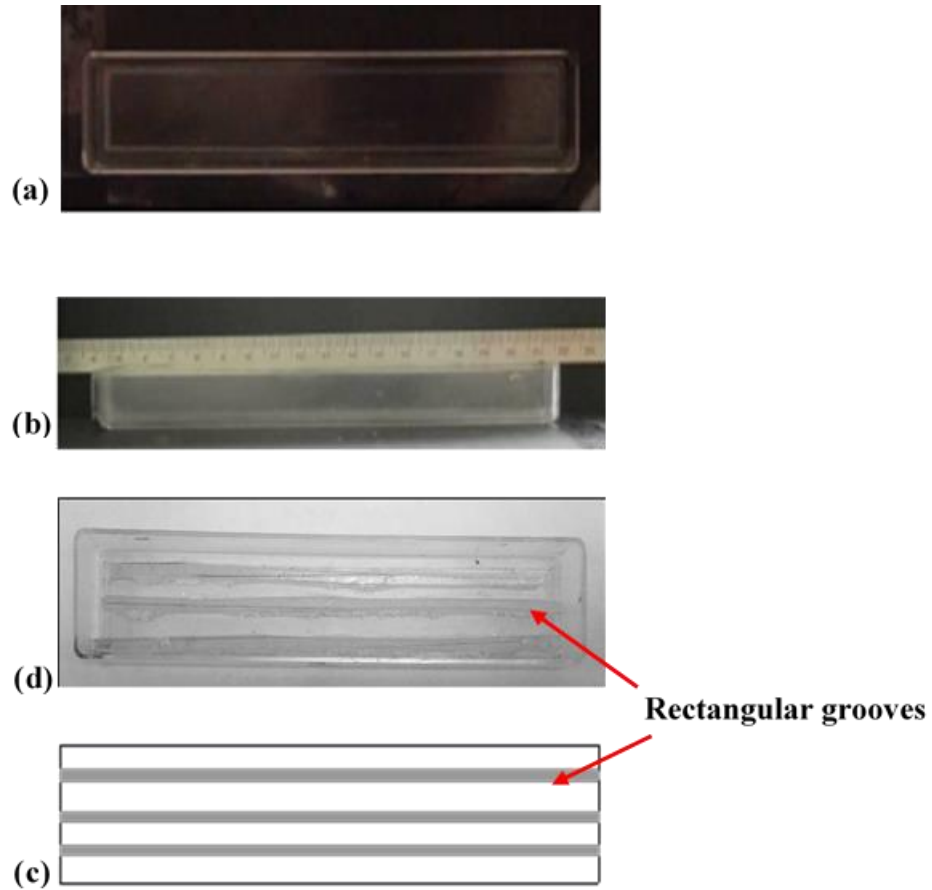


Figure 4.16 The rectangular Perspex mold; (a) top view, (b) front view, (c) Top view after gluing the rectangular pieces, (d) schematic drawing of the groove patterns (using $\text{MgCl}_2 \cdot 6\text{H}_2\text{O}$)

For the soil mixture of 75% kaolin and 25% bentonite, two soil specimens were prepared at similar initial water content of 90.19 % and dry density of 7.848 kN/m^3 . One sample was prepared in the circular plate and then inundated with the saturated salt solution of calcium nitrate tetrahydrate ($\text{Ca}(\text{NO}_3)_2 \cdot 4\text{H}_2\text{O}$) provided a suction of 92 MPa measured by using WP4-T (Decagon (1998-2003), (see Figure 4.17). The other specimen was prepared in the rectangular perspex mold and then submerged with Magnesium Chloride Hexahydrate solution

($\text{MgCl}_2 \cdot 6\text{H}_2\text{O}$) which provided a suction of 152 MPa measured by using WP4-T (Decagon (1998-2003), see Figure 4.18.

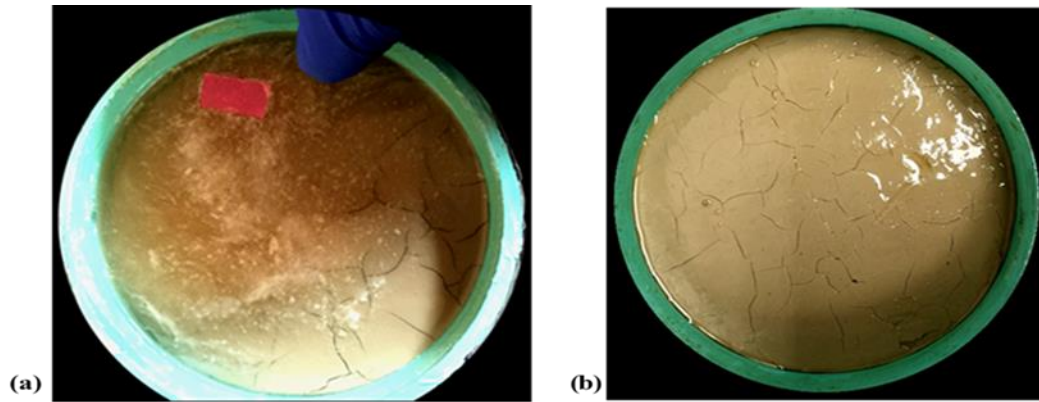


Figure 4.17 (a) & (b) Crack patterns of a fully saturated soil sample consisted of 75% kaolin and 25% bentonite submerged in $\text{Ca}(\text{NO}_3)_2 \cdot 4\text{H}_2\text{O}$ ($w = 90.19\%$, $\rho_d = 7.848 \text{ kN/m}^3$)

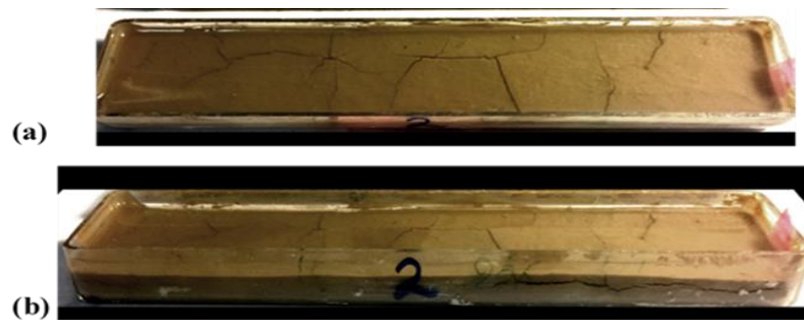


Figure 4.18 (a) & (b) Crack patterns of a fully saturated natural soil submerged in $\text{MgCl}_2 \cdot 6\text{H}_2\text{O}$ ($w = 66 \%$, $\rho_d = 7.848 \text{ kN/m}^3$)

For the natural soil, one fully saturated soil specimen (slurry) was prepared at initial water content of 66 % and dry density of 7.848 kN/m^3 . The soil was placed in two layers to the desired

initial dry unit weight using the same circular plate used previously for the artificial soil mixture. A very light tamping was subjected to each layer in order to remove all the air bubbles from the soil sample. Then the sample was immediately inundating with a fully saturated salt solution (calcium nitrate tetrahydrate, $\text{Ca}(\text{NO}_3)_2 \cdot 4\text{H}_2\text{O}$). Photos were taken by a digital camera to capture the crack patterns (Figure 4.19).

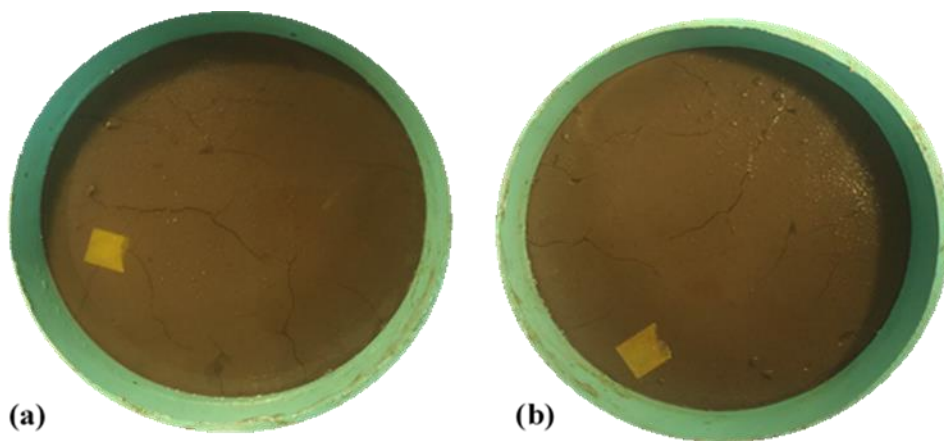


Figure 4.19 (a) & (b) Crack patterns of a fully saturated natural soil submerged in $\text{Ca}(\text{NO}_3)_2 \cdot 4\text{H}_2\text{O}$ ($w = 66\%$, $\rho_d = 7.848 \text{ kN/m}^3$)

4.4.3 Results and discussion

Figure 4.17, Figure 4.18 and Figure 4.19 show the evolution of cracks under constrained condition while inundated in fully-saturated salt solutions. It was observed that when the specimens were inundated with salt solutions, cracks developed within few minutes. However, the salt solution made the photos blurred and unclear for analyzing purposes.

It is apparent that our finding is completely contradict with the crack mechanism that reported by Shin and Santamarina (2011). Shin and Santamarina (2011) reported that cracks initiate when the air invades the saturated soil, resulting in an increase in the suction. Accordingly, based on the observation of evolution of the cracks under salt solution, it is clear that the mechanism of air invading is not reasonable and reliable to interpret the formation of desiccation-induced cracks.

4.5 Digital Image Correlation analysis (DIC) for soil cracking

Digital Image Correlation (DIC) which is also known as Particle Image Velocimetry (PIV) is an image-based deformation measurement technique in progressively widespread use in multidisciplinary fields, such as, fluid, solid and soil mechanics. The use of DIC analysis provides full and continuous measurments of displacemnets/strains fields that would be equivalent to numerous of sensors. Thus, this method could be low-priced, easier, and more competitive than other techniques in the research area. DIC technique was originally developed in the area of the solid mechanics (i.e., Sutton et al., 1983) to measure the field of strains on the surface of a specimen subjected to mechanical loading. In the beginning of the late 1990s, some researchers started to study the failure mechanism of soils using image-based deformation measurements (White et al., 2003, Costa et al., 2008a, 2008b, Stirling et al., 2015). They invistigated the variations of field displacements/strains during soil cracking using the digital image correlation (DIC) analysis method. They have realized that the DIC technique is capable to enhance our understanding of soil mechanics in geotechnical applications (White et al., 2001, 2003, Costa et al., 2008a, 2008b, Take, 2015, Stirling et al., 2015, QI el al., 2017). Therefore, more research based on DIC analysis is still growing in the area of the soil mechanics.

Previous and recent research have employed different computer programs for DIC analysis, such as, the Geo-PIV and MATLAB. In our study a MATLAB code developed by (Mori & Chang, 2003), was utilized for computing full displacement fields of the cracked soil surface. In this section, the DIC method was employed to capture the displacement fields of the deformed soil during drying/wetting cycles Digital Image Correlation (DIC) technique.

The Digital Image Correlation technique (DIC) detects planer displacements (2D) of a deformed surface by correlating between a pair of images captured before and after deformation. The DIC analysis method is contactless, and full fields of displacements can be determined without introducing sensors into the soil specimen. The soil behavior herein is explored within the context of stress-strain behavior with incorporating cracking behavior and displacement fields for interpreting the complete behavior of soil when exposed to wetting/drying cycles.

The DIC analysis significantly includes image-based computer analysis of pixel movement measured between a pair of digital images. The two images involve the reference image which is captured before any deformation occurs, and the second image captured when deformation takes place at certain time (see Figure 4.20). Initially, the surface of the undeformed-soil specimen which is corresponding to the reference image is textured (dotted) by using an artificial speckle pattern. At different time intervals, a number of images are then taken for the surface of the deformed specimen. A correlation of the corresponded points in the dotted surface between the reference (undeformed) and deformed images is then conducted by using DIC analysis software. The accuracy and precision of DIC analysis significantly depends on the capability to capture the variation in the pixel intensity values between two images.

The speckle pattern is a significant criterion should be well considered in the DIC analysis. The soil's surface is textured by applying speckle pattern, either by using seed particles, such as sand (Costa, et al., 2008b), or by using paint. There are two primary components for a suitable speckle pattern. Firstly, the speckles (points) should be small enough and well-distributed on the whole surface, so that the camera can capture their motion in every subset. Secondly, high contrast must be maintained for distinguishing the speckle pattern during image capture, hence, ensure matching the points. Poor speckle pattern may cause mis-recording of the incremental displacements in some subsets.

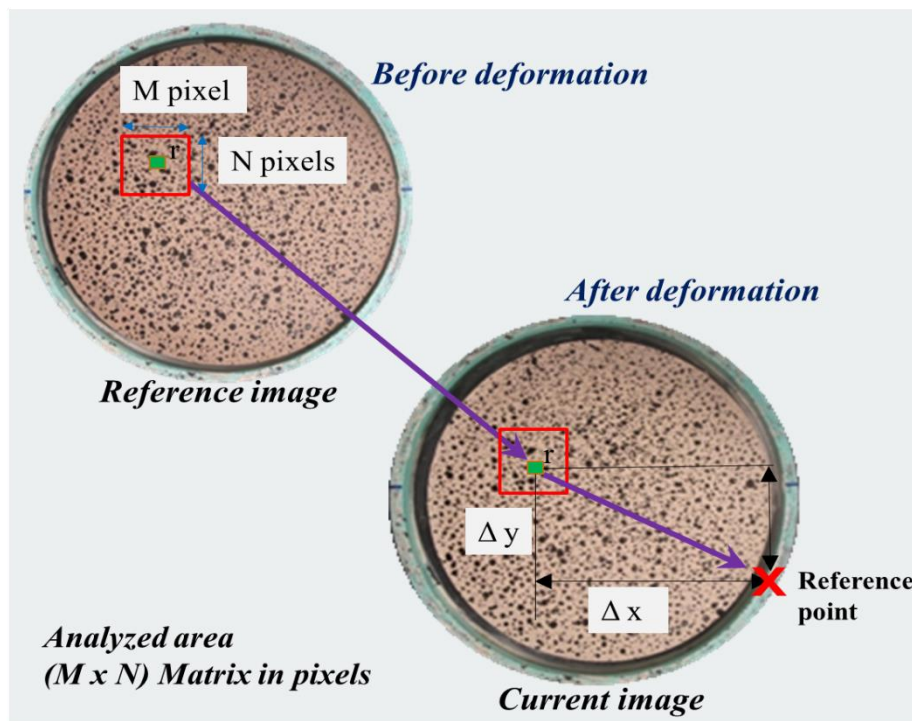


Figure 4.20 Digital Image Correlation principle

4.5.1 DIC experimental set up and materials

Two identical soil specimens were prepared at similar initial water content of about 50% (+12% of optimum moisture content) and compacted at the same dry unit weight of 10.34 kN/m^3 (85% of γ_{dmax} as determined from the standard Proctor test, ASTM D698), and degree of saturation of about 87.13%. The smooth and circular-spiral-grooved base desiccation plates that used previously were employed for free and restrained conditions. The notion from these test is to interpreting some previous findings of desiccation tests presented in this chapter. In particular, why the soil develops cracks when wetted?

The best strategy to obtain high-quality images for DIC analysis is typically ensured by creating an appropriate speckle pattern on the soil's surface. The surface of the soil specimen was prepared for the DIC monitoring by applying speckle pattern. This was accomplished by using black aerosol paint sprayed from an appropriate distance and angle to achieve good prevalence and coverage, as shown in Figure 4.21. In this study, it was not applicable to use seed particles, such as sand (Costa et al., 2008b) to create speckle pattern on the specimen's surface. The only reason is that when specimen wetted, the speckles leave their places in response to adding the water not in response of soil behavior. This leads to missing out the reference coordinates of the speckles, resulting in significant errors in the actual movement of the particles in response to soil behavior during wetting.

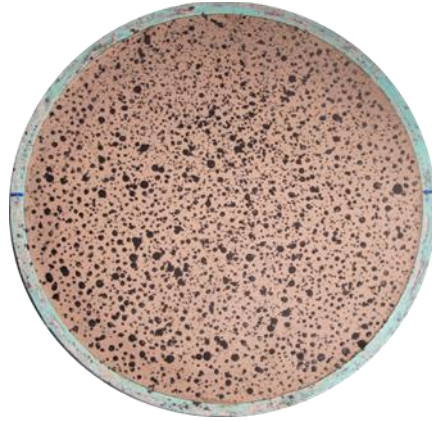


Figure 4.21 Speckle patterns on the surface of the specimen for DIC analysis

A digital camera (Canon Camera-*Power Shot G11*) with the highest resolution of (3648-pixel x 2736-pixel) was mounted directly above the soil specimen (perpendicularly) to capture a series of photos during the cyclic processes. Image capture was performed automatically by using remote control connected to the camera every 30 minutes during testing. Cold light sources were positioned to maintain high contrast of the speckle pattern on surface during testing. The experimental set-up is described in Figure 4.22.

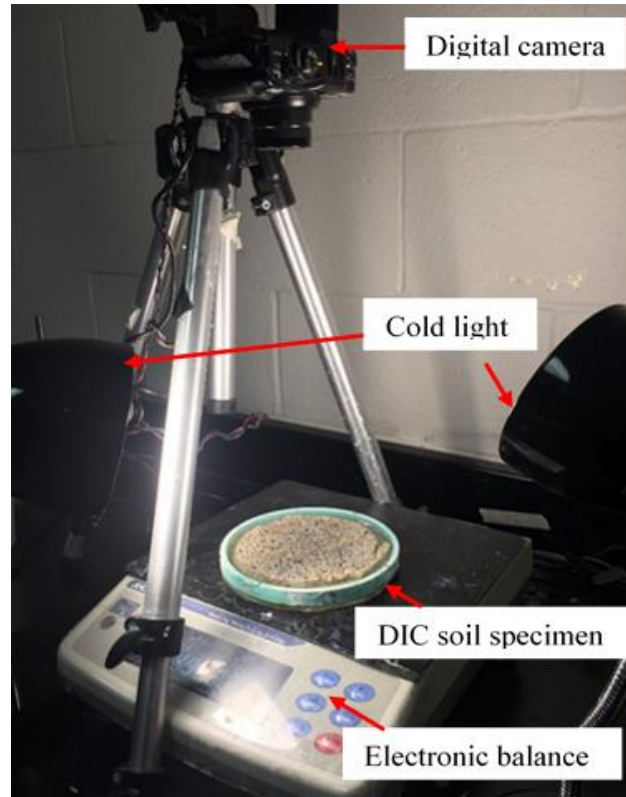


Figure 4.22 Experimental set up for DIC analysis

4.5.2 Results of DIC analysis

A series of digital images were taken for every wetting/drying process for measuring the displacement fields at different time intervals, particularly when soil cracked. For DIC analysis, the reference image was taken at the beginning of the wetting or drying process, and then all the images were captured every 30 minutes. Initially, the TrueColor/RGB images were processed by using *Image J* software to be prepared for DIC based-MATLAB analysis. Firstly, the digital image (TrueColor/RGB) of soil sample was converted to a grayscale image. The grayscale image was obtained by converting the image to the type of 8-bit. Afterward, the background of the image had

been subtracted from the image. Then, the grayscale image was converted to a binary black-and-white (B & W) image. The image processing procedure is described in Figure 4.23.

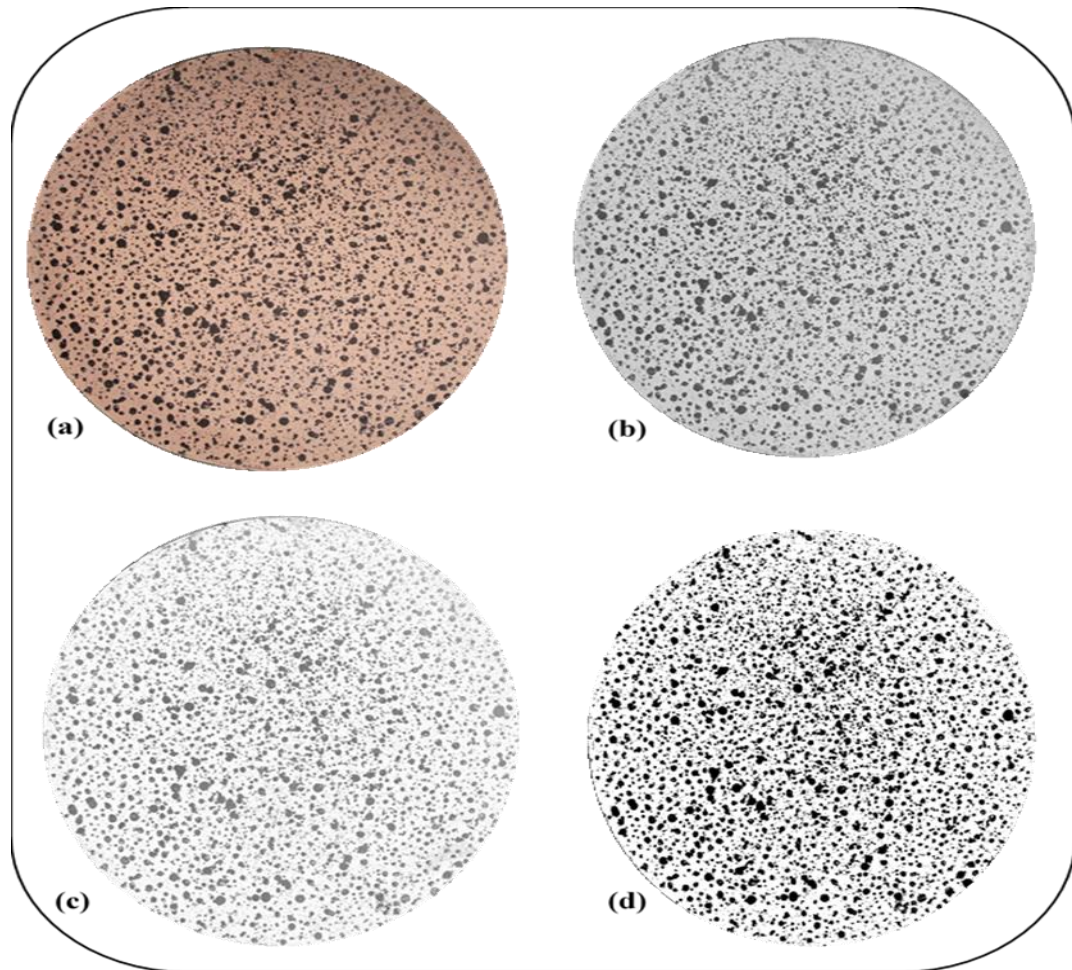


Figure 4.23 Image processing for DIC analysis; (a) TrueColor/RGB image, (b) grayscale (8 bit), (c) subtract background, (d) binary

4.5.2.1 DIC results of free restrained specimen

The specimen was subjected to three wetting/drying cycles under free restricted condition. Full displacement fields have been developed for representative the hydro-mechanical behavior of the specimen. The displacement fields are provided for every wetting/drying process. Within each time series, similar scale has been used. Based on the MATLAB code (Mori & Chang, 2003) that used for DIC analysis, the smoothing process of unrealistic changes (i.e., red vectors) in vectors is highly recommended when use 50% overlap ratio. The overlap is held when two cameras capture two images with overlap between them. In our experiment, one camera was utilized, and hence no overlap option is considered in the results.

Figure 4.24 and Figure 4.25 present the displacement localization after 30 hours and near the end of the first drying, respectively. As expected for free desiccation test, the specimen exhibited isotropic shrinkage with no cracks development in the first drying. The specimen dried equivalently in both directions of x and y , when drying proceeded, the specimen continued isotropic shrinkage without crack formation. Unforeseen results were then obtained upon wetting; the specimen expanded instantaneously in nonuniform way, as consequence, few cracks developed, as shown in Figure 4.26. This is strongly related to the changes in soil structure involving configurations of soil particles and stress state. In the first drying, initially the soil particles arranged in different way than that after the first drying, for example, from parallel to flocculated configurations. This developed roughness contacts between the soil particles resulting in tensile stresses. Upon wetting, the soil particles tended to expand due to water absorption and changed its arrangement from flocculated to parallel, thus cracks developed.

During the second drying, it was clearly observed that the displacement vectors in the middle part of the soil are smaller than those of the boundary ones. This is assured on having constraining shrinkage during drying, as seen in Figure 4.27 and Figure 4.28. Upon the second wetting, it was observed healing and closure of the primary crack that developed in the second drying, while soil continued expansion new cracks formed, as show in Figure 4.29.

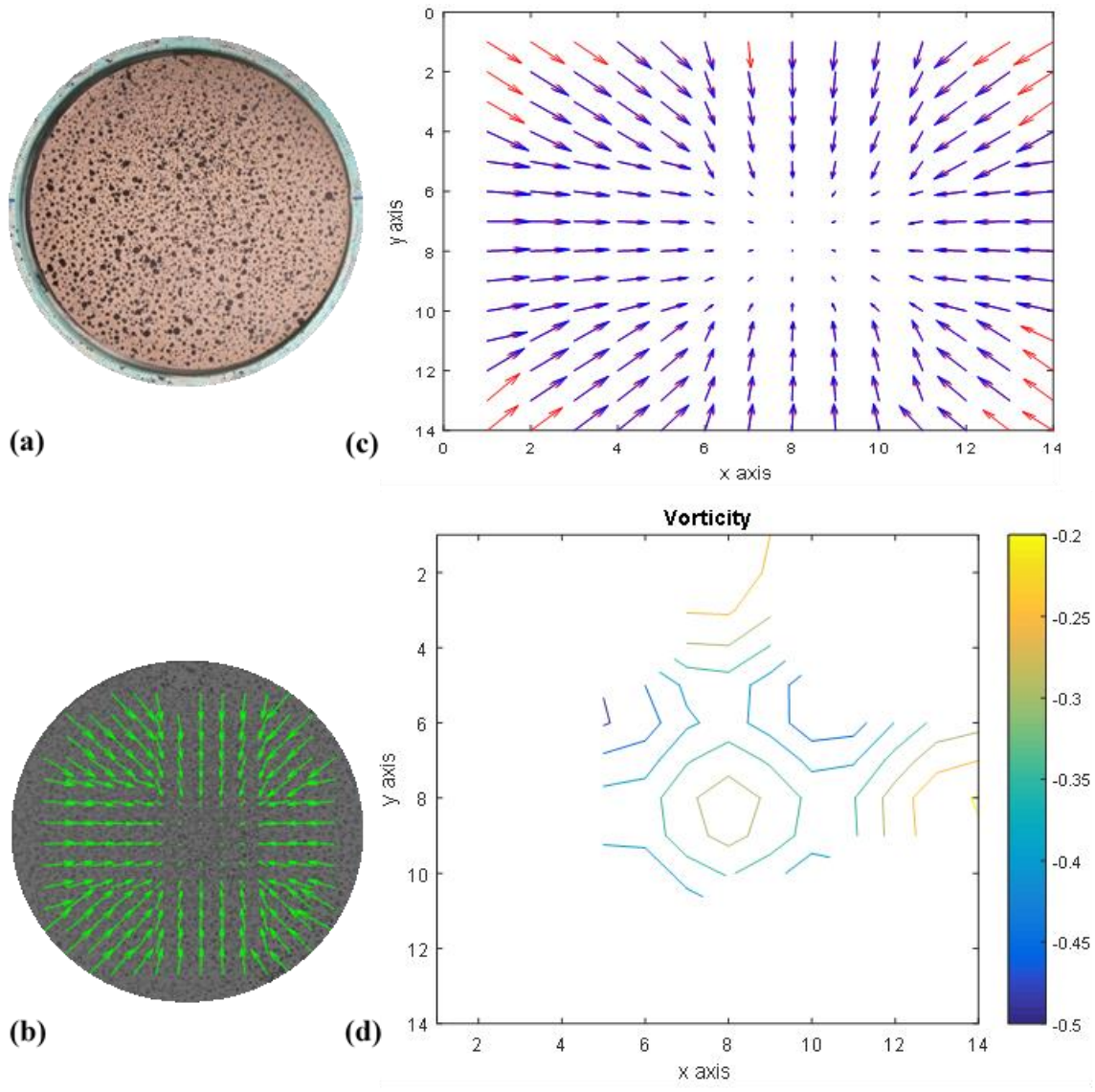


Figure 4.24 Compacted specimen during 1st drying at $t= 30$ hrs; (a) a true color photo; (b) specimen with displacement vectors; (c) displacement fields in x & y (*pixels*); (d) vorticity contours

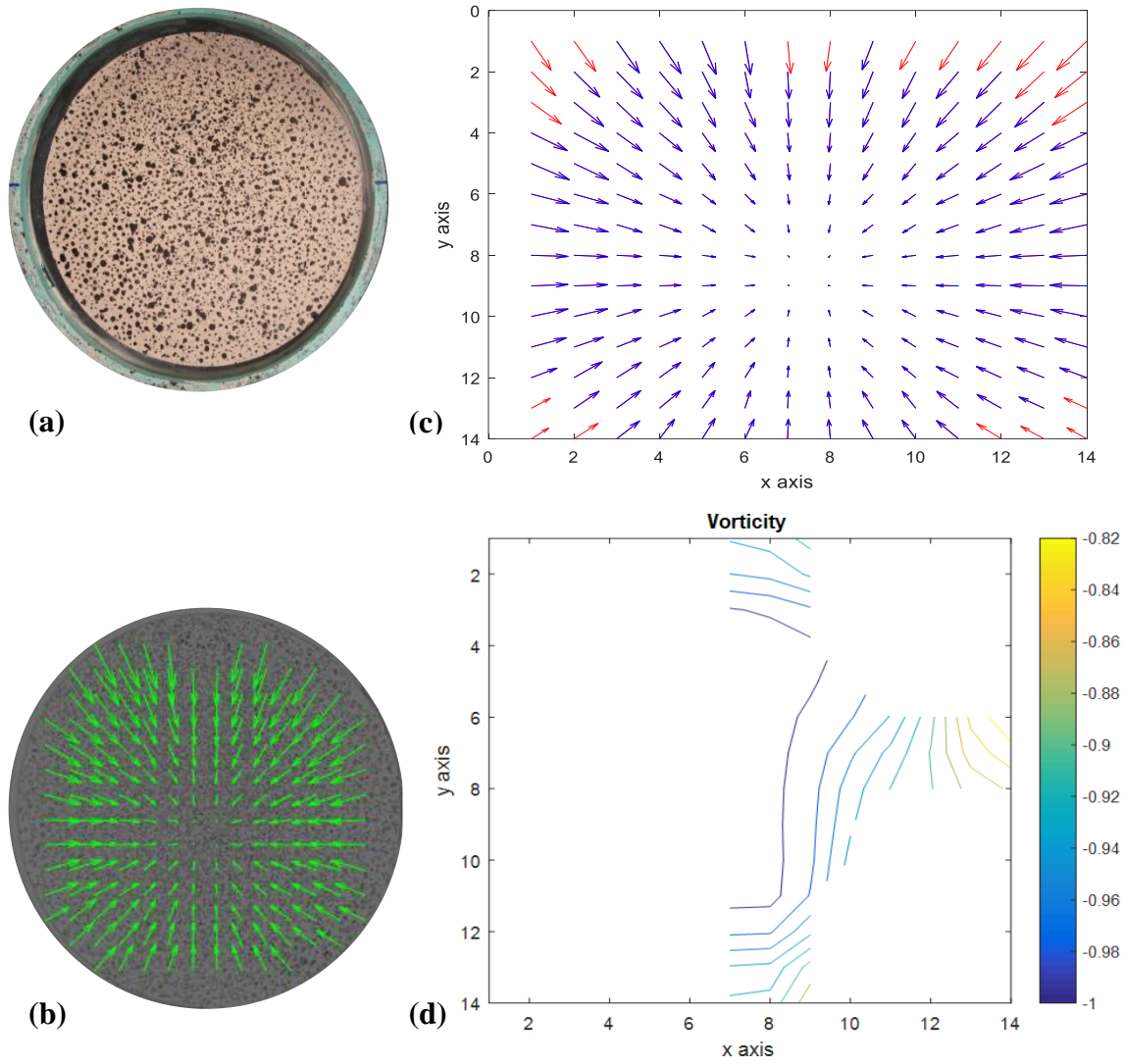


Figure 4.25 Compacted specimen during 1st drying; at $t = 133.5$ hrs; (a) a true color photo; (b) specimen with displacement vectors; (c) displacement fields in x & y (pixels); (d) vorticity contours

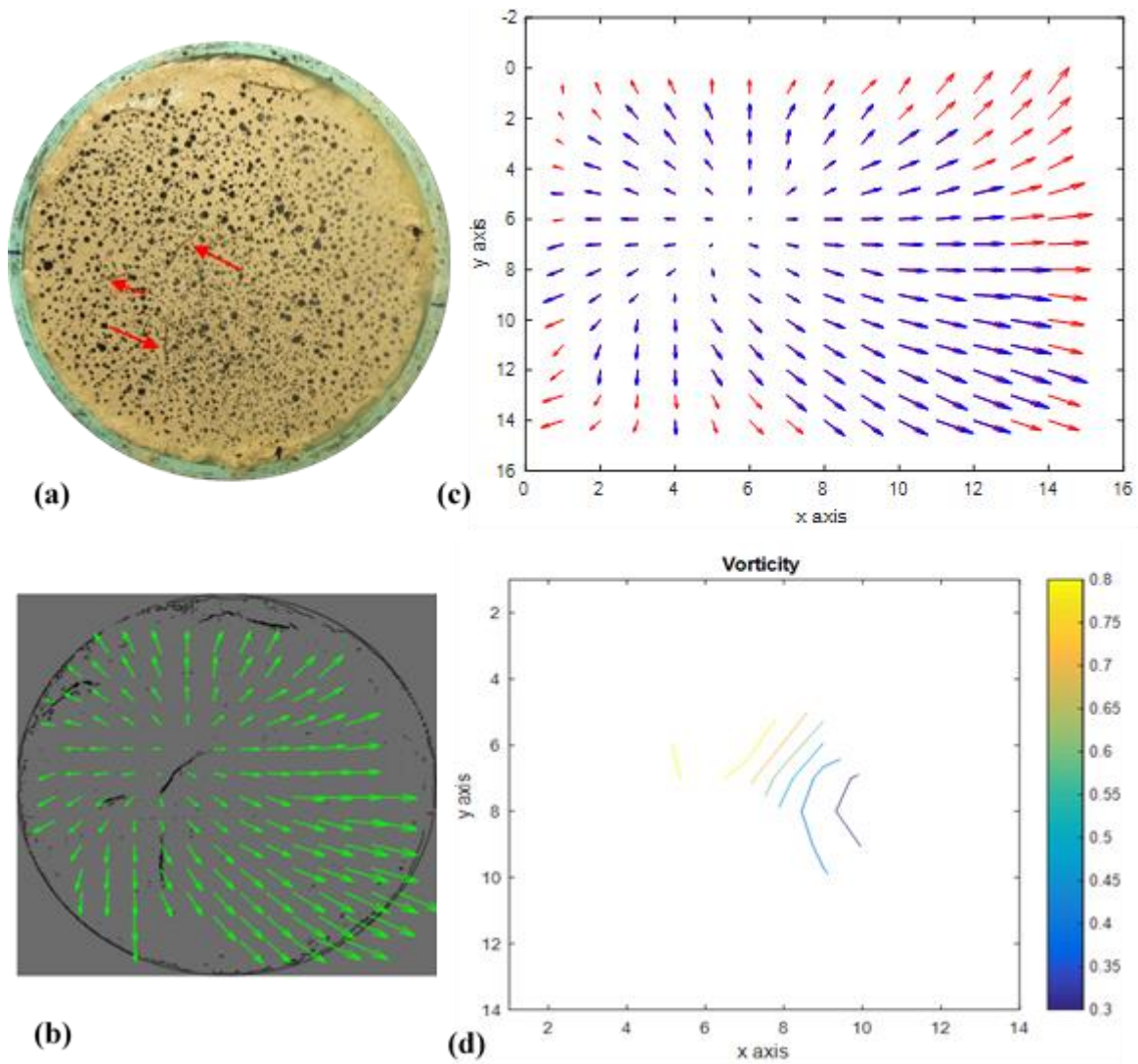


Figure 4.26 Immediately after 1st wetting; (a) a true color photo; (b) specimen with displacement vectors; (c) displacement fields in x, y (pixels) (d) vorticity contours

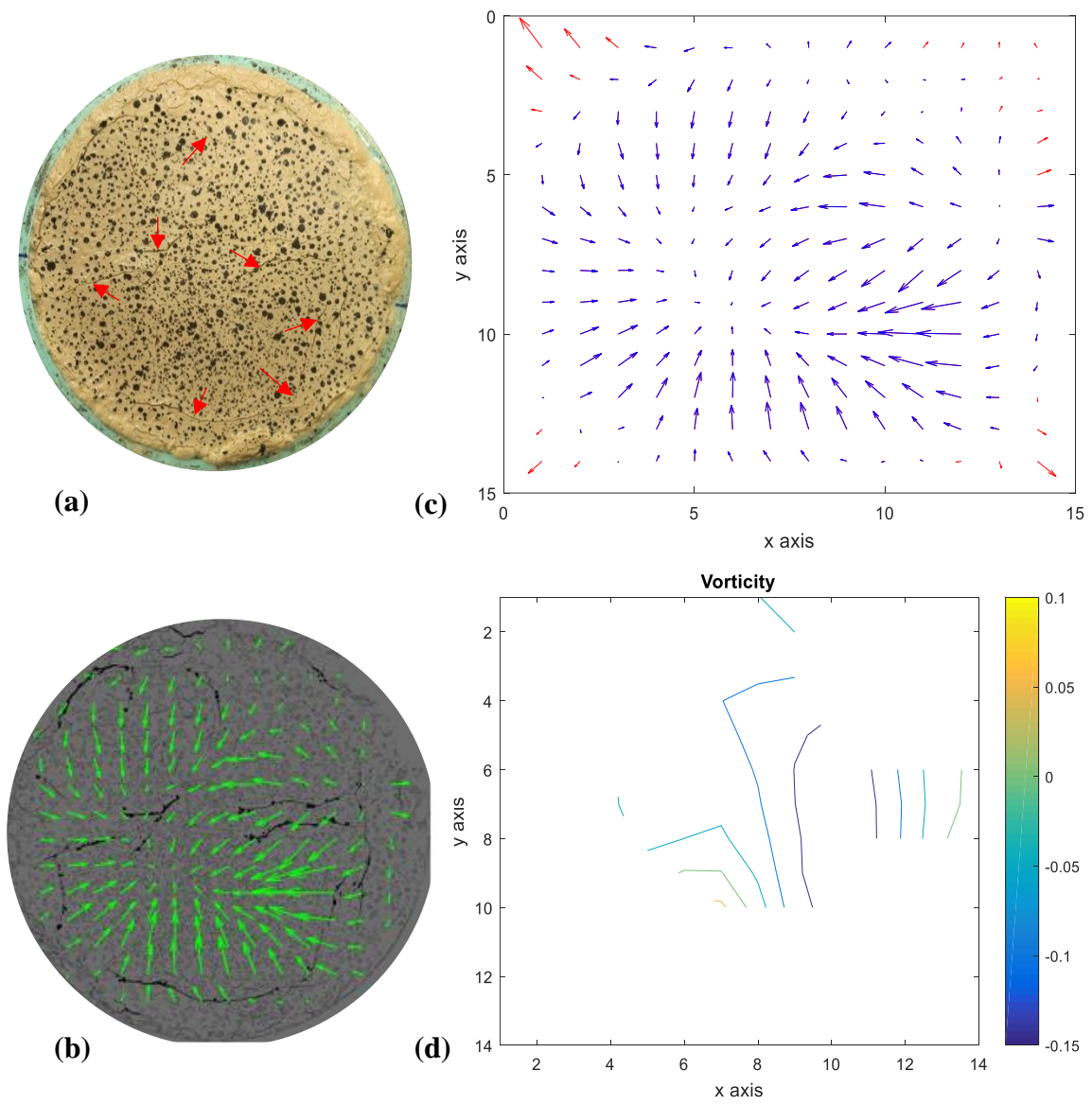


Figure 4.27 After 6 hours from 2nd drying; (a) a true color photo; (b) specimen with displacement vectors; (c) displacement fields in x, y (in pixels); (d) vorticity contours

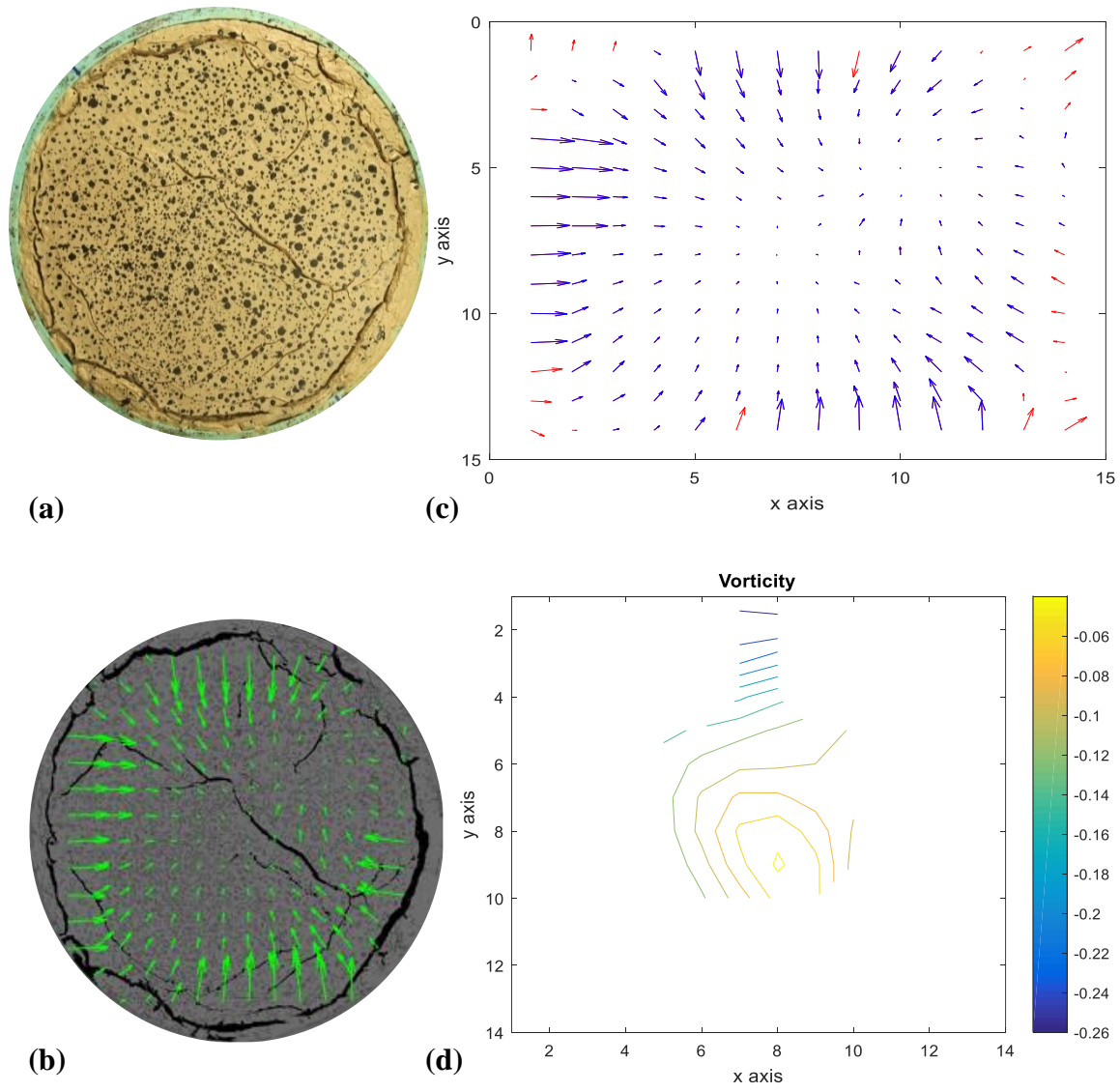
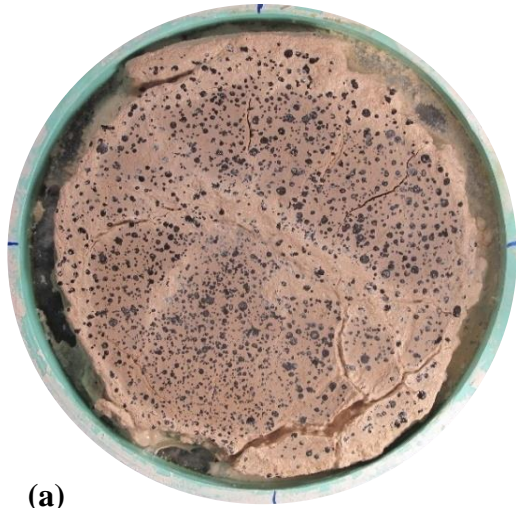
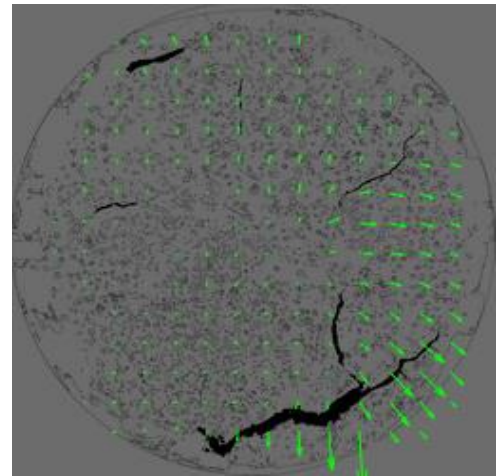


Figure 4.28 At failure-2nd drying: (a) a true color photo; (b) specimen with displacement vectors; (c) displacement fields; (d) vorticity contours



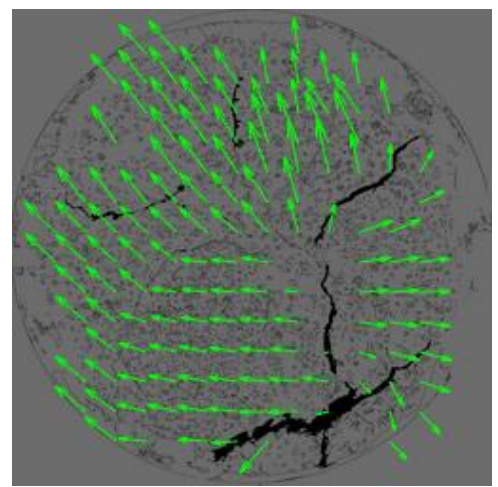
(a)



(b)



(c)



(d)

Figure 4.29 Immediately after 2nd wetting; (a) true color photo; (b) specimen with displacement vectors, at end of 2nd wetting; (c) true color photo; (d) specimen with displacement vectors

4.5.2.2 DIC results of constrained specimen

The displacement vectors during the first drying are presented in Figure 4.30, Figure 4.31 and Figure 4.32. In the first drying, the small displacement vectors indicate that the specimen was shrinking under restrained condition. This restrained is presumed to arise due to the circular-spiral grooves at the soil bed. The initiation of the crack is clearly observed in Figure 4.30. It was observed large displacement vectors obtained perpendicularly to the crack, while small ones in the rest of the specimen. While the drying process proceeded, the specimen was shrinking under restrained condition. When the tensile stresses exceeded the tensile strength of the material, the crack formed at defect or weaker region. Upon the first wetting, the specimen exhibited nonuniform expansion. This resulted in healing of the present cracks and developing a very small crack, as shown in Figure 4.33. In the second drying, the specimen experienced nonuniform shrinkage where more cracks propagated, as seen in Figure 4.34. During the second wetting, the specimen expanded in nonuniform way where no crack healing was obtained, as presented in Figure 4.35. More cracks formed over the third drying (Figure 4.36).

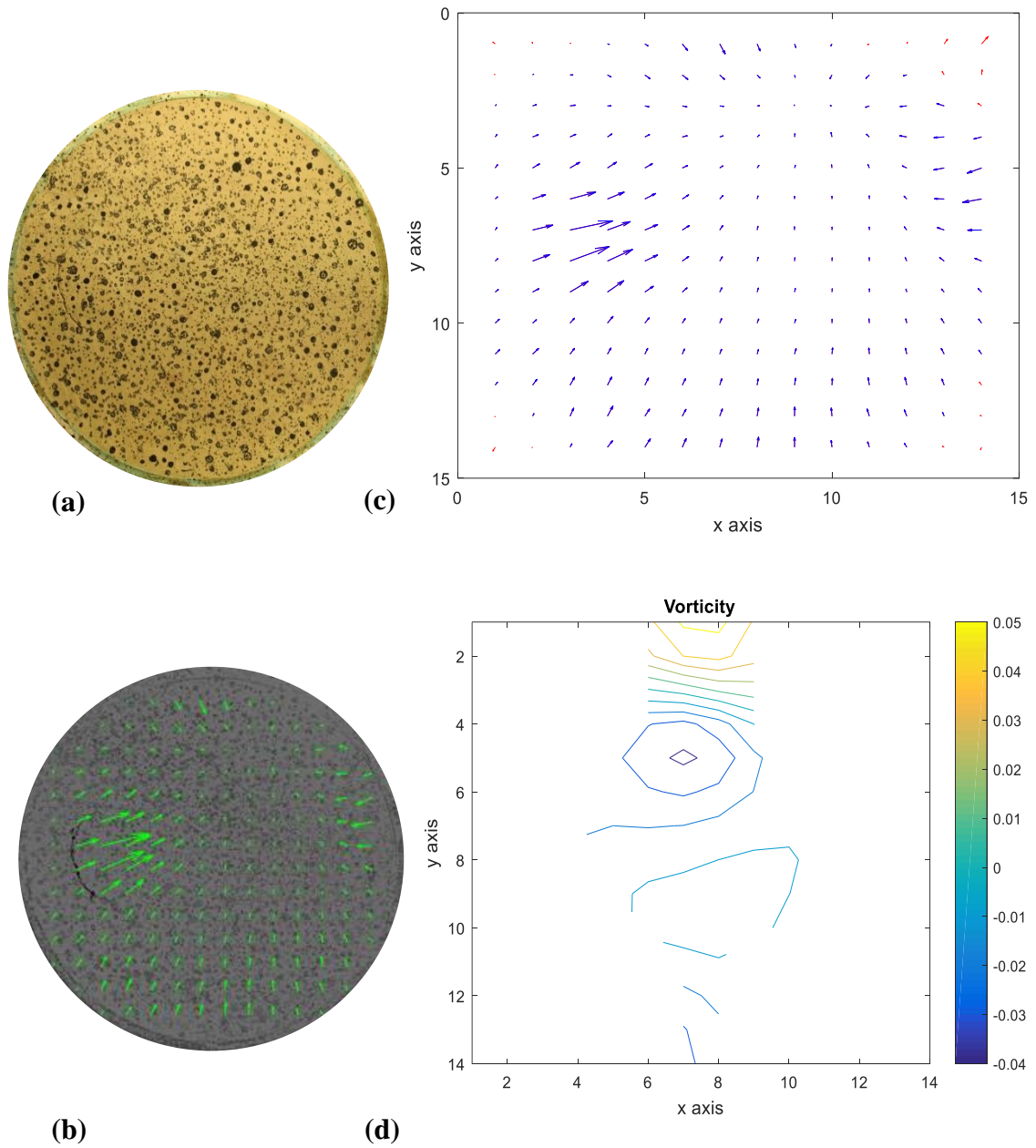


Figure 4.30 At initial crack-(5 hours)-1st drying: (a) a true color photo; (b) specimen with displacement vectors; (c) displacement fields; (d) displacement fields after smoothing

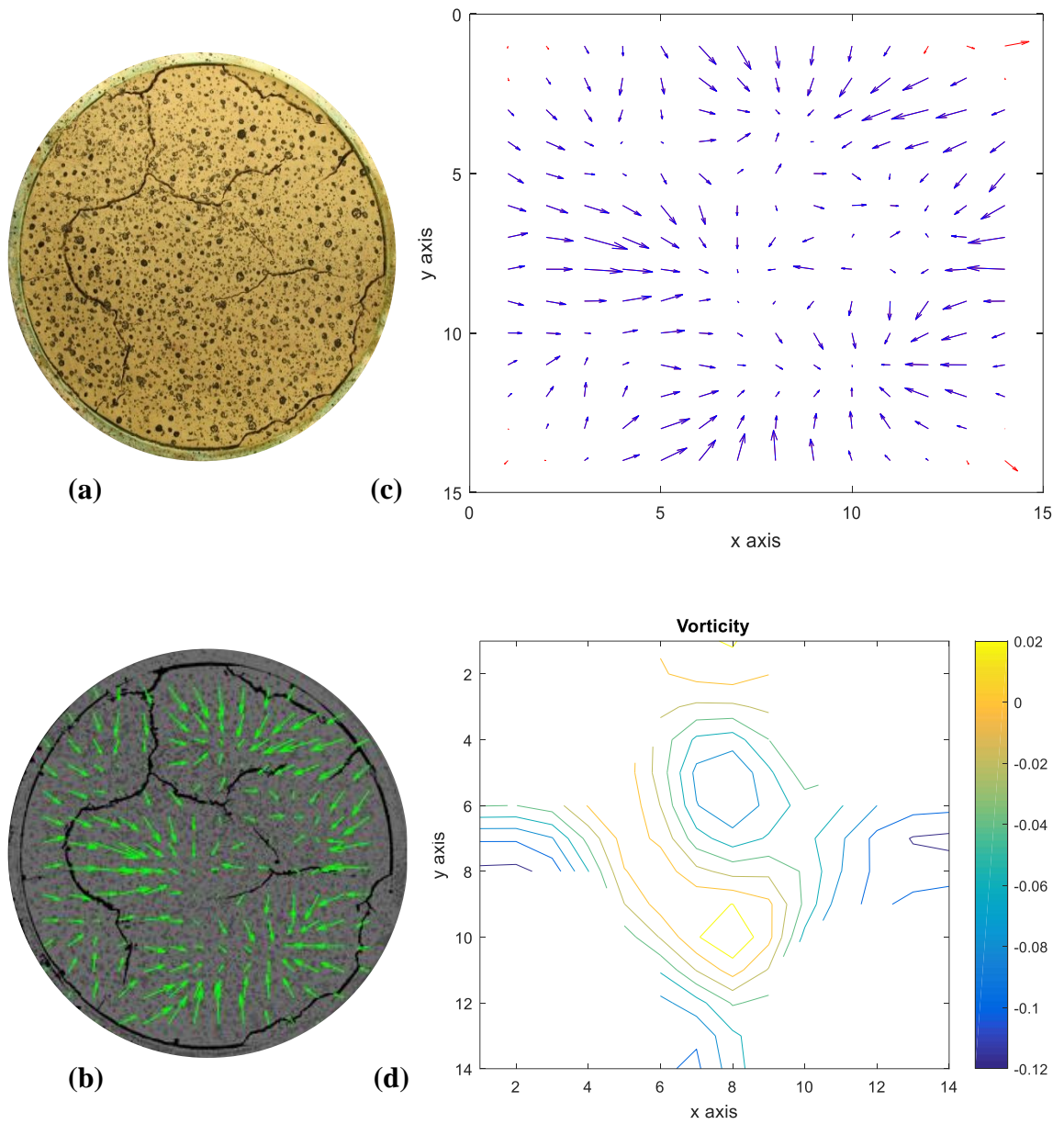


Figure 4.31 After 16 hours 1st drying: (a) a true color photo; (b) specimen with displacement vectors; (c) displacement fields; (d) Vorticity

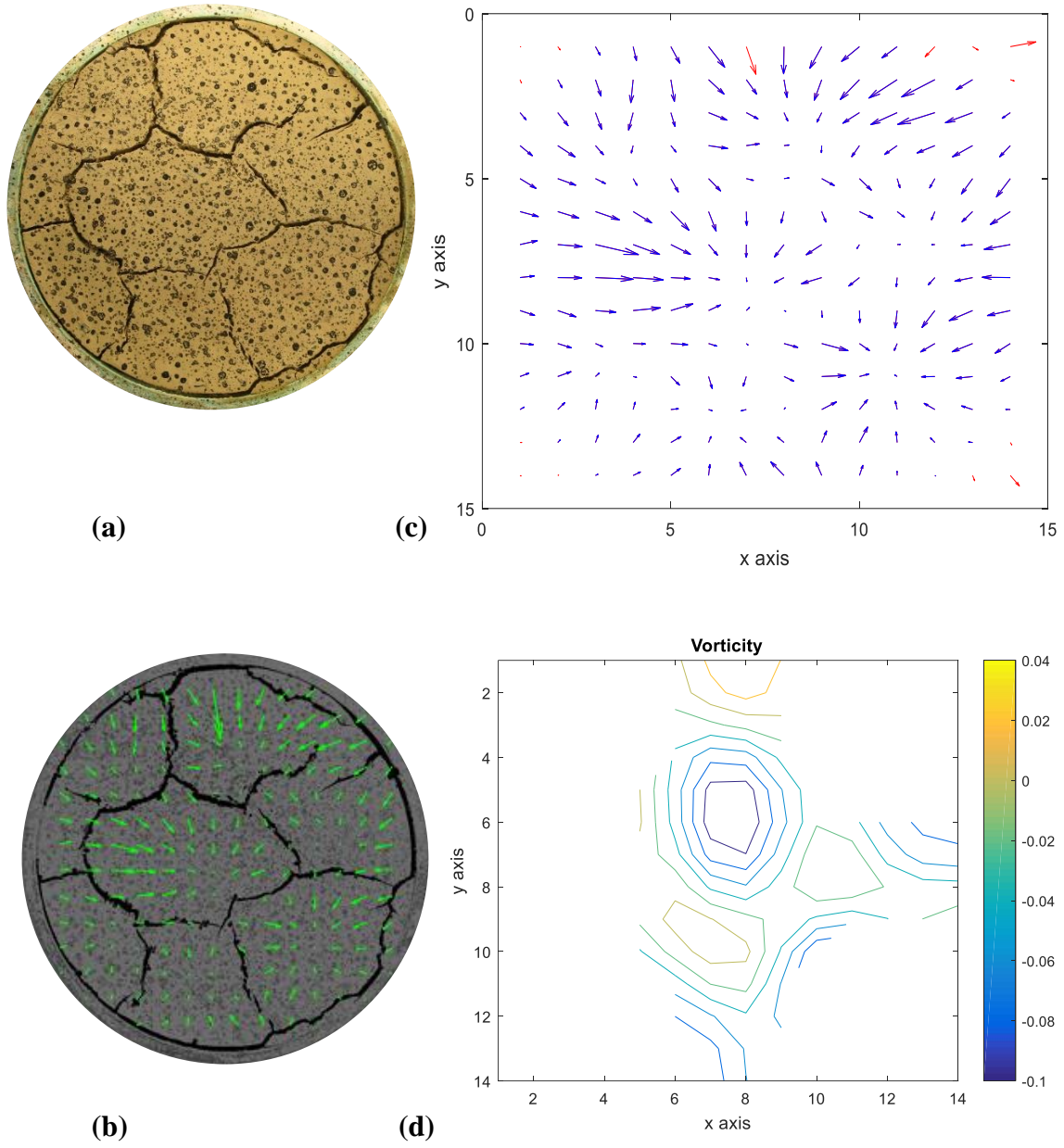


Figure 4.32 After 24 hours 1st drying: (a) a true color photo; (b) specimen with displacement vectors; (c) displacement fields; (d) Vorticity

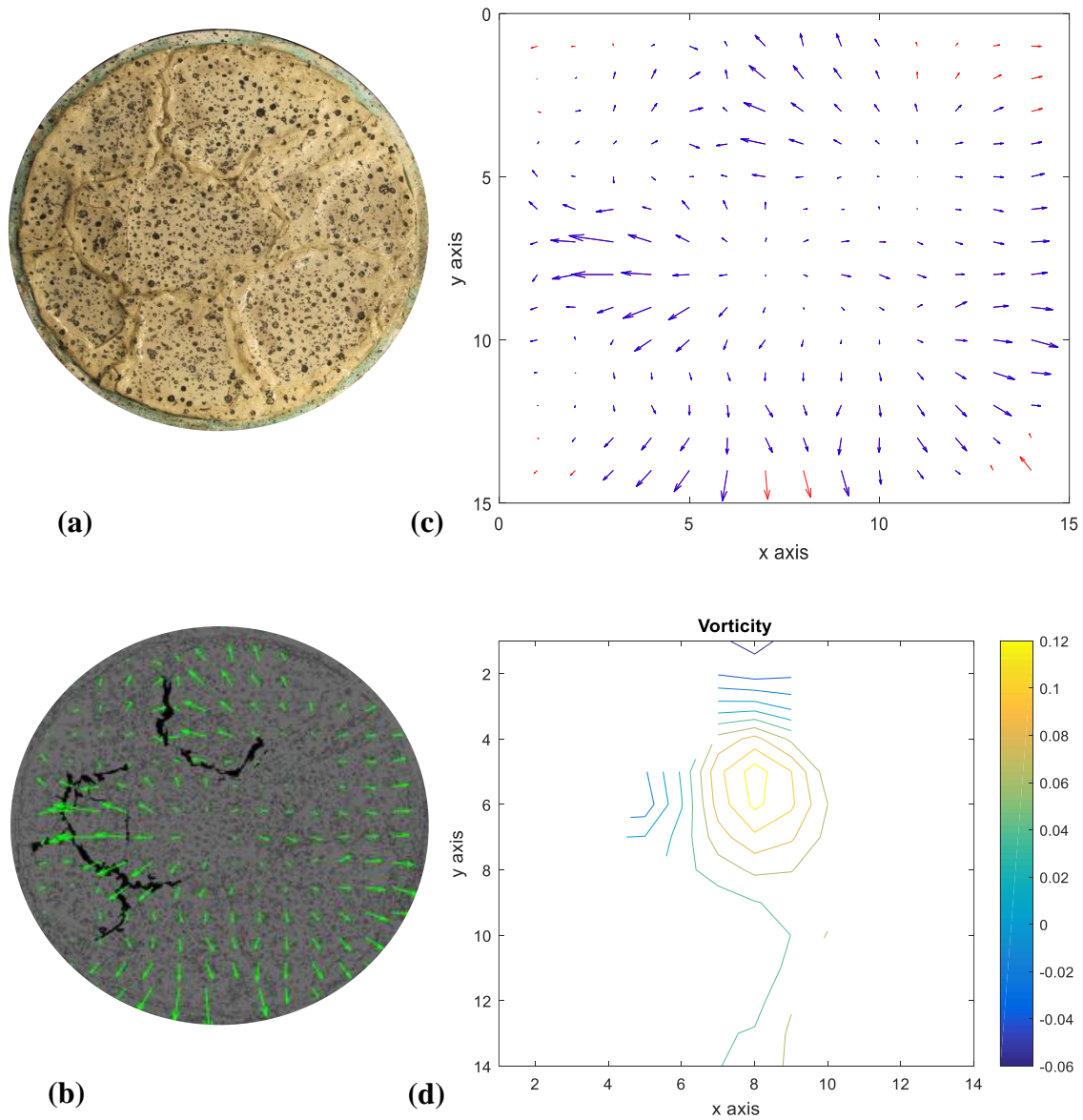


Figure 4.33 After 22 minutes 1st wetting: (a) a true color photo; (b) specimen with displacement vectors; (c) displacement fields; (d) Vorticity

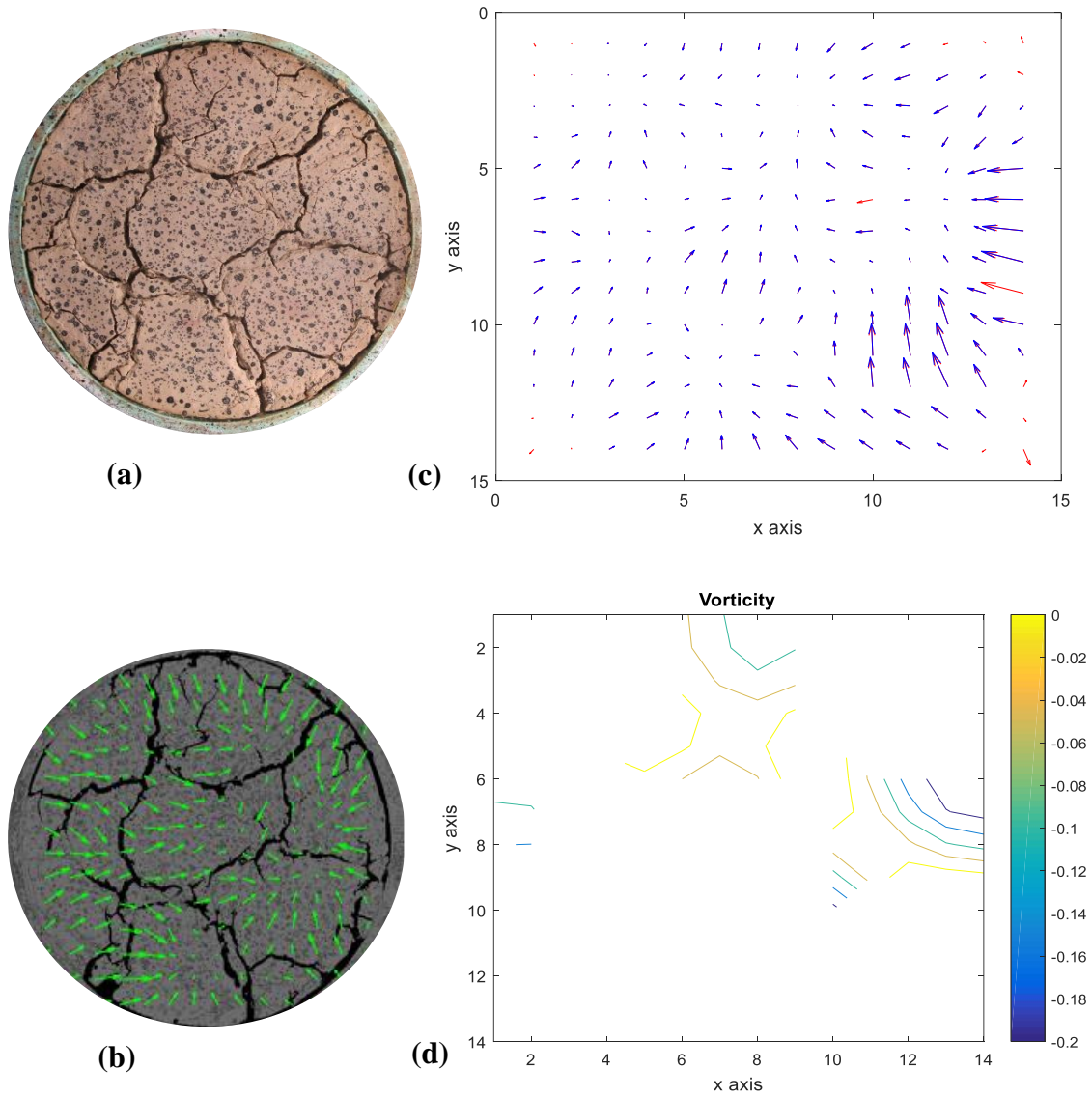


Figure 4.34 After 24 hours 2nd drying: (a) a true color photo; (b) specimen with displacement vectors; (c) displacement fields; (d) Vorticity

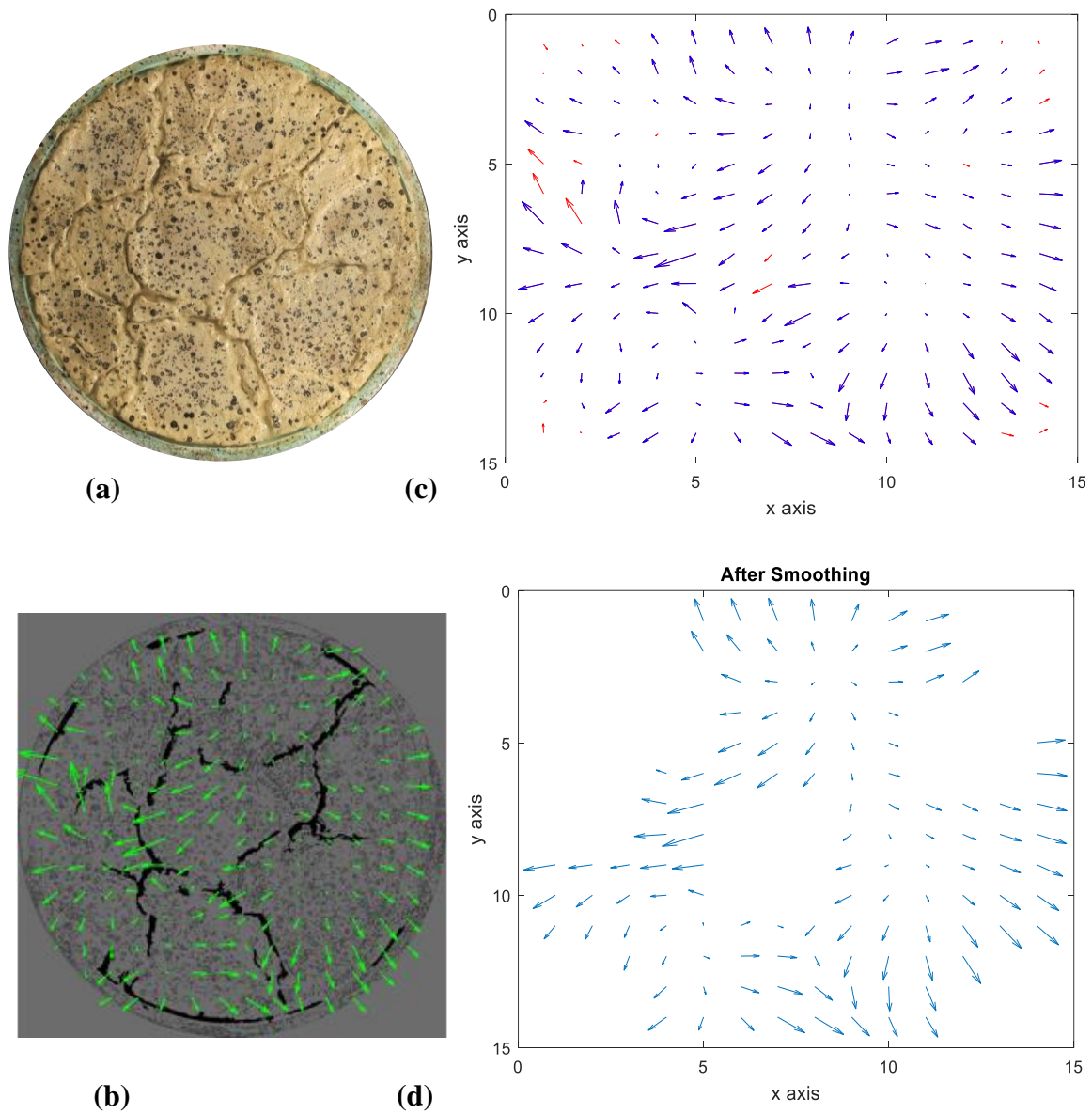
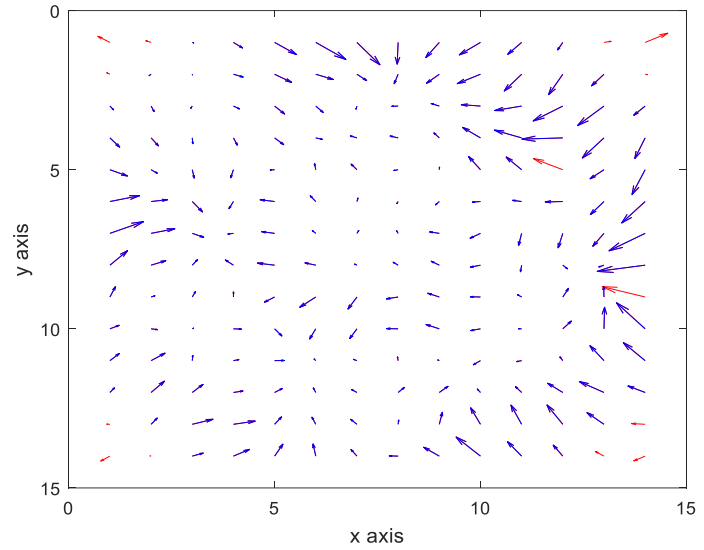


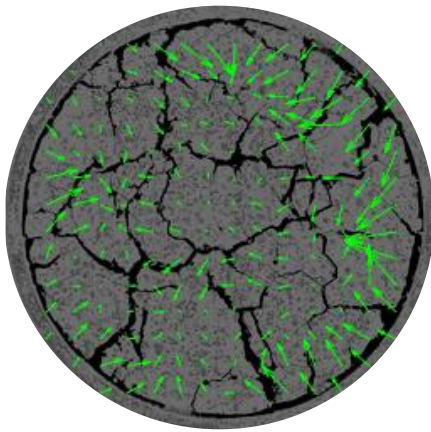
Figure 4.35 Immediately after 2nd wetting: (a) a true color photo; (b) specimen with displacement vectors; (c) displacement fields; (d) displacement field after smoothing



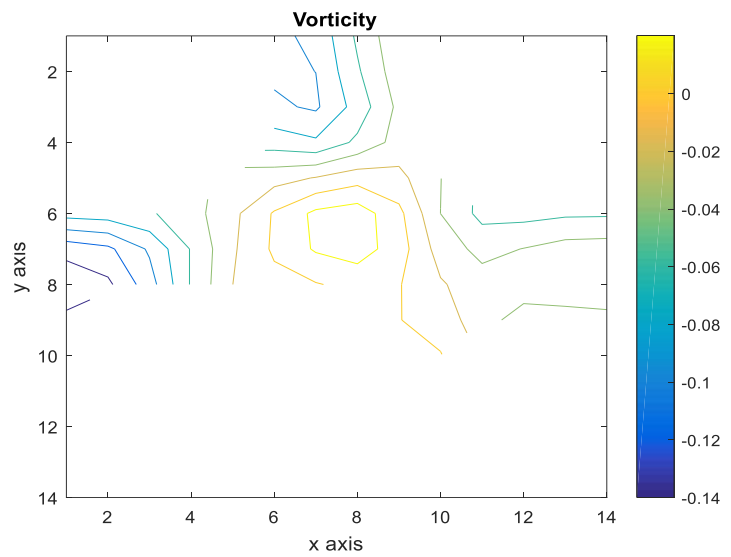
(a)



(c)



(b)



(d)

Figure 4.36 After 24 hours 3rd drying: (a) a true color photo; (b) specimen with displacement vectors; (c) displacement fields; (d) vorticity

4.6 Concluding remarks

- In general, the constrained specimens experienced more cracks than the free ones. Although negligible constrains were provided between the soil and the smooth interface, the free specimens experienced cracks during cycles. This indicates that the interface factor can't be taken as the only factor for inducing cracks in soils.
- The significant effect of the cyclic wetting/drying processes on the evolution and propagation of cracks in soils can be highlighted in this study. More cracks developed each cycle till reach to an equilibrium state of no significant cracks formed.
- The initial saturation condition has a significant effect on desiccation cracking where the saturated specimens experienced more cracks than those of unsaturated ones.
- Although all unsaturated and saturated samples were compacted at high compaction energy, where this degree is highly recommended to compact some geotechnical structures, such as embankments (i.e., 94.4% of γ_{dmax} as determined from the standard Proctor test, ASTM D698), they all experienced cracks when subjected to alternatives wetting/drying cycles regardless to the restriction conditions at the soil boundaries (i.e., soil-interface) and the initial saturation conditions.
- It is believed that DIC technique can be a beneficial tool for analyzing stresses and strains distribution during cracking.
- Formation and propagation of cracks in soil are strongly related to the variations in the configurations of soil's particles and stress state that occur during alternative shrinkage and swelling/expansion when subjected to drying and wetting, respectively.
- The most interesting finding in this study is that cracks may develop during wetting.

CHAPTER V

A NEW INNOVATIVE DEVICE FOR MEASURING TENSILE STRENGTH OF SOILS DURING WETTING/DRYING CYCLES

5.1 Introduction

Many geotechnical problems arise from variations of moisture content and volume; for example, swelling and shrinkage in expansive clays. During wet seasons, soil may experience swelling or expanding in the volume. While during dry seasons, soil may exhibit reduction in volume (shrinkage), resulting sometimes in crack formation. Cracking in soil is a common phenomenon which occurs due to evaporation of water from soils during dry climate. These desiccation cracks may take place in naturally deposited soils as well as engineered soils, such as roadway embankments, compacted fills, slopes, hydraulic barriers, and buffers. Desiccation cracks may turn into a preferential passageway for water flow and contaminates transport in soils (McBrayer. et al., 1997, Albrecht and Benson, 2001, Greve et al., 2010). Also, presence of cracks may cause large variations in the hydraulic and mechanical characteristics of the intact soils, and this may become critical and destructive on the performance of a number of geotechnical, geo-environmental, and geological projects, such as landfill cover, clay liner, and industry waste (Omidi et al., 1996, Albrecht and Benson, 2001, Tang, et al., 2011).

In this chapter, the effect of cyclic wetting/drying processes on the evolution and propagation of cracks has been examined. Soil cracking propagates after every new cyclic wetting/drying till approaches to the equilibrium state in which no significant cracks develop. This phenomenon is strongly relevant to the variations of hydro-mechanical characteristics of soils.

Tensile strength is a useful indicator for studying the mechanical behavior of soils. It plays a significant role in several engineering applications. Over many years, the mechanism of tensile failure has been paid attention by several researchers to interpret many failures of earthen structures. This chapter introduces the first generation of a new tensile device for determining tensile strength of soil during sequential drying/wetting cycles. The determination of tensile strength has been coupled with the study of desiccation cracking during cyclic wetting/drying. The acceptability and feasibility of the new device and procedure have been evaluated.

5.2 Objectives

The underlying objective herein was to investigate the variations of tensile behavior of soils subjected to multiple drying and wetting cycles when exposed to circumstances as in field. The motivation of this work was stemmed from the observation of crack propagation under successive drying/wetting cycles. Most researchers come into an agreement that accumulated irreversible deformations, such as swelling and shrinkage, may occur upon multiple wetting and drying cycles associated with significant variations in soil fabric. These changes may influence on hydro-mechanical response of soil, and as a result cracks propagate. Under drying, soil may experience irreversible deformations in fabric resulting in crack formation, while upon wetting, soil may undergo softening/weakening response in which sometimes provides healing and closure to the cracks that formed in the drying process. However, these cracks remain weak region and under the alternate drying cycle, the cracks re-open and propagate increasingly. After a certain number of drying/wetting cycles, the cracks remain unchanged. In response to that, considerable research has been triggered herein to investigate the variations of tensile behavior of soils during wetting and drying cycles.

Of particular significant in understanding of cracking mechanism, a new approach of tensile testing is utilized in this work to examine tensile strength during sequential wetting and drying cycles. This new approach consists of subjecting the soil to drying process in which the tensile stresses may develop at soil-interface due to an increment in matric suction, and thus cracks form. Previous laboratory tensile studies have been hindered a numerous of difficulties comprising; the soil sampling, detachment between the soil sample and tensile mold during the test, and the very high-water content of the soil sample. Consequently, my research had promoted more crucial improvements on tensile testing which simulates the natural conditions of soils as in field.

5.3 Methodology

5.3.1 Design of experiment and test principle

A new approach has been developed to examine the variations of tensile strength of soil when subjected to wetting/drying cycles. The fundamental concept of the new testing method is that the soil develops tensile stresses when exposed to natural circumstances during drying process as in the field without employing any external tensile stresses. The tensile tests were performed under fully restricted condition in which no motion was allowed for the free part of the device. This was performed by completely holding the free part by the load cell to prevent the lateral displacement during shrinkage and expansion when drying and wetting, respectively.

The soil experiences either increase of suction under drying or decrease under wetting. This results in generating tensile stresses during drying or stress releasing (i.e., reduction in the tensile stresses) upon wetting. To induce tensile stresses, restraints were provided during cyclic processes through employing protrusions at the soil bed. Rectangular protrusions were fabricated to induce

and mobilize tensile stresses at the soil bed during drying /wetting cycles. When the tensile stresses exceed the tensile strength of the soil cracks develop. Also, the protrusions can provide an attachment at soil-bed where the load cell which is attached to the side and the bed of the free jaw, can measure the developed tensile forces.

The new tensile device consists of two halves of jaws with the square dimensions of the closure 150 mm x 150 mm and 25.4 mm of thickness. One half is fixed and the other one sets on ball bearings to induce free movement with minimal friction between the base and the surface. A small gap is introduced where the two halves join in order to prevent developing tensile forces between the two halves. U-shaped channel is mounted directly below the gap for allowing the excess water to drain when the soil sample subjected to wetting process. A micro sized load cell with the dimensions of 19.1 mm x 19.1 mm x 6.4 mm is connected to the movable half of the tensile box to measure the developed tensile loads during wetting and drying cycles. The only reason of using a micro load cell is to prevent the soil specimen undergoing fracture failure due to the weight of the load cell during the test. The load cell has the capacity up to 200 N (50 lb) with a full resolution of 0.01% (0.02 N or 0.0045 lb). Figure 5.1 provides more details in the new tensile apparatus.

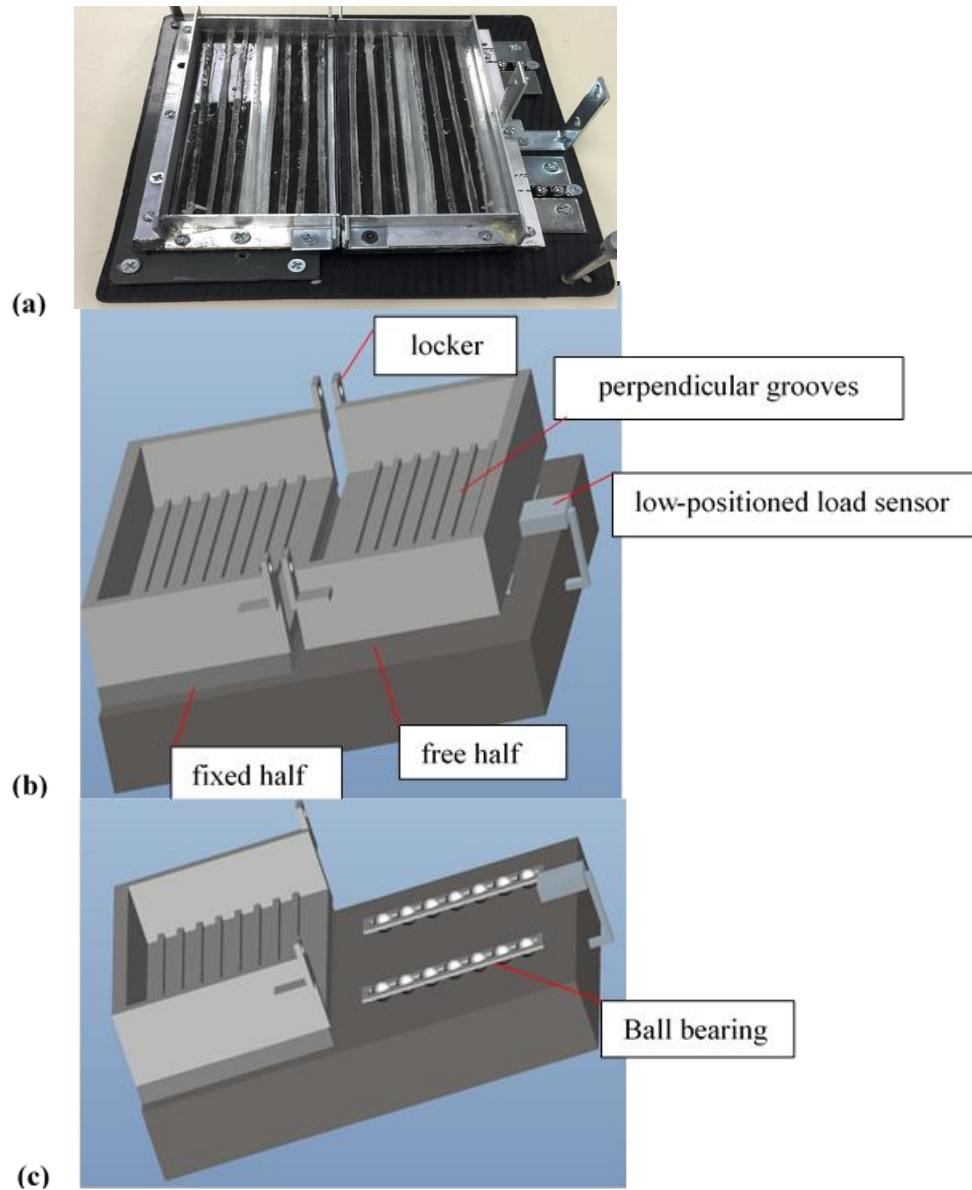


Figure 5.1 (a) the new tensile device; (b) & (c) schematic drawings for the device

5.3.2 Materials and methods

Tensile tests were performed on compacted specimens of a high expansive soil mixture consisted of 75% kaolin and 25% bentonite, (see Table 3.1 & 3.2). The physical properties of the

soil mixture are presented in Table 5.1. Liquid limit (LL) was 88% while plasticity index (PI) was about 48%. Two soil specimens were prepared at similar initial water content of about $42.7\% \pm 0.7\%$ (+4.7% of optimum moisture content) and dry unit weight of 11.4 kN/m^3 (94.4% of γ_{dmax} as determined from the standard Proctor test, ASTM D698), see Table 5.1. Each specimen was tested under different condition to examine the acceptability and validity of the new testing procedure in this research. More details are provided in the next sections.

Table 5.1 Physical properties and initial conditions of 75% kaolin & 25% bentonite mixture

Liquid limit (%)	88
Plasticity index (%)	48
Specific gravity	2.67
USUC ^a classification	^a CH
Optimum water content (%)	36.0
Maximum dry unit weight (kN/m^3)	12.16
<u>Compacted specimens</u>	
Initial water content (%)	42.7 ± 0.7
Initial dry unit weight (kN/m^3)	11.40
Initial void ratio	1.29

^aUnified Soil Classification System, ^bLL: Liquid limit

5.3.2.1 Sample preparation and test procedure

For soil preparation, the soil mixture was blended thoroughly with distilled water to the specific water content and the desired dry density (see Table 5.1). Then the soil was kept in a sealed bag for 24 hours to promote moisture equilibrium. The tensile device was calibrated before compacting the soil. The calibration process included the two steps; calibrating the free part of the device on the top of the ball bearing, and then setting a small gap between the two halves of the

box by utilizing a plastic spacer. Two screws were used to maintaining the gap which were then removed after completion of preparation and before starting the test (see Figure 5.2). Two soil specimens were prepared at similar initial water content and dry unit weight and then tested at two different conditions.

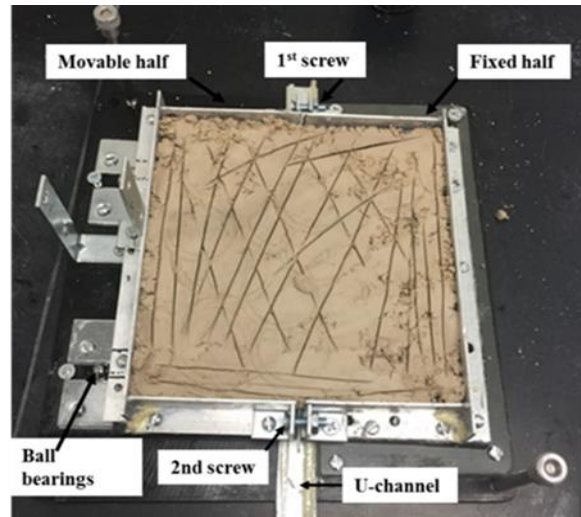


Figure 5.2 The new tensile device during preparation of the soil sample; the first layer of the soil sample

The variations of water mass during drying and wetting cycles were determined by placing the tensile device on the top of an electronic balance with the maximum capacity of 8100 g and repeatability of 0.01 g. A digital camera (Canon Camera-Power Shot G11) with the highest resolution of (3648-pixel x 2736-pixel) was fixed directly above the soil specimen (perpendicularly) to capture a series of photos during the cyclic processes. Figure 5.3 presents the experimental set-up of testing procedure including the tensile device, the electronic balance, and the overhead camera. Initially, the specimen was allowed to dry naturally under controlled

laboratory temperature and relative humidity ($24\pm 1\text{ C}^\circ$, $\text{RH} = 52\pm 2\%$). When the developed tensile stresses exceeded the tensile strength of the specimen, the soil failed. The process was terminated when the weight of the sample was constant or no significant change observed.

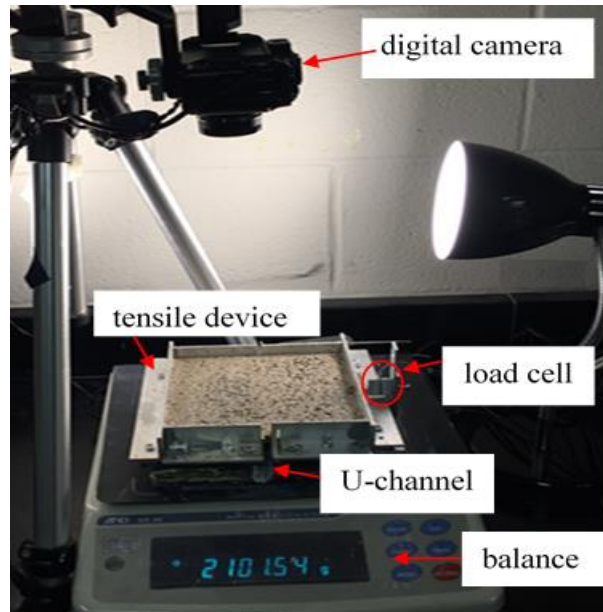


Figure 5.3 Testing Set-up of the new tensile procedure

The wetting process was an important issue taken into our consideration in the new tensile testing method. Significant issues had been opted to wet the soil sample successfully inside the new device. On one hand to ensure that the soil sample had homogenous water content. On the other hand, to make sure that measured water loss by using the electronic balance was for the soil sample and not for the excess free water in the device. During wetting, the soil sample was gradually inundated with distilled water by using a filling syringe. Firstly, the surface of the sample was subjected to wetting, and then all the boundaries and the soil bed of the sample were wetted

as well. Upon wetting, the soil exhibited swelling, and then expanded toward the walls of the tensile device, resulting in a reduction and release in the tensile force. The developed force that determined during wetting process is referred to lateral-induced expansion force (LIEF). A complete or/and partial healing and closure of the current cracks was observed. The secondary cracks usually healed, however, sometimes the primary cracks subjected to negligible healing.

5.3.2.2 Locking and unlocking test procedure

Two identical soil specimens were tested under two different conditions in order to examine the validation and acceptability of the testing method. One test was performed with maintaining the gap between the two parts of the tensile device unlocked during the drying/wetting cycles. While the other one was performed with locking the gap by using two screws after the failure where the maximum tensile force was determined. For the locking test, the load cell was disconnected at the end of the drying process. Then the force sensor was reconnected before the wetting process for measuring the lateral-induced expansion forces (LIEF) during wetting. At the end of wetting, the force sensor was disconnected again and then reconnected for the next drying process. This scenario was performed in all cycles. The main purpose of the latter method was that to start every drying and wetting process with zero/null force. Also, to allow the cracks propagate without the effect of gap existence.

5.3.3 Quantitative analysis by using image technique

Digital image analysis technique (by using *image j software*) was employed to study the morphology of crack patterns on the surface of the samples at the end of each wetting-drying cycle. The procedures of digital image analysis were illustrated by (Atique et al., 2009). The procedure that opted herein for image analysis technique is presented in Figure 5.4. Firstly, the digital image

(TrueColor/RGB) of soil sample was converted to a grayscale image. The grayscale image was obtained by converting the image to the type of 8-bit. Afterward, the background of the image had been subtracted from the image. Then, the grayscale image was converted to a binary black-and-white image (B & W). In this stage, the binary image has replaced all pixels in the grayscale image with luminance greater than a threshold value of 1(white) and the other pixels with the value 0 (black). So that, the binary image consists of only 1's and 0's, which represents the un-cracked and cracks areas respectively. Finally, an outline operation had been performed where the cracks and un-cracked areas can be obtained. Then the ratio of crack areas to the total area of the soil sample at the end of drying or wetting process can be determined as the crack intensity factor (CIF).

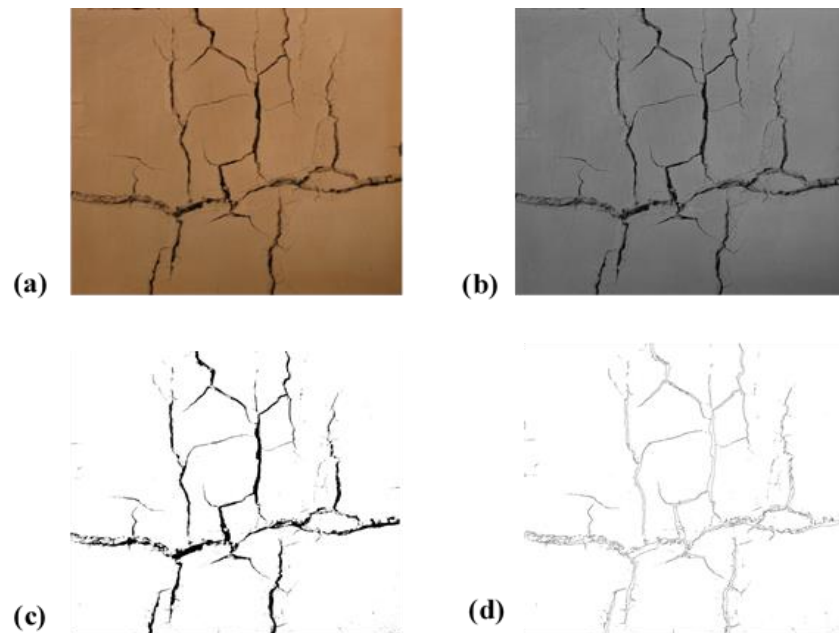


Figure 5.4 Image processing: a) A TrueColor (RGB) image; b) converting the RGB image to a grayscale (8-bit); c) subtracting background and converting to a binary image; and d) outline operation

5.4 Results and discussion

Two series of tensile testing results are presented and described herein; one series for unlocked-gap sample and the other one for locked-gap sample. The variation of tensile and lateral-induced expansion forces over time was determined for all drying and wetting processes, respectively. Also, the variation of tensile forces as a function of water content was determined. Cracking network was characterized at the end of each cycle by using the Crack Intensity Factor (CIF). In this study, the soil specimen which was tested with unlocked-gap is referred to “Mixture-Compacted Unlocked” (MC-U). While the soil specimen that was tested with locked-gap is referred to “Mixture-Compacted Locked” (MC-L).

Upon drying, the tensile forces increased up to a maximum tensile force coinciding with the inception of crack formation in the soil sample. Afterward, the tensile force decreased when drying proceeded and the cracks fully propagated. In this study, the tensile failure corresponded to the crack initiation in the same direction of the gap (Y-axis) and perpendicular to the restrictions in X-direction, see Figure 5.5. The crack in the X-direction initiated and propagated in which the soil specimen remained in a state to resist the failure. When drying proceeded, the crack in Y-direction initiated and fully propagated at which the tensile failure occurred.

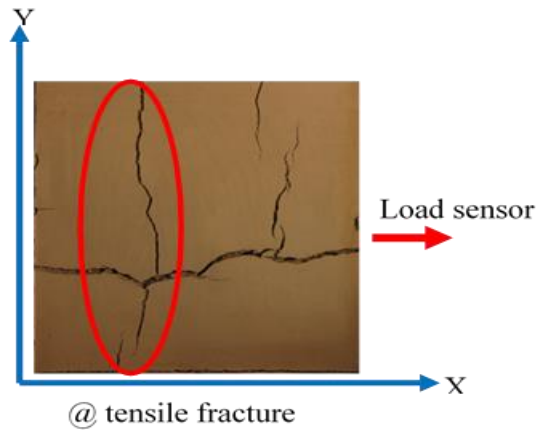


Figure 5.5 Y-direction crack corresponded to the tensile failure

During the first drying, the soil developed a fully crack just after the peak load where it decreased as drying proceeded and the crack propagated in the soil specimen. Based on that the tensile force was carried by the full cross-sectional area of the soil.

The tensile strength was calculated by dividing the maximum tensile force by the cross-sectional area of the soil specimen. The cross-sectional area was determined at failure by using image analysis technique. Compare to the initial cross-sectional area of specimen, it was found that the lateral shrinkage and the vertical change in the thickness were calculated at failure to be insignificant. Accordingly, either areas can be opted for calculating the tensile strength.

Upon wetting, the soil exhibited swelling, and then expanded toward the load sensor. This resulted in a reduction in tensile force and then increase in the lateral-induced expansion force (LIEF). A complete or/and partial healing and closure of the current cracks was observed. The secondary cracks usually healed, however, primary cracks subjected to negligible healing. For the next drying process, the soil sample resisted the tensile failure due to crack healing in the first

drying process. When the drying proceeded, the sample failed whenever a fully Y-direction crack developed.

5.4.1 Results of unlocked-gap test

The soil specimen (MC-U) was subjected to five wetting/drying cycles. The variation of water content over time during drying is presented in Figure 5.6. The water content gradually decreased over time till approached equilibrium at the end of drying process. For wetting, the sample was wetted to more or similar water content compared to the initial water content-as compacted, as shown in Figure 5.6.

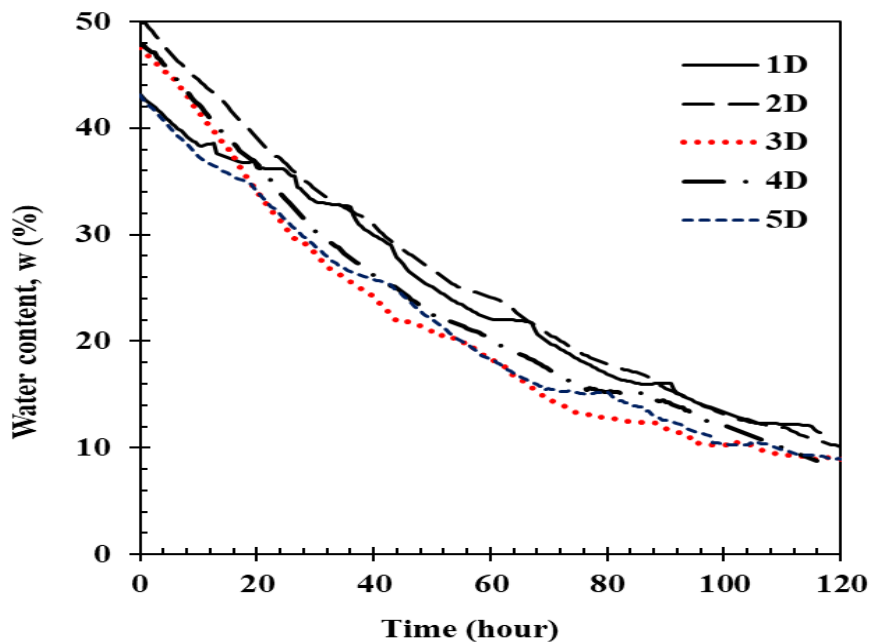


Figure 5.6 Variation of water content over time for the compacted specimen (MC-U) during drying processes; D: Drying

Figure 5.7 provides information regarding the variation of void ratio and volume of soil specimen for a given change in water content for shrink paths through drying cycles. The primary

volumetric change occurred between the saturation lines of 80% and 50%, and this is similar to the experimental results published by Tripathy et. al., (Tripathy et al., 2002).

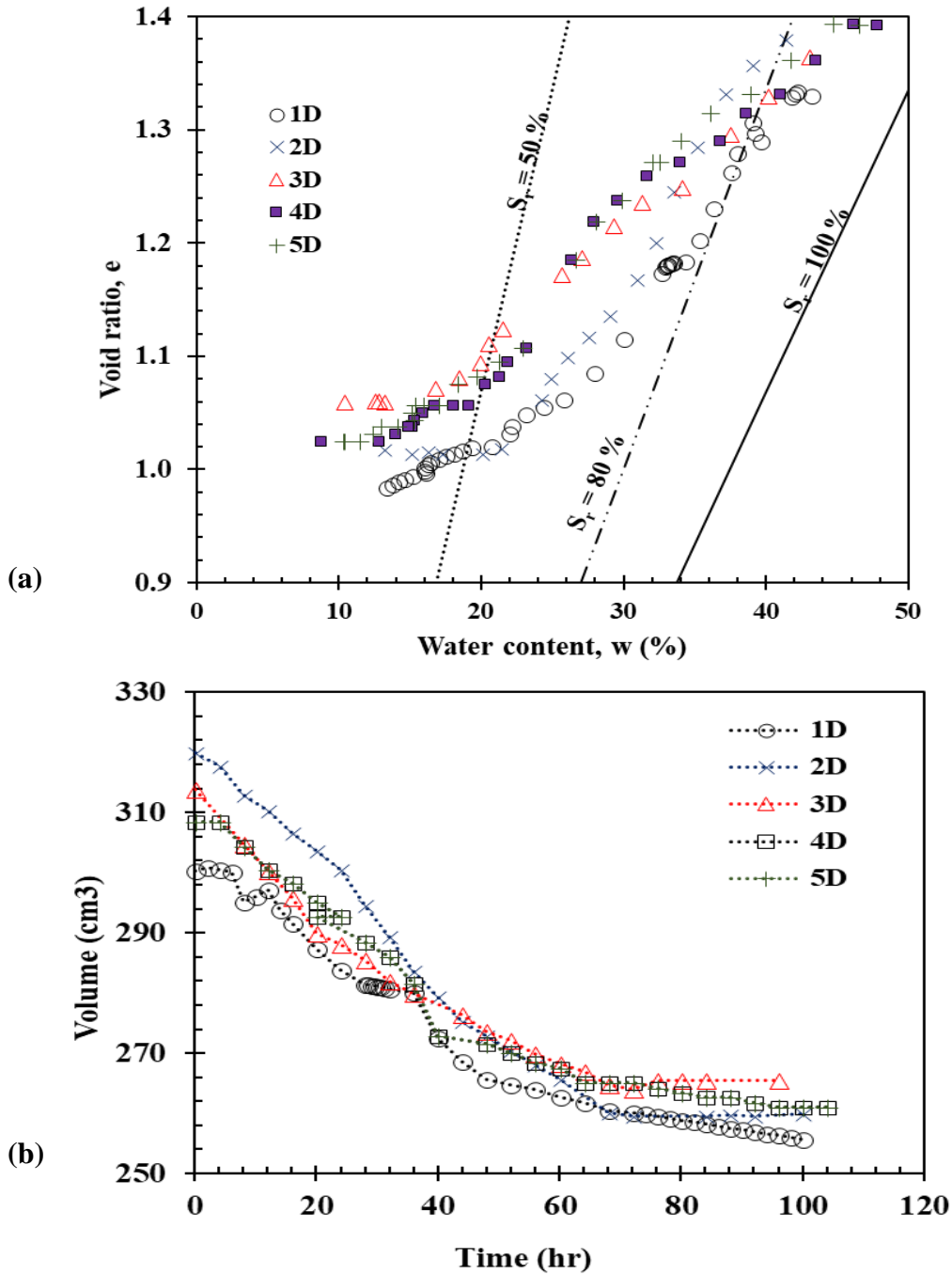


Figure 5.7 (a) Variation of void ratio vs. water content during drying cycles, (b) variation of soil's volume over time

5.4.1.1 Effect of cyclic drying/wetting on tensile tests

In this thesis, a positive sign convention was opted for the tensile force, and a negative sign for the lateral-induced expansion force (LIEF). The variation of forces over time through drying and wetting processes are presented in

Figure 5.8 and Figure 5.9, respectively. In the first drying, the soil sample exhibited much higher tensile force compared to the other drying processes. The tensile forces gradually increased up to the peak value and then decreased when drying proceeded and the cracks fully propagated. When approached the equilibrium at the end of the first drying, negligible force maintained. Upon wetting, the soil sample exhibited an instantaneous reduction in the tensile force, and then generated the lateral induced-expansion force due to swelling/expansion where healing and closure of some crack openings were observed. In the second, third, fourth and fifth drying cycles, the soil sample exhibited much lower tensile forces compared to that of the first drying. After the failure, the tensile forces decreased to constant remaining values till approached the equilibrium at the end of the second, third, fourth, and fifth cycles.

It is believed that the soil structure (fabric and the inter-particle forces) was exposed to irrecoverable deformations/deteriorations during the first drying, resulting in considerable decrease in the strength. After that cycle, the tensile strength extremely decreased. It was obtained that the tensile strength increased in the fourth and the fifth drying compared to third one, however, the increase is very small compared to that one in the first cycle.

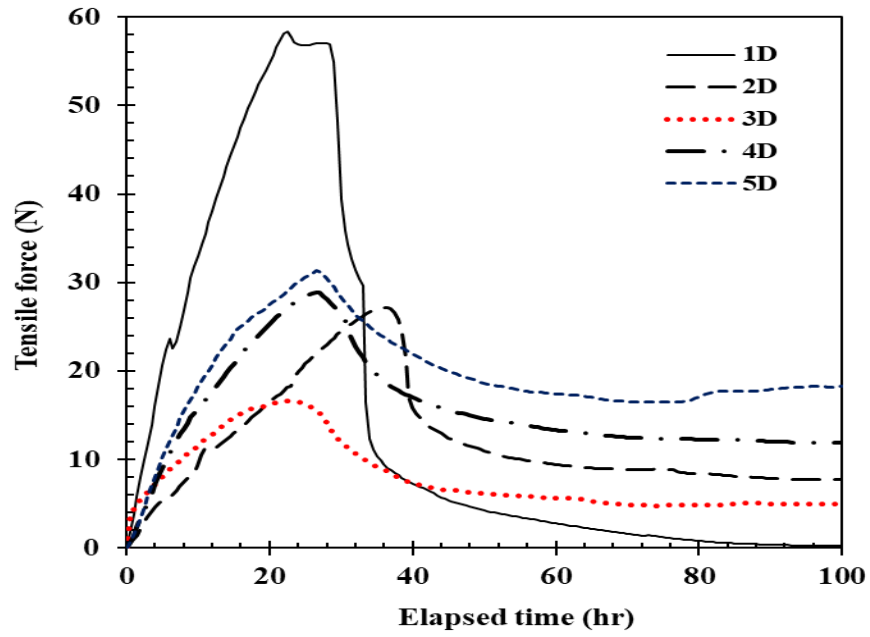


Figure 5.8 Variation of tensile forces over time for MC-U during five drying cycles; D: Drying, U: Unlocked-gap after failure

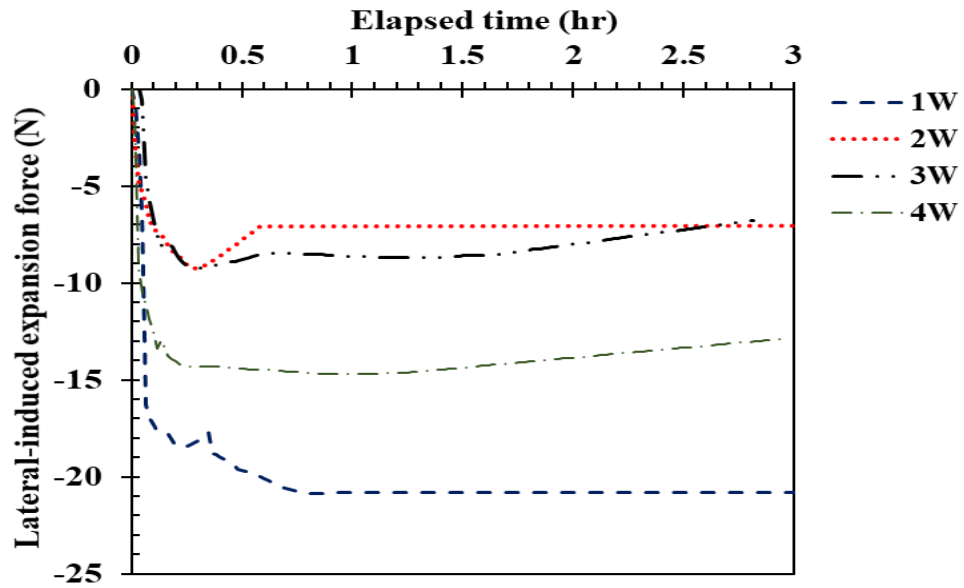


Figure 5.9 Variation of lateral-induced expansion force (LIEF) over time for MC-U during four wetting cycles; W: Wetting, U: Unlocked-gap after failure

Figure 5.10 (a & b) show the variation of tensile forces as a function of degree of saturation and water content change during drying cycles, respectively. In general, the tensile failure of all drying curves occurred within the degree of saturation range between 77% to 64% and the corresponding cracking water content over a range of 30% to 33.5 %. Figure 5.11 presents the variation of maximum tensile and lateral-induced expansion forces during drying and wetting processes, respectively. In general, the results show that the maximum tensile forces decrease in non-linear trend over drying processes. Similar trend was observed for the maximum lateral expansion forces during wetting, however in very limited range from 20.5 N to 14.7 N.

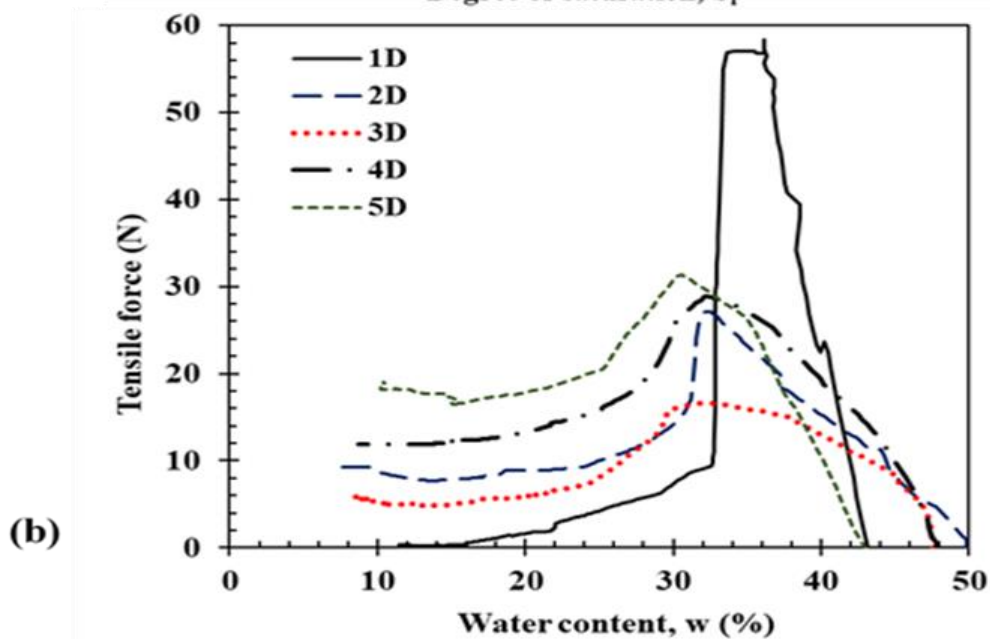
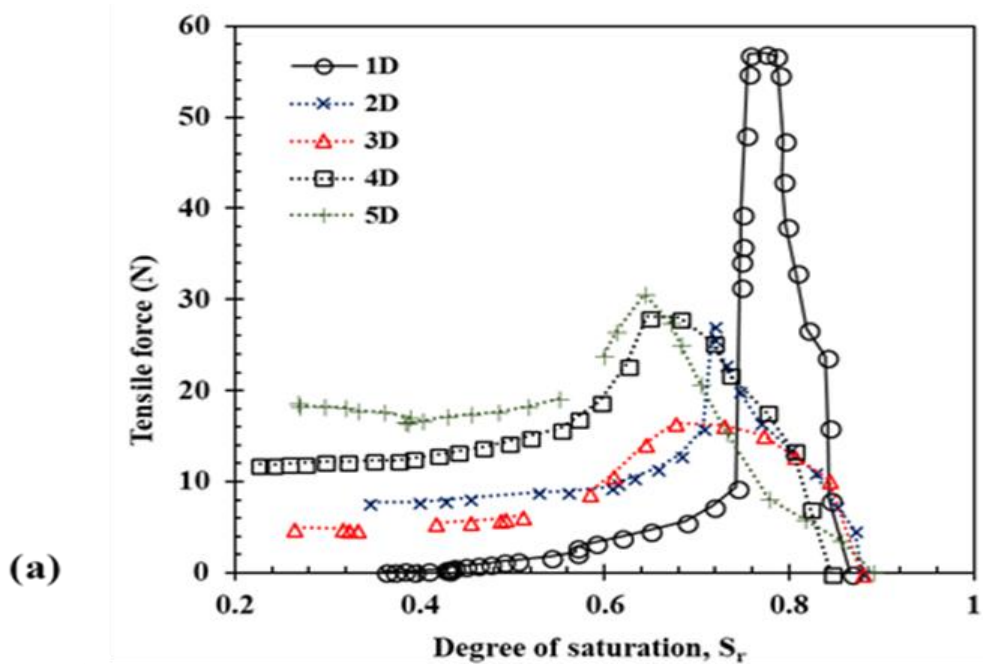


Figure 5.10 Variation of tensile forces as a function of (a) degree of saturation, (b) water content for MC-U; D: Drying, U: Unlocked-gap after failure

It is clearly observed the impact of cyclic wetting/drying on the tensile strength of specimen, where the maximum strength was determined in the first drying and decreasing is determined for the other drying processes, as shown in Figure 5.12.

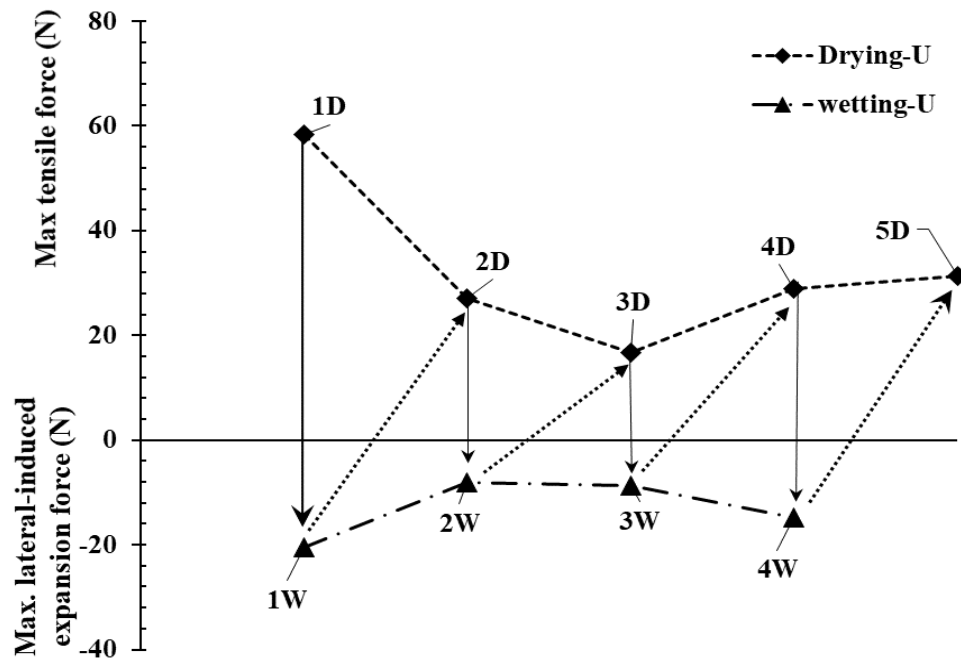


Figure 5.11 Variation of maximum tensile and lateral-induced expansion forces over cycles for (MC-U); D: Drying, W: Wetting, U: Unlocked-gap after failure

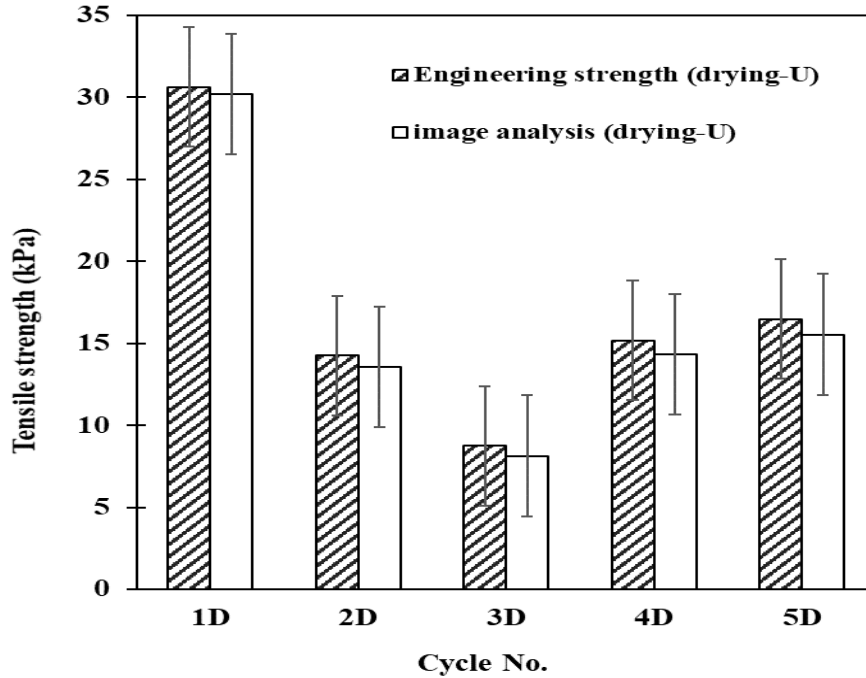


Figure 5.12 Variation of tensile strengths of the compacted specimen (MC-U); D: Drying, U: Unlocked-gap after failure

5.4.1.2 Effect of cyclic drying/wetting on cracking

Figure 5.13 presents the crack networks at the end of every drying/wetting cycle of the compacted sample that tested under unlocked-gap condition. Relative to the direction of the tensile stresses that developed due to the restriction provided in x-direction, only the cracks in y-direction corresponded to the tensile failure of the soil specimen (Figure 5.5). In the first drying, a primary crack was initially formed in x-direction subdivided the sample into two blocks. Afterward, a fully propagated crack in the y-direction was formed approximately after 28.5 hours from the beginning of the test. When drying proceeded more cracks propagated in the same direction. Upon wetting, the water inundation resulted in healing and closure of some of the visible cracks that formed in the first drying. It seems that the crack network helped the water to penetrate readily without

changing of the patterns and that resulted in closure of some cracks. In the second drying, the large cracks that previously formed in the first drying reopened and more cracks developed. Also, it was observed that more cracks propagated over cycles.

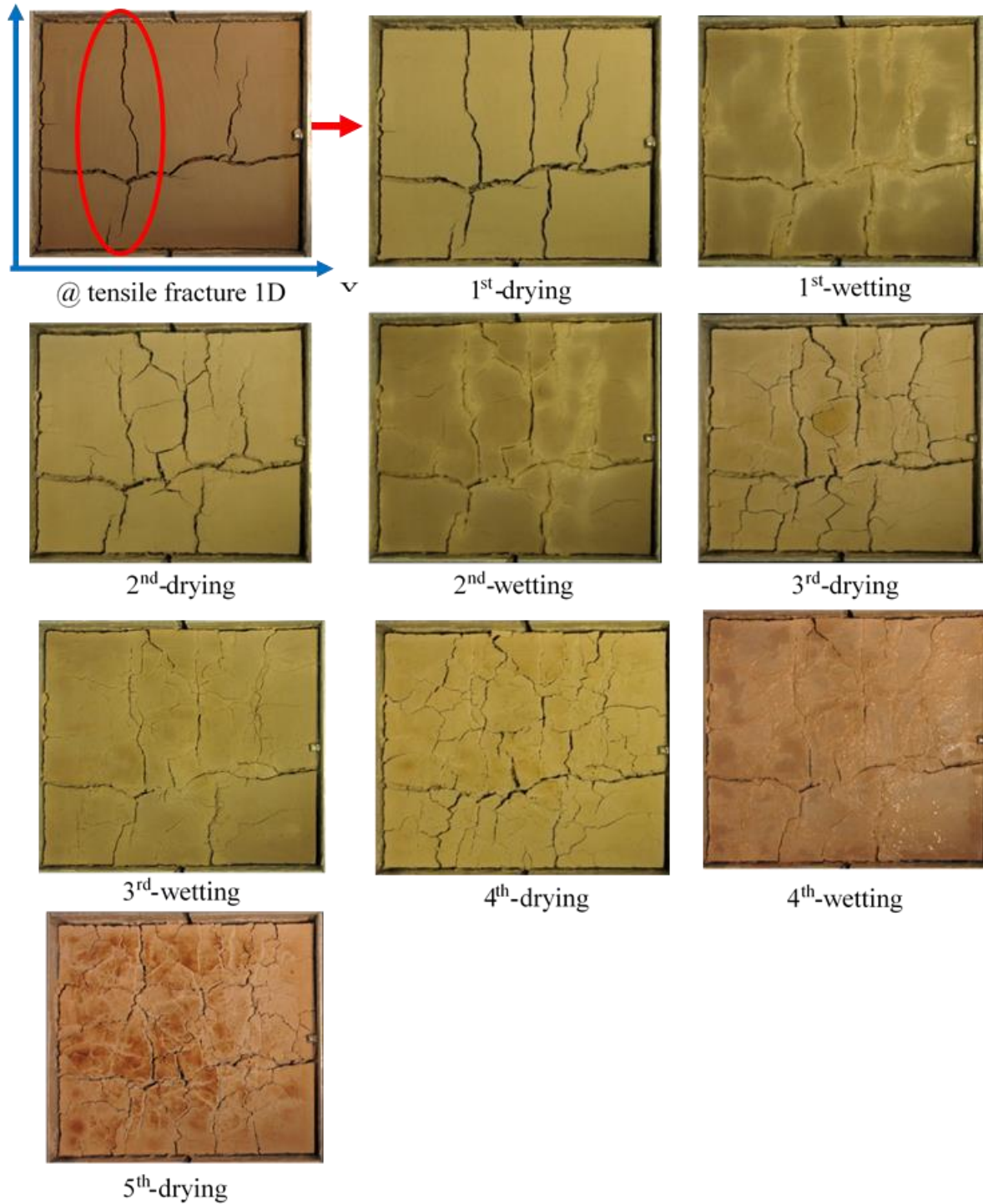


Figure 5.13 Crack patterns of MC-U specimen subjected to the new tensile test in cyclic wetting/drying

The soil specimen experienced crack propagation when subjected to alternatives wetting/drying cycles with the maximum CIF of about 5% at the end of the third drying. After the third drying (i.e., fourth and fifth drying), the soil sample exhibited a reduction in the CIF's, as shown in Figure 5.14. Almost constant CIF's were determined at the end of the wetting processes (CIF = 2%). For every drying/wetting cycle, the average crack aperture was calculated by averaging the widths of all cracks observed on the surface. Upon wetting process, it was observed healing some of the current cracks and then when subjected to the next drying, new cracks formed. Figure 5.14 shows the variation of Crack Intensity Factor (CIF) and crack aperture during wetting/drying cycles. For the drying cycles, CIF and crack aperture increased up to the third drying, then decreased in the fourth and fifth drying. While during wetting, CIF is nearly constant while the crack aperture gradually decreased. The increase of the CIF in the fourth and fifth cycles are consistent with the results of tensile strength; the strength decreased up to third drying and then increased in the fourth and fifth cycles.

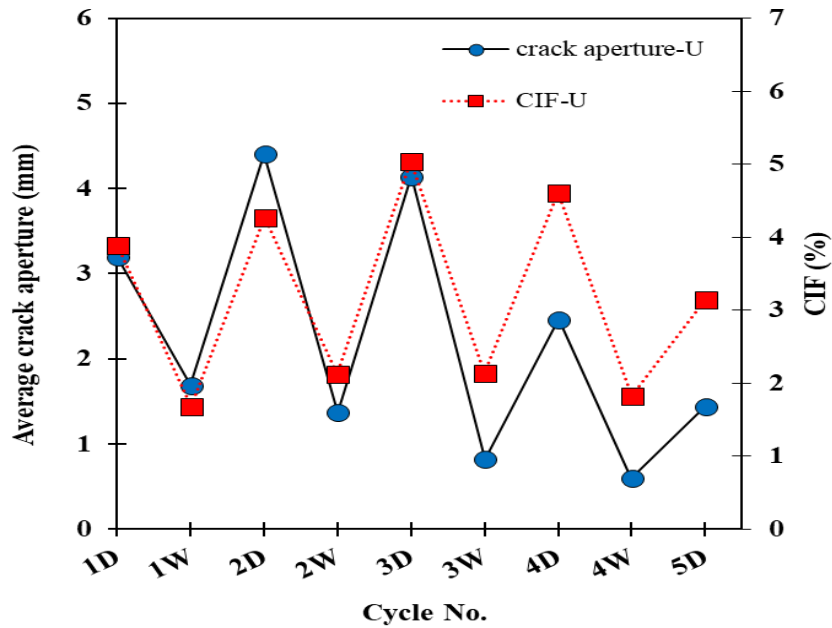


Figure 5.14 Variation of CIF and average crack aperture over wetting/drying cycles of unlocked-gap specimen

5.4.2 Results of locked-gap test

The soil specimen (MC-L) was subjected to five wetting/drying cycles. The variation of water content over time during drying is presented in Figure 5.15. The water content gradually decreased over time till approached equilibrium at the end of drying process. For wetting, the sample was wetted to water content similar to the initial water content-as compacted.

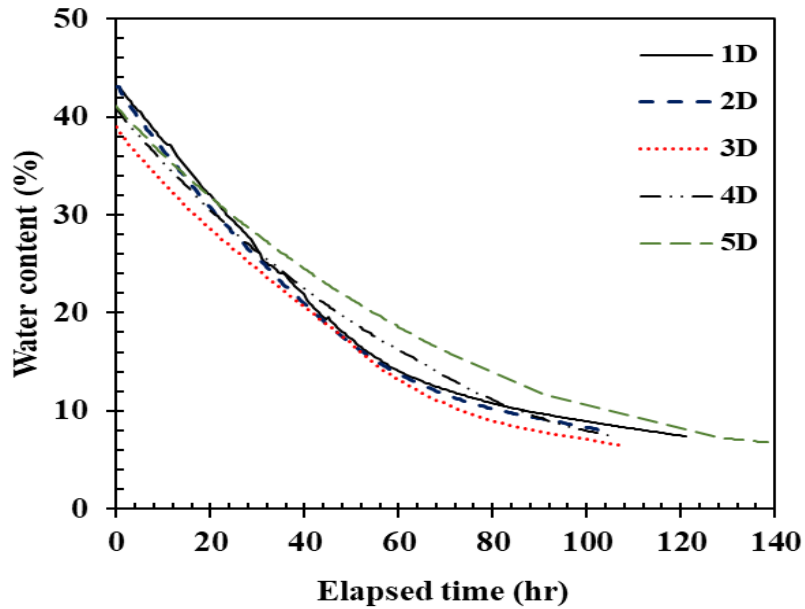


Figure 5.15 Variation of water content over time for the compacted specimen (MC-L) during drying processes; D: Drying

The variations of void ratio and volume of soil specimen were provided in Figure 5.16 (a & b) for a given change in water content for shrink paths through drying cycles. Similar to the unlocked-gap results, the primary volumetric change occurred between the saturation lines of 80 % and 50 %, and this is similar to experimental results published by Tripathy et al., (Tripathy et al., 2002).

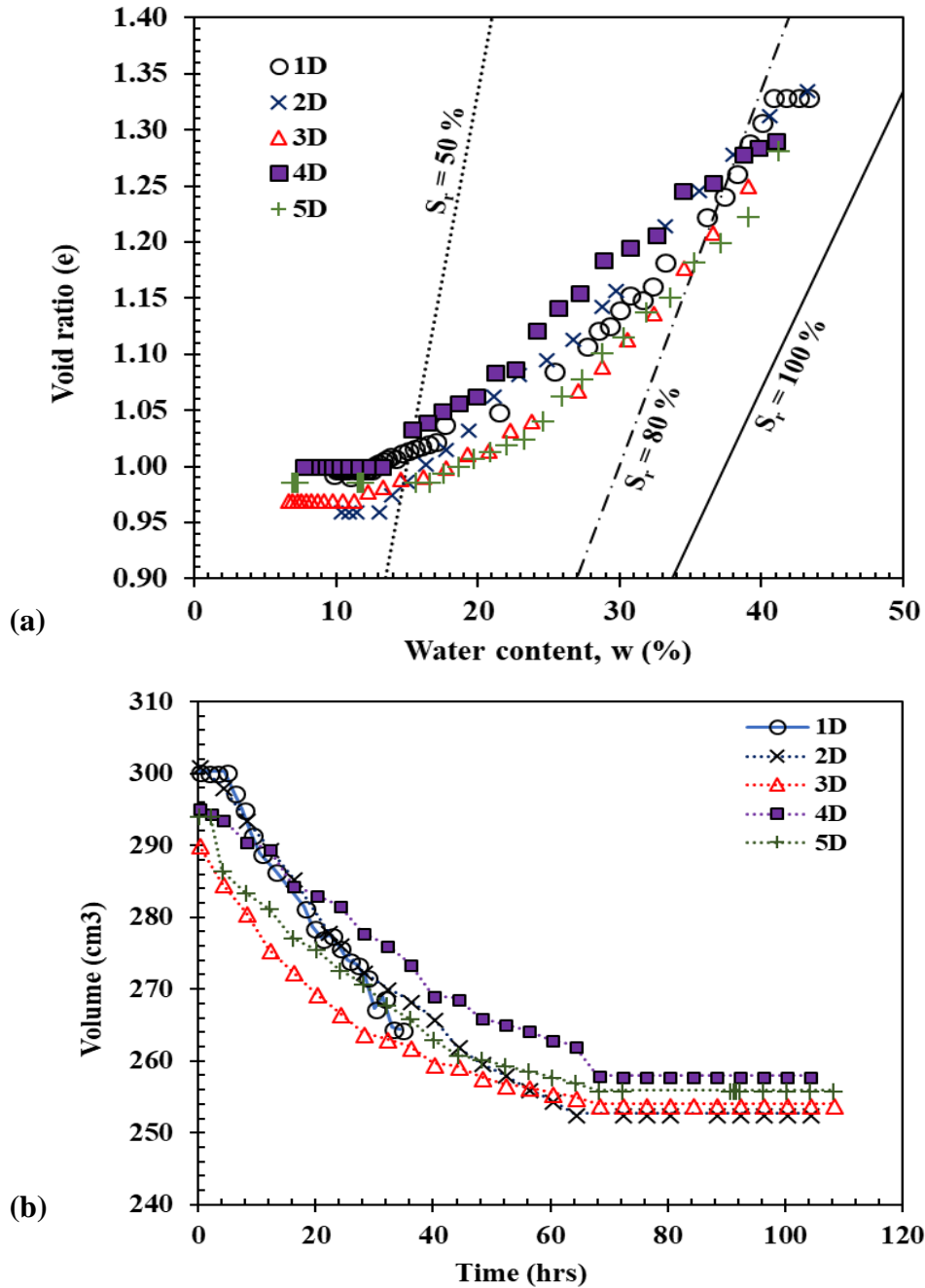


Figure 5.16 Variation of (a) void ratio vs. water content, and (b) soil's volume over time

5.4.2.1 Effect of drying/wetting cycles on tensile tests

Figure 5.17 presents the variation of tensile forces over time during drying processes. Figure 5.18 shows the developing of the lateral-induced expansion forces (LIEF) when the soil subjected to wetting. All drying curves have similar trends to those of unlocked-gap sample in which the curves decreased to almost constant values till approached the equilibrium. The variations of tensile forces as functions of degree of saturation and water content through drying cycles are presented in Figure 5.19 (a & b), respectively. For all drying cycles, the specimen exhibited tensile failure at nearly similar degree of saturation within the range between 73% to 68 % and the corresponding water content over a range of 29 % to 31.5 %. The results show that the soil experienced much higher tensile strength in the first drying than that of the other cycles (Figure 5.20 and Figure 5.21).

In the first drying, the soil sample experienced much higher tensile force compared to the other drying processes. The tensile forces gradually increased up to the peak value and then decreased when drying proceeded and the cracks fully propagated. Upon wetting, the soil sample exhibited a quick reduction in the tensile force in very short time. After that, the soil developed lateral-expansion forces due to swelling/expansion where healing and closure of some crack openings were observed. In general, the soil exhibited much lower tensile forces in the other six drying cycles compared to that one of the first drying, and this trend similar to that one captured for the unlocked-gap specimen. In addition, it was determined that the tensile strength increased again after the third drying similarly to unlocked-specimen.

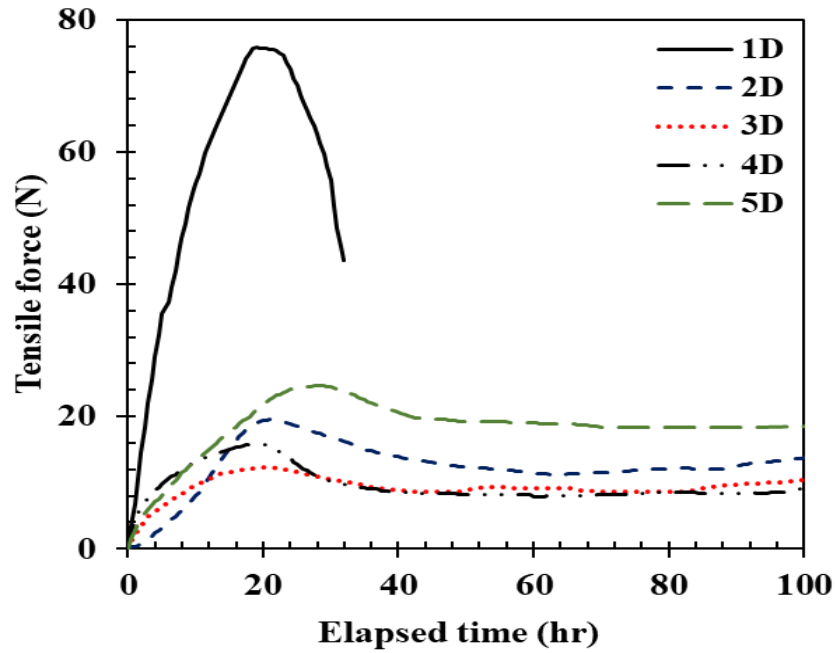


Figure 5.17 Variations of tensile forces over time for the compacted specimen (MC-L) during five drying cycles; D: Drying, L: Locked-gap after failure

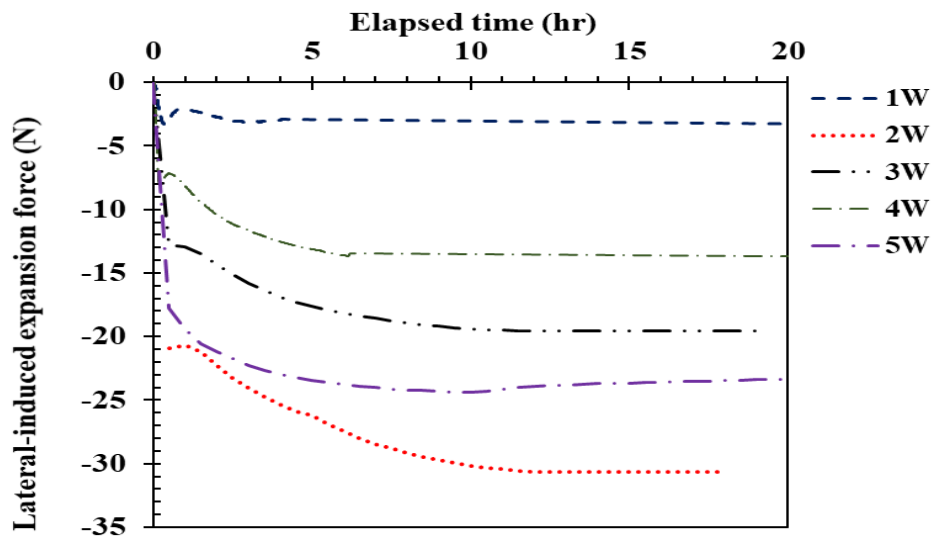


Figure 5.18 Variation of lateral-induced expansion forces over time for the compacted specimen (MC-L) during wetting cycles; W: Wetting, L: Locked-gap

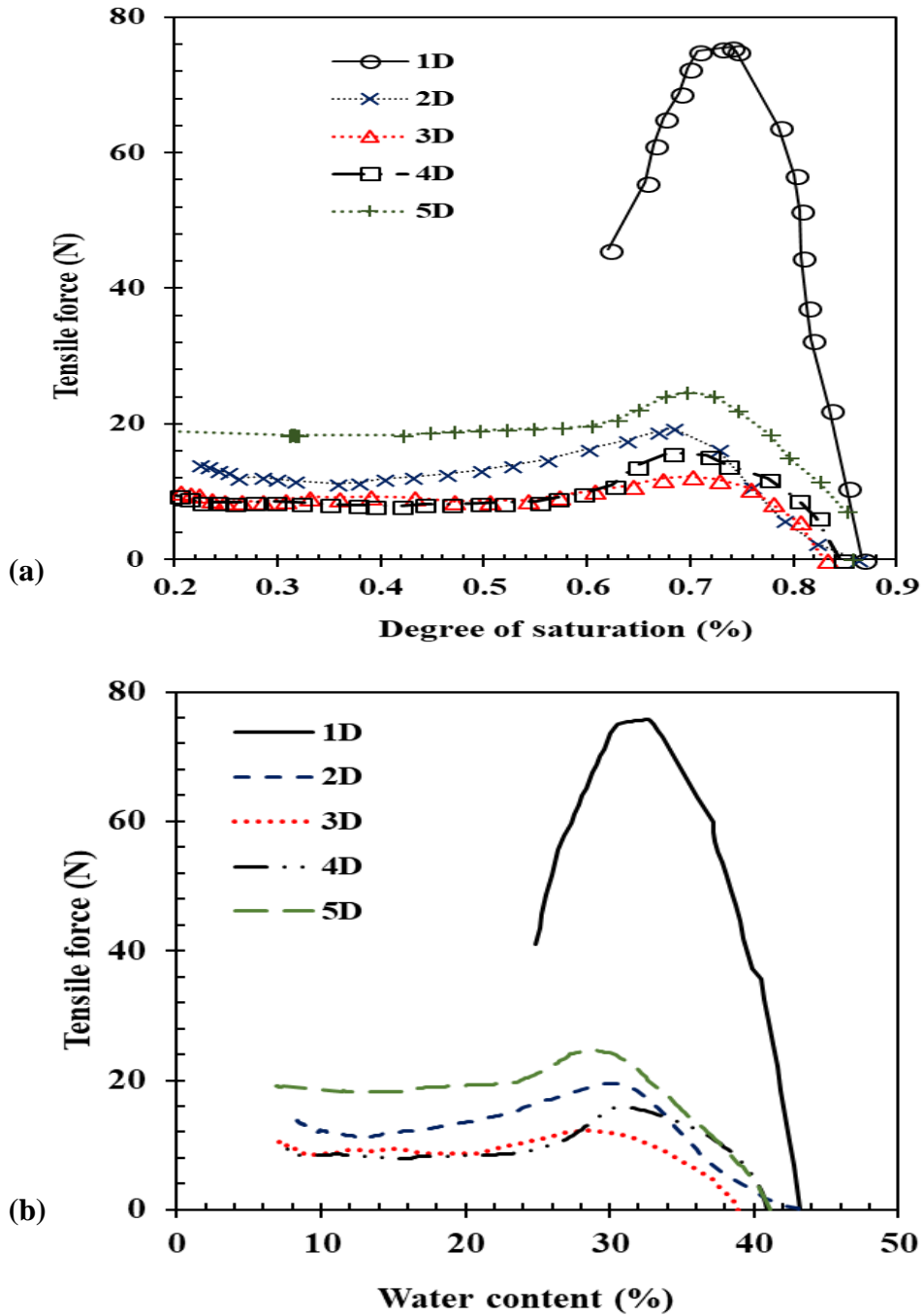


Figure 5.19 Variations of tensile forces with changes of (a) degree of saturation and (b) water content for MC-L during drying cycles; D: Drying,

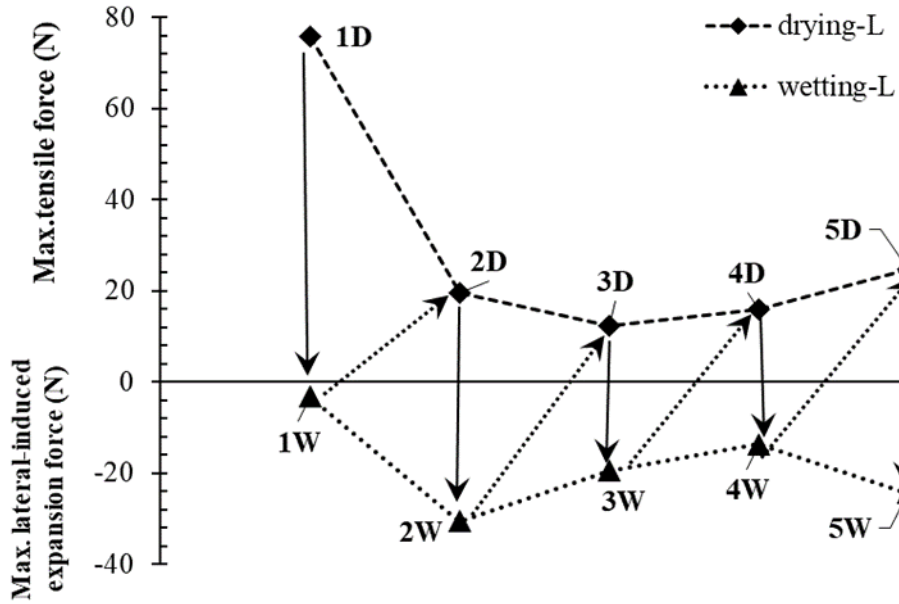


Figure 5.20 Variation of max. tensile and lateral-induced expansion forces over cycles for MC-L; D: Drying, W: Wetting, L: Locked-gap after failure

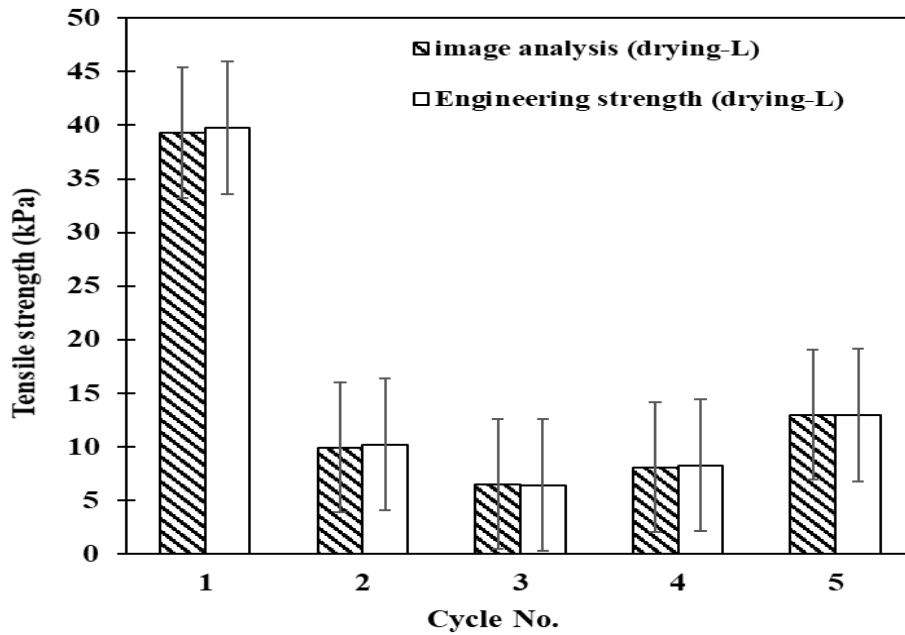


Figure 5.21 Variation of tensile strengths over cycles for MC-L; D: Drying, L: Locked-gap after failure

5.4.2.2 Effect of cyclic drying/wetting on cracking

Figure 5.22 and Figure 5.23 present the crack patterns at the end of every drying/wetting cycle of the compacted sample that tested under locked-gap condition. Similar to the unlocked-gap soil sample, a crack was initially formed in x-direction and then another primary crack formed in the y-direction which fully propagated after 24.5 hours. When drying proceeded more cracks propagated in the same direction. Upon wetting, the water inundation resulted in healing and closure of some of the visible cracks that formed in the first drying. In the second drying, the large cracks that previously formed in the first drying reopened and more new cracks developed. More cracks propagated when the soil specimen subjected to the next wetting/drying processes.

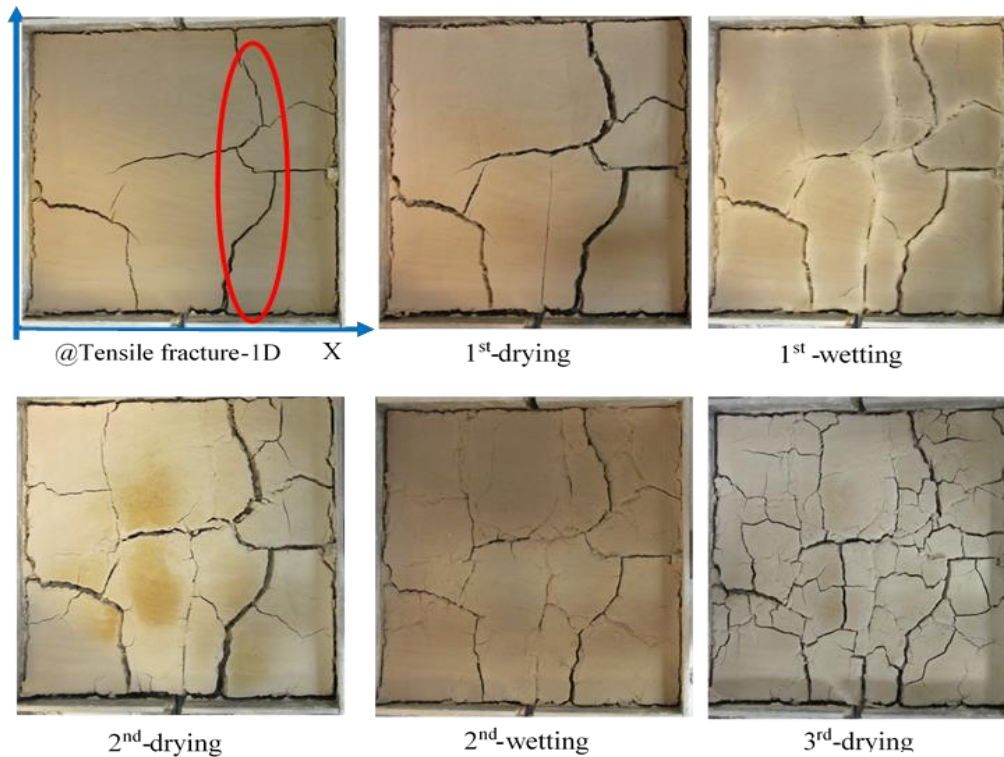


Figure 5.22 Crack patterns of the compacted sample (MC-L) subjected to cyclic wetting/drying in the new tensile test,

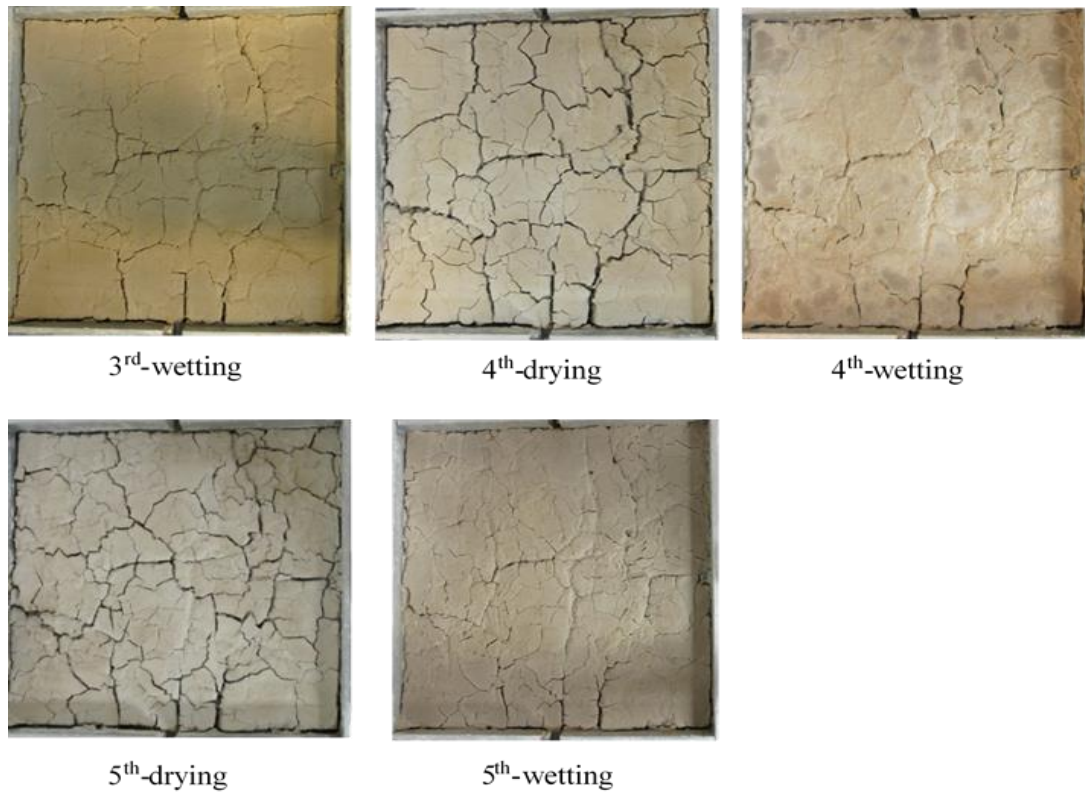


Figure 5.23 Continued: crack patterns of the compacted sample (MC-L) subjected to cyclic wetting/drying in the new tensile test

It was clearly observed the influence of alternative wetting/drying cycles on desiccation cracking of the soil sample. The maximum CIF was determined about 6 % at the end of the third drying. After the third drying, the soil sample generally exhibited a slight reduction in the CIF's. Figure 5.24 shows the variation of Crack Intensity Factor (CIF) and crack aperture during wetting/drying cycles. For the drying cycles, nonlinear trend is obtained for CIF and crack aperture where both increased up to the second drying, then decreased largely in the fourth and fifth cycle.

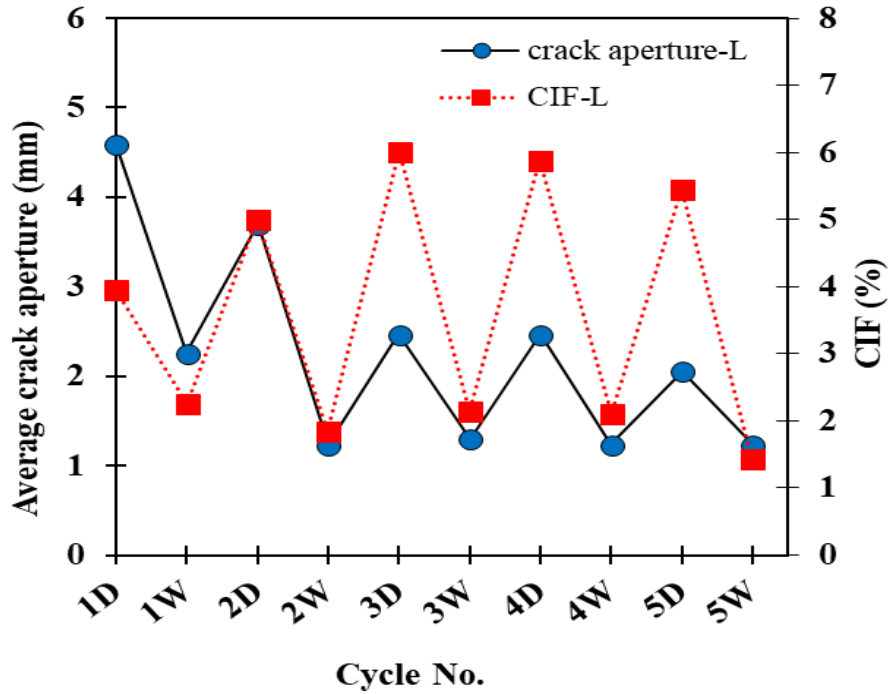


Figure 5.24 Variation of CIF and average crack aperture over wetting/drying cycles of locked-gap specimen

5.4.3 Comparison between the unlocked and locked-gap tests

Two identical soil specimens were tested under two different conditions in order to examine the acceptability and validity of the new tensile testing method. One test was performed with maintaining the gap unlocked between the two halves of the tensile device during the drying/wetting cycles. The other one was performed with locking the gap by using two screws after the failure where the maximum tensile force was determined. For the locking test, the load sensor was disconnected at the end of every wetting/drying cycle, and then reconnected before the start of the next process. The main purpose of this was that to start every drying and wetting process

with zero/null force. Also, to allow the cracks to propagate after failure without the effect of gap existence.

Figure 5.25 shows a comparison between the variation of the tensile strengths of the unlocked and locked-gap tests during multiple drying/wetting cycles. The results of the first drying cycle show that the tensile strength of the locked-gap specimen is higher than that of the unlocked-gap one. While the tensile strengths of unlocked-specimen are higher than those of the locked-gap specimen in the other drying processes (second, third, fourth and fifth drying). For each drying cycle, the reduction in tensile strength was calculated relative to that one of the first drying, as follows:

$$\textit{Reduction in tensile strength} = \frac{\sigma_{t_1} - \sigma_{t_n}}{\sigma_{t_1}} \quad (5.1)$$

where σ_{t_1} is the tensile strength in the first drying (kPa), σ_{t_n} is the tensile strength in (n) drying cycle (kPa); for example, $n = 2, 3, 4, \dots$ etc. Figure 5.26 presents the reduction in the tensile strength of unlocked and locked-gap specimens. Both tests almost give similar expressions where non-linear reduction in the tensile was obtained.

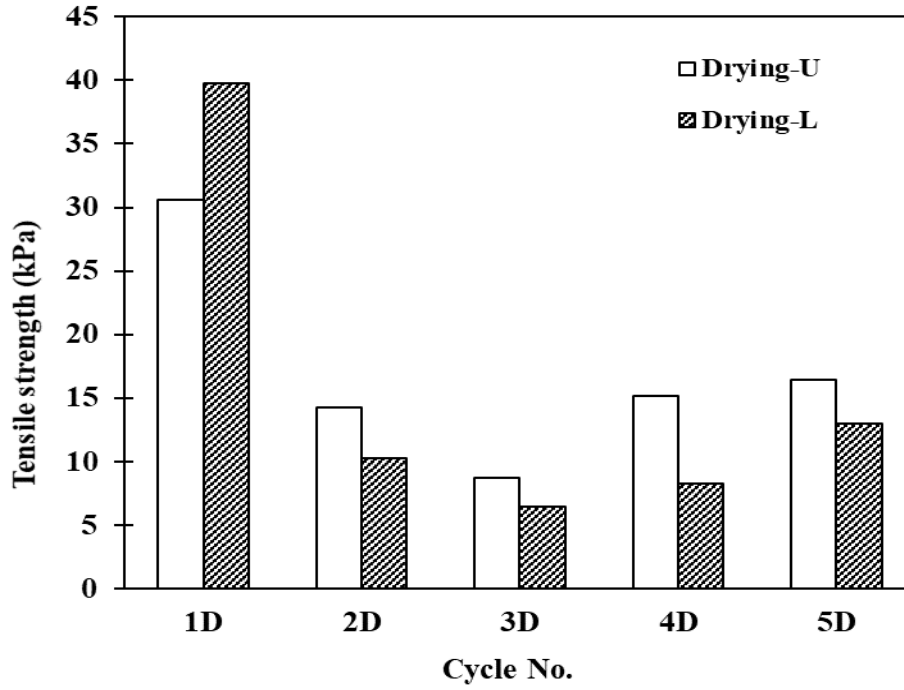


Figure 5.25 Variations of tensile strength of unlocked and locked-gap compacted specimens subjected to several wetting/drying cycles

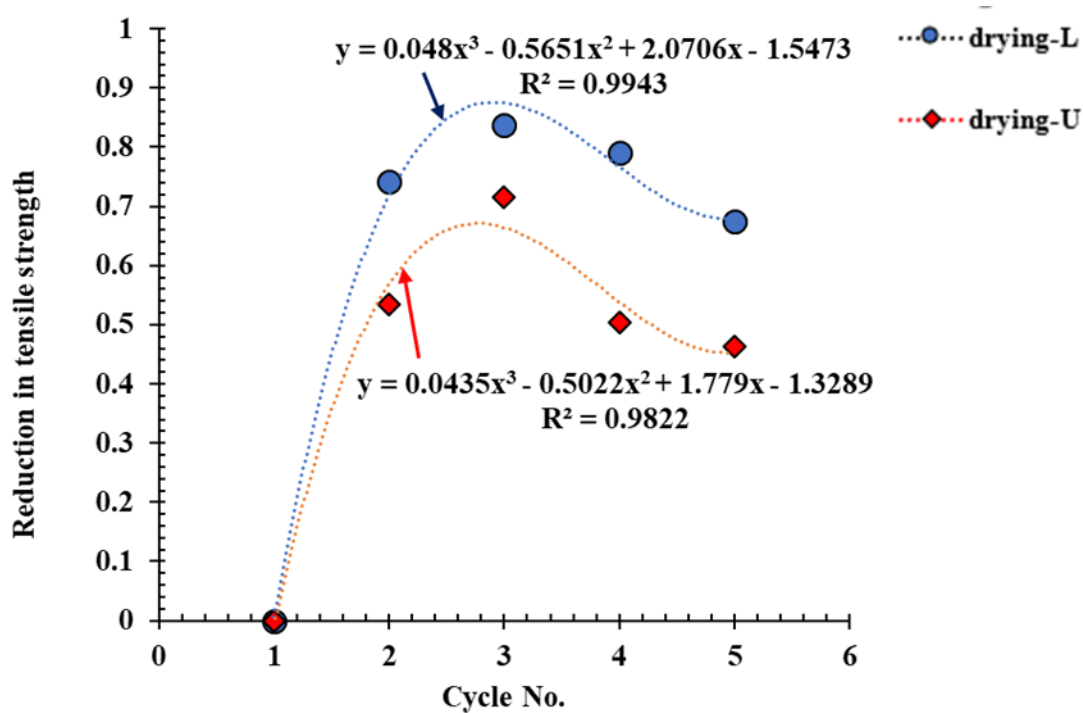


Figure 5.26 Reduction in tensile strength of unlocked and locked-gap specimens for all drying cycles

Moreover, comparative analysis is made between the two tests in the context of cracking patterns. The CIF's of the two tests are presented in Figure 5.27. The experimental data has been fitted and gives almost similar expressions. CIF(s) of the locked-gap test are higher compared to those of unlocked test, except for the first drying. This is consistent with the results of the tensile strength, where the locked-gap specimen experienced lower tensile strengths than those of the other one, and this caused in more cracks. Both tests have almost similar CIF values in the wetting cycles.

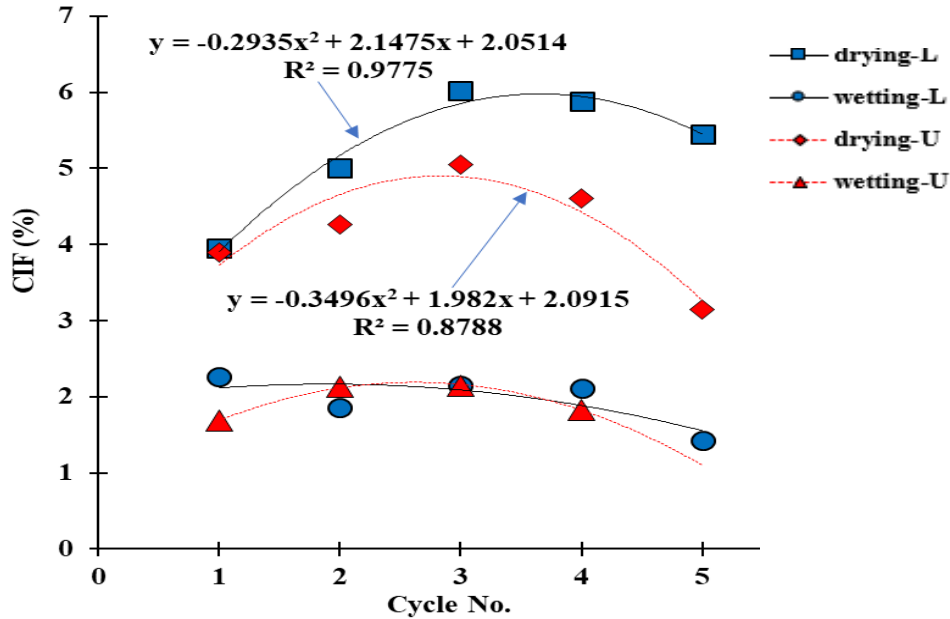


Figure 5.27 Variations of CIF's of unlocked and locked-gap compacted specimens subjected to several wetting/drying cycles

5.5 Digital Image Correlation (DIC) analysis

The new developed tensile test had been set up as described in section 5.3.2.1. This chapter presents a unique tensile-DIC test conducted on the soil mixture of 75% kaolin and 25% bentonite. The soil specimen was prepared at initial water content of about 45 % (+7% of optimum moisture content), dry unit weight of 10.25 kN/m³ (84 % of γ_{dmax} as determined from the standard Proctor test, ASTM D698), and degree of saturation of about 77.2%.

The best strategy to obtain high-quality images for DIC analysis is typically ensured by creating an appropriate speckle pattern on the soil's surface. In this study, the surface of the soil specimen was prepared for the DIC monitoring by applying speckle pattern. This was accomplished by using black aerosol paint sprayed from an appropriate distance and angle to achieve good prevalence and coverage, as shown in Figure 5.28. In this study, it was not applicable

to use seed particles, such as sand (Costa et al., 2008b) to create speckle pattern on the specimen's surface. The only reason is that when specimen wetted, the speckles leave their places in response to adding the water not in response of soil behavior. This leads to missing out the reference coordinates of the speckles, resulting in significant errors in the actual movement of the particles in response to soil behavior during wetting.

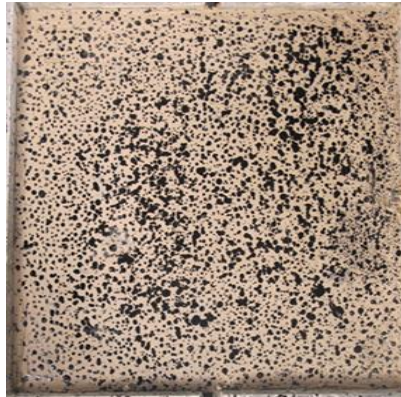


Figure 5.28 Speckle pattern on the surface of the soil specimen for tensile-DIC test

A digital camera (Canon Camera-Power Shot G11) with the highest resolution of (3648-pixel x 2736-pixel) was mounted directly above the soil specimen (perpendicularly) to capture a series of photos during the cyclic processes. Image capture was performed automatically by using remote control connected to the camera every 30 minutes during testing. Cold light sources were positioned to maintain high contrast of the speckle pattern on surface during testing. The variations of water mass during drying and wetting cycles were determined by placing the tensile device on the top of an electronic balance with the maximum capacity of 8100 g and repeatability of 0.01 g. The complete set-up of the new tensile DIC test described in Figure 5.29.

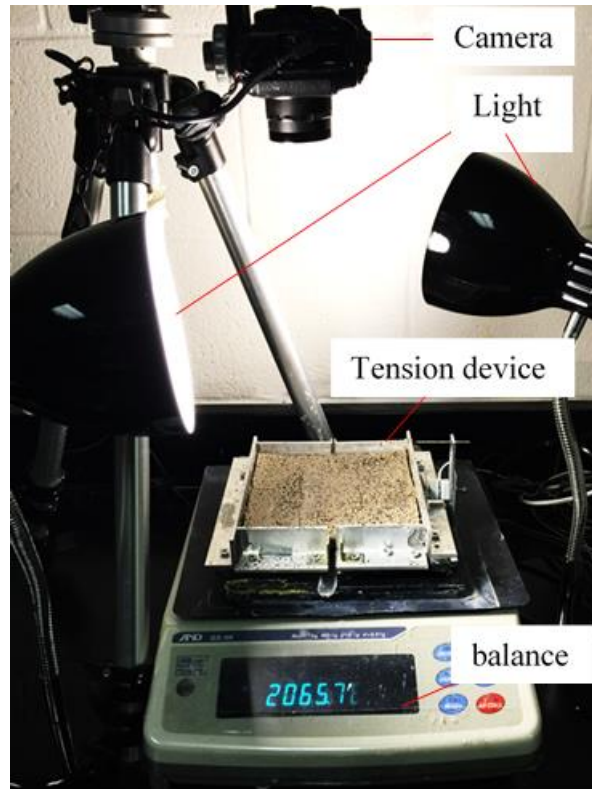


Figure 5.29 The new tension-DIC test set up

5.5.1 Image processing for DIC analysis

A series of digital images were taken for every wetting/drying process for measuring the displacement fields at different time intervals, particularly at tensile fracture. For DIC analysis, the reference image was taken at the beginning of the wetting or drying process, and then all the images were captured every 30 minutes. Initially, the TrueColor/RGB images were processed by using *Image J* software to be prepared for DIC based-MATLAB analysis. Firstly, the digital image (TrueColor/RGB) of soil sample was converted to a grayscale image. The grayscale image was obtained by converting the image to the type of 8-bit. Afterward, the background of the image had

been subtracted from the image. Then, the grayscale image was converted to a binary black-and-white (B & W) image. The image processing procedure is described in Figure 5.30.

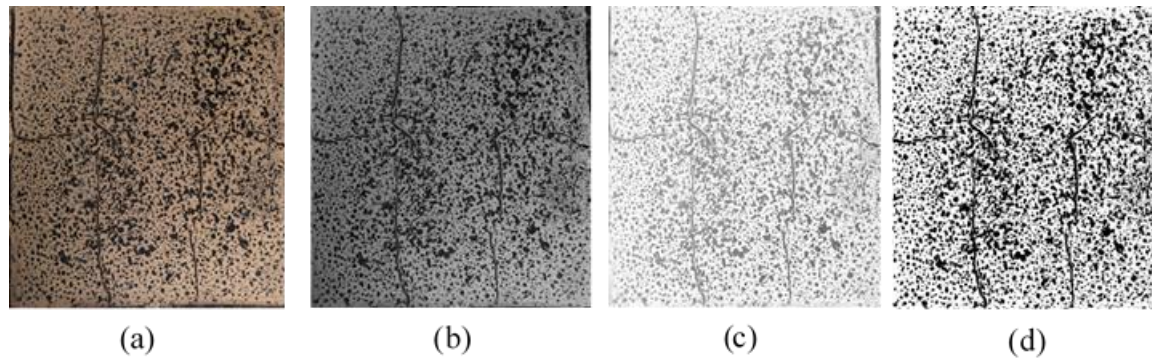


Figure 5.30 Image processing for PIV analysis; (a) TrueColor/RGB image, (b) grayscale (8 bit), (c) subtract background, (d) binary

5.5.2 Results of tensile tests

The new tensile testing was used to study the impact of wetting/drying cycles on tensile and cracking behavior using DIC analysis. A high expansive soil was subjected to sequential wetting/drying cycles, tensile stresses generated during drying due to the restrictions provided at the soil bed. Constraints were provided at the soil bed through rectangular protrusions fabricated in such a way for allowing the force sensor to measure the tensile stresses that were expected to be largest. While no tensile stresses were expected to be in the other direction. During drying, the first crack initiated in which no tensile stresses were expected. Over time, more cracks propagated in which the tensile stresses were expected to be largest and then fully propagated when tension failure occurs. Full displacement fields have been developed for representative the tensile tests of

the soil. The compacted soil specimen used in the DIC analysis is referred to “Mixture-Compacted” (MC-DIC).

The soil specimen (MC) was subjected to wetting/drying cycles. The variation of water content over time during drying is presented in Figure 5.31. Similar trends were observed for all drying curves indicating the gradual reduction of the water content over time till approached equilibrium state at the end of drying process. For wetting process, the sample was wetted to water content nearly similar to the initial water content-as compacted.

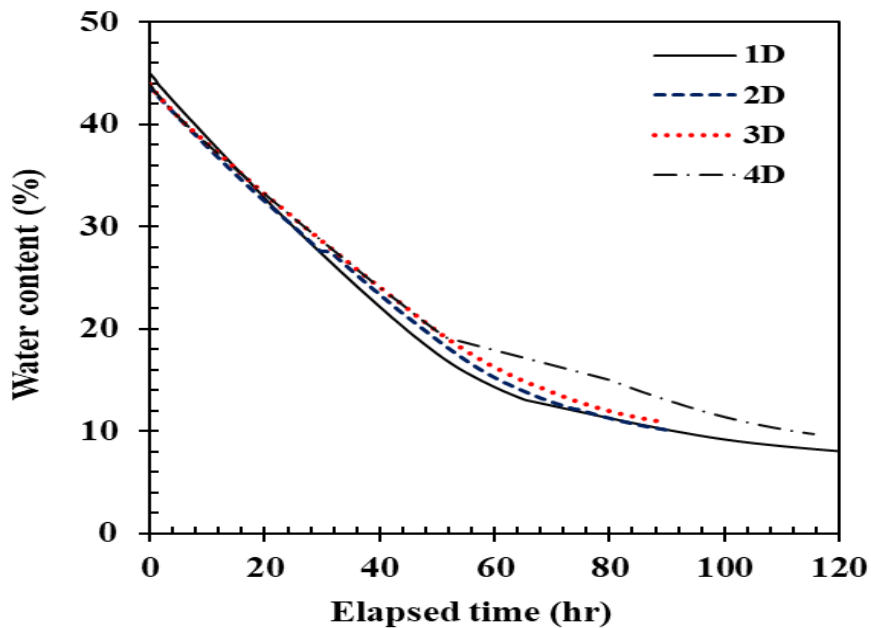


Figure 5.31 Variations of water content over time for the compacted specimen (MC3-DIC) during drying processes; D: Drying

The variation of tensile and compression forces over time through drying and wetting processes are presented in Figure 5.32 and Figure 5.33, respectively. Similar trends of all tensile curves are observed indicating gradual increase of tensile force overtime till approached to the

peak value at failure and then a reduction till maintained a residual tensile value due to locking the gap between the free and fixed parts of the device. In general, MC3-DIC specimen nearly exhibited similar tensile behavior to that of specimens previously tested under similar scenarios in the previous chapter.

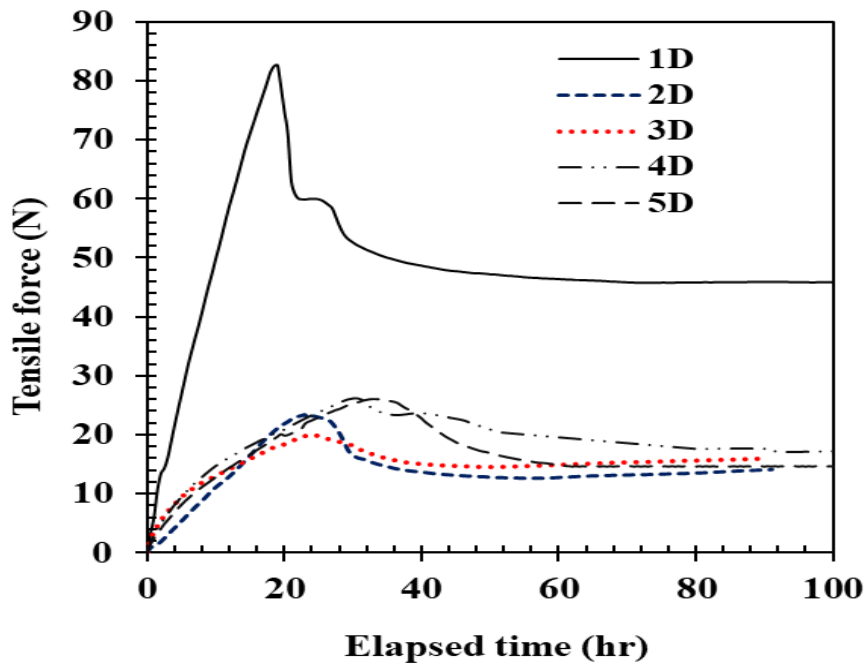


Figure 5.32 Variation of tensile forces over time for the compacted specimen (MC3-DIC) during drying cycles; D: Drying

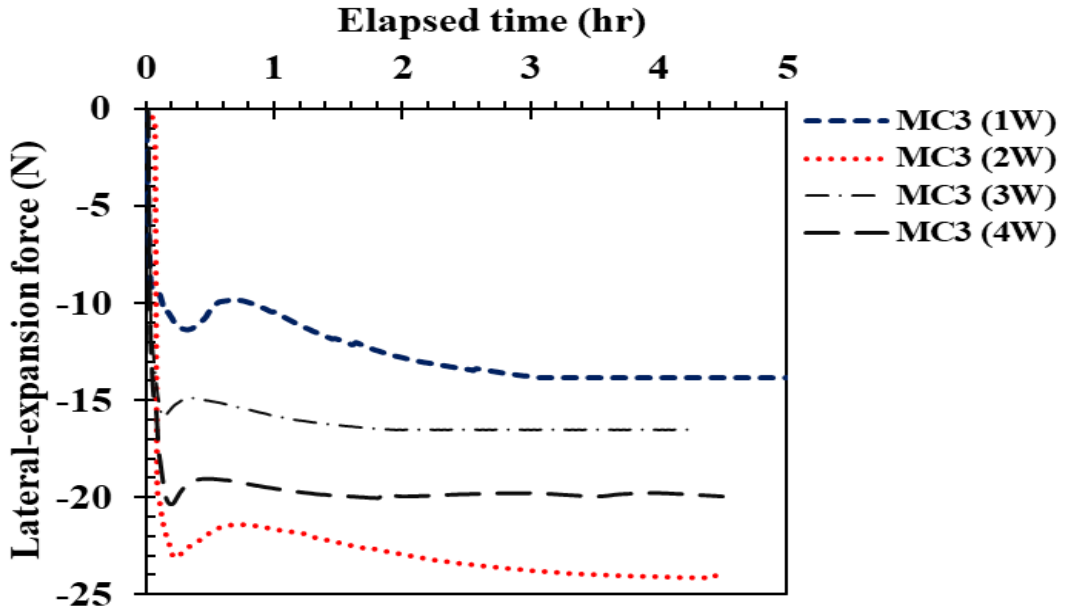


Figure 5.33 Variation of compression forces over time for the compacted specimen (MC3-DIC) during wetting processes; W: Wetting

Figure 5.34 shows the variation of tensile forces as a function of water content during drying. The inception of cracking is determined at the cracking water content of the specimen coincided with the water content at the peak tensile forces. It was found that the cracking water contents of the specimen are obtained over the range of 29.4 % to 33.89 %.

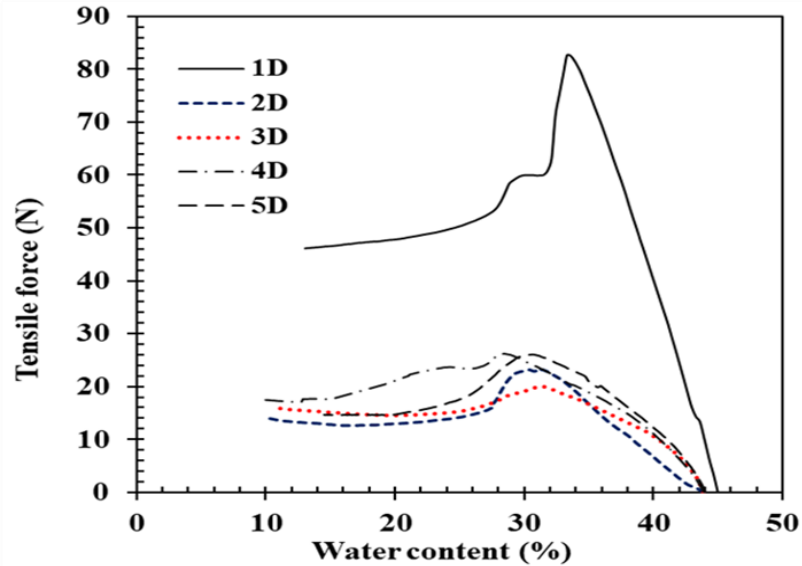


Figure 5.34 Variations of tensile forces as a function of water content for the MC3-DIC during drying processes; D: Drying, locked-gap after failure

The lateral shrinkage and the vertical change in the thickness of the soil specimen were calculated at failure to be insignificant compared to the initial state of the specimen. Based on that, the cross-sectional area change was neglected, so that the tensile strength was calculated by dividing the peak tensile force by the initial cross-sectional area of the specimen. Figure 5.35 shows the variation of tensile strength of MC3-DIC specimen during drying processes.

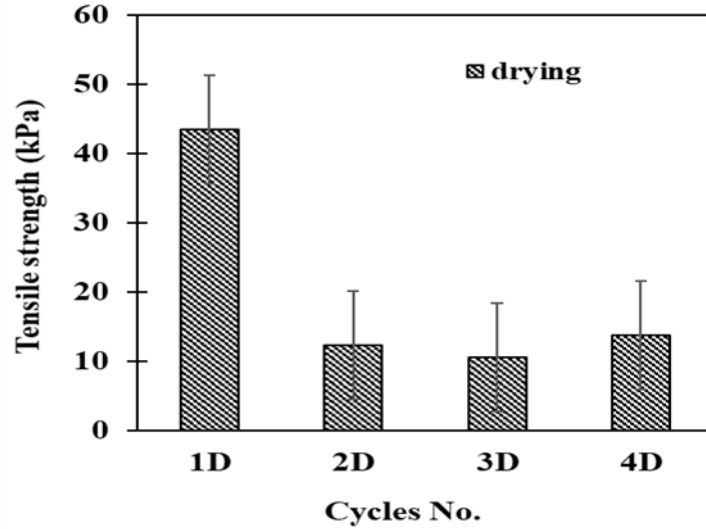


Figure 5.35 Effect of wetting/drying cycles on tensile strength of the compacted specimen (MC3-DIC)

Soil specimen (MC3-DIC) exhibited the largest tensile strength in the first drying (Figure 5.35). The tensile force gradually increased over time till approached to the peak value at failure and then a residual tensile value maintained due to locking the gap between the free and fixed parts of the device. Similar trend was observed in all drying processes.

Upon wetting, the soil sample exhibited an instantaneous decrease in the tensile force, and then compression forces developed due to swelling/expansion in which healing and closing of some crack openings were observed. The largest compression force was determined in the second wetting process indicating in which largest expansion was obtained.

It is believed that the soil structure (fabric and the inter-particle forces) was exposed to large deteriorations during the first drying. This may cause irrecoverable deformations in the soil structure and as a result a reduction in the tensile strength. In third drying, the soil sample exhibited

slight decrease in the tensile strength compared to the second drying. While the tensile strength increased again in the fourth drying.

5.5.3 Digital Image Correlation (DIC) results

Full displacement fields have been developed for representative tension tests of a soil specimen tested in the new tensile device and subjected to drying/wetting cycles. The displacement fields are determined at time series to illustrate the development of soil cracking during drying. Every wetting/drying cycle, the displacement fields are provided. Within each time series, similar scale has been used. Figure 5.36 (a)-(d) presents the behavior of the specimen after 6 hours from the first drying. Initially the specimen was shrinking more in the longitudinal direction (parallel to the gap) than the lateral one. This is clearly observed from the large displacement vectors in the longitudinal direction (parallel to the gap) and the small ones in the lateral direction (orthogonal to the gap). This is due to having the protrusions in the longitudinal direction in which the free movement was allowed, while restrained in the lateral direction. In the early stage of the drying time, the cracks initiated at which the displacement vectors became in opposite direction.

While drying proceeded, the displacement vectors in Figure 5.37 depict more closely isotropic shrinkage of the specimen. However, more large displacement vectors are obtained in the longitudinal direction than the other one. Due to decreasing of moisture content and increasing of the corresponded suction, the soil's particles were allowed to rearrange themselves in the shrinkage process. This is attributed to the concept of the strain energy release. Any material has a strain energy stored by its particles in the closed system; once the particles allowed to rearrange their configurations due to any external process, such as thermal and chemical reactions, the strain energy will be released resulting in distortion or changing in the whole system. Figure 5.38

presents the crack dynamics when the specimen reached to the peak value in the tensile curve after 20 hours from the first drying. Figure 5.39 presents the crack widening after 21 hours from the beginning of the first drying period and after 1 hour when the failure occurred. In this stage, the displacement vectors showing the direction of soil particles and how the crack formed during drying process.

Figure 5.40 shows the disconnected displacement vectors surrounded the crack regions. In this stage, the soil particles continued their shrinking in nonuniform way with no more cracks formed. Figure 5.41 (a) –(d) presents the displacement fields immediately after the first wetting. The most interesting finding in that figure is that a longitudinal crack evolved immediately after the wetting process. It seems that when the soil subjected to drying process, the soil particles rearranged themselves in random configurations in which some defected regions may develop somewhere within the soil mass. Based on the concept of the uniform behavior of soil during compression or swelling, the stresses are equal in all directions. However, in our case, the stresses which represented by the displacement vectors are unequal, hence, this resulted in crack formation. As expected, more cracks developed and propagated in the second drying. This is consistent with the previous tensile result in which the specimen experienced much lower tensile strength and more crack propagated.

Figure 5.42 shows the displacement field vectors at the peak stage in the tensile curve. The configurations of the vectors indicate that the specimen didn't act as one mass during the second drying. On the contrary, the soil mass experienced discontinuity wherever the defected regions found. Therefore, the specimen exhibited lower tensile strength and more cracks compared to those of the first drying.

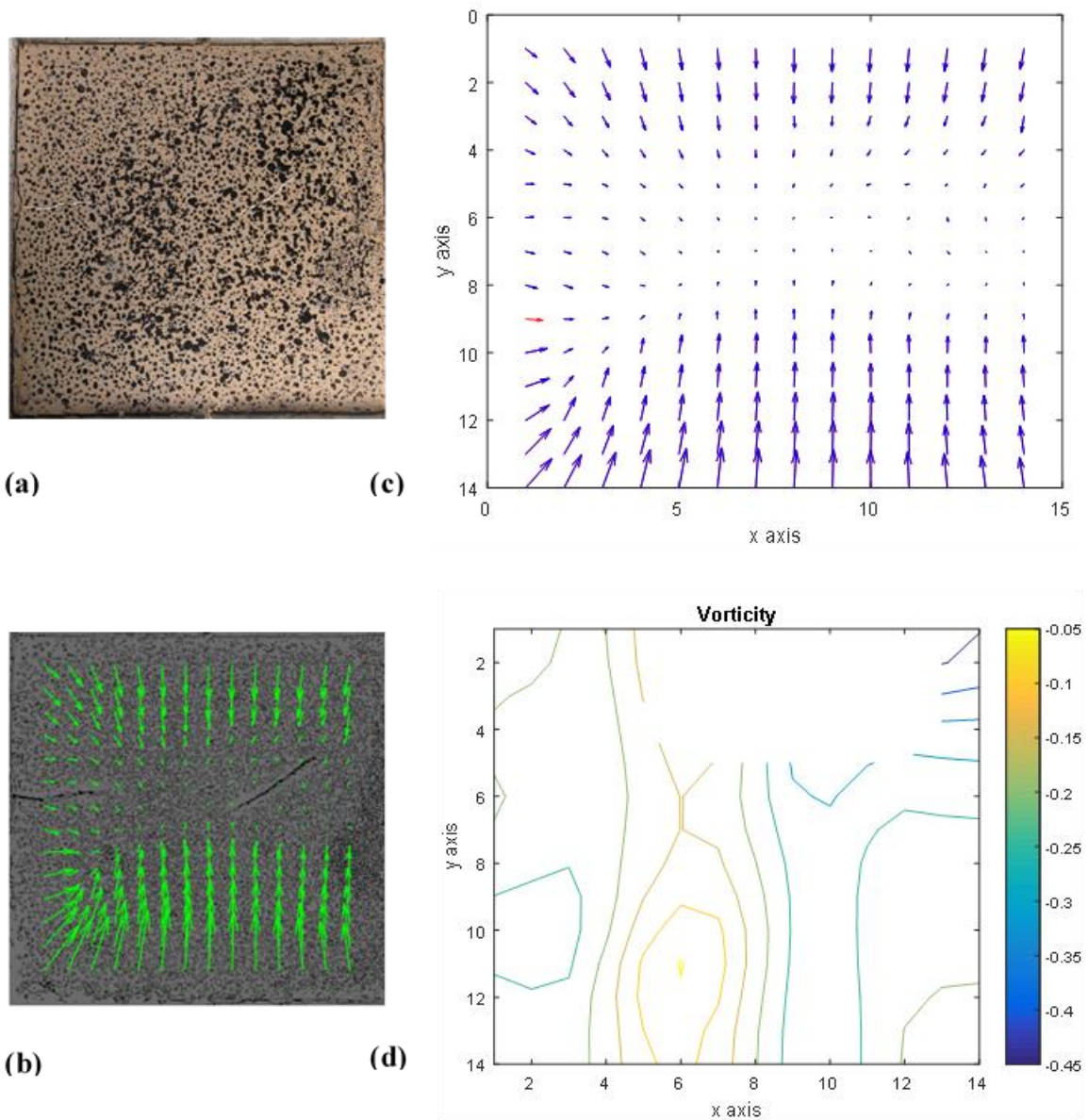


Figure 5.36 The tensile specimen when cracks initiated after 6 hours during 1st drying; (a) a true color photo; (b) specimen with displacement vectors; (c) displacement fields in x & y(pixels); (d) vorticity contours

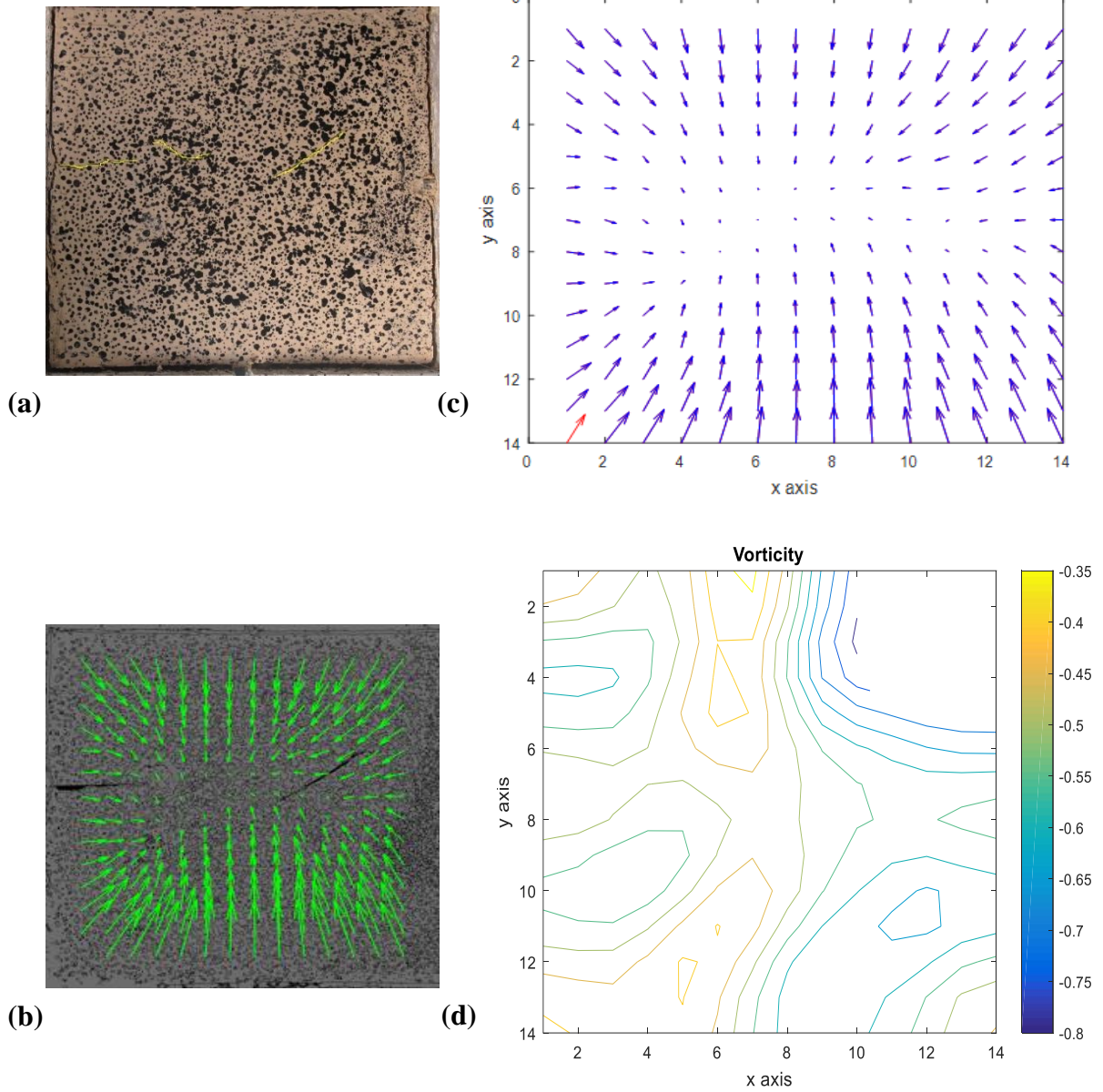


Figure 5.37 After $t = 10$ hours during 1st drying; (a) a true color photo; (b) specimen with displacement vectors; (c) displacement fields in x & y (pixels); (d) vorticity contours

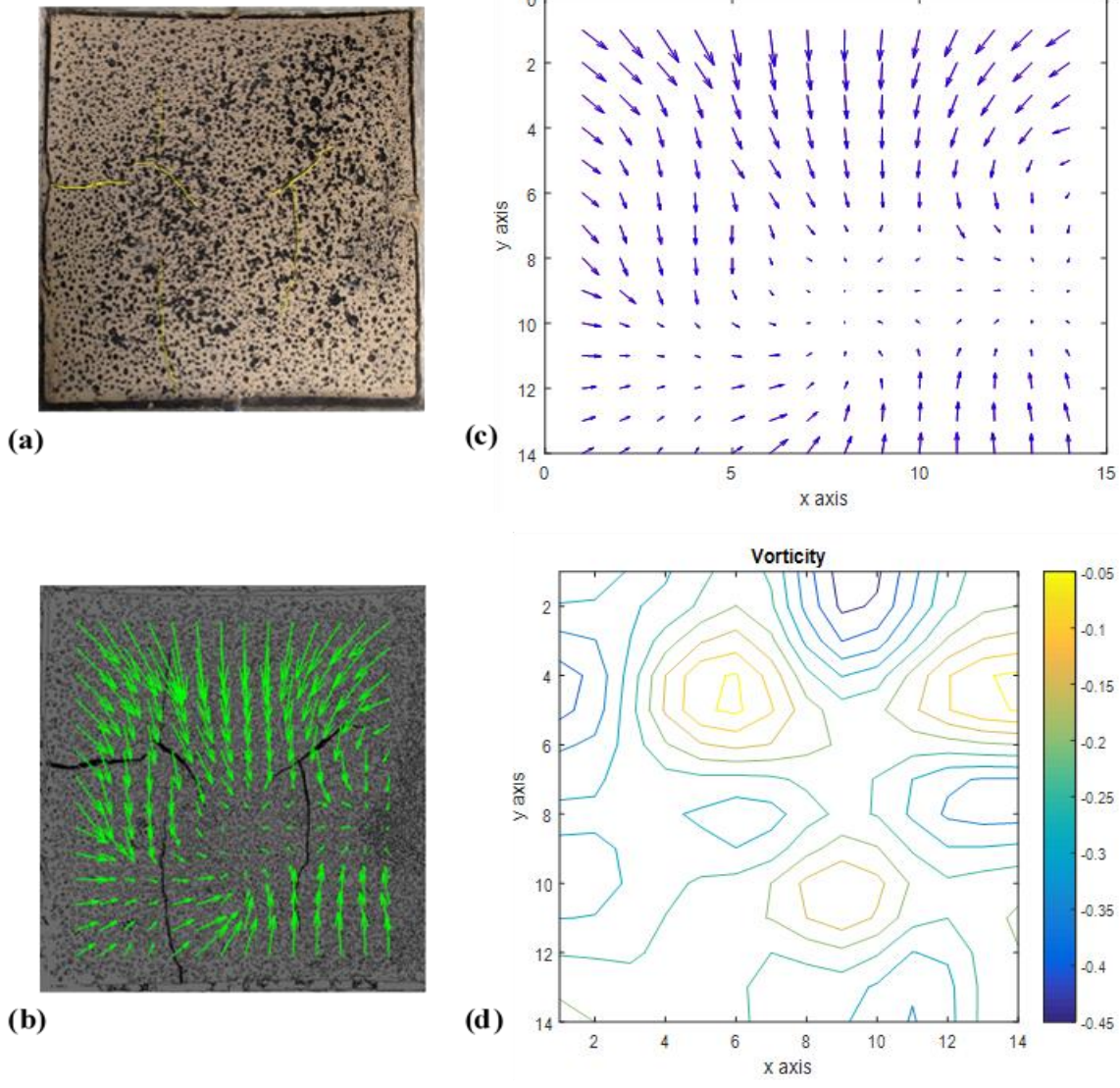
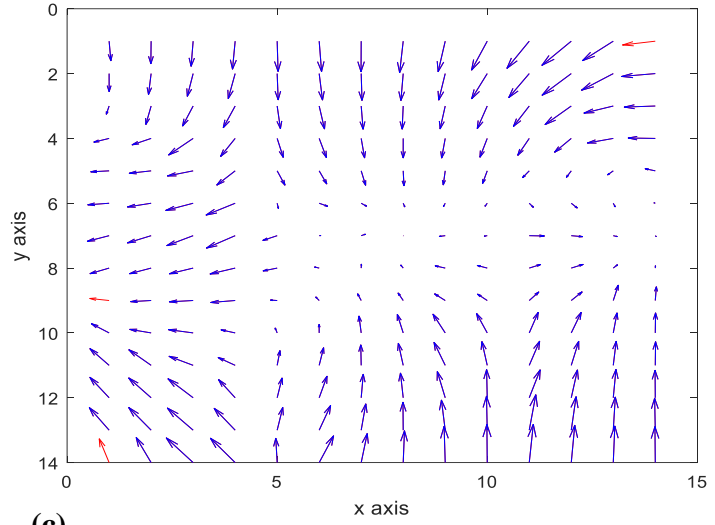


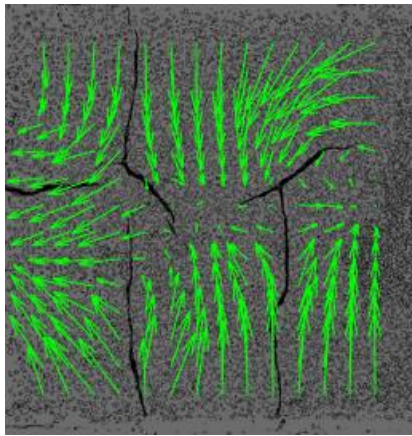
Figure 5.38 At the peak, after $t = 20$ hours during 1st drying; (a) a true color photo; (b) specimen with displacement vectors; (c) displacement fields in x & y (pixels); (d) vorticity contours



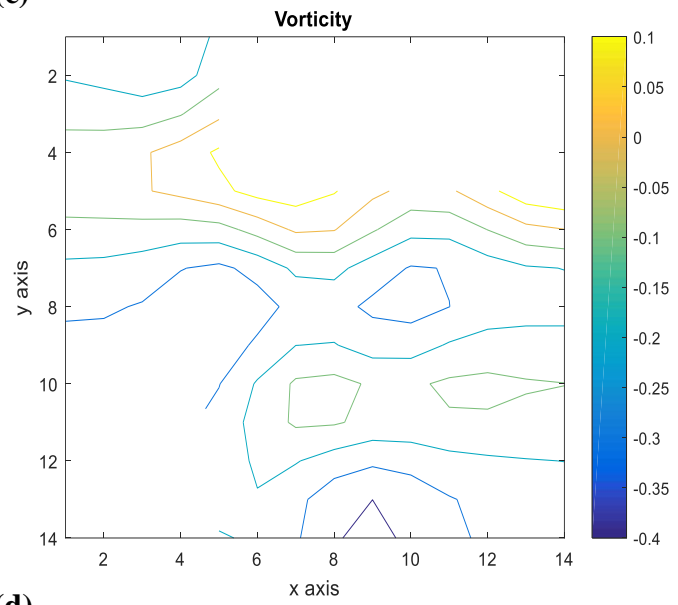
(a)



(c)



(b)

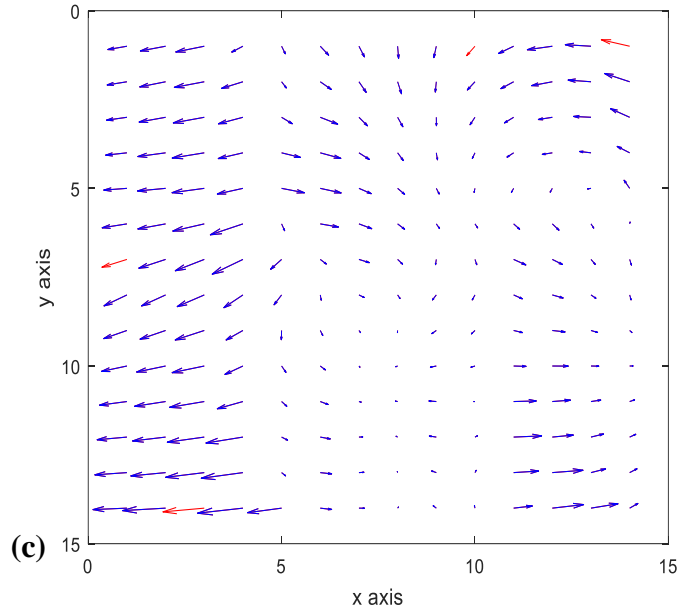


(d)

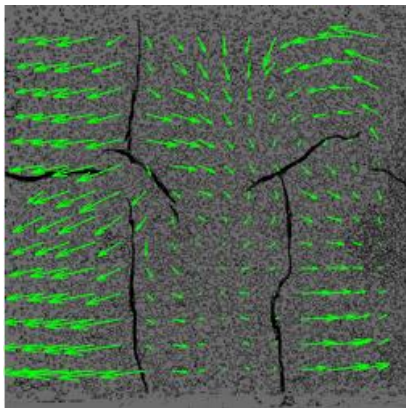
Figure 5.39 Crack widening after $t = 21$ hours from 1st drying; (a) a true color photo; (b) specimen with displacement vectors; (c) displacement fields in x & y (pixels); (d) vorticity contours



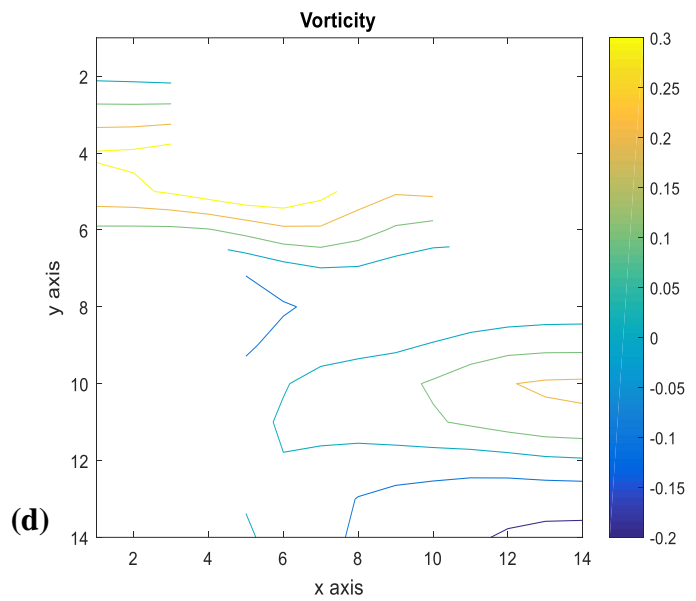
(a)



(c)



(b)



(d)

Figure 5.40 Fully crack propagated at the end of 1st drying; (a) a true color photo; (b) specimen with displacement vectors; (c) displacement fields in x & y (pixels); (d) vorticity contours

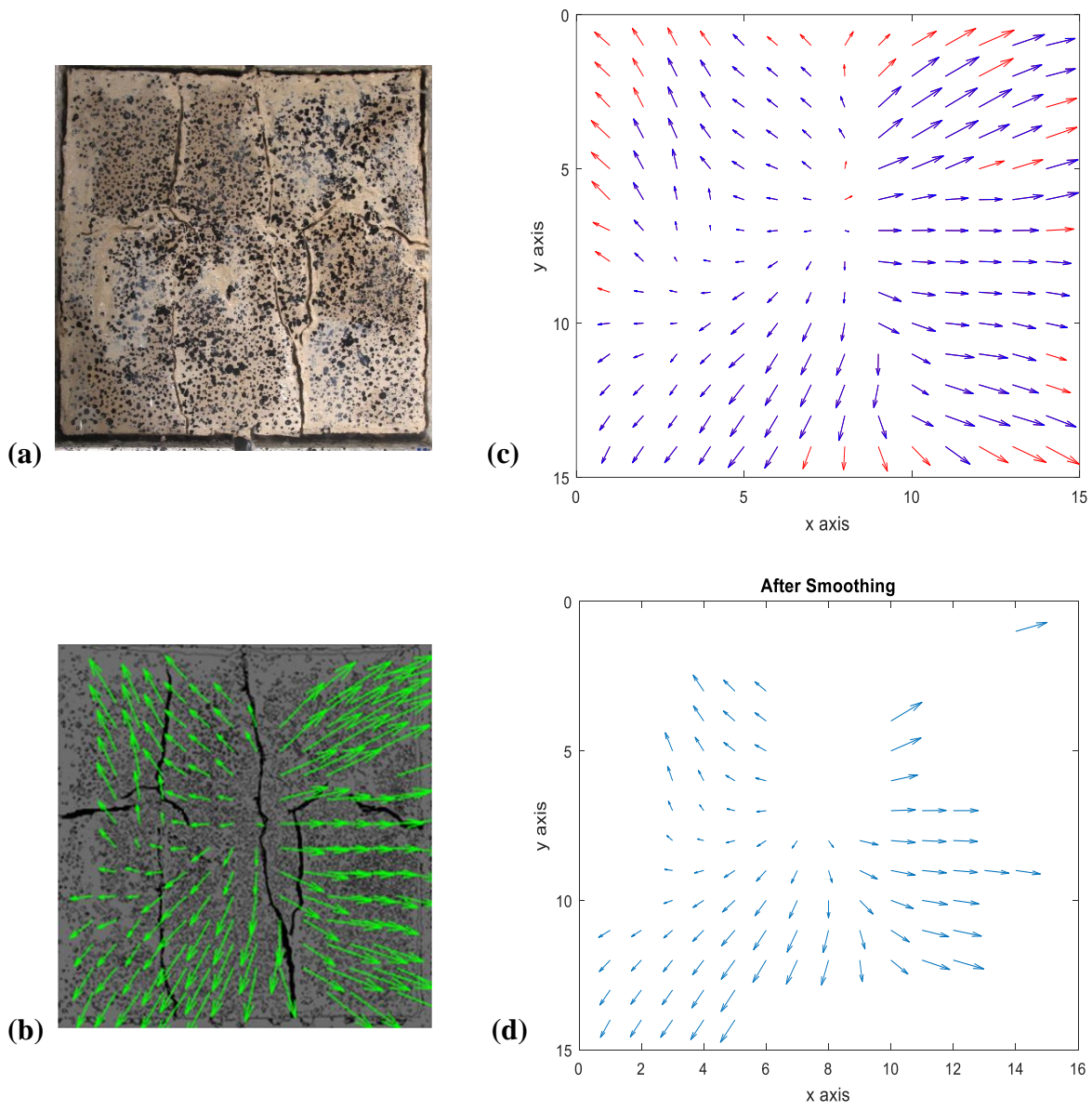


Figure 5.41 Immediately after 1st wetting; (a) a true color photo; (b) specimen with displacement vectors; (c) displacement fields in x & y (pixels); (d) displacement fields after smoothing

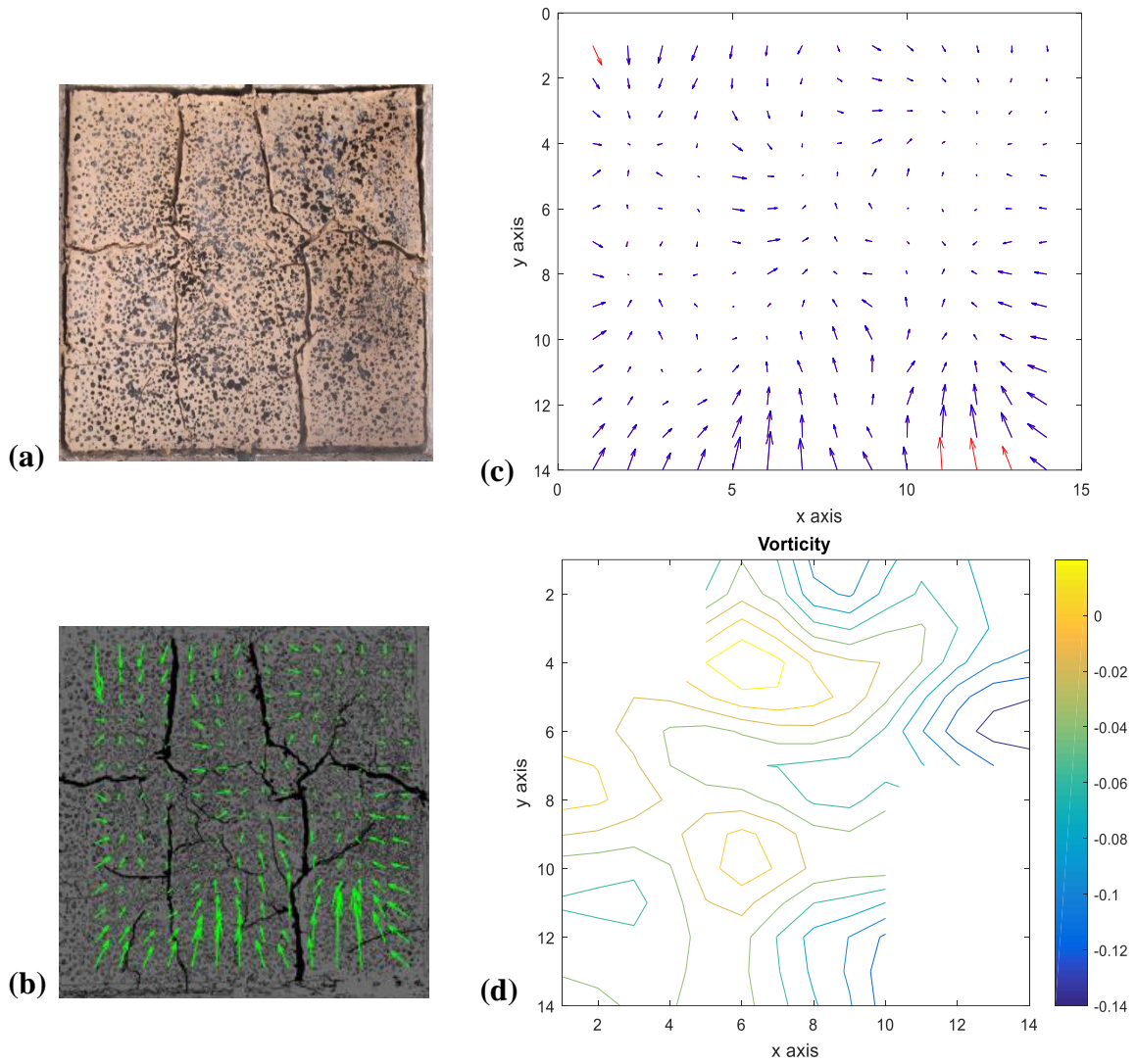


Figure 5.42 At the peak, 2nd drying; (a) a true color photo; (b) specimen with displacement vectors; (c) displacement fields in x & y (pixels); (d) vorticity

5.6 Concluding remarks

A new innovative tensile testing device was developed to examine the tensile strength and cracking behavior of soils subjected to cyclic wetting/drying processes. This apparatus was designed for continuous determination of tensile forces and lateral-induced expansion forces during drying and wetting, respectively. Two scenarios of application were performed in order to inspect the validity and feasibility of the device for determining the accurate tensile strength of soil. Several findings are highlighted below:

1. There are some differences between the tensile results of unlocked and locked-gap applications, and this may due to residual forces carried by the load sensor or/and by the soil, in which results in higher tensile values for unlocked-gap specimen than those of the other one, except in the first drying. However, the fitted curves of the tensile strengths and CIF (s) of both specimens are almost consistent.
2. The scenario of locked-gap is more appropriate for the accurate determination of the tensile strength of soil subjected to wetting/drying cycles.
3. The locked-gap specimen developed higher tensile force than that of the unlocked-one in the first drying, and this may due to lubricating of the device's walls in unlocked-gap scenario in which the edges of the specimen freely curled up, and hence didn't involve in tensile resistance. Consequently, lower tensile force generated in the unlocked-gap application in the first drying.
4. The trend of the tensile curve under drying condition shows that the tensile force increases with decreasing water content and increasing the corresponded suction up

to the failure. After that, the tensile force decreases with increasing suction where no significant contribution is made on the soil strength.

5. It should be mentioned that the tensile strength of soil decreased up to the third cycle. However, the tensile strength increased again in the fourth and fifth cycles for unlocked-gap specimen and in the fifth cycle for the locked specimen compared with second cycle. This may potentially due to healing and closure of some cracks during wetting cycles. For unlocked-gap specimen, the average crack aperture decreased in the fourth and fifth cycle in which previous cracks healed and new cracks developed in smaller width. Similarly, for the locked-gap specimen, the present cracks healed and new ones formed over cycles but in smaller crack aperture in the fifth cycle. Therefore, the raise of tensile strength after the third cycle is likely due to decreasing of the crack aperture over cyclic wetting/drying processes in which the soil tensile strength had boosted.
6. The Digital Image Correlation (DIC) technique can interpret the cracking mechanism of soils during wetting/drying cycles.

CHAPTER VI
TENSILE BEHAVIOR OF SOILS UNDER PARTIALLY RESTRICTED CONDITION
DURING WETTING/DRYING CYCLES

6.1 Introduction

The performance of the new tensile device had been deeply explored in different contexts involving; specimen's thickness and size, directional restriction, and soil structure. The tensile tests herein were conducted under partially restrained condition which is different than what was presented and described in chapter V. Partially restrained condition was provided through allowing the free part of the device to move in response to the soil shrinkage and expansion during drying and wetting, respectively. The determination of the tensile forces has been coupled with the study of the desiccation cracking of a high expansive soil mixture consisted of 75 % kaolin and 25 % bentonite during sequential wetting/drying cycles.

6.2 Objectives

The study herein aimed to gain better understanding the tensile and cracking behavior of clays in different contexts. The main specific objectives can be highlighted below:

- To investigate the performance of the new tensile testing method under partially restrained condition.
- To explore the influence of specimen's size and thickness on tensile and cracking behavior of compacted soils.
- To investigate the effect of the directional restriction on tensile behavior of soils.

- To examine the effect of initial conditions and soil structure on tensile and cracking behavior during wetting/drying cycles.

6.3 Experimental methodology

Desiccation cracking behavior is a complex phenomenon to understand where it is presumed to be developed due to a number of factors, such as clay content, mineral composition, aspect ratio, specimen's size, and boundary conditions. In this chapter, a number of factors were taken into consideration for measuring the tensile forces and characterizing desiccation cracking of soil when subjected to a number of wetting/drying cycles. These factors include the soil structure, the initial condition, specimen's size, thickness and directional restriction.

The fundamental concept of the testing method herein resembles to that one adapted in the previous chapter (chapter V), except the restricted condition. The testing method hither was performed under partially restricted condition which was achieved through allowing the base of the free jaw of the tensile device to move during drying and wetting processes. This was accomplished by mounting the load sensor in a high-positioned to measure the developed tensile forces and lateral displacements during drying cycles. To induce tensile stresses in this study, restraints were provided through employing protrusions at the soil bed, when the tensile stresses exceed the tensile strength of the soil, cracks develop. Also, the protrusions can provide an attachment at soil-bed where the load cell which is attached to the side and the bed of the free jaw, can measure the developed tensile forces

The soil exhibited shrinkage toward the gap and expansion away from the gap during drying and wetting, respectively. The lateral displacements were obtained by using a non-contact LVDT (*Macro Sensor SE 750-500*). This LVDT was intentionally utilized to prevent any friction

may influence on the natural movement of the soil specimen when dried or wetted. The micro-sized load cell was used, similar to that one used in the previous chapter, to measure the tensile forces with the capacity up to 200 N (50 lb) and a full resolution of 0.01% (0.02 N or 0.0045 lb). To allow the movement of the free jaw during shrinkage/expansion, the load sensor was high-positioned on L-shaped angle which is attached to the free jaw at a distant of 2.54 cm from the base of the free jaw (see Figure 6.1).

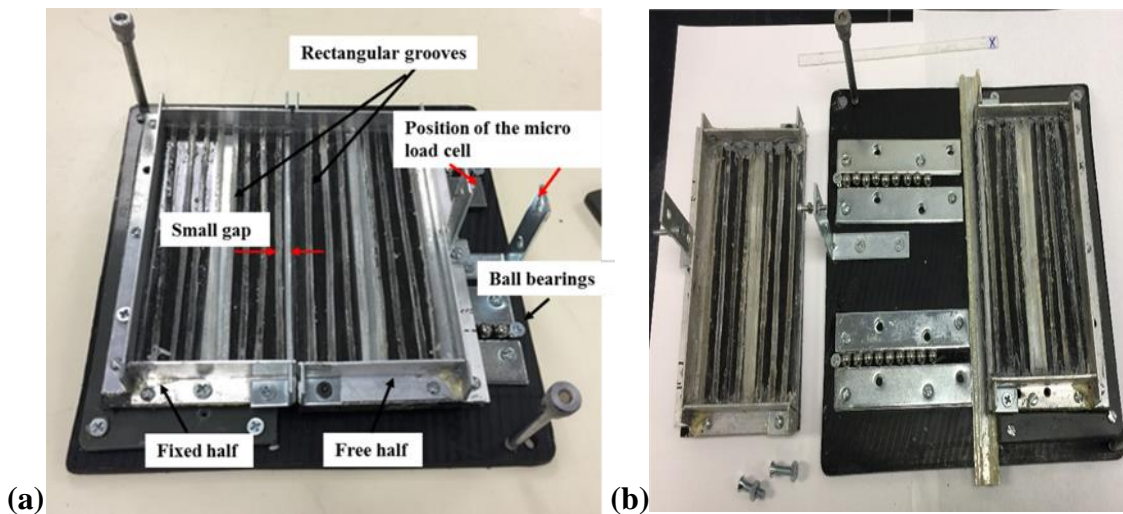


Figure 6.1 (a) & (b) The new tensile testing device with a high positioned micro-load sensor

The water loss was monitored during drying and wetting cycles by an electronic balance with the maximum capacity of 8100 g and repeatability of 0.01 g. A digital camera (Canon Camera-Power Shot G11) with the highest resolution of (3648-pixel x 2736-pixel) was mounted directly above the soil specimen (perpendicularly) to capture a series of photos during the cyclic drying and wetting. Figure 6.2 presents the experimental set-up of testing procedure including the

tensile device, the electronic balance, and the overhead camera. The soil used herein was as same as that one used in chapter V. Soil specimen was initially allowed to dry naturally under controlled laboratory temperature and relative humidity (24 ± 1 Co, $RH = 52\pm 2\%$). The drying process was terminated when the weight of the sample was constant or no significant change observed. Afterward, the soil specimen was wetted in the same procedure that performed in the tensile tests of chapter V (fully-restricted condition). The soil specimen was subjected to a number of sequential wetting/drying cycles. The tensile forces and the 2D-desiccation cracking were obtained. A full procedure of cracking characterization is presented in chapter V (section 5.3.3).

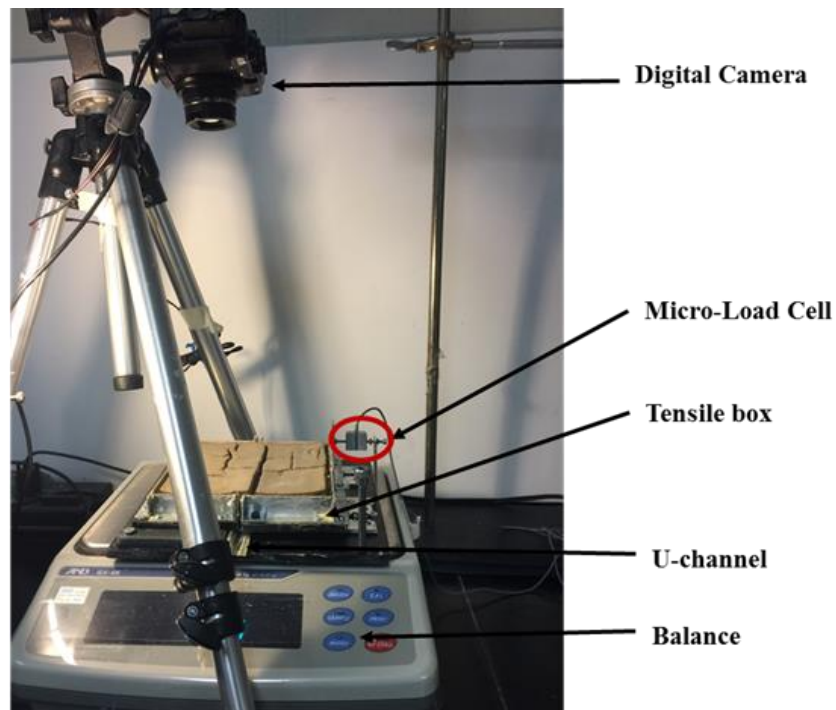


Figure 6.2 Experimental set-up of the testing procedure

Four unsaturated-compacted specimens were prepared at initial water content of about 42.7% (+4.7% of optimum moisture content) and dry unit weight of 11.4 kN/m³ (94.4% of γ_{dmax} as determined from the standard Proctor test, ASTM D698). The specimens namely MC1, MC2, MC3, and MC4 were tested in the context of the following factors; reference case, specimen's thickness, specimen's size, and directional restriction, respectively. One additional specimen namely MS was prepared at water content of 90.1% and dry unit weight of 7.848 kN/m³ and tested for studying the effect of initial water content and soil structure on tensile and cracking behavior. Figure 6.3 shows the selected points for the tensile tests in the compaction curve of the soil mixture of 75 % kaolin and the 25 % bentonite.

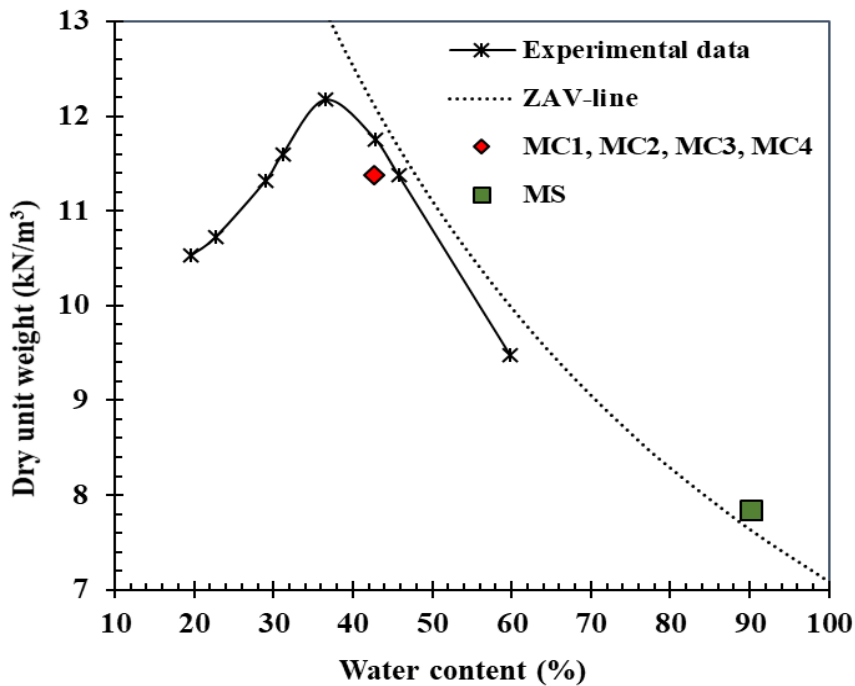


Figure 6.3 Selected points for tensile tests from compaction curve of the soil mixture of 75 % kaolin and 25 % bentonite

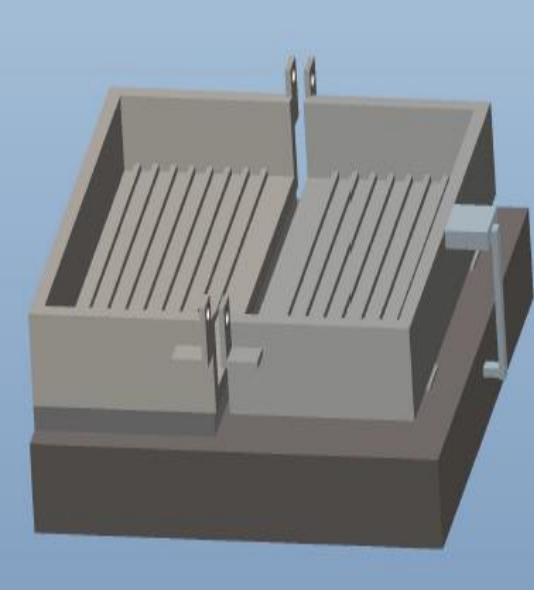
For specimen preparation, the soil was compacted in the tensile device in two layers to achieve the required dry unit weight at desired water content. Laboratory compaction composed of tamping with a 20-mm diameter metal rod to achieve approximately uniform application of compaction energy to the top of each layer. While the fully-saturated specimen (MS) was prepared in the tensile device in two layers by using very light tamping and vibration applied to the soil specimen to get rid of the air bubbles. The small gap between the two halves of the tensile device was maintained by using a plastic spacer during specimen preparation. In addition, two screws were utilized for preventing closing the gap during soil preparation, and then removed after completion of preparation and before starting of the test. Table 6.1 shows all cases opted for conducting the tensile tests under different conditions.

Figure 6.4 presents schematic drawings for the new tensile device in different cases. The crack morphology was determined for every test by using the image analysis technique to analyzed and interpreted the effects on the outcome; more details of the image technique is provided in chapter IV (see section 4.3.2.3).

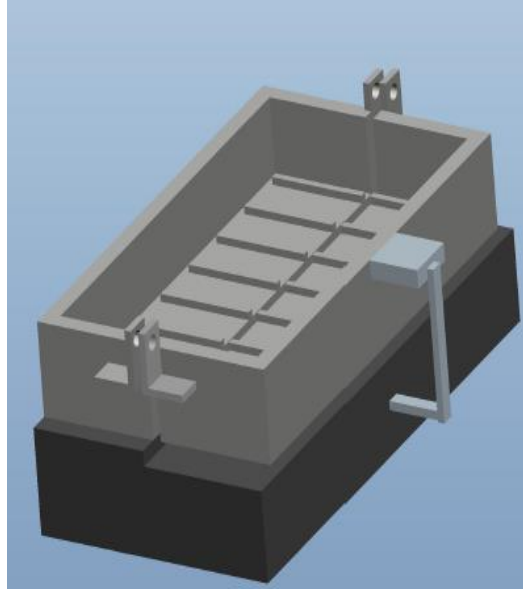
Table 6.1 Test reference for tensile tests

Test reference	Specimen type	w ₀ (%)	γ _d (kN/m ³)	Soil thickness (mm)	Soil dimensions (mm) width * length	Aspect ratio width: thickness	Base restriction	size ratio relative to MC1	Factor
MC1	compacted	43.1	11.4	12.7	150*150	11.81: 1	orthogonal	_	reference case
MC2	compacted	43.0	11.4	25.4	150*150	5.91: 1	orthogonal	2: 1	aspect ratio (thickness)
MC3	compacted	42.67	11.4	12.7	75*150	5.91: 1	parallel	0.5: 1	(specimen's size) directional restriction
MC4	compacted	42.6	11.4	12.7	150*150	11.81:1	parallel	1: 1	directional restriction
MS	slurry	90.1	7.84	12.7	150*150	11.81:1	orthogonal	1: 1	soil structure

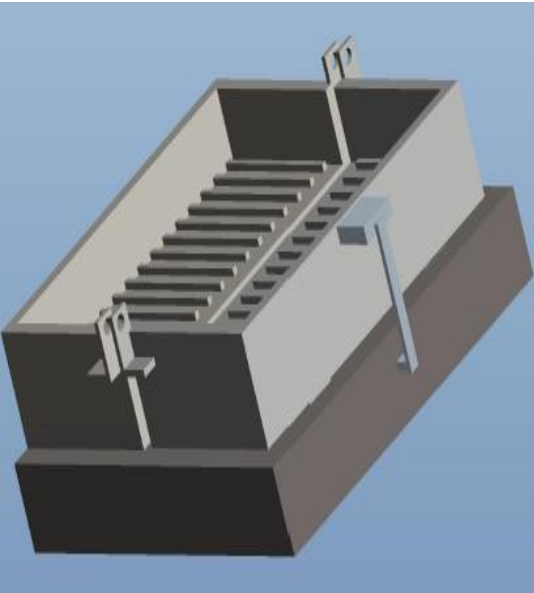
Note: MC: unsaturated-compacted soil specimen, MS: fully-saturated soil specimen
base restriction is relative to tension's direction transmitted to load sensor
size ratio = size of specimen: size of MC1
width is perpendicular to the gap
length is parallel to the gap



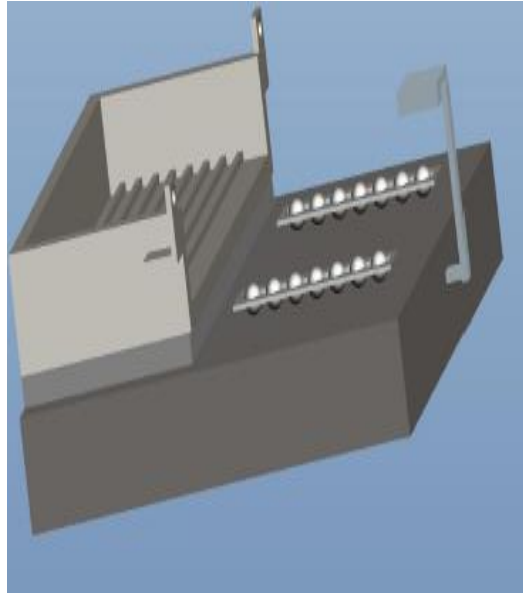
(a)



(b)



(c)



(d)

Figure 6.4 the tensile device with high-positioned load sensor (a) perpendicular grooves for MC1, MC2; (b) parallel grooves for smaller size (MC3); (c) parallel grooves for MC4; (d) sectional view with perpendicular grooves

6.4 Results and discussion

The experimental campaign in this chapter aimed to study the tensile and cracking behavior of soils when imposing partially restricted condition and subjected to multiple wetting/drying cycles. The study was performed in the context of some factors including; specimen's thickness (aspect ratio), specimen's size, directional restriction, initial water content, and soil structure. The results of each test are presented and described in the following sections.

6.4.1 Reference case/ unsaturated-compacted soil specimen (MC1)

The compacted soil specimen namely MC1 was prepared at initial water content of about 43.1% and dry unit weight of 11.4 kN/m³, (see Figure 6.3). MC1 was subjected to five wetting/drying cycles. The variation of water content over time during drying is presented in Figure 6.5. The water content gradually decreased over time till approached equilibrium state at the end of drying process. For wetting process, the sample was wetted to similar and/or slightly higher water content compared to the initial one as-compacted. In this chapter, for all presented figures, the letter D refers to drying cycle, and the letter W refers to wetting cycle. The numbers 1 to 5 refer to the number of drying or wetting cycle, for example, the number 1 refers to the first cycle and so on.

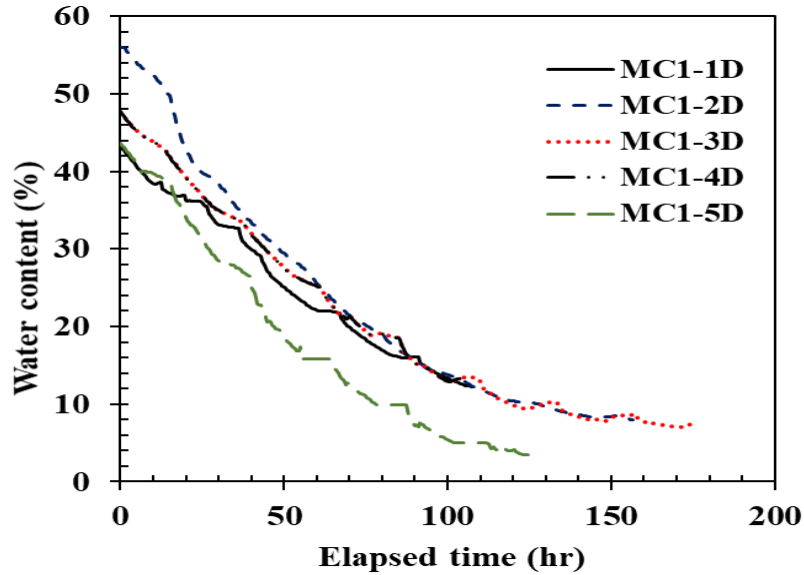


Figure 6.5 Variation of water content over time for MC1 specimen

Photographs were taken to monitoring the area and thickness changes of the specimen during drying and wetting processes. Image analysis technique was employed for calculating the volume change in the specimen at different time intervals. Only the intact soil was considered; the crack and gap areas were excluded from the calculation. Accordingly, the degree of saturation, variations of void ratio and volume were determined at different time periods through drying cycles.

More information related to void ratio and volumetric changes of soil specimen are presented in Figure 6.6 (a & b). An essential linear shrinkage of soil was determined within the range of degree of saturation 80% to 50%. While curvilinear shrinkage was determined in the beginning and at the end of the volume change. All curves present similar trend over drying cycles.

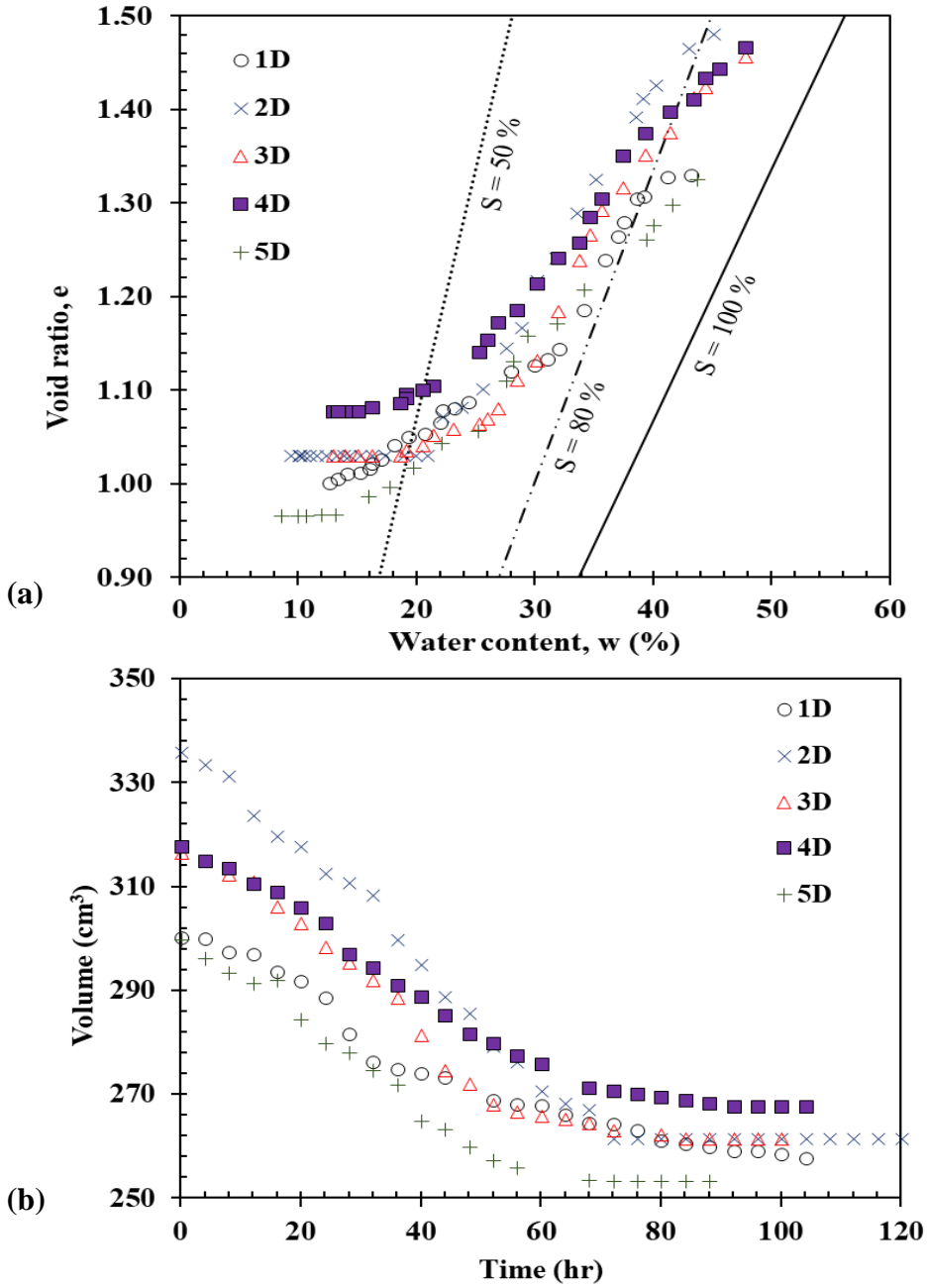


Figure 6.6 Variations of (a) void ratio vs. water content, and (b) soil's volume over time for MC1

6.4.1.1 Effect of cyclic drying/wetting on tensile behavior

Similar to what was adopted in chapter V, a positive sign convention is opted for presenting the developed tensile forces during drying cycles. The developed force during wetting was namely Lateral-Induced Expansion Force (LIEF); a negative sign convention is opted for this one. The variations of tensile and lateral-induced expansion forces over time through drying and wetting cycles are presented in Figure 6.7 and Figure 6.8, respectively. Figure 6.9 shows the variation of lateral displacements during drying cycles. Figure 6.10 (a & b) presents the variations of tensile forces as a function of degree of saturation and water content during drying cycles, respectively. The relationship between the lateral displacements and tensile forces during drying is established in Figure 6.11.

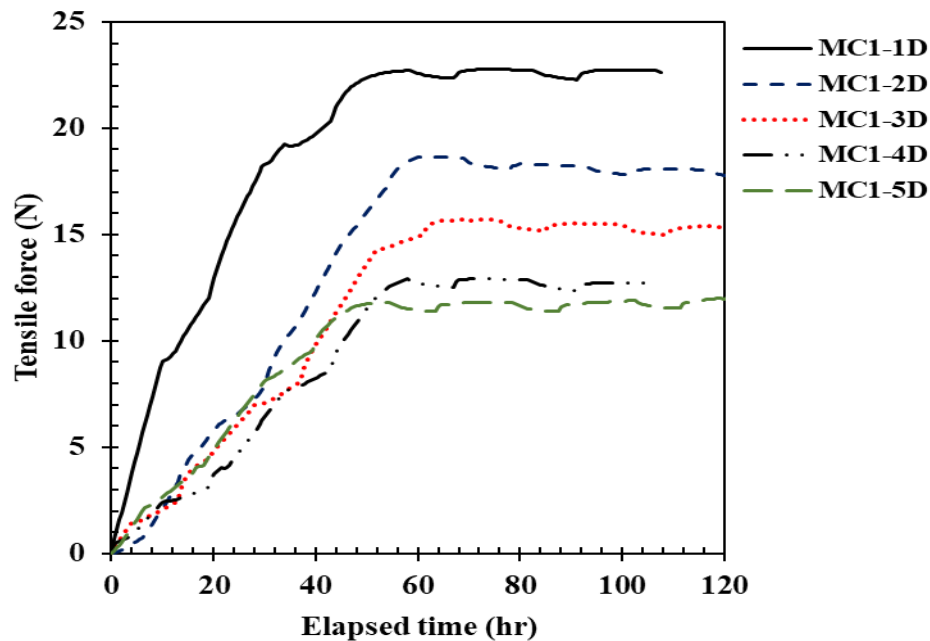


Figure 6.7 Variations of tensile forces over time for MC1; D: drying

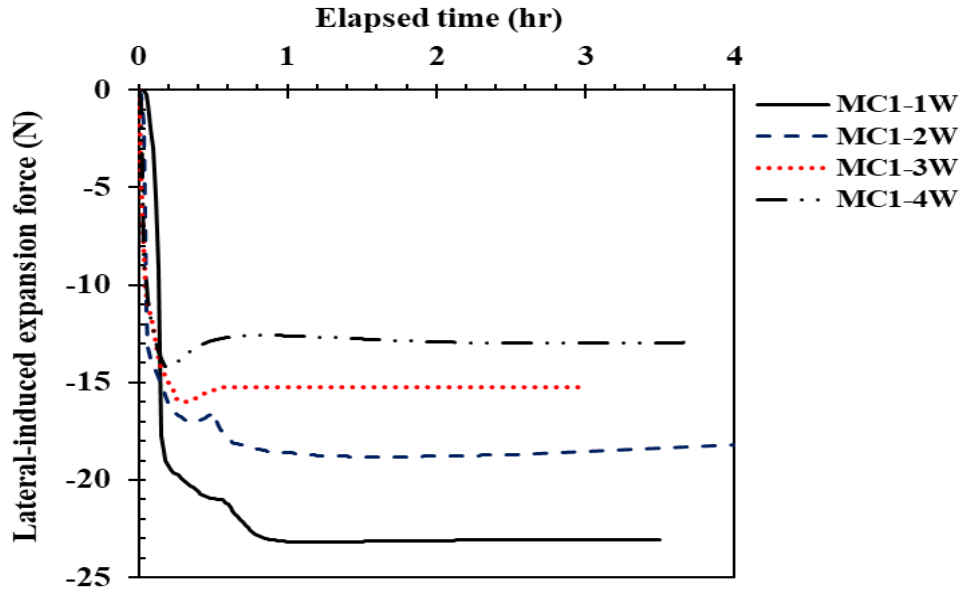


Figure 6.8 Variations of lateral-induced expansion forces over time for MC1; W: wetting

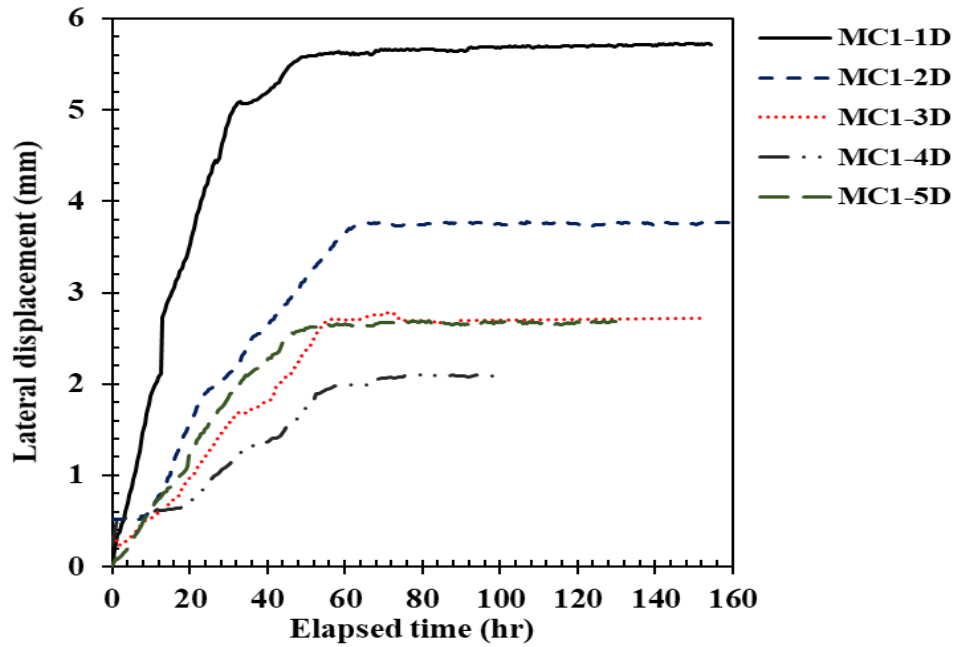


Figure 6.9 Variations of lateral displacement over time for MC1; D: drying

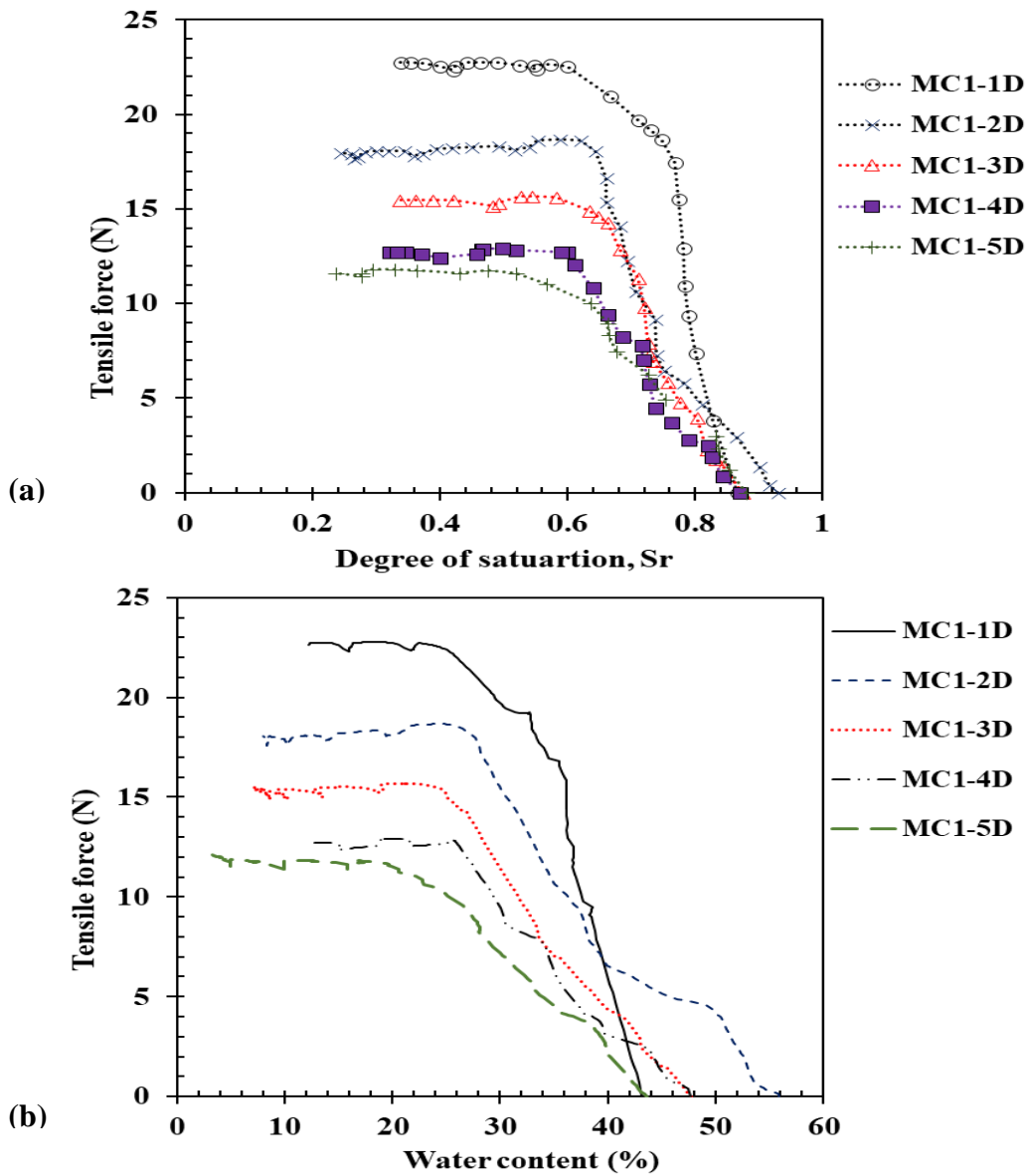


Figure 6.10 Variations of tensile forces as a function of (a) degree of saturation, and (b) water content for MC1; D: drying

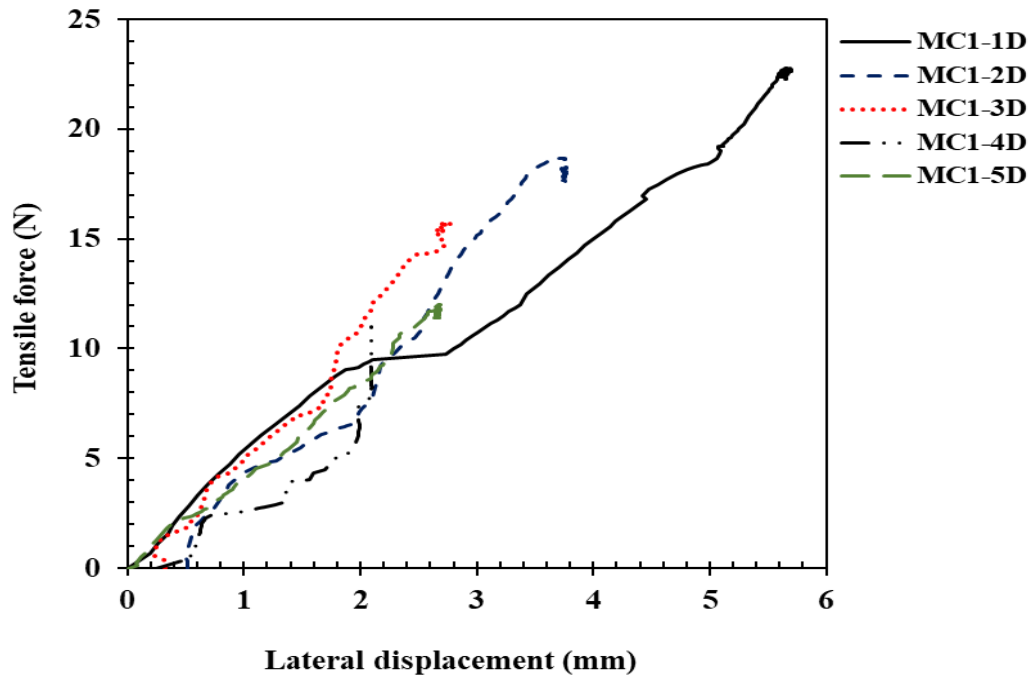


Figure 6.11 Lateral displacements vs. tensile forces for MC1 during five drying cycles

Upon drying, the tensile forces gradually increased up to a constant value and maintained till drying proceeded and the cracks fully propagated. Similar trend was obtained for all drying curves where the tensile forces increased with decreasing of water contents and then maintained constant till drying process was terminated. While during wetting, the tensile force released instantaneously and then reduced till approached to zero value. After that, lateral-induced expansion forces readily generated and then increased to values ranged from 12.5 N to 22.5 N till approached to a constant value. No variation was obtained on the lateral expansion forces after 1 hour where the soil sample reached to a constant water content. All drying curves reached to constant tensile forces at almost the water content of 25 %. A reduction in the tensile resistance was observed over cycles where the maximum tensile force was determined in the first drying (i.e., 22.7-N). More cracks propagated during the sequential wetting/drying cycles.

6.4.1.2 Effect of cyclic drying/wetting on desiccation cracking

Figure 6.12 and Figure 6.13 present the crack networks at the end of every drying/wetting cycle of the unsaturated-compacted specimen (MC1). In the first drying process, a primary crack was initially formed in x-direction subdivided the sample into two blocks followed then by a crack in the y-direction. During wetting, the soil exhibited expansion/swelling due to water absorption accompanied with changing in the stress state. This caused large deformations/deteriorations in the soil structure resulted in significant healing and closure of the present cracks that formed in the first drying, in addition to new cracks developed during wetting. More cracks developed over successive wetting/drying cycles. In general, the results of tensile and cracking behavior are consistent; more cracks were developed with decreasing of the peak tensile forces through drying cycles. Over cycles, the CIF increased and the crack aperture decreased up to the fourth cycle, as shown in Figure 6.14. In the fifth drying, it was observed decreasing in CIF and crack aperture. It seems that some cracks healed during the fourth wetting, resulting in less cracks in the fifth drying. The most interesting finding observed herein is that the present cracks healed during wetting process, and when the specimen subjected to the next drying, most of the healed cracks remained closed and new cracks developed in different regions in the soil mass. However, the healed cracks remained weak regions in the specimen. This interprets why the specimen experienced lower

tensile resistance through cycles until approached to equilibrium state in which no any further changes in tensile strength and desiccation cracking.

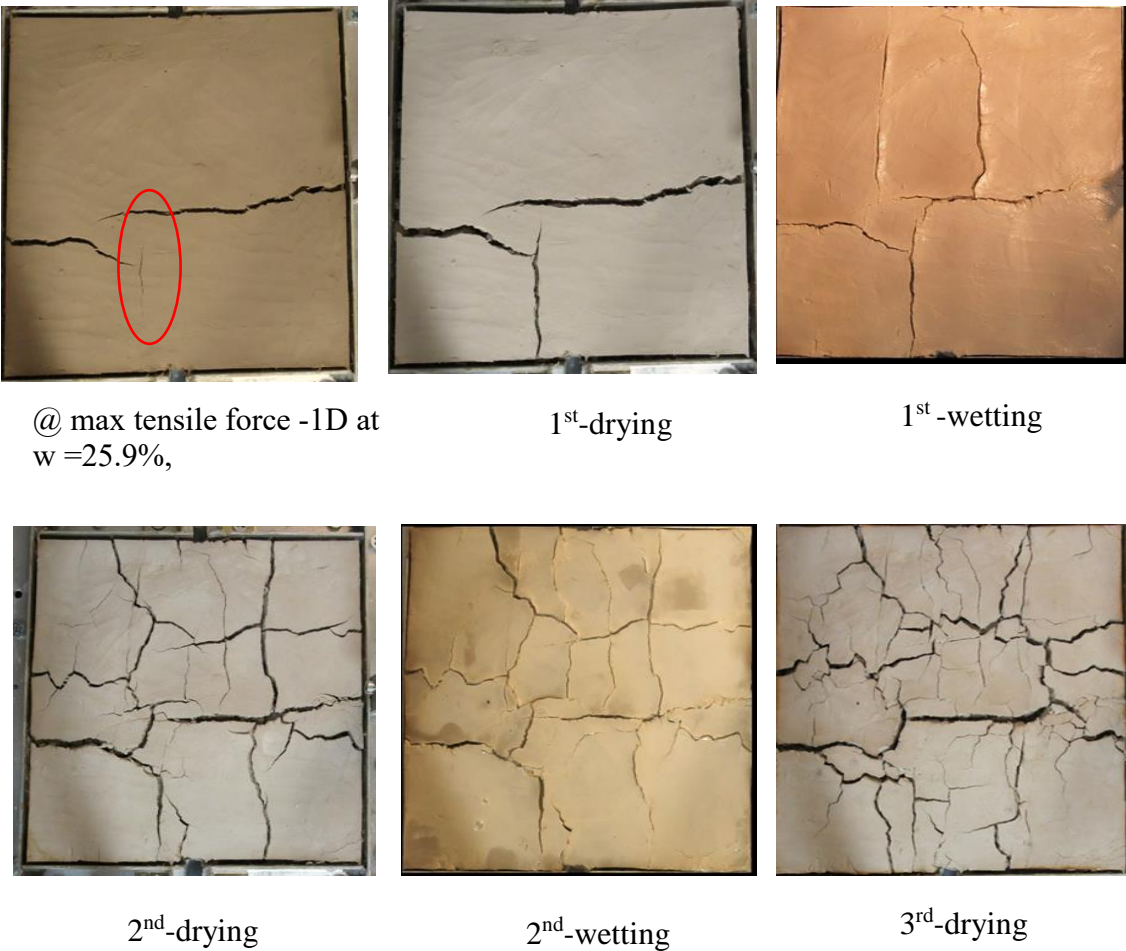


Figure 6.12 Crack patterns at the end of the cycle for the unsaturated-compacted specimen (MC1)



3rd-wetting



4th-drying



4th-wetting



5th-drying

Figure 6.13 Continued crack patterns at the end of the cycle for MC1

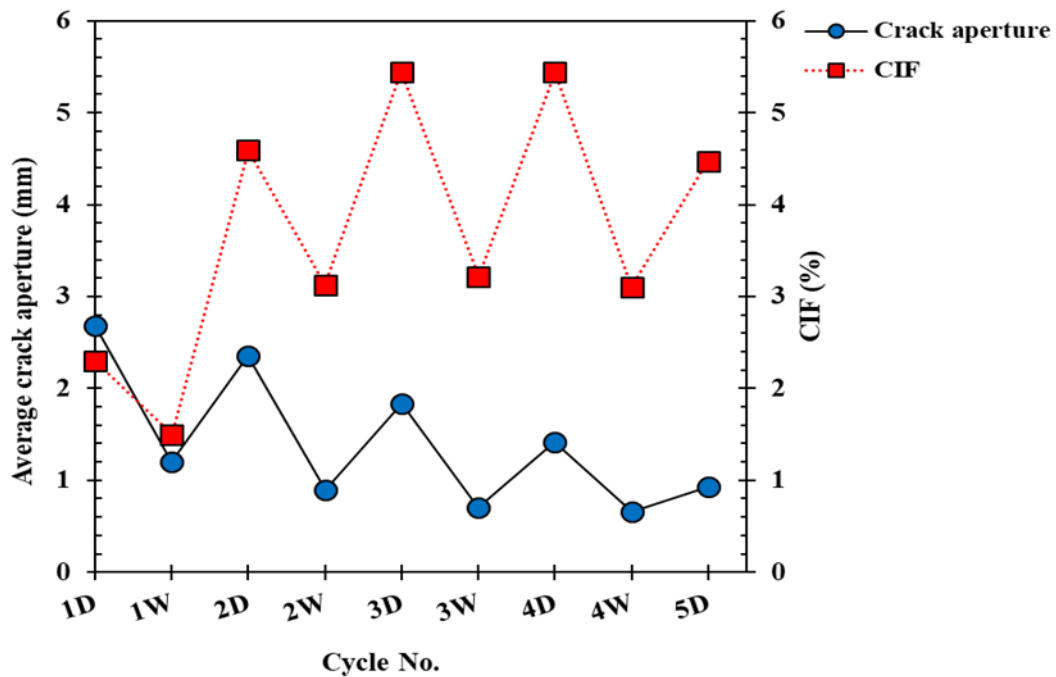


Figure 6.14 Crack Intensity Factor (CIF) and average crack aperture at the end the cycle for MC1; W: Wetting, D: Drying

6.4.2 Specimen's thickness /Unsaturated-compacted specimen (MC2)

The aspect ratio of the specimen is defined as the proportional relationship between its width to its thickness. The size ratio is the relationship between two specimen's sizes indicating how many times the first size contains the second size (reference size). The two ratios had been considered to study their effects on tensile and cracking behavior of soil. For MC2 specimen, the aspect ratio was 5.91: 1 and the size ratio was 2: 1 considering MC1 as a reference (second number in the ratio), as shown in Table 6.1. The MC2 specimen was prepared at similar initial conditions (i.e., water content and dry density) and double thickness compared with those of MC1 specimen. The variation of water content over time during drying is presented in Figure 6.15. The water content gradually decreased over time till approached equilibrium at the end of drying process. For

wetting, the sample was wetted to lower water content compared to the initial water content as-compacted. More information related to void ratio and volume changes is presented in Figure 6.16.

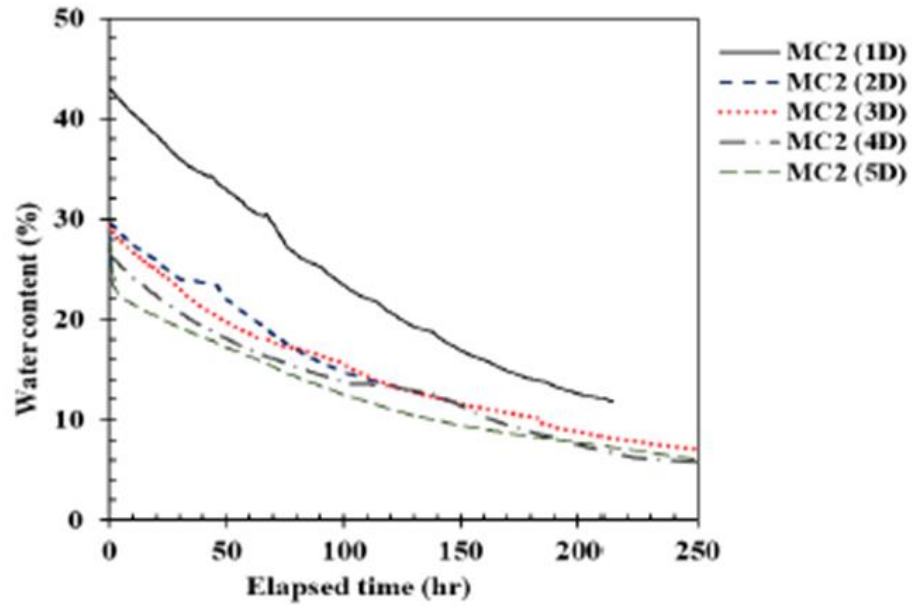


Figure 6.15 Variations of water content over time for MC2; soil thickness of 25.4 mm

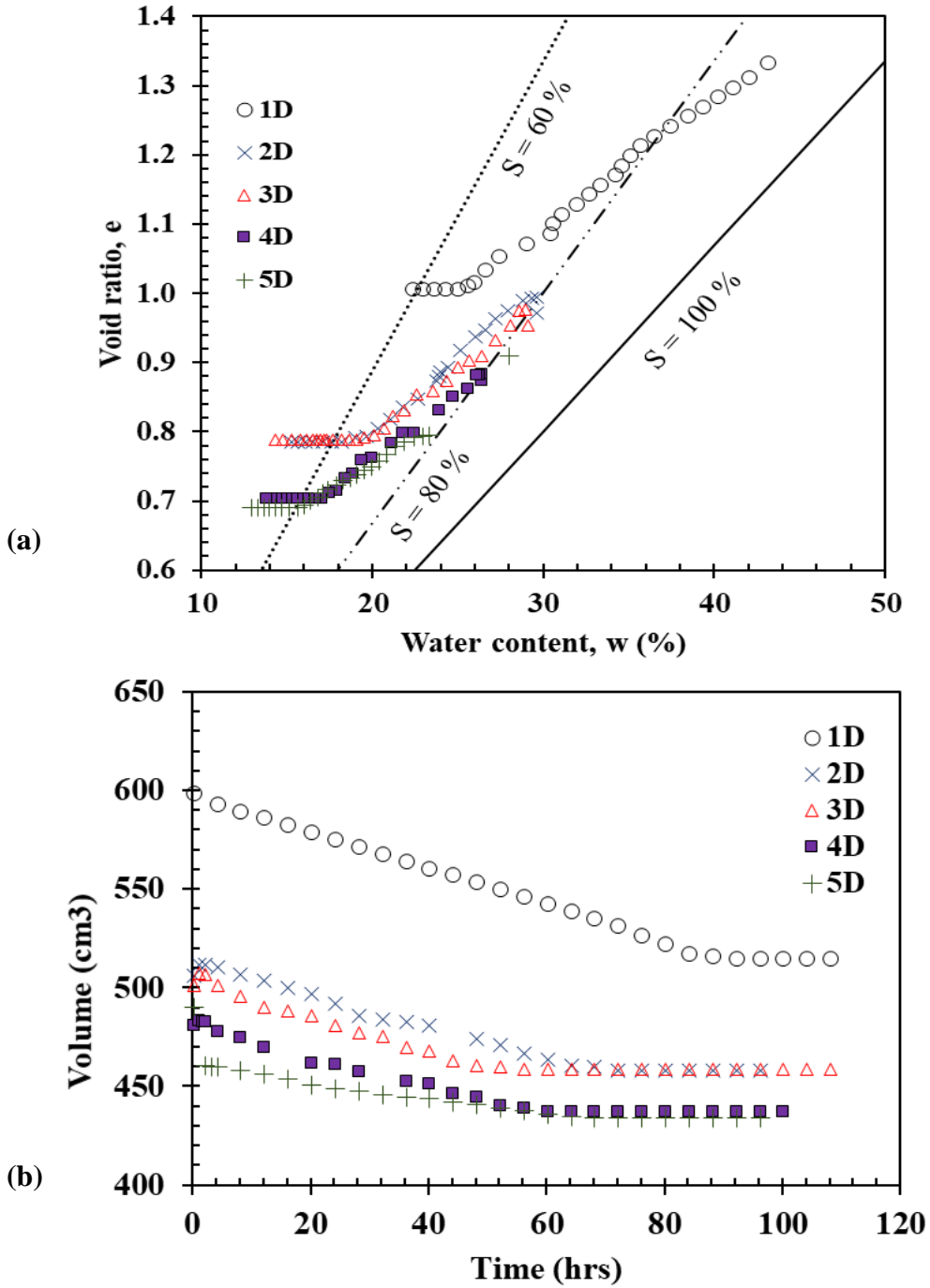


Figure 6.16 (a) Variations of void ratio vs. water content, (b) volume change over time for MC2; soil thickness of 25.4 mm

6.4.2.1 Effect of cyclic drying/wetting on tensile tests

Figure 6.17 and Figure 6.18 present the variation of tensile and lateral-induced expansion forces over time through drying and wetting cycles, respectively. Figure 6.19 shows the lateral displacements experienced by MC2 over time during drying processes. Figure 6.20 (a & b) shows the tensile forces functions of degree of saturation and water content. Figure 6.21 presents the lateral displacements over time during drying cycles. The trends of drying curves are similar to those of MC1, where the tensile force reached to a constant value and maintained till drying process was terminated.

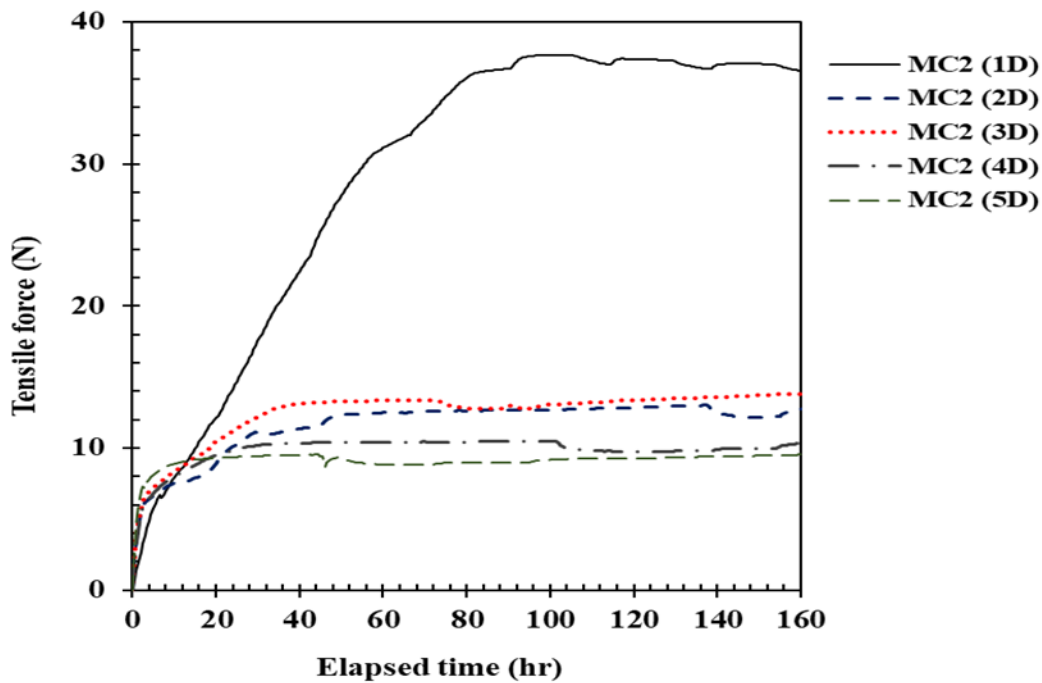


Figure 6.17 Variation of tensile forces over time for MC2 subjected to five drying processes; soil thickness of 25.4 mm

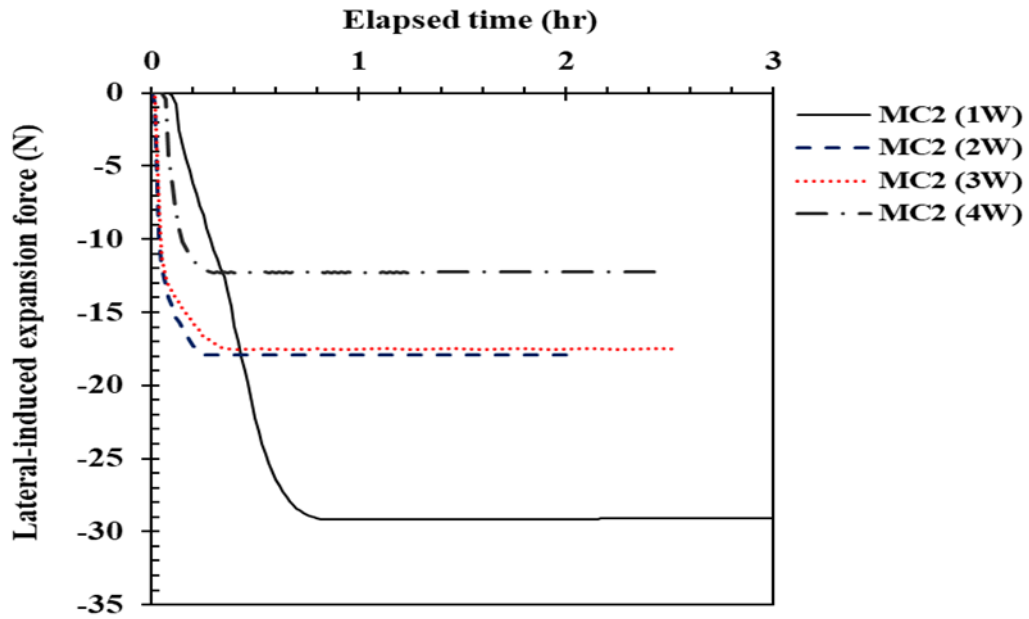


Figure 6.18 Variation of lateral-induced expansion forces over time for MC2

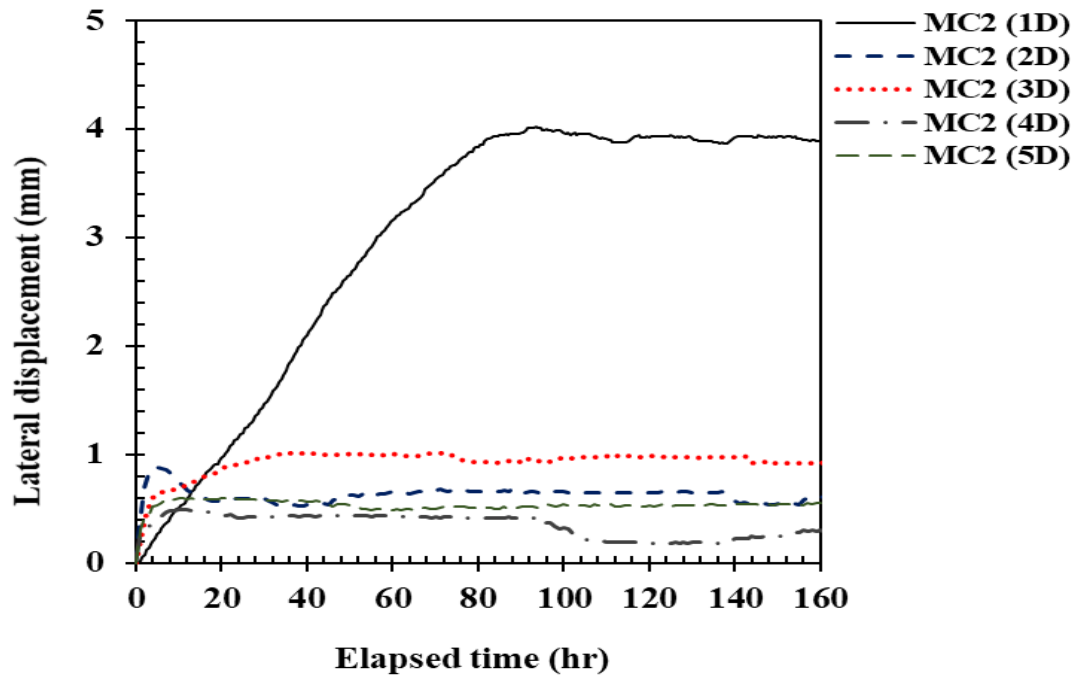


Figure 6.19 Variation of lateral displacement over time for MC2

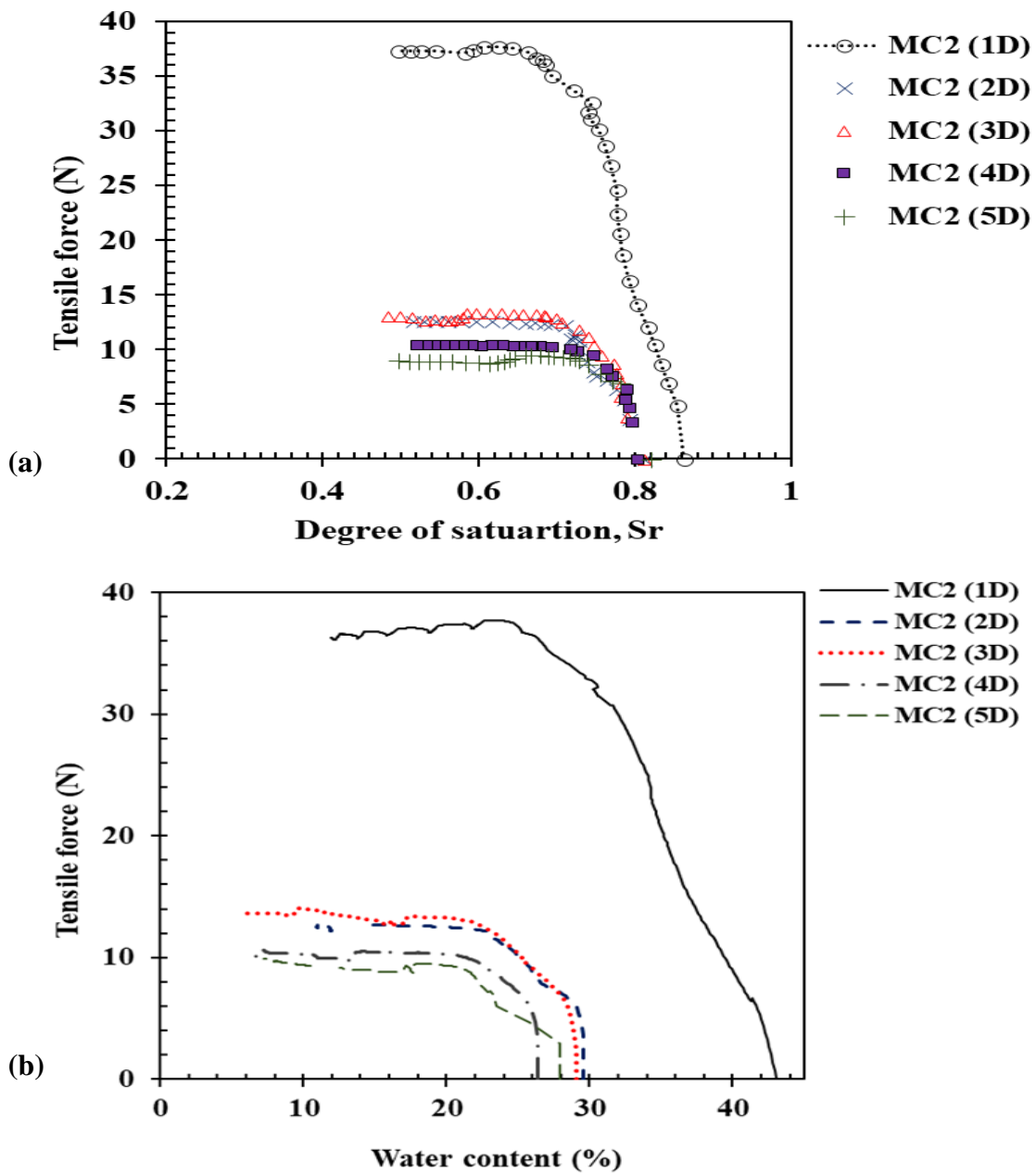


Figure 6.20 Variations of tensile forces for MC2 as a function of (a) degree of saturation, (b) water content

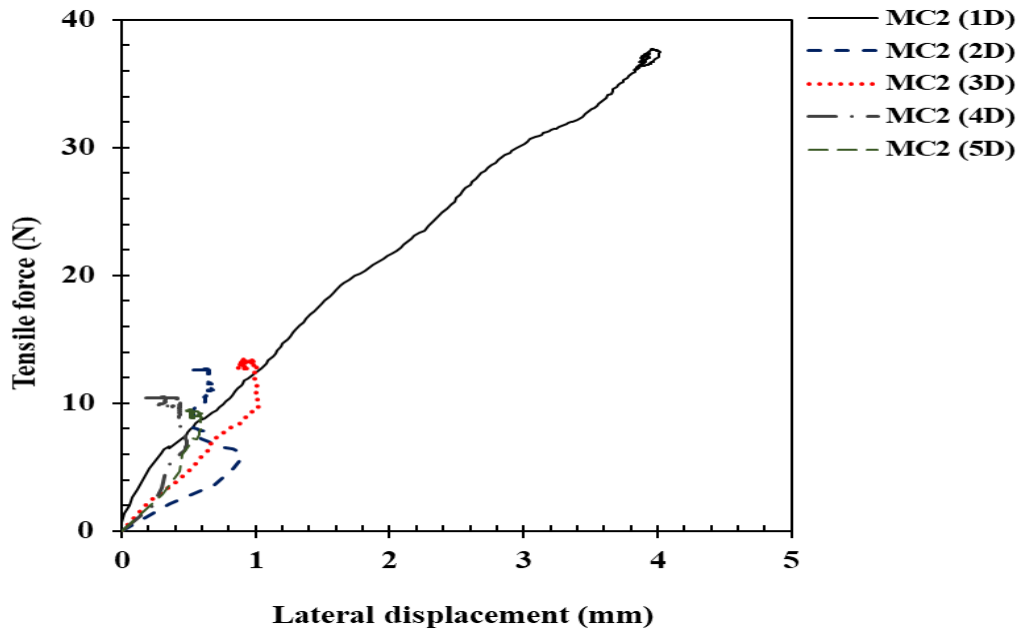


Figure 6.21 Lateral displacement vs. tensile forces over drying cycles for MC2

6.4.2.2 Effect of cyclic drying/wetting on desiccation cracking

Figure 6.22 and Figure 6.23 presents the crack networks at the end of each cycle for the unsaturated-compacted specimen (MC2). No cracks developed in the first drying, and this is related to the higher tensile resistance that experienced by the specimen. On the other hand, cracks formed and propagated over the other cycles in which lower tensile forces generated. The results in Figure 6.24 show that crack intensity factors (CIF) and crack aperture increased over drying cycles while no variation was obtained during wetting cycles, except in the first one.

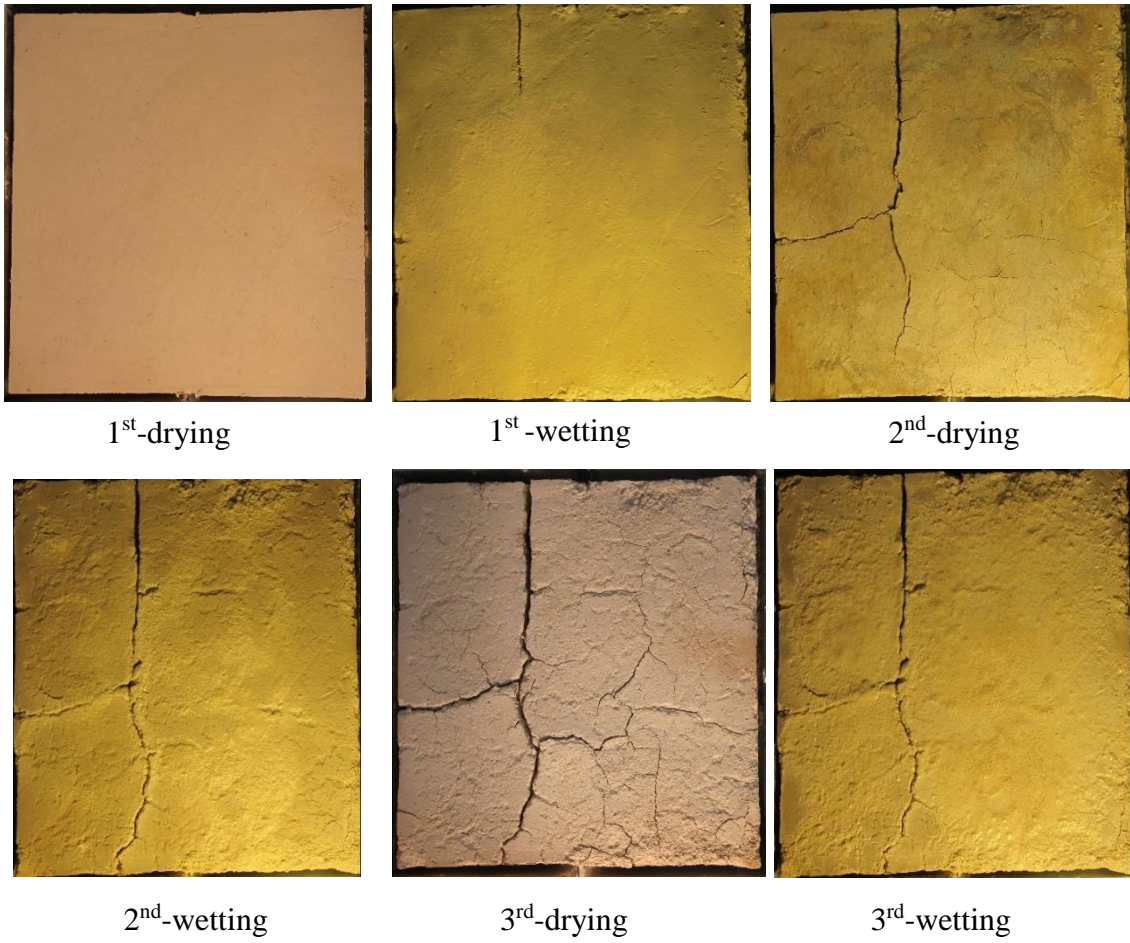


Figure 6.22 Crack patterns at the end of the cycle for the unsaturated-compacted specimen (MC2)



4th-drying



4th-wetting



5th-drying

Figure 6.23 Continued crack patterns at the end of the cycle for MC2

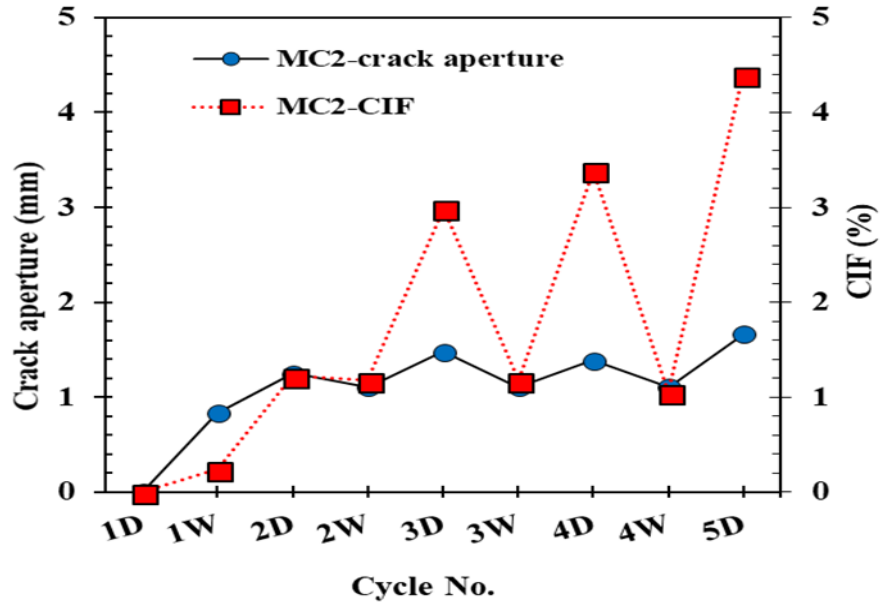


Figure 6.24 Variations of CIF and crack aperture for MC2 at the end of the cycle

6.4.3 Specimen's size and directional restriction/ MC3

The compacted soil specimen namely MC3 was prepared at similar initial conditions of those of MC1. The experiment herein was performed to study the coupled effect of specimen's size and directional restraining condition on the tensile and cracking behavior of soil by using the new tensile device. Figure 6.25 shows a photo of the new tensile device with reduced width and length by using additional partitions installed inside the device for the desired dimensions. MC3 was prepared at a half size of the that of MC1. The dimensions of the tensile device were reduced for this test, as follows; 75mm in width; 75 mm in length; and maintained 12.7 mm in the height. The variation of water content over time during drying is presented in Figure 6.26. Void ratio and volume changes are presented in Figure 6.27.

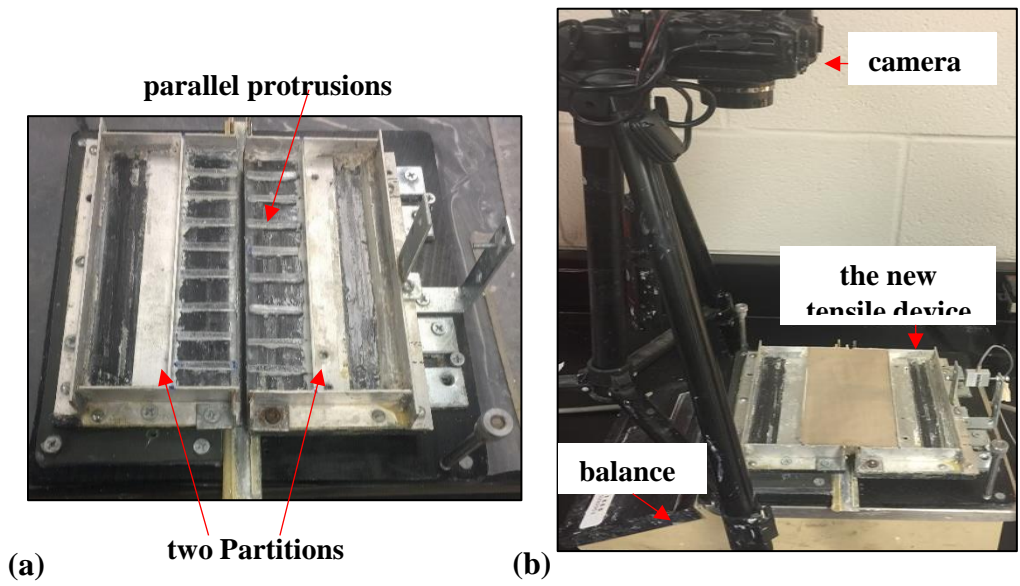


Figure 6.25 (a) A plane view of the reduced-dimensional tensile device, (b) experimental set-up of the test

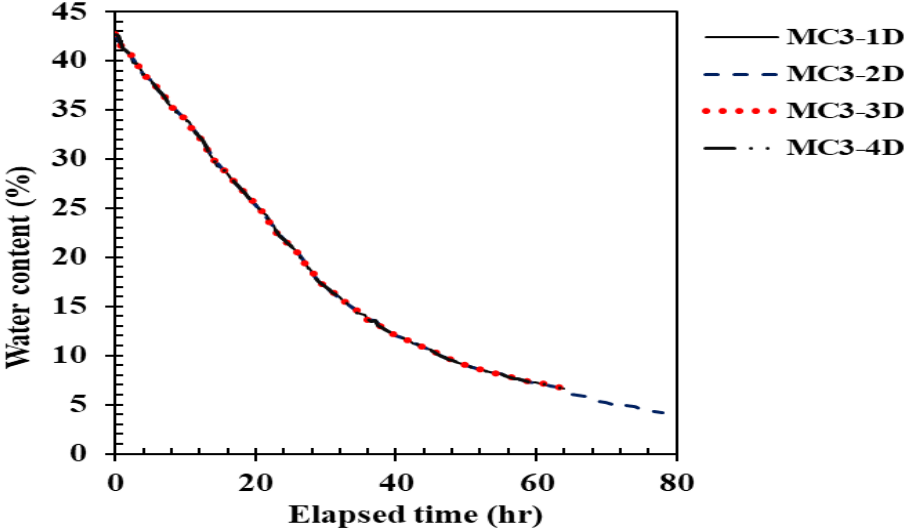


Figure 6.26 Variation of water content over time for MC3 during cycles

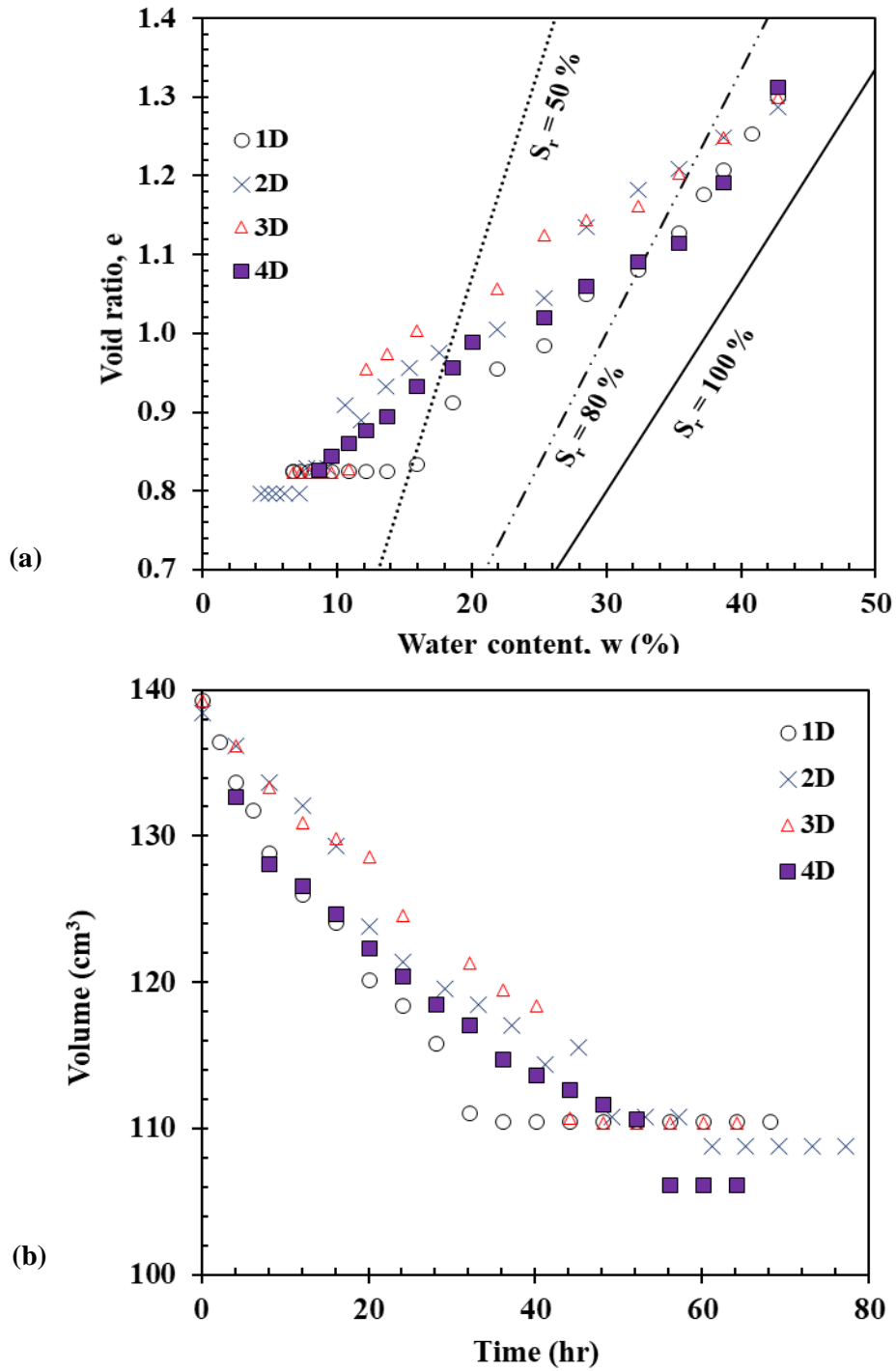


Figure 6.27 (a) Variation of void ratio with water content change, (b) Volume change over time for MC3

6.4.3.1 Effect of cyclic drying/wetting on tensile tests

The variations of tensile and lateral-induced expansion forces over time are presenting in Figure 6.28 and Figure 6.29 during drying and wetting, respectively. Figure 6.30 shows the variation of tensile forces as a function of water content over time during drying cycles. The tensile results of MC3 are different than those of MC1 where the MC3 exhibited nearly a bell-shaped curve in the first drying. In this cycle, the tensile force reached to a peak value and then gradually decreased when drying proceeded. The tensile curve in the second drying is slightly lower than that one of the first drying. In the third and fourth cycles, the maximum tensile forces decreased to the half magnitude compared to that one in the first and second cycles. All the tensile curves generally have similar trend and shape. Upon wetting, the behavior of MC3 resembles to that one of MC1 where the tensile forces decreased instantaneously till reached to zero value. After that, the lateral expansion forces readily generated and then increased to the values ranged from 2 N to 14 N till approached to equilibrium state where no significant changes occurred.

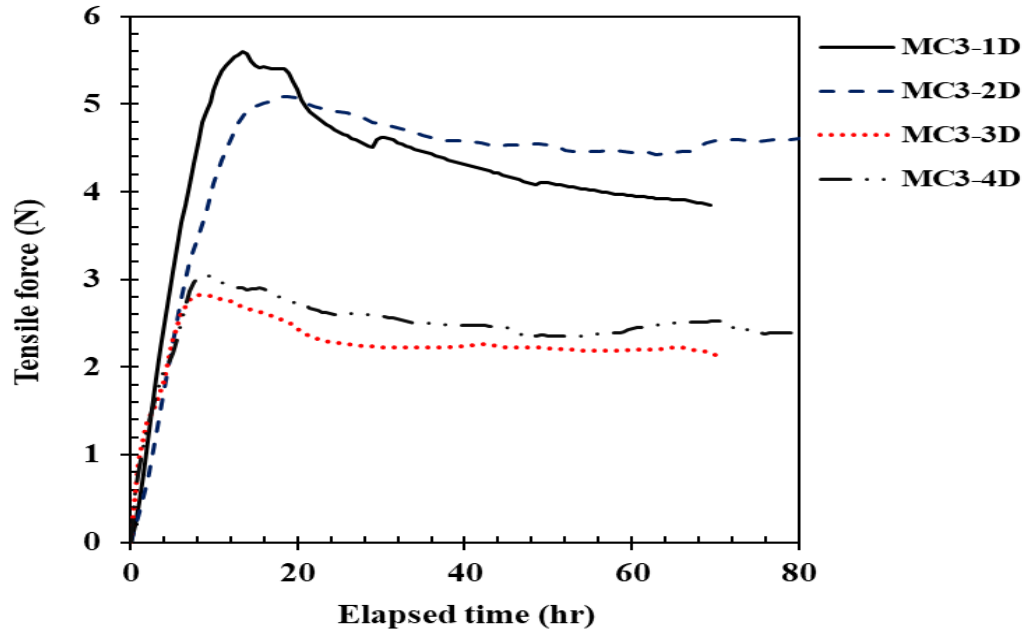


Figure 6.28 Variation of tensile forces over time for MC3 during drying cycles

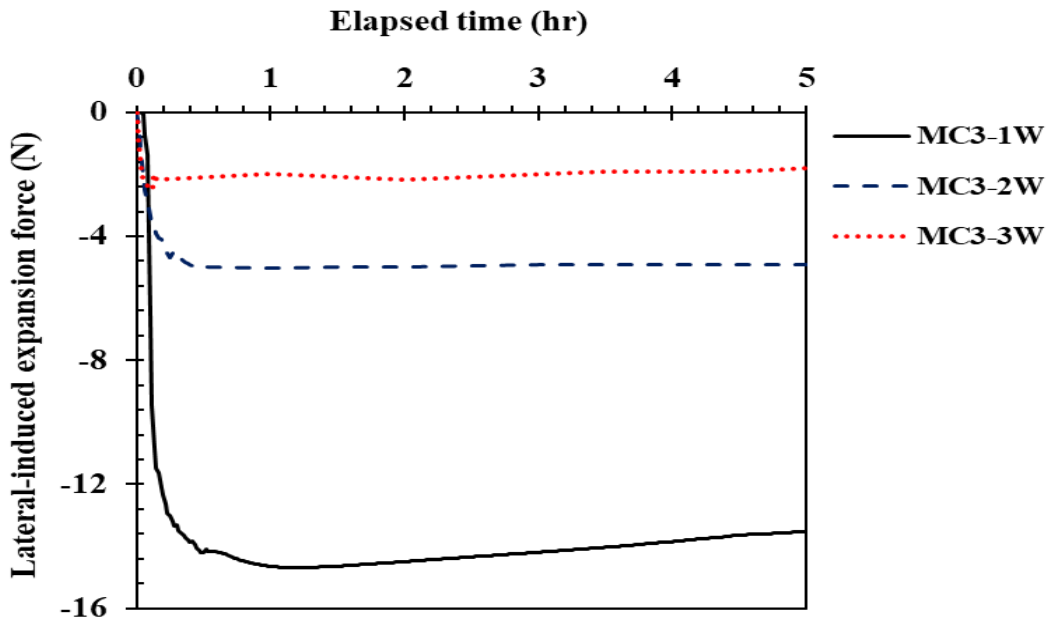


Figure 6.29 Variation of lateral-induced expansion forces over time for MC3; W: Wetting

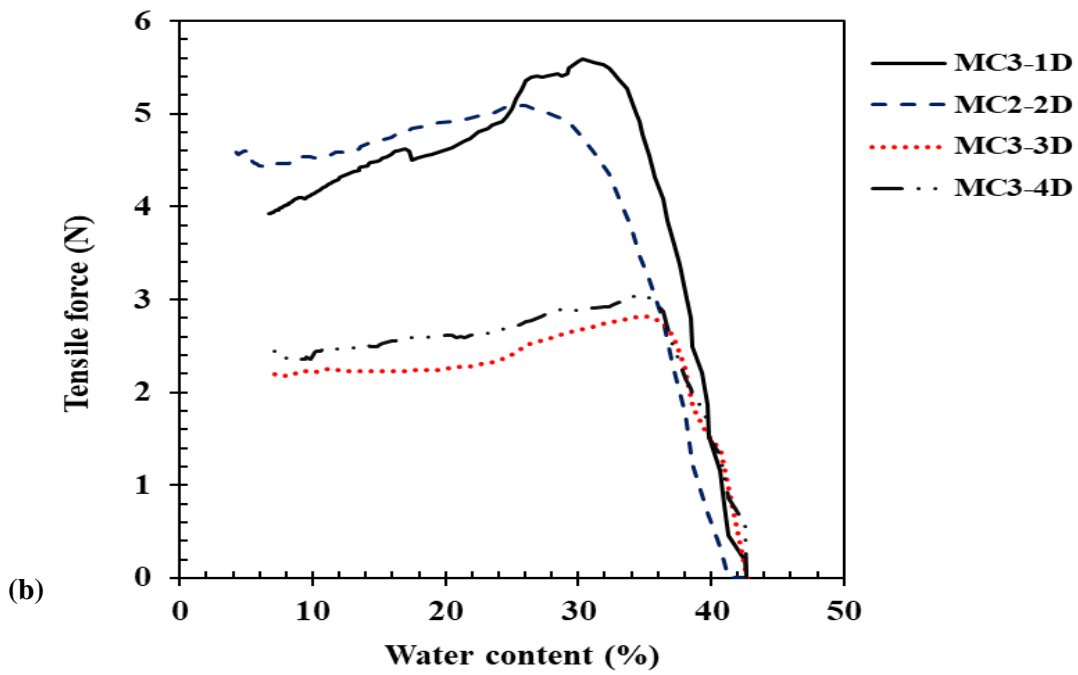
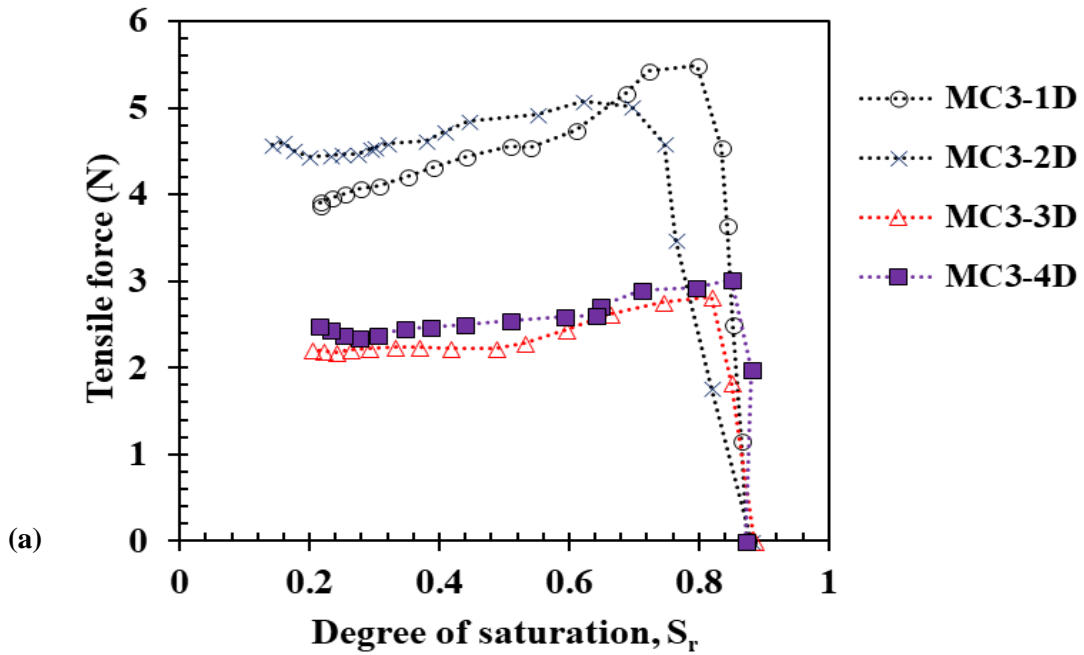


Figure 6.30 (a) Variation of tensile forces as a function of degree of saturation (b) tensile force vs water content for MC3; D: Drying

6.4.3.2 Effect of cyclic drying/wetting on cracking

At the end of the first drying, it was observed that the two edges of the specimen curled up where invisible two cracks developed beneath the surface, as shown in Figure 6.31. This interprets the presence of the peak in the tensile curve in the first drying. Immediately when the specimen was wetted, the two cracks fully developed on the surface at the two curled edges. The morphology of cracks at the end of each cycle for the specimen (MC3) is presented in Figure 6.32. Very few cracks formed over the other cycles in which lower tensile forces generated. However, the cracks only developed in X-direction responding to restraining direction. The results in Figure 6.33 show that crack intensity factors (CIF) and crack aperture increase up to the second cycle and then maintained constant till the fourth cycle.

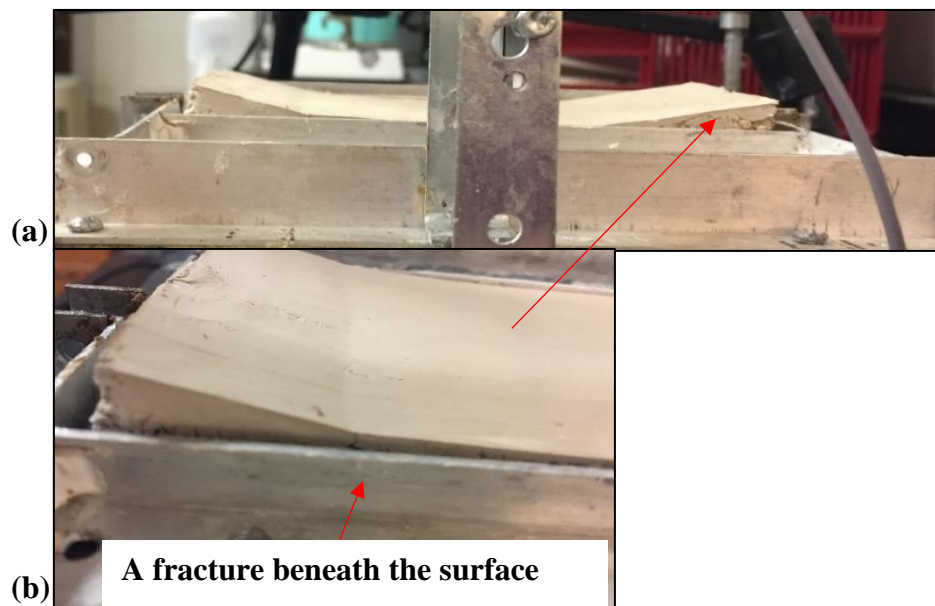


Figure 6.31 Side view of the MC3 at the end of first drying, (b) a curled edge with invisible crack beneath the surface

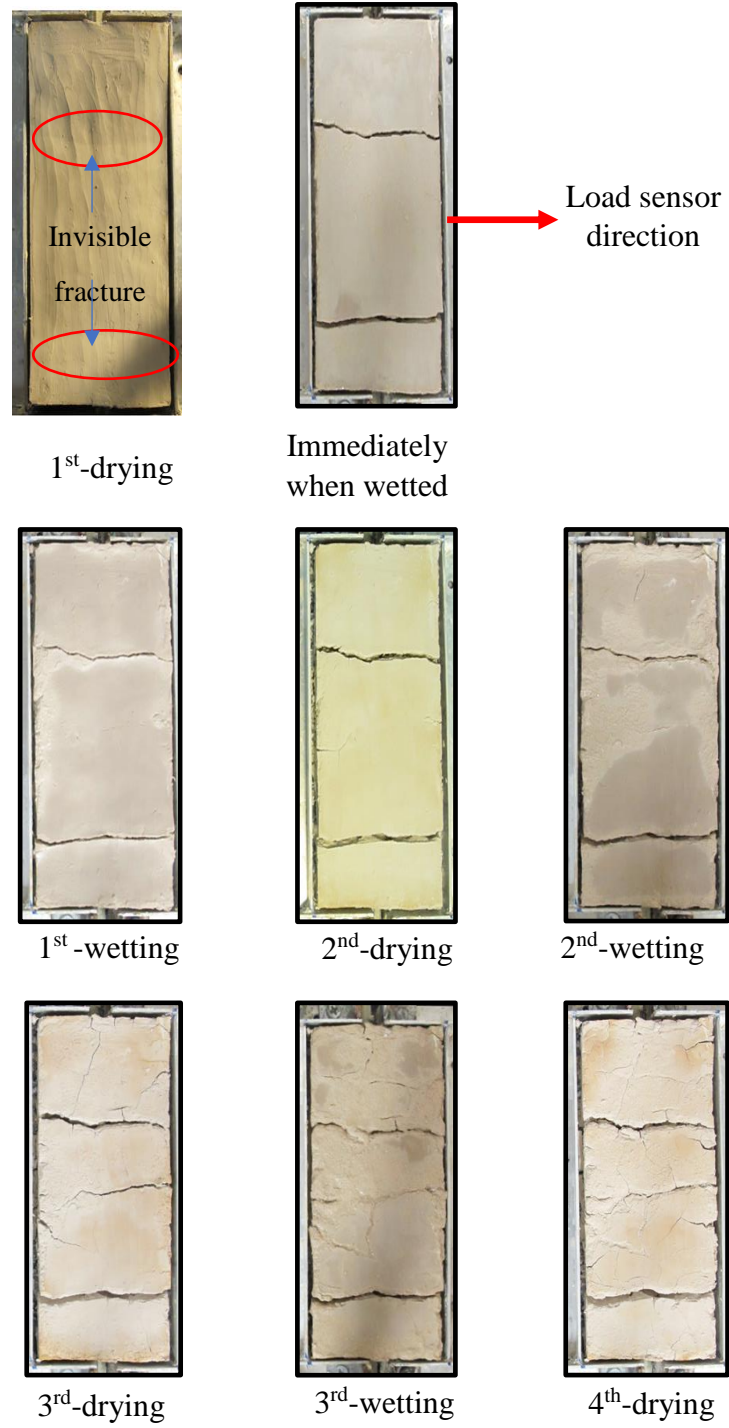


Figure 6.32 Crack patterns at the end of each cycle for the MC3

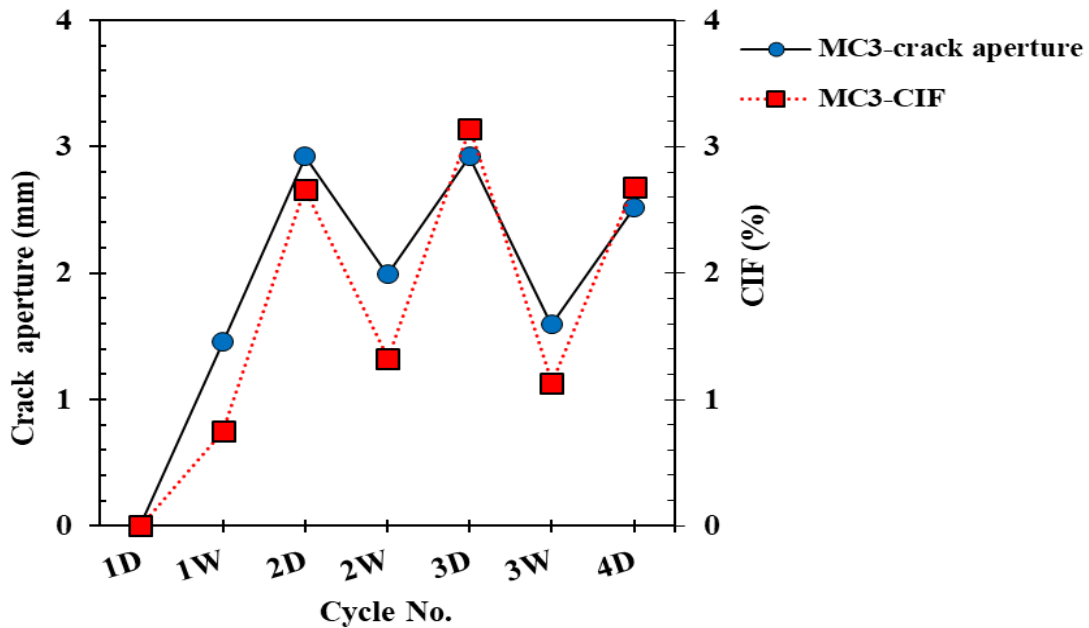


Figure 6.33 Variation of crack intensity factors (CIF) and average crack aperture for the MC3 over cycles

6.4.4 Directional restriction/unsaturated-compacted specimen (MC4)

In this section, only the effect of directional restriction had been studied by using a constrained pattern different than the one used for the specimens of MC1, MC2 and similar to that one for MC3. The compacted soil specimen namely MC4 was prepared at similar initial conditions of those of MC1, as shown in Figure 6.3. Different constraining condition was applied to the specimen by fabricating the protrusions to be perpendicular to the direction of the gap and in the same direction of the movement. In this case, the lower restraints will be provided in the direction of movement (perpendicular to the gap) in which lower tensile stresses will generate. While the higher tensile stresses will be in the other direction (parallel to the gap). Figure 6.34 shows a photo

of the tensile device with parallel constraining patterns. The specimen MC4 was subjected to one drying process. The variation of water content over time is showing in Figure 6.35.

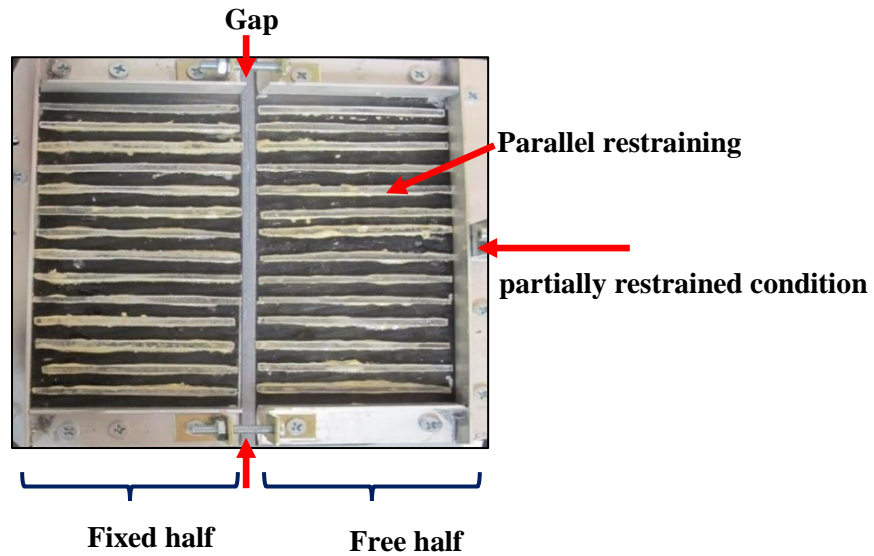


Figure 6.34 A photo of the new tensile device with parallel restraining condition

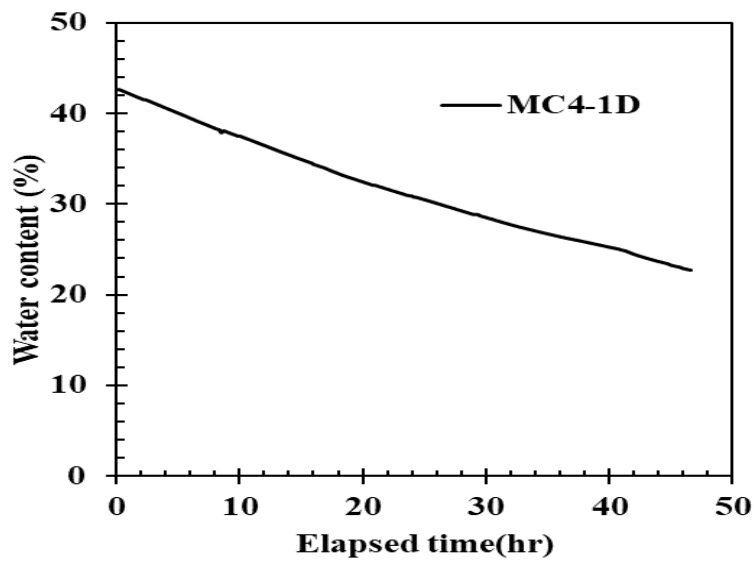


Figure 6.35 Variation of water content over time during the first drying process for the specimen MC4

6.4.4.1 Tensile and cracking behavior

The variations of tensile over time during the first drying is presenting in Figure 6.36. Figure 6.37 shows the variation of tensile forces as a function of water content over time during drying cycles. The tensile force increased gradually up to a peak value of 10 N after 19.53 hours from the beginning of the test at the cracking water content of 32.9 % and then decreased to an equilibrium state where the test was terminated. Initially, uncompleted horizontal cracks initiated at the both sides of the specimen. then an uncompleted longitudinal crack developed in responding to the restraints at the soil bed. In case of free shrinkage, the soil shrinks isotopically in which no stress localization occurs. However, in the case of restrained shrinkage, the soil shrinks in random configurations in responding to the constraints, as a consequence stress and displacement localizations generate, and this resembles to our case herein. Also, it was clearly observed that the crack always initiated at the early stage of the drying process. Figure 6.38 shows the crack patterns at some time intervals for the specimen MC4 during the first drying process.

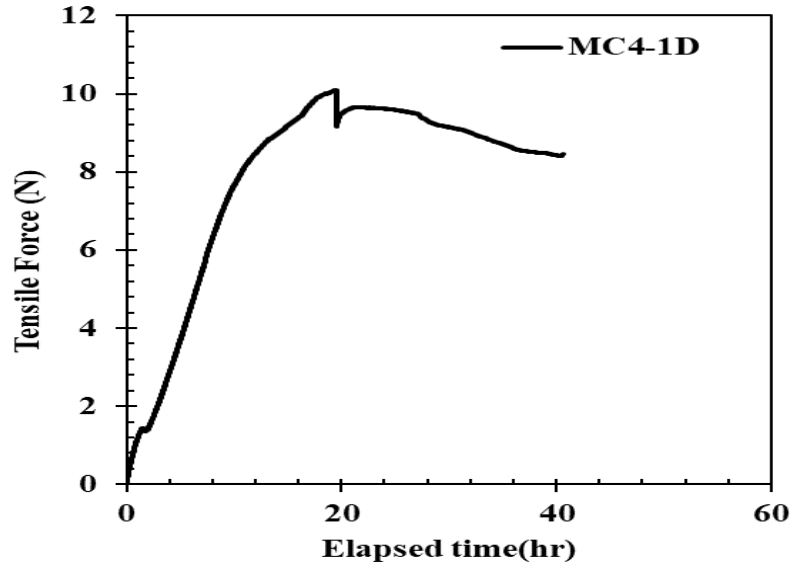


Figure 6.36 Variation of tensile force over time during the first drying process for the specimen MC4

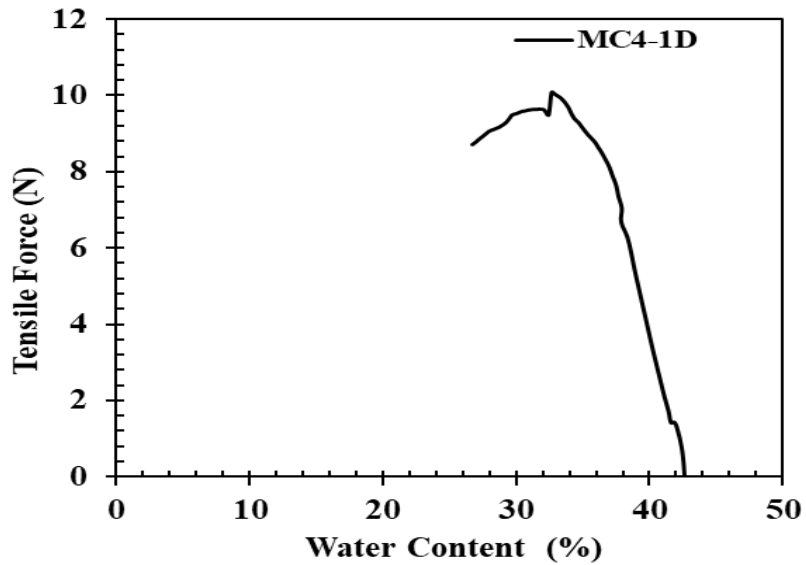


Figure 6.37 Variation of tensile force as a function of water content during the first drying process for the specimen MC4



after 11-hour at $w = 37\%$



after 14.6-hour at $w = 35\%$



at maximum tensile force, after 19.5-hour, $w = 32.9\%$



after 36-hour, $w = 26\%$

Figure 6.38 Crack patterns at some time intervals for the specimen MC4 during the first drying process

6.4.5 Soil structure/fully-saturated specimen (MS)

A fully saturated (slurry) specimen was prepared at the initial water content of about 90.19% \pm 0.5% (\approx LL) and dry unit weight of 7.848 kN/m³. The soil was prepared in the tensile device in two layers with maintaining a small gap between the two halves by utilizing a plastic spacer. Two screws were used to preventing closing the gap and facilitating soil preparation, and then they were removed after completion of soil preparation and before starting the test. Very light tamping and vibration were applied to the soil specimen to get rid of the air bubbles. The fully-saturated (slurry) soil specimen is referred herein to “Mixture-Slurry” (MS). The specimen MS was subjected to four wetting/drying cycles. For each drying process, the gap between the fixed and free jaws was locked after the tensile failure occurred. Then the crack propagation continued till reached to the equilibrium state. The variations of water content over time during drying is presented in Figure 6.39. For wetting process, the sample was wetted to lower water content compared to the initial water content as-prepared. Figure 6.40 (a & b) present the changes in void ratio and volume during drying cycles in the fully saturated soil specimen.

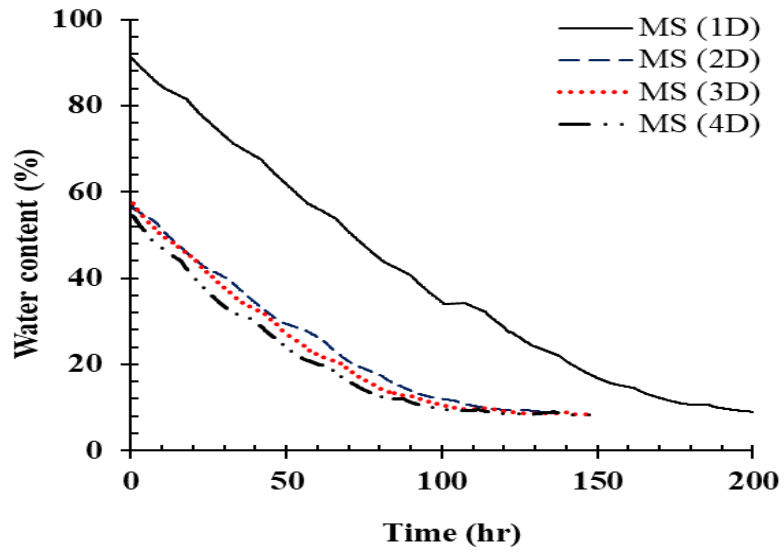


Figure 6.39 Variations of water content over time for the fully-saturated specimen (MS) during four wetting-drying cycles; D: Drying

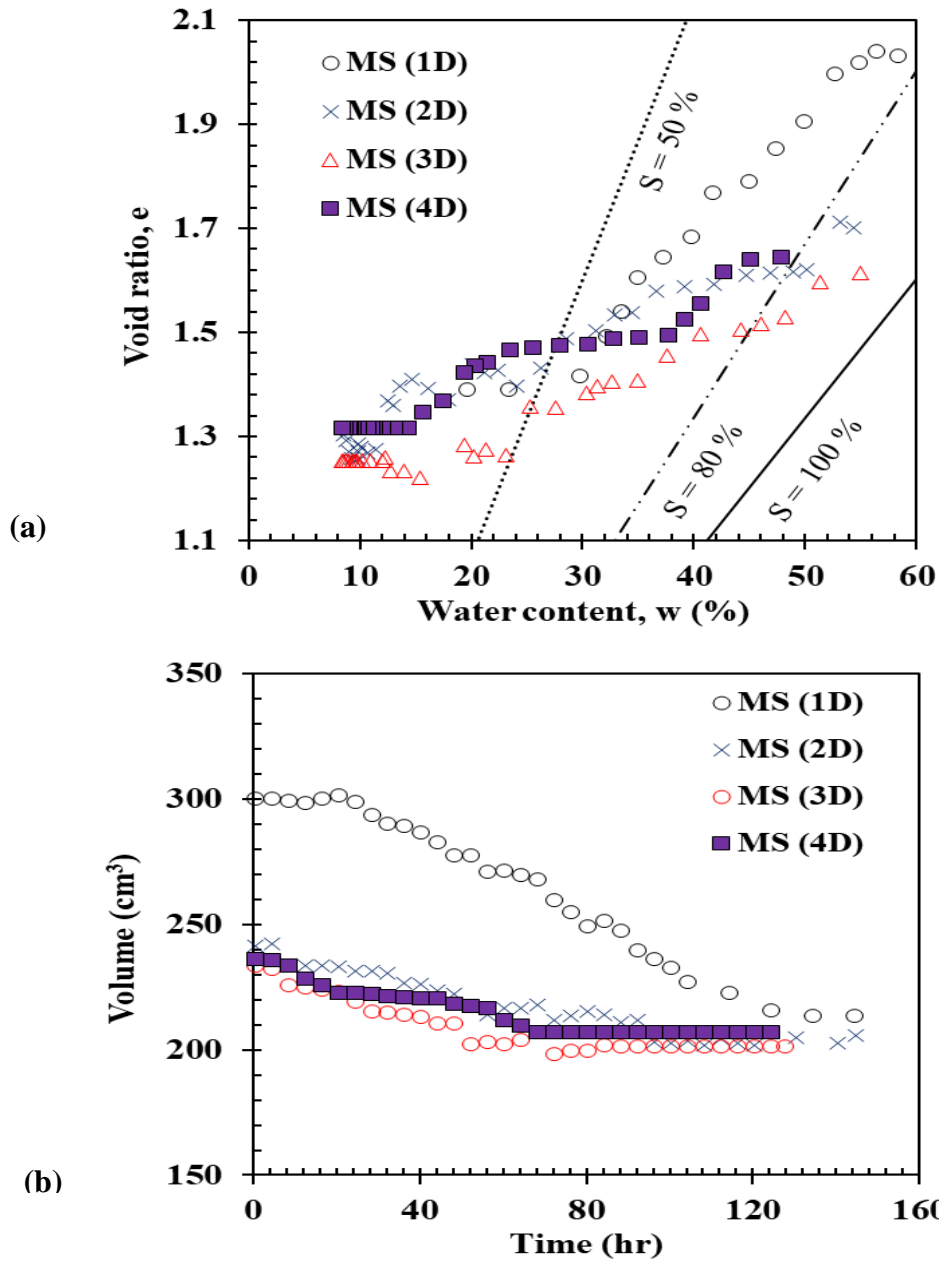


Figure 6.40 (a) Void ratio vs. water content, (b) volume change over time for fully-saturated specimen

6.4.5.1 Effect of cyclic drying/wetting on tensile behavior

The variation of tensile and lateral-induced expansion forces over time through drying and wetting processes are presented in Figure 6.41 and Figure 6.42, respectively. Figure 6.43 shows the lateral displacement of the fully-saturated specimen during drying processes. Upon drying, the tensile forces gradually increased up to the peak value and then decreased when drying proceeded and the cracks fully propagated. When approached the equilibrium at the end of the drying, the force maintained at constant value after the peak. This due to locking the gap after the failure which helped in maintaining the force. The maximum lateral displacement of the soil specimen was measured in the first drying of about 3.9 mm. While the soil specimen moved less in the other drying cycles with the maximum displacement of about 0.69 mm.

Upon wetting, the tensile force decreased instantaneously till reached to zero value, where the soil experienced swelling/expansion due to water absorption. After that, the lateral-induced expansion force generated and then increased to very small values ranged from 0.5 N to 2.5 N till approached to a constant value. No variation was observed on the lateral expansion forces after 1 hour in which the soil specimen reached to a constant water content.

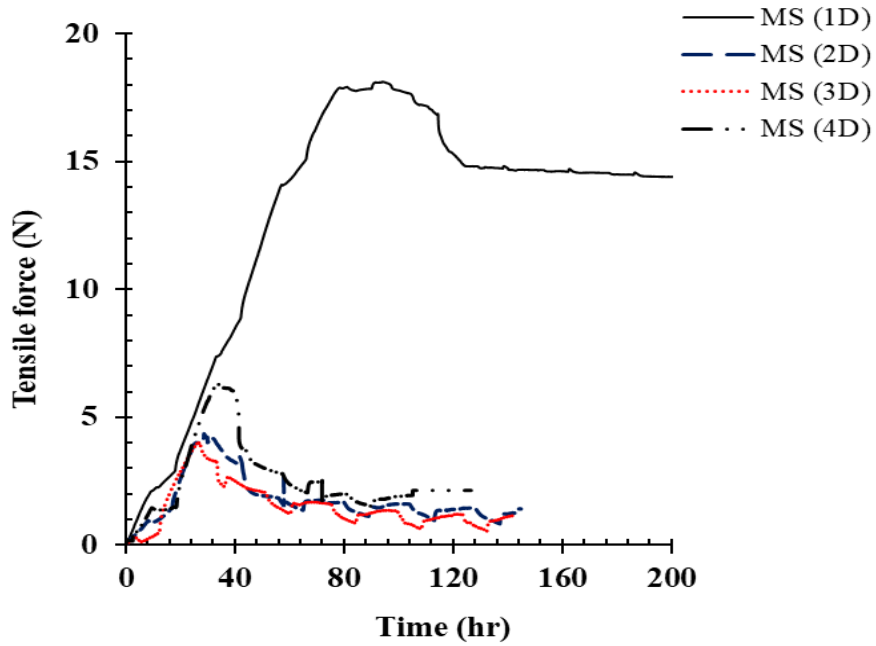


Figure 6.41 Variations of tensile forces over time for the fully-saturated specimen (MS) during four drying cycles; D: Drying, with locking after failure

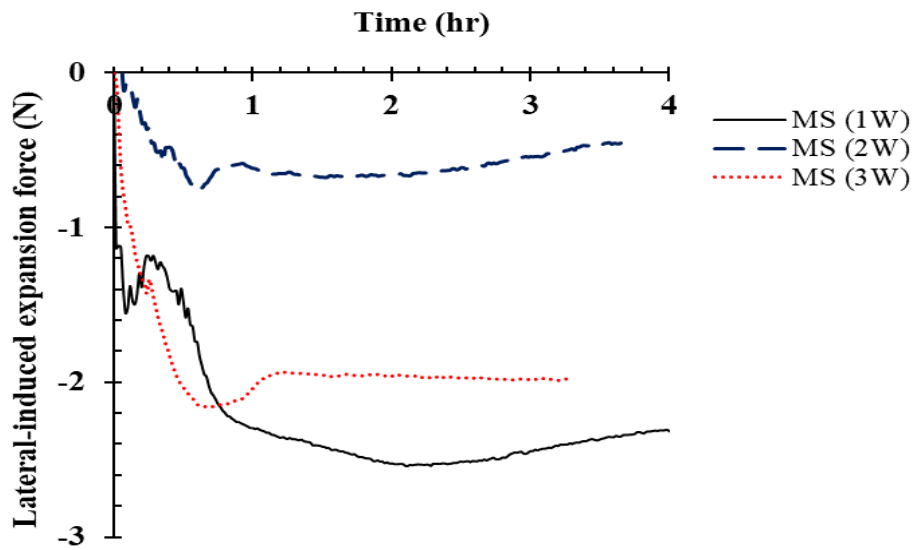


Figure 6.42 Variations of lateral-induced expansion forces over time for MS specimen

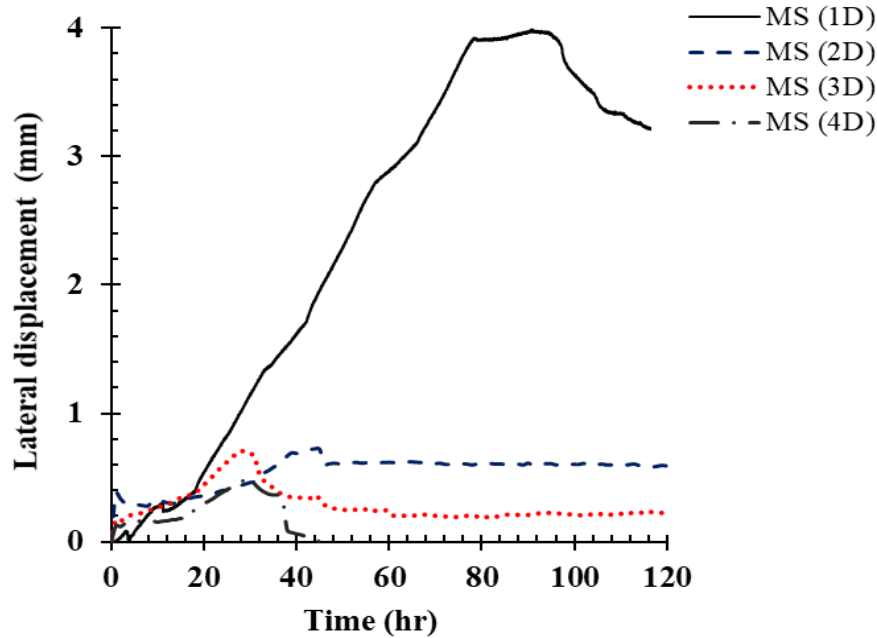


Figure 6.43 Lateral displacements over time for the fully-saturated specimen (MS) during drying; D: drying, with locking after failure

Figure 6.44 (a & b) show the variation of tensile forces as functions of degree of saturation and water content during four sequential wetting/drying cycles, respectively. For all cycles, the tensile force increased with the decreasing of moisture content and increasing of the corresponding suction. When specimen failed, the tensile force decreased, while drying proceeded. This nonlinear relationship between tensile strength and water content was previously investigated by Nahlawi et al (2004). However, they conducted the tensile tests on soil at different water contents.

In the first drying, the soil exhibited much higher tensile strength than those of the other cycles. The first crack in the y-direction was determined at the water content of 44.3 % for the first drying. For the other drying curves, the soil exhibited tensile failure at the water contents of 38.3 %, 35.7 %, and 29.5 % in the second, third, and the fourth drying, respectively. No more new

cracks observed in the y-direction. More details regarding of the tensile cracking are provided in chapter V (section 5.4.1).

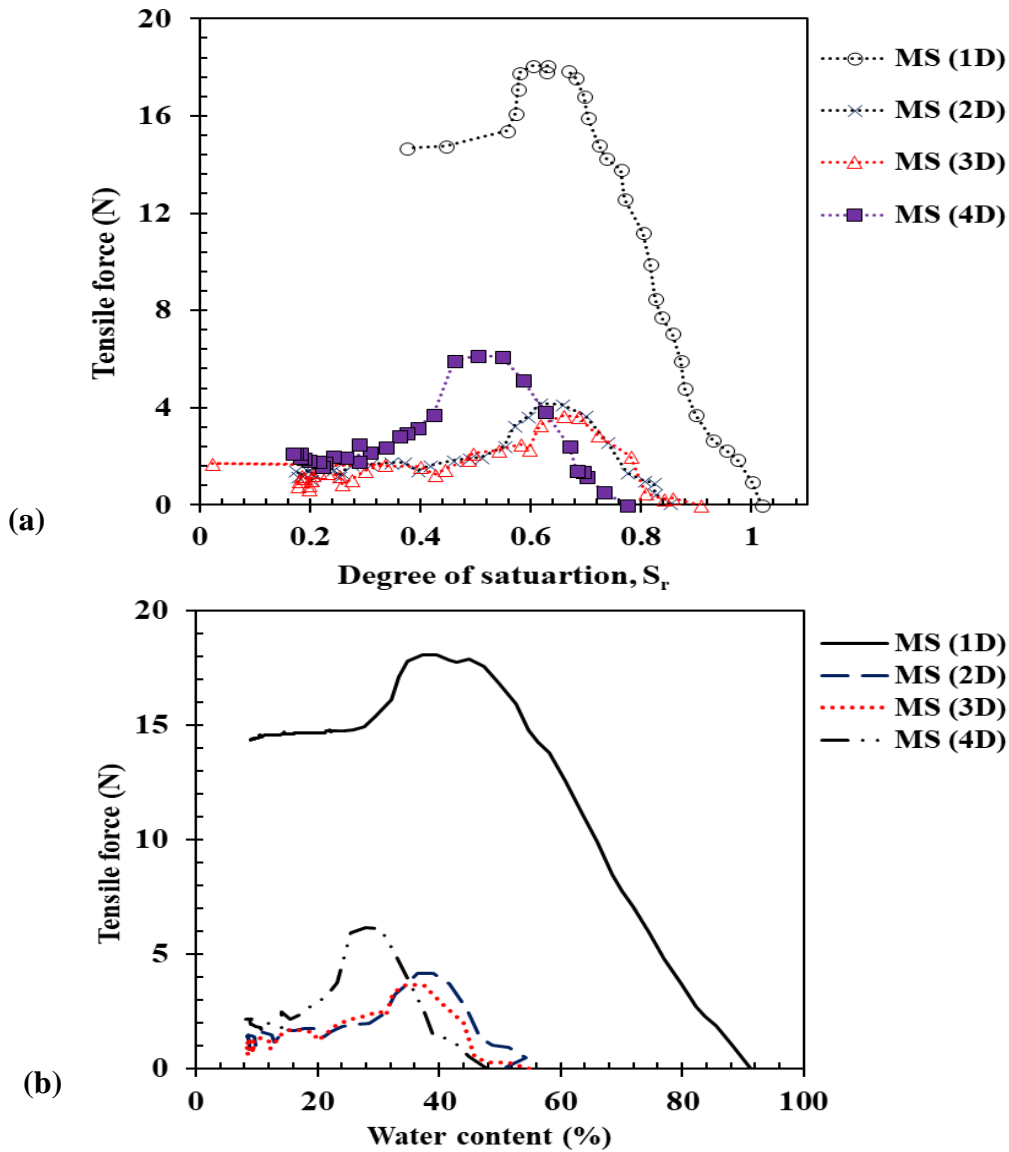


Figure 6.44 (a) Variations of tensile forces as a function of degree of saturation, (b) tensile force vs. water content for the fully-saturated specimen (MS)

In the first drying, the soil experienced much higher peak force (i.e., 17.8-N) compared to the other drying processes. At the end of the first drying, the primary cracks of the soil specimen developed and propagated. In the second and the third drying, the peak forces were determined to be 4.3 N and 4.02 N, respectively. While in the fourth drying, the peak tensile force was obtained 6.4 N which was slightly higher than those of the second and third drying. It is believed that the soil structure (fabric and the inter-particle forces) was exposed to deteriorations during the first drying. This may cause irrecoverable deformations in the soil structure resulting in a reduction in the strength after the first drying.

6.4.5.2 Effect of cyclic drying/wetting on desiccation cracking

Figure 6.45 and Figure 6.46 present the crack patterns at the end of every drying/wetting cycle of the fully-saturated sample tested under locked-gap condition after failure. In the first drying process, a primary crack was initially formed in x-direction subdivided the sample into two blocks. After that, a fully propagated crack in the y-direction was formed approximately after 105 hours. When drying proceeded more cracks propagated in the both directions. Upon wetting, the soil specimen was not wetted to the water content similar to the initial one-as prepared. Hence, less deformations were observed during drying and wetting. This resulted in insignificant healing and closing of the present cracks that formed in the first drying. Moreover, no more considerable crack propagation was observed in the second, third, and fourth drying processes.

It was obviously observed that the soil specimen didn't experience significant crack propagation when subjected to alternatives wetting/drying cycles. In the first drying, the soil exhibited CIF of about 8.7 % and increased slightly to 9.1 % in the second drying. No more cracks were obtained over cycles; the maximum CIF was determined of about 9.6 %, as shown in Figure

6.47. This may be interpreted due to the small deformations and deteriorations that the soil exhibited during wetting/drying because the soil was not wetted to the initial water content-as initially prepared.

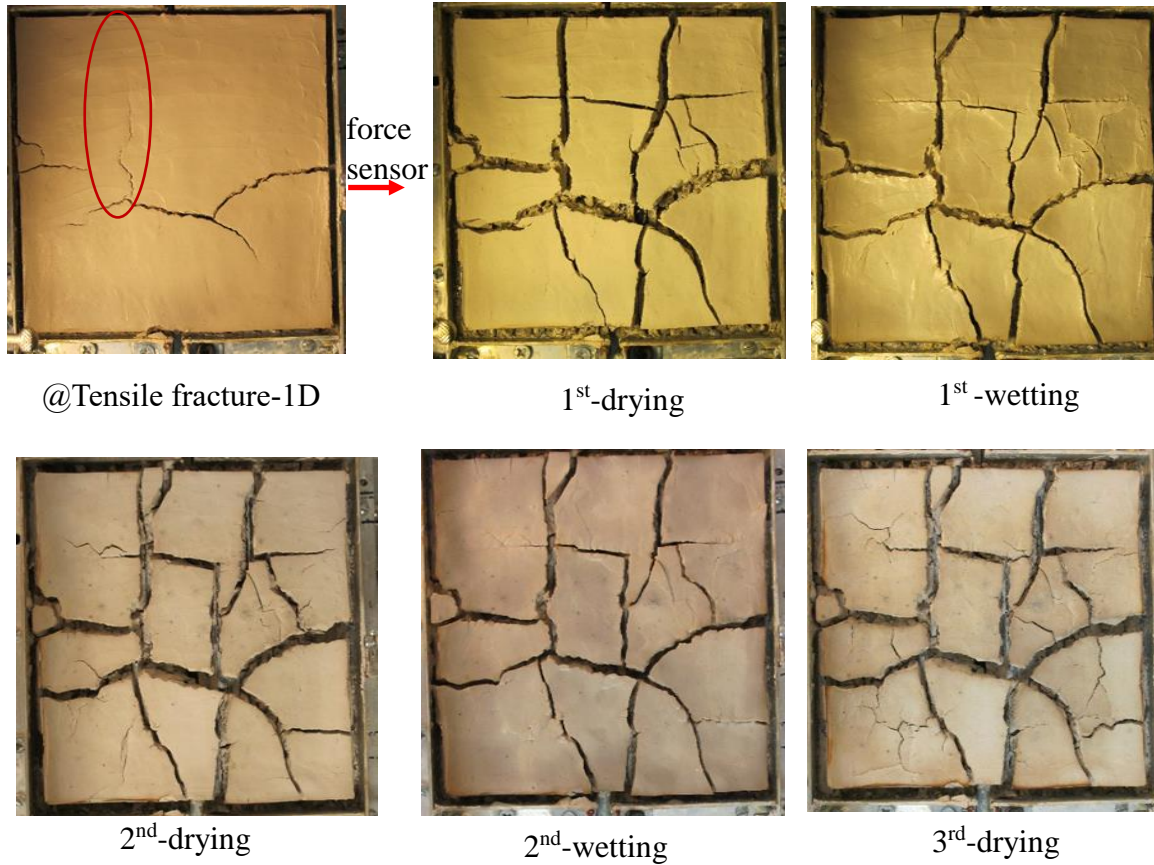


Figure 6.45 Crack patterns of a fully saturated sample (slurry) (MS) subjected to the new tensile test in cyclic wetting/drying, with locked-gap scenario after failure

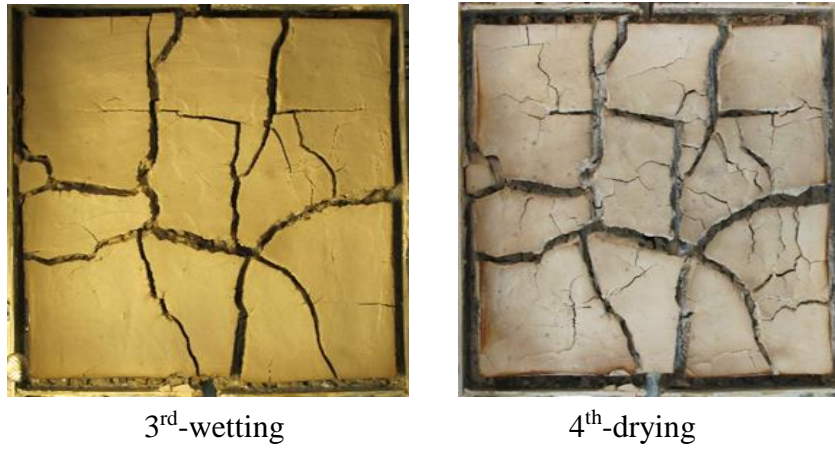


Figure 6.46 Continue. crack patterns of a fully saturated sample (slurry) (MS) subjected to the new tensile test in cyclic wetting/drying, with locked-gap scenario after failure

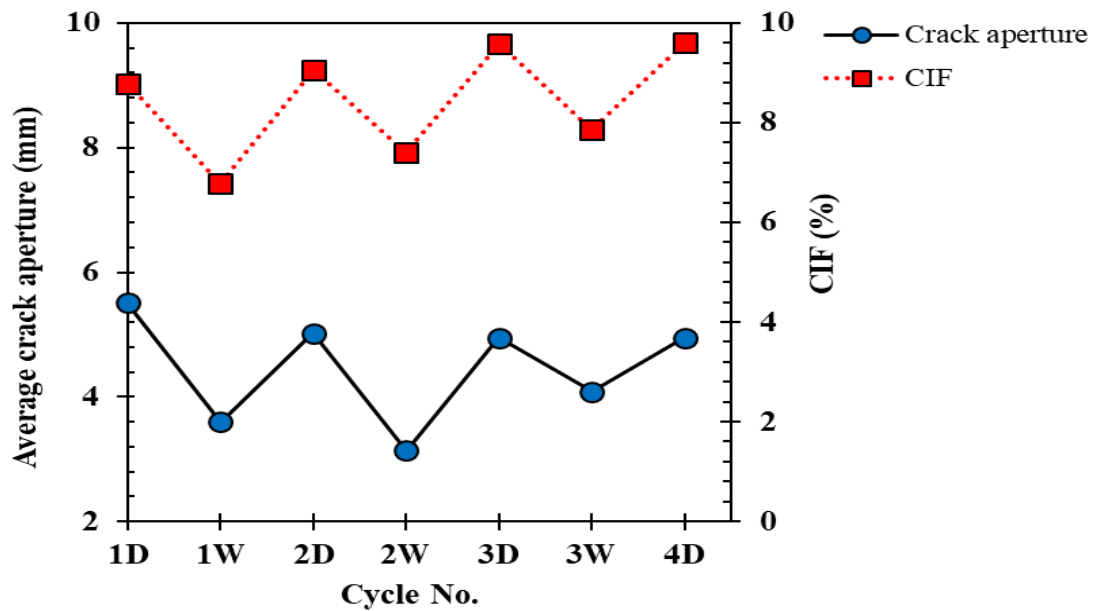


Figure 6.47 Crack Intensity Factor (CIF) and average crack aperture at the end of every wetting/drying process for the fully-saturated specimen (MS); Locked-gap after failure

6.4.6 Effect of specimen's thickness, size, restraining condition and soil structure on tensile and cracking behavior

The effect of four factors has been investigated on tensile and cracking behavior of a high expansive soil under partially restrained condition. These factors involve specimen's size, thickness, constraining condition, and soil structure. Figure 6.48 presents the variations of the maximum tensile and lateral expansion forces for all specimens through cycles. Figure 6.49 (a & b) shows the variations of Crack Intensity Factors (CIF) and average crack aperture that experienced by specimens over cyclic wetting-drying processes, respectively.

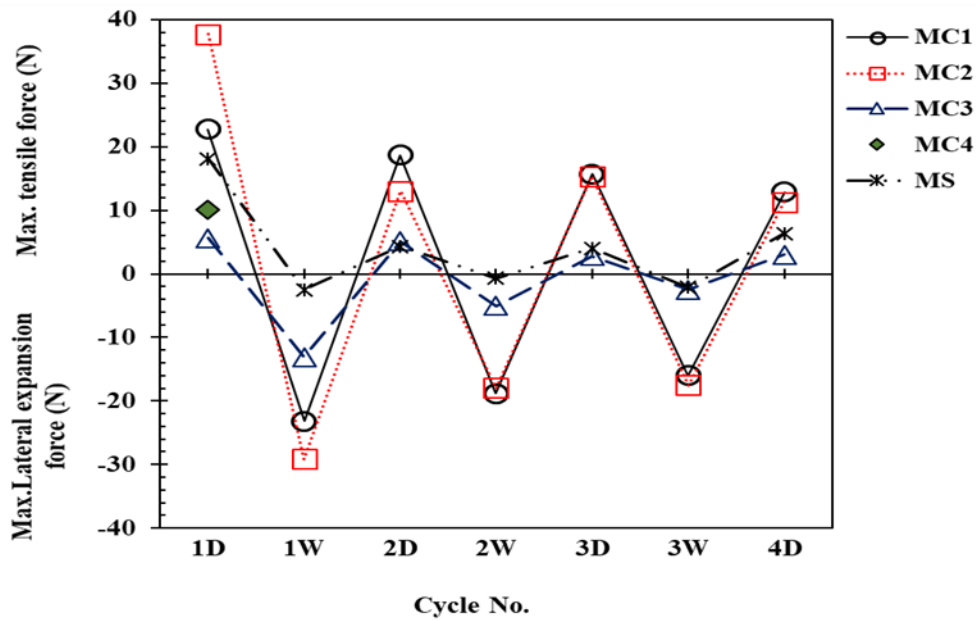


Figure 6.48 Variation of tensile and lateral-induced expansion forces over cycles for MC1, MC2, MC3, MC4, & MS; W: Wetting, D: Drying

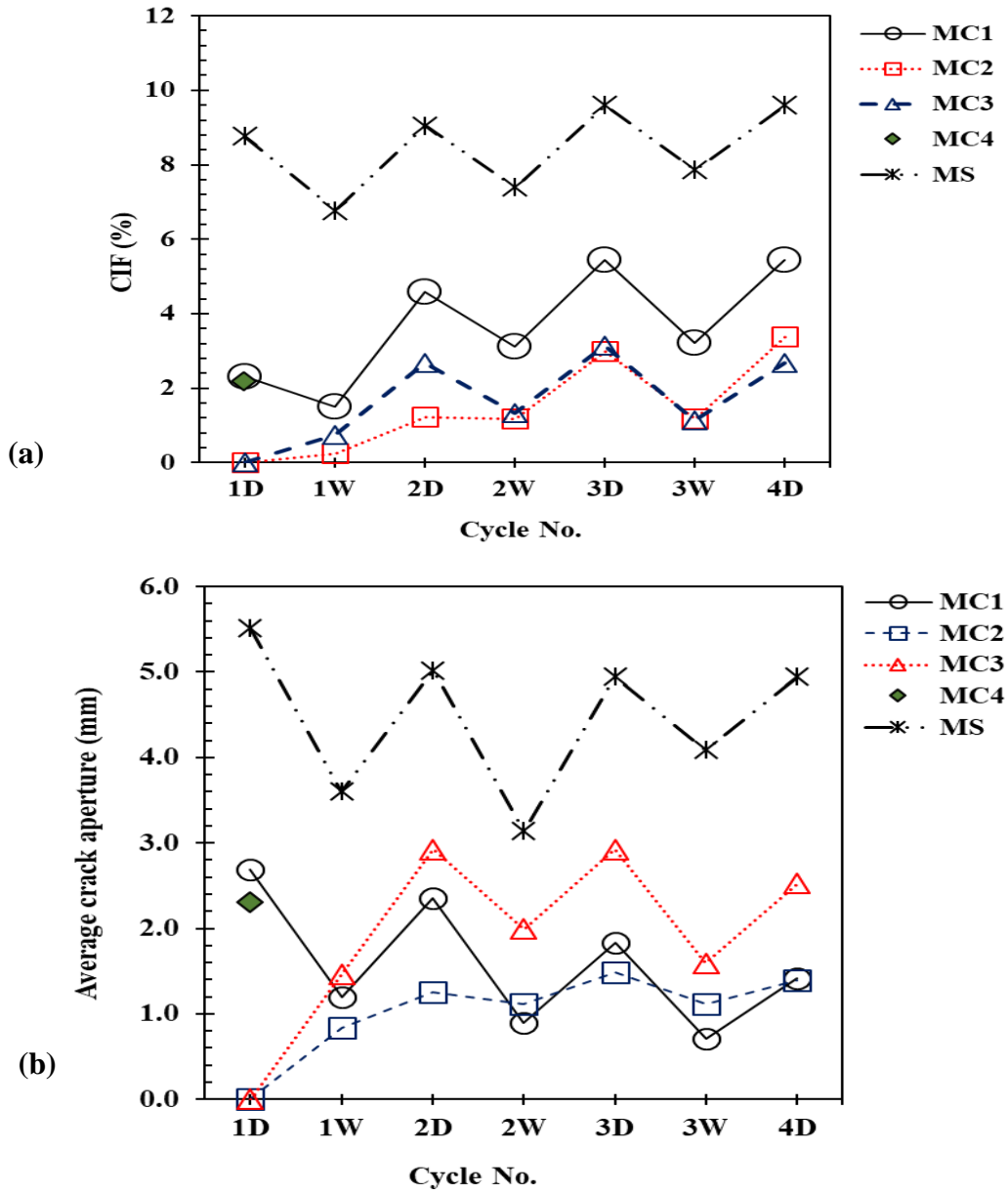


Figure 6.49 (a) Variation of Crack Intensity Factor (CIF); (b) variation of average crack aperture over cycles for MC1, MC2, MC3, MC4, & MS; W: Wetting, D: Drying

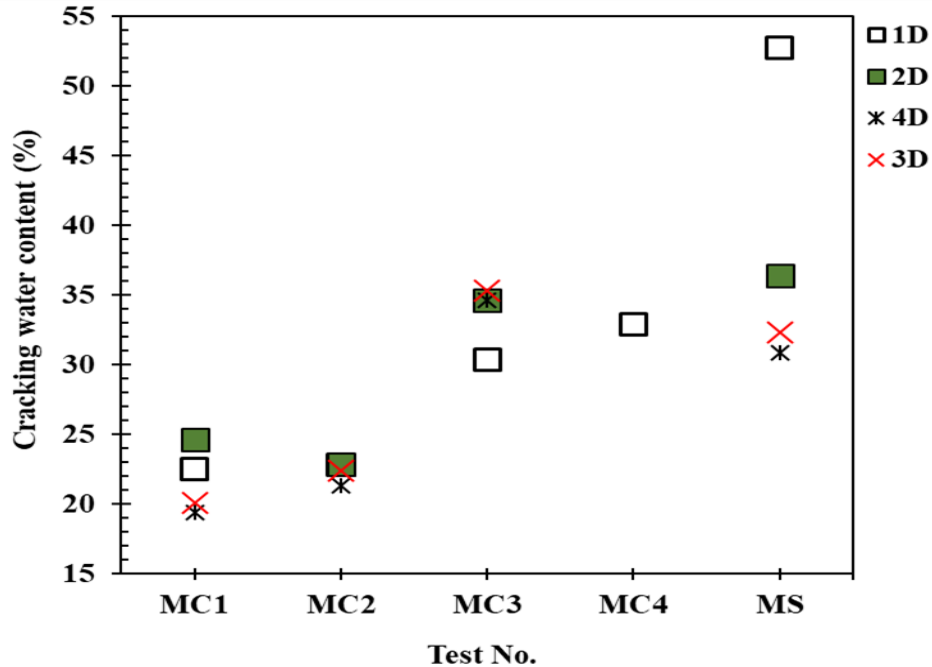


Figure 6.50 Variation of cracking water content over drying cycles for MC1, MC2, MC3, MC4, & MS; D: Drying

6.4.6.1 Effect of specimen's thickness

A comparison between the results of MC1 and MC2 is presented in Figure 6.48. In the first drying, MC2 exhibited higher peak tensile force than that of MC1. However, unlike our expectation, MC2 developed similar maximum tensile forces to those of MC1 over the other cycles. This similarity may be due to two potential reasons; the first one is that no significant effect of specimen's thickness after the first wetting/drying, the second reason is that due to wetting the MC2 to lower water contents compared to the initial one as compacted.

Upon wetting, similar behavior was obtained for MC2 and MC1. MC2 exhibited an instantaneous decrease in the tensile forces during wetting; the tensile forces reduced till reached

to zero value. After that, the lateral expansion forces readily generated and then increased to the values ranged from 12 N to 29 N till approached to equilibrium.

Compared to cracking results of MC1, MC2 exhibited lower CIF(s) over cycles, as shown in Figure 6.49. In general, both specimens were initially cracked at almost similar water contents although the MC2 was wetted to lower water contents during wetting cycles. For MC2 the cracks initiated at the same water content of about 22 % in all drying cycles. While the cracks initiated at the range of water content of about 21 to 24% for MC1.

6.4.6.2 Coupled effect of specimen's size and directional restriction

MC3 specimen was prepared at identical initial conditions of those of the reference specimen (MC1), except the size and constraining condition were different. Two comparisons were made, as follows; the first one compared with the reference specimen MC1 for investigating effect of specimen's size and directional restriction, and the second one compared with MC4 for the effect of directional constraining only. For the first comparison, MC3 experienced lower tensile and lateral-expansion forces compared to those of MC1 during drying and wetting, respectively, as shown in Figure 6.48 .Fewer cracks developed in MC3 responding to the constraining direction at the soil bed; while no cracks developed in the other direction (i.e., y-direction). It seems that the strength of soil specimen is smaller when the ratio of length to width becomes higher. Accordingly, it can be concluded that the specimen's size influences on crack patterns where smaller size developed fewer cracks and lower tensile resistance.

Compared with MC4, different cracks patterns were obtained between the two specimens. This is mainly attributed to the size ratio where specimen with smaller size ratio generates lower tensile resistance. Also, it should be mentioned herein that directional restriction doesn't influence

on crack patterns for identical compacted specimens (i, e., MC1 compared to MC4), even though MC1 experienced double tensile force of that one of MC4 in the first drying.

6.4.6.3 Effect of directional restriction

Parallel and perpendicular restrictions were employed for studying the effect of directional restrictions on tensile behavior and desiccation cracking of two identical prepared specimens. The reference specimen MC1 was tested in the new tensile device with perpendicular restriction relative to the direction of the partial motion introduced at the soil bed. While a parallel restriction was employed for testing the specimen MC4. The comparison is performed herein only for the first drying cycle, since MC4 was subjected to one drying process. The results presented in Figure 6.48 and Figure 6.51 show that MC1 experienced higher tensile resistance than that of MC4. This meets our expectation that the perpendicular restriction induces higher tensile forces than those of the parallel one. However, the crack patterns in the two cases are similar in the first drying, as shown Figure 6.52. The results of image analysis show almost similar crack patterns of nearly identical CIF(s) of 2.3% and 2.2% and crack apertures of 2.7 mm and 2.3 mm experienced by MC1 and MC4, respectively. Therefore, it can be concluded that the directional restriction impacts on

the tensile strength of soil where higher one developed for the soil-perpendicular interface. No significant effect was observed on cracking patterns in two cases (Figure 6.52).

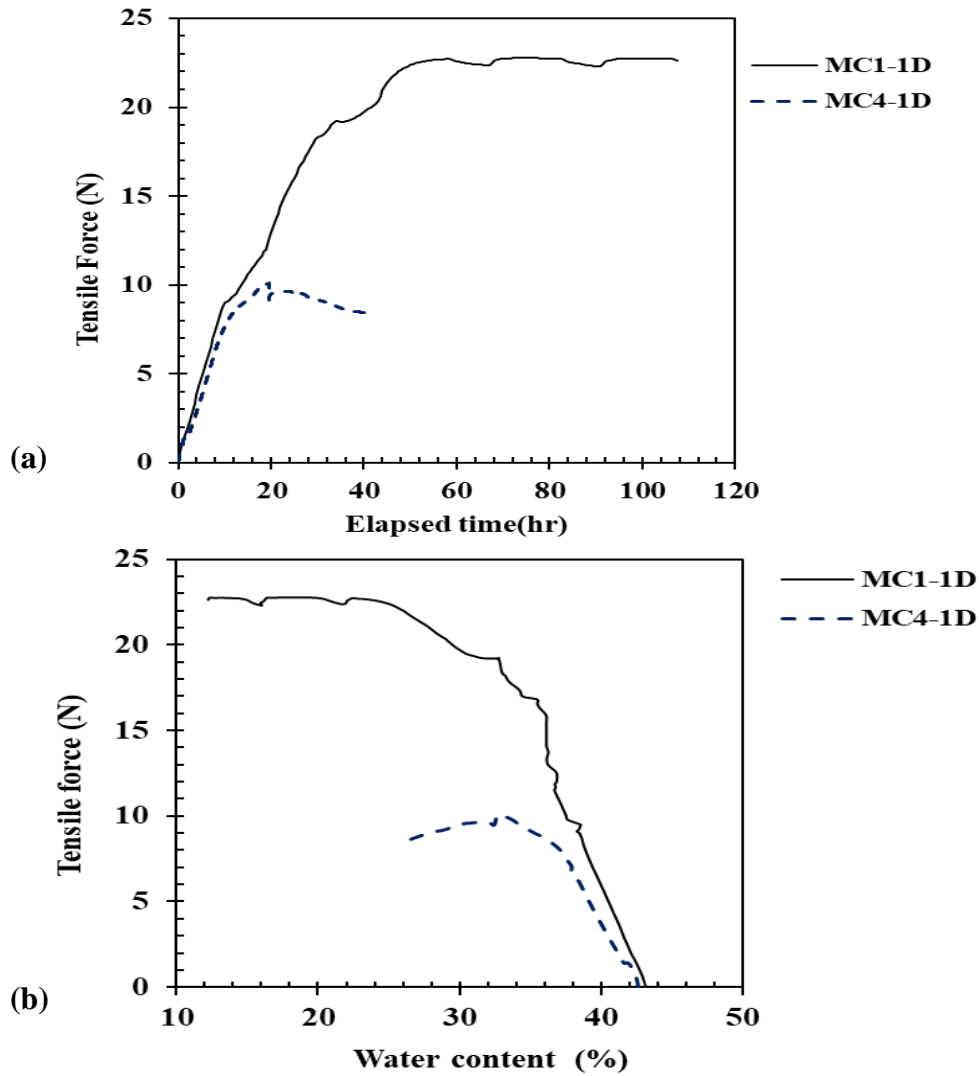
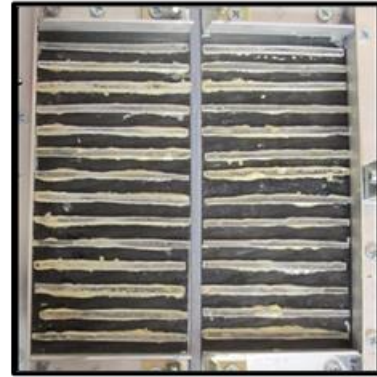
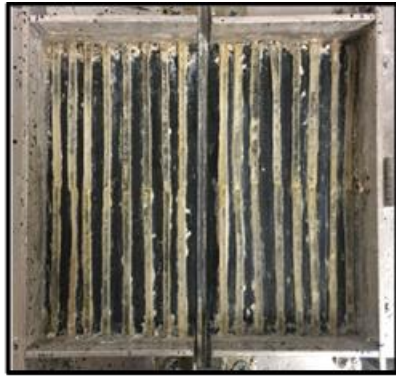
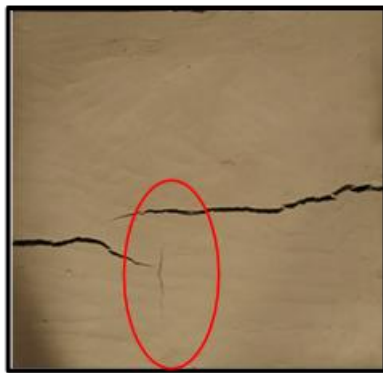


Figure 6.51 Comparison between MC1 and MC4 for the first drying cycle; (a) tensile forces over time, (b) tensile forces as a function of water content



(a)



(b)

MC1: @ peak, $t = 50$ -hour,
 $w = 25.9\%$

MC4: @ peak, $t = 20$ -hour,
 $w = 35\%$



(c)

Figure 6.52 Comparison between crack patterns for MC1 and MC4; (a) constraining case; (b) at the peak; (c) at the end of the first drying

6.4.6.4 Effect of soil structure

Compared to MC1, the fully-saturated specimen MS experienced lower tensile strength in the first drying and decreased more through cycles. More cracks were experienced by the fully-saturated specimen (MS) compared to the compacted specimens (i.e., MC1, MC2, MC3, and MC4). This is owing to the effect of soil structure in which the slurry specimen has lower interparticle strength and different soil particles configurations than those of compacted one. However, the MS experienced higher tensile strength in the first drying for MC3 and MC4 and nearly equal one through the other cycles for MC3. This may relate to differences in the size ratio in case of MC3 and constraining condition in case of MC4.

6.5 Concluding remarks

A number of factors had been considered to investigate the performance of the new tensile device involving; specimen's thickness and size, directional restriction, and soil structure. Several findings are highlighted below:

1. In general, the orthogonal constraining condition induces higher tensile forces than those of parallel one.
2. For the same parallel restraining and different size ratios, the specimen of smaller size ratio experienced lower tensile strength (i.e., compare MC3 & MC4). For example, in the first drying, MC3 experienced the peak tensile force of 5.6 N which is half of that developed by MC4 (10.1 N).
3. For orthogonal restraining, the thicker specimen developed higher tensile forces than those of thinner one in the first drying. However, no significant changes were observed over the other cycles (i.e., compare MC1 & MC2).

4. For the orthogonal constraining, the compacted specimens developed higher tensile forces and fewer cracks compared to those of fully-saturated specimen (i.e., compare MS with MC1 & MC2).
5. No peak tensile forces were obtained for MC1 and MC2 in which indicates that these specimens can resist more tensile stresses. Also, this indicates that the tensile strengths of these specimens are higher than the values determined in the tensile tests under partially restrained condition.

CHAPTER VII

CONCLUSIONS AND RECOMMENDATIONS

7.1 Introduction

This research aimed to study the hydro-mechanical behavior of soils subjected to multiple drying and wetting cycles. This has been stemmed from the observation of crack propagation of soil when exposed to successive drying/wetting cycles. Under drying, soil may develop irreversible deformations in fabric resulting in crack formation, while upon wetting, soil may undergo softening/weakening which provides healing and closure to the present cracks that formed in the previous drying. However, these cracks remain weak region and under alternate drying the cracks re-open and propagate increasingly. After a certain number of drying/wetting cycles, the cracks remain unchanged without any propagation. In this chapter, the main goals achieved are highlighted below:

- A laboratory investigation which covers the physical and hydro-mechanical soil characteristics was carried out. Some of these properties involve the volumetric behavior of soil when subjected to cyclic wetting/drying processes, water retention curves of fully-saturated and compacted soils, and others.
- An experimental campaign was carried out to study the influence of soil-interface on unsaturated and saturated shearing strength of soil.
- A laboratory investigation to study the impact of soil-interface coupled with the effect of different initial conditions of soils on the inception and propagation of cracks. Moreover,

the soil's particles were tracked during drying and wetting by using the Digital Image Correlation (DIC) analysis.

- A new innovative tensile device was designed and developed for measuring the tensile strength of soil subjected to circumstances similar to those in field, with an adequate recognition of the limitations of this approach, if any. In addition, the DIC analysis was employed to track the soil's particles during cyclic shrinkage and swelling.
- A laboratory exploration was performed to examine the validity and feasibility of the new tensile device. In this campaign, the effects of some parameters on tensile and cracking behavior of soil were examined. These parameters included the specimen's size and thickness, directional restriction, and soil structure.
- The effect of cyclic wetting and drying processes was quantitatively examined by employing two contactless techniques involving; image analysis for capturing some key variables, such as, crack aperture, crack propagation, and volume change, and Digital Image Correlation (DIC) method for tracking the the displacement field vectors of the deformed soil.

In this chapter, the results and observations leading to general conclusions which are presented corresponding to each accomplished goal listed above.

7.2 Shear strength of unsaturated and saturated soil interfaces

The directional shear strengths were examined between compacted soils and four different interfaces involving; perpendicular, circular, parallel and smooth surfaces. The results have revealed that the shearing behavior of the soil is strongly affected by the interface patterns. The strength of unsaturated compacted soil was found higher than that of saturated one. The higher

strength is determined for the soil-soil and the lower one was obtained for those experiments involving smooth interface. The strength for the case of perpendicular grooves with respect to the shear direction is higher compared to the ones of circular, parallel, and smooth cases. The strengths of circular patterns are determined between the ones for perpendicular and parallel interfaces. The influence of different interfaces is mainly observed in the linear envelopes that used to define the shear strength parameters; the friction angles and the cohesion values.

7.2.1 Contributions and future recommendations

The experimental campaign herein provides a comprehensive knowledge of the effect of different interface patterns on the shear behavior of unsaturated and saturated compacted soils. These findings can provide significant improvements on the designing criteria of some ge-structures in the field. The results are also valuable for testing the validity of any cracking model. Future recommendations will involve large-scale study under circumstances similar to those in the field which would be beneficial to capture the actual and accurate determination of the shear strength of soil interfaces.

7.3 Desiccation plate tests

A comprehensive series of desiccation plate-tests was conducted on thin layers of the soil mixture using two different soil-interfaces subjected to unsaturated and saturated conditions. Two different counter-faces; including smooth and circular groove, were used to study the effect of soil-interface on the cracking patterns. The effect of alternative cycles wetting/drying on the crack patterns had been investigated as well. The morphology of crack patterns was determined using the image analysis technique to analyzed and interpreted the effects on test outcome. Moreover, the Digital Image Correlation (DIC) technique was employed for understanding the emerging

phenomenon behind soil cracking, particularly, during wetting process. The conclusions are highlighted below:

- In general, the constrained specimens developed more cracks than the free ones. Even though negligible constrains were provided between the soil and the smooth interface, the free specimens developed cracks during the wetting/drying cycles. This indicates that the interface factor can't be taken as the only factor for inducing cracks in soils.
- More cracks developed each cycle till reach to an equilibrium state of no significant cracks formed. Accordingly, the significant effect of the cyclic wetting/drying processes on the evolution and propagation of cracks in soils can be highlighted in this study.
- The saturated soils developed more cracks than unsaturated ones in which indicating that the initial saturation condition has a significant effect on cracking behavior.
- Although all unsaturated and saturated samples were compacted at high compaction energy, where this degree is highly recommended to compact some geotechnical structures, such as embankments (i.e., 94.4% of γ_{dmax} as determined from the standard Proctor test, ASTM D698), they all experienced cracks when subjected to alternatives wetting/drying cycles regardless to the restriction conditions at the soil boundaries (i.e., soil-interface) and the initial saturation conditions.
- It is believed that DIC technique can be a useful tool for analyzing stresses and strains distribution during cracking.
- Crack formation and propagation in soil are strongly related to the variations in the configuration of soil particles and stress state that occur during alternative shrinkage and swelling/expansion when subjected to drying and wetting, respectively.

- The most interesting finding in this study is that soil cracking may develop during wetting.
- Based on the results of evolution of the cracks under salt solution, it is clear that the mechanism of air invading is not reasonable and reliable to interpret the formation of desiccation-induced cracks.

7.3.1 Contributions and future recommendations

The laboratory investigating herein provide better understanding the effect of interfaces and initial conditions on soil cracking during multiple wetting/drying processes. The DIC analysis was a beneficial technique for tracking the soil's particle movements during cyclic shrinkage and expansion in drying and wetting processes, respectively.

For future work, the large-scale study will give significant information to improve our understanding of the cracking mechanism in soil. Moreover, this study can include studying the effect of some factors on cracking, such as, aspect ratio, sample size, and others. Laboratory tests such as SEM (Scanning Electron Microscope) and MIP (Mercury Intrusion Porosimetry), will be useful to gain comprehensive understanding of the micro-structure of cyclic shrink/swell of soil.

7.4 A novel tensile device for the accurate determination of tensile strength

A novel tensile device was developed for studying the tensile strength and desiccation cracking of soils when subjected to a number of wetting/drying cycles. The fundamental concept of the new testing method is that the soil develops tensile stresses when exposed to natural circumstances during drying process as in the field without employing any external tensile stresses. This new testing approach allowed for capturing some key variables associated with the desiccation cracking involving as follows; water content, suction, crack initiation, crack propagation, crack aperture, and volume change.

The new tensile device was found to yield accurate determination of tensile strength of soil. This technique has provided a significant advance over the other testing methods that are inherently limited to determine the tensile strength of soil at a constant water content. Two scenarios of application were performed in order to inspect the validity and feasibility of the device for determining the accurate tensile strength of soil. In addition, the effects of some factors on tensile and cracking behavior of soil, such as, thickness and size of specimen, directional restriction, and soil structure, have been studied. The evolution and propagation of cracking were captured during wetting/drying cycles by using a digital camera.

Crack dynamics was also captured by monitoring the displacement field vectors on the soil's surface by using the Digital Image Correlation (DIC) technique. This technique has advanced our understanding of cracking mechanism of soils when subjected to sequential wetting/drying cycles. Several findings are highlighted below:

- The scenario of locked-gap is more appropriate for the accurate determination of the tensile strength of soil subjected to wetting/drying cycles. This application can prevent any potential residual forces that may be carried out by the load sensor or/and the soil after every drying/wetting cycle.
- The trend of the tensile curve under drying condition shows that the tensile force increases with decreasing water content and increasing the corresponded suction up to the failure. After that, the tensile force decreases with increasing suction where no significant contribution is made on the soil strength. Upon wetting, the tensile forces decrease till approached to zero and then the lateral-induced expansion forces develop and remained constant at constant moisture content.

- The soil specimen experienced high reduction in the tensile strength after the first drying. Based on the Digital Image Correlation (DIC) technique, it was found that, the configurations of the vectors indicate that the specimen didn't act as one mass during the second, and third drying cycles. On the contrary, the soil mass experienced discontinuity wherever the defected regions found. Therefore, the specimen exhibited lower tensile strength and more cracks compared to those of the first drying.
- The DIC technique revealed that the soil may crack during wetting due to two reasons, as follows; the random and weak configurations of soil's particles that occurred during the first drying, and the specimen exhibited antistrophic expansion accompanying with different stress states within the material.
- The tensile and cracking behavior of soil rely on some factors, but not limited to them, including; specimen's thickness and size, directional restriction, and soil structure. The effects of these factors had been investigated under partially restrained condition by using the new tensile device. The results revealed that the tensile behavior of soil varies based on these factors in which different maximum tensile forces and different crack patterns were obtained.

7.4.1 Contributions and recommendations for future work

The new tensile device was designed and developed to study the tensile and cracking behavior of soils. This apparatus provided a novel approach over the previous ones that were limited to measuring the tensile strength of soils at constant water content in which did not stimulate the environmental circumstances as in the field. Accompanied with DIC analysis, this

testing method can be used to model the hydro-mechanical behavior of soils; for example, displacement fields of soil can be employed to estimate its deformation, strain and stress distribution during cyclic wetting/drying processes.

For future work recommendations, more improvements on the device will include direct suction measurements and enhance the wetting process.

REFERENCES

- Albercht, B. A., & Benson, C. H. (2001). Effect of desiccation on compacted natural clay. *J. Geotech. Geoenviron. Eng.*, 67(1), 67-75. doi:10.1061/(ASCE) 1090-0241
- Al-Jeznawi, D. (2015). Experimental studies of soil behavior subjected to drying. *Master thesis. Dept. of Civil Engineering, Texas A & M University.* .
- Alonso, E. E., Romero, E., Hoffmann, C., & Carcia-Escudero, E. (2005). Expansive bentonite-sand mixture in cyclic controlled-suction drying and wetting. *Eng. Geol.*, 8, 213-226.
- Amarasiri, A., Kodikara, J., & Costa, S. (2011). Numerical modelling of desiccation cracking. *Int J Numer Anal Meth Geomech*, 35, 82-96.
- ASTM. (2005). "Soil and rock (I)." D 420–D 5611, West Conshohocken, Pa.
- ASTM D3080/D3080M. Standard Test Method for Direct Shear Test of Soils Under Consolidated Drained Conditions. (2011). American Society for Testing and Materials.
- Atique, A., Sánchez, M., & Romero, E. (2009). Investigation of crack desiccation in soil from a flood protection embankment. *CRC Press*, 413-418.
- Ayad, R., Soulié, M., & Konrad, J. (1997). Desiccation of a sensitive clay: application of the model CRACK. *Can. Geotech. J.*, 34, 943-951.
- Baer, J. U., Kent, T. F., & Anderson, S. H. (2009). Image analysis and fractural geometry to characterize soil desiccation cracks. *Geoderma*, 154, 153-163.
- Benson, C. H., & Daniel, D. E. (1990). Influence of clods on hydraulic conductivity of compacted clay. *J. Geotech Engrg*, 116(8), 1231-1248.
- Bishop, A., & Garga, V. (1969). Drained tension tests on London clay. *Geotechnique*, 19, 309-313.
- Borana, I., Yin, J., Singh, D., & Shukla, S. (2016). Interface behavior from suction-controlled direct shear test on completely decomposed granitic soil and steel surfaces. *Int. J. Geomech.* , 16(6), D4016008.
- Boukpeti, N., & White, D. (2017). Interface shear box tests for assessing axial pipe-soil resistance. *Géotechnique* , 67(1), 18-30. [<http://dx.doi.org/10.1680/jgeot.15.P.112>].
- Boynton, S., & Daniel, D. (1985). Hydraulic conductivity tests on compacted clay. *J. Geotech. Engineering*, 111(4), 465-478.
- BYK Additives & Instruments. Material name: Bentonite H, Safety data sheet. (2015). 194, version # 04.

- Cardoso, R., Romero, E., Lima, A., & Ferrari, A. (2007). A comparative study of soil suction measurement using two different high-range psychrometers. *In Experimental Unsaturated Soil Mechanics*, 79-93 Springer Berlin Heidelberg.
- Cerato, A., Miller, G., & Hajjat, J. (2009). Influence of clod-size and structure on wetting-induced volume change of compacted soil. *Journal of Geotechnical and Geoenvironmental Engineering*, 135(11).
- Chai, J., & Saito, A. (2016). Interface shear strengths between geosynthetics and clayey soils. *Int. J. of Geosynth. And Ground Eng.* , 2(19), DOI 10.1007/s40891-016-0060-8.
- Chen, W., Zhou, W., & Jing, X. (2017). Effects of shear direction on the shearing behavior of a soil-structural interface using discrete element method. *Proceedings of the 19th International Conference on Soil Mechanics and Geotechnical Engineering, Seoul*.
- Corte, A., & Higashi, A. (1960). Experimental research on desiccation cracks in soil. *U.S. Army Snow, Ice and Permafrost Research Establishment, Hanover, N.H. Research report 66*.
- Costa, S., Kodikara, J., & Thusyanthan, N. (2008a). Study of desiccation crack evolution using image analysis. *E-UNSAT 2008, First European conference on unsaturated soil, Durham, united Kingdom*.
- Costa, S., Kodikara, J., & Thusyanthan, N. (2008b). Modelling of desiccation crack development in clay soils. *The 12th International Conference of International Association for Computer Methods and Advances in Geomechanics (IACMAG), Goa, india*.
- Daniel, D. E., & Wu, Y. K. (1993). Compacted clay liners and covers for arid sites. *Journal of Geotechnical Engineering, ASCE*, 119(2), 223-237.
- EdgarMineral. (2018). EdgarMineral, EPK. <http://edgarminerals.com/EPK-Clay.html>.
- Escario, V., Juca, J. F., & Coppe, M. (1989, August 13-18). Strength and deformation of partly saturated soils. *In proceeding of the 12 th International Conference on Soil Mechanics and Foundation Engineering, Rio de Janeiro, 1*, 43-46.
- Estabragh, A. R., Parsaei, B., & Javadi, A. A. (2015). Laboratory investigation of the effect of cyclic wetting and drying on the behaviour of an expansive soil. *Soil and Foundations*, 55(2), 304-314.
- Fredlund, D. G., Xing, A., & Huang, S. (1994). Predicting the permeability function for unsaturated soils using the soil-water characteristic curve. *Canadian Geotechnical Journal*, 31(4), 533-546.
- Fredlund, D., & Rahardjo, H. (1993). Soil mechanics for unsaturated soils. *John Wiley & Sons, Inc*.

- Frydman, S. (1964). The applicability of the Brazilian (indirect tension) test to soils. . *Australian journal of applied science* , 15, 335-343.
- Gallage, C., & Uchimura, T. (2016). Direct shear testing on unsaturated silty soils to investigate the effects of drying and wetting on shear strength parameters at low suction. *J. Geotech. Geoenviron. Eng.*, 142(3).
- Ghosh, A., & Subbarao, C. (2006). Tensile strength bearing ratio and slake durability of class F fly ash stabilized with lime and gypsum. *Journal of Materials in Civil Engineering*, 18(1).
- Greve, A., Andersen, M., & Acworth, M. (2010). Investigations of soil cracking and preferential flow in a weighing lysimeter filled with cracking clay soil. *Journal of Geotechnical and GeoEnvironmental Engineering*, 393, 105-113.
- Hamid, T., & Miller, G. (2009). Shear strength of unsaturated soil interfaces. *Can. Geotech. J.*, 46, 595-606.
- Hamid, T., & Miller, G. (2009). Shear strength of unsaturated soil interfaces. *Can. Geotech. J.*, 46, 595-606.
- Harrison, J. A., Hardin, B. O., & Mahboub, K. (1994). Fracture toughness of compacted cohesive soils using ring test. *Journal of Geotechnical Engineering*, 120(5), 872-891.
- Hossain, M., & Yin, J. (2013). Unsaturated soil-cement interface behaviour in direct shear tests. *Australian Geomechanics*, 48(3), 141-154.
- Hueckel, T. (1992). Water-mineral interaction in hygro-mechanics of clays exposed to environmental loads: a mixture-theory approach. *Canadian Geotechnical Journal*, 29(6), 1071-1086. doi: doi:10.1139/t92-124.
- Jacinto, A., Villar, M., & Ledesma, A. (2012). Influence of water density on the water-retention curve of expansive clays. *Geotechnique* 62, No. 8, 657–667, 62(8), 657-667. Retrieved from [<http://dx.doi.org/10.1680/geot.7.00127>]
- Kim, T. H., Kim Ta, H., & Kang, G. C. (2012). Factors influencing crack induced tensile strength of compacted soil. *Journal of Materials in Civil Engineering*, 24(3), 315-320.
- Kim, T., & Hwang, C. (2003). Modeling of tensile strength on moist granular earth material at low water conten. *Engineering Geology*, 69, 233-244.
- Kiviranta, L., & Kumpulainen, S. (2011). Quality Control and Characterization of Bentonite Materials. Working Report 2011-84, POSIVA.
- Kleppe, J. H., & Olson, R. E. (1985). Desiccation cracking of soil barriers. (*ASTM STP 874*), A. J. Johnson, R. K. Frobel, N. J. Cavallis and C.B. Pettersson, eds., ASTM, Philadelphia, Pa, 263-275.

- Kodikara, J. K., & Choi, X. (2006). In: Miller GA, Zapata CE, Houston SL, Fredlund DG, editors. Unsaturated soils, vol. 2. ASCE Geotechnical Special Publication. *Simplified analytical model for desiccation cracking of clay layers in laboratory tests*, 2558-2567.
- Kodikara, J., Barbour, S., & Fredlund, D. (2000). Desiccation cracking of soil layers. *Proceedings of Asian Conference on Unsaturated Soils: From Theory to Practice, Singapore*, 693-698.
- Konrad, J. M., & Ayad, R. (1997). An idealized framework for the analysis of cohesive soils undergoing desiccation. *Canadian Geotechnical Journal*, 34(4), 477-488.
- Lakshmikantha, M. R., Prat, P. C., & Ledesma, A. (2012). Experimental evidences of size-effect in soil cracking. " *Can. Geotech. J.*, 49(3), 264-284.
- Lakshmikantha, M., Prat, P., & Ledesma. (2009). Image analysis for the quantification of a developing crack network on a drying soil. *Geotechnical Testing Journal*, 32(6), Paper ID GTJ102216.
- Lakshmikantha, M., Prat, P., & Ledesma, A. (2009). Image analysis for the quantification of a developing crack network on a drying soil. *Geotech Test J*, 32(6), 505-515.
- Lall, P., Dornala, K., Zhang, D., Xie, D., & Zhang, A. (2014). Transient dynamics model and 3D-DIC analysis of new-candidate for JEDEC JESD22-B111 test board. *Electronic Components and Technology Conference (ECTC), 2014 IEEE 64th*, DOI: 10.1109/ECTC.2014.689.
- Liu, Q., Yasufuku, N., Omine, K., & Hazarika, H. (2012). Automatic soil water retention test system with volume change measurement for sandy and silty soils. *Soils and Foundations*, 52(2), 368-380.
- Lopez-Bellido, R. J., Munoz-Romero, V., & Lopez-Bellido, F. J. (2016). Crack formation in a mediterranean rainfed vertisol: effect of tillage and crop rotation. *Geoderma*, 281, 127-132.
- Lu, H., He, W., Liao, Z., & Chen, W. (2013). The swelling, shrinkage and cracking properties of compacted clay. *EJGE*, Vol. 18.
- Manzoli, O., Sánchez, M., Maedo, M., Hajjat, J., & Guimarães, L. (2017). An Orthotropic FE interface damage model for simulating drying processes in porous materials. *Acta Geotechnica*, DOI 10.1007/s11440-017-0608-3.
- McBrayer, M., Mauldon, M., & Drumm, E. (1997). Infiltration Tests on Fractured Compacted Clay. *Journal of Geotechnical and GeoEnvironmental Engineering*, 123(5).
- Miller, C., Mi, H., & Yesiller, N. (1998). Experimental analysis of desiccation crack propagation in clay liners. *Journal of the American, Water Resources Association*, 34(3).

- Miller, G. A., & Hamid, T. B. (2007). Interfaces direct shear testing of unsaturated soil. *Geotechnical Testing Journal*, 30(3), 182-191. doi:10.1520/GTJ13301
- Miller, G., Hassanikhah, A., & Varsei, M. (2015). Desiccation crack depth and tensile strength in compacted soil. *Unsaturated Soil Mechanics-From Theory to Practice: Proc., 6th Asia Pacific Conf. On Unsaturated Soils, CRC Press*. Boca Raton, FL.
- Mitchell, A. R., & Van Genuchten, M. T. (1992). Shrinkage of bare and cultivated soil. *Soil Sci. Soc. Am. J.*, 56, 1036-1042.
- Mori, N., & Chang, K. (2003). Introduction to MPiV, user reference manual. 14p "<http://www.oceanwave.jp/software/mpiv>".
- Morris, P. H., Graham, J., & Williams, D. J. (1992). Cracking in drying soils. *Canadian Geotechnical Journal*, 29, 263-277.
- Nahlawi, H. (2004). *Behavior of reactive soil during desiccation. Master's Thesis, Monash University, Australia.*
- Nahlawi, H., & Kodikara, J. (2006). Laboratory experiments on desiccation cracking of thin soil layers. *Geotech Geol Eng.*, 24(6), 1641-1664.
- Nahlawi, H., Chakrabarti, S., & Kodikara, J. (2004). A direct tensile strength testing method for unsaturated geomaterials. *Geotechnical Testing Journal*, 27, 356-361.
- Nawamooz, H., & Masrouri, F. (2008). Hydromechanical behaviour of an expansive bentonite/silt mixture in cyclic suction-controlled drying and wetting tests. *Eng. Geol.*, 101, 154-164.
- Omidi, G., Thomas, J., & Brown, K. (1996). Effect of desiccation cracking on the hydraulic conductivity of a compacted clay liner. *Water Air Soil Pollution*, 89, 91-103.
- Peron, H., Hueckel, T., & Laloui, L. (2009a). Fundamentals of desiccation cracking of fine-grained soils: experimental characterization and mechanisms identification. *Can. Geotech. J.*, 46, 1177-1201.
- QI, C., Zheng, J., Zuo, D., & Chen, G. (2017). Measurement on soil deformation caused by expanded-base pile in transparent soil using particle image velocimetry (PIV). *Journal of Mountain Science*, 14(8), 1655-1665 DOI: 10.1007/s11629-016-4025-0.
- Rayhani, M., E.K. Yanful, E., & Fakher, A. (2008). Physical modeling of desiccation cracking in plastic soils. *Engineering Geology*, 97, 25-31.
- Rodríguez, R., Sánchez, M., Lloret, A., & Ledesma, A. (2007). Experimental and numerical analysis of a mining waste desiccation. *Can Geotech J.*, 44, 644-658.

- Sánchez, M., Atique, A., Kim, S., Romero, E., & Zielinski, M. (2013). Exploring desiccation cracks in soils using a 2D profile laser device. *Acta Geotechnica*, 8, 583-596, DOI 10.1007/s11440-013-0272-1.
- Sánchez, M., Manzoli, O., & Guimarães, L. (2014). Modeling 3-D desiccation soil crack networks using a mesh fragmentation technique. *Computers and Geotechnics*, 62, 27-39.
- Shin, H., & Santamarina, J. C. (2011). Desiccation cracks in saturated fine-grained soils particle level. *Geotechnique*, 11, 961-972.
- Shin, H., & Santamarina, J. C. (2011). Desiccation cracks in saturated fine-grained soils: particle-level phenomena and effective-stress analysis. *Geotechnique*, 61(11), 961-972.
- Shit, P., Bhunia, G., & Maiti, R. (2015). Soil crack morphology analysis using image processing techniques. *Model. Earth Syst. Environ*, 1(35), DOI 10.1007/s40808-015-0036-z.
- Stirling, R., Hughes, P., Davie, C., & Glendinning, S. (2015). Tensile behavior of unsaturated compacted clay soils-A direct assessment method. *Applied Clay Science*, 112-113, 123-133.
- Sutton, M., Walters, W., Peters, W., Ranson, W., & and McNeil, S. (1983). Determination of displacements using an improved digital correlation method. *Image and Vision Computing*, 1(3), 133-139 doi.org/10.1016/0262-8856(83)90064-1.
- Take, W. (2015). Advances in visualization of geotechnical processes through digital image correlation. *Can. Geotech. J.*, 52, 1199-1220 dx.doi.org/10.1139/cgj-2014-0080.
- Tamrakar, S., Mitachi, T., Toyosawa, Y., & Itoh, K. (2005). Development of a New Soil Tensile Strength Test Apparatus. *Site Characterization and Modeling*, 1-10. doi:10.1061/40785(164) 26
- Tang, C., Cui, Y., Shi, B., Tang, A., & An, N. (2016). Effect of wetting-drying cycles on soil desiccation cracking behaviour. *E3S Web of conferences 9, 12003, E-UNSAT 2016*, DOI: 10.1051/e3sconf/20160912003.
- Tang, C., Cui, Y., Shi, B., Tang, A., & Liu, C. (2011). Dessication and cracking behaviour of clay layer from slurry state under wetting-drying cycles. *Geoderma*, 111-118.
- Tang, C., Pei, X., D, W., Shi, B., & Li, J. (2015). Tensile Strength of Compacted Clayey Soil. *Journal of Geotechnical and Geoenvironmental Engineering*, 141(4), -1--1.
- Tang, S., Shi, B., Liu, C., Suo, B., & Gao, L. (2011). Experimental characterization of shrinkage and desiccation cracking in thin clay layer. *Applied Clay Science*, 52, 69-77.
- Trabelsi, H., Jamei, M., Guiras, H., Zenzri, H., Romero, E., & Olivella, S. (2010). Some investigations about the tensile strength and the desiccation process of

- unsaturated clay. *14th International Conference on Experimental Mechanics*. doi:10.1051/epjconf/20100612005
- Trabelsi, H., Jamei, M., Zenzri, H., & Olivella, S. (2012). Crack patterns in clayey soils: experiments and modeling. *nt J Numer Anal Meth Geomech*, 36(11), 1410-1433.
- Tripathy, S., Rao, S., & Fredlund, D. (2002). Water content – void ratio swell-shrink paths of compacted expansive soils. *Can. Geotech. J.*, 39, 938-959 DOI: 10.1139/T02-022.
- Tsakiroglou, C., Klint, K., Nilsson, B., Theodoropoulou, M., & Aggelopoulos, C. (2012). From aperture characterization to hydraulic properties of fractures. *Geoderma*, 181-182, 63-77.
- Uday, K., & Singh, D. (2013). Investigation on cracking characteristics of fine-grained soils under varied environmental conditions. *Drying Technology*, 31, 1255-1266.
- UMS GmbH, M. (2009). T5/T5X Pressure transducer tensiometer, Manual. Version 12.
- Van Genuchten, M. (1978). Calculating the unsaturated hydraulic conductivity with a new closed-formed analytical model. *Water Resources Research*, 37(11), 21-28.
- Vanicek, I. (2013). The importance of tensile strength in geotechnical engineering. *Acta Geotechnica Slovenica*, 1, 5-17.
- Varsei, M., Miller, G., & Hassanikhah, A. (2016). Novel approach to measuring tensile strength of compacted clayey soil during desiccation. *International Journal of Geomechanics c ASCE*.
- Vesga, L. F. (2009). Direct tensile-shear test (DTS) on unsaturated kaolinite clay. *Geotechnical Testing Journal*, 32(5), 397-409.
- Villar, M. V. (2002). Thermo-hydro-mechanical characterisation of a bentonite from Cabo de Gata: A study applied to the use of bentonite as sealing material in high level radioactive waste repositories. *Madrid, Spain: Publicacio ´n Te ´cnica ENRESA*.
- Villar, M. V., Sánchez, M., & Gens, A. (2008). Behaviour of a bentonite barrier in the laboratory: Experimental results up to 8 years and numerical simulation. *Physics and Chemistry of the Earth*, 33, S476-S485. doi:10.1016/j.pce.2008.10.055.
- Wang, D., Tang, C., Cui, Y., Shi, B., & Li, J. (2016). Effects of wetting-drying cycles on soil strength profile of a silty clay in micro-penetrometer tests. *Engineering Geology*, 206, 60-70, <https://doi.org/10.1016/j.enggeo.2016.04.005>.
- Wheeler, S., Sharma, R. S., & Buisson, M. S. (2003). Coupling of hydraulic hysteresis and stress-strain behaviour in unsaturated soils. *Geotechnique*, 53(1), 41-54.
- White, D., Take, W., & Bolton, M. (2003). Soil deformation measurement using particle image velocimetry (PIV) and photogrammetry. *Geotechnique*, 53(7), 619-631.

- White, D., Take, W., Bolton, M., & Munachen, S. (2001). A deformation measurement system for geotechnical testing based on digital imaging, close-range photogrammetry, and PIV image analysis. *15th International Conference on Soil Mechanics and Geotechnical Engineering, Istanbul, Turkey*, 539-542. pub. Balkema, Rotterdam.
- Yesiller, N., Miller, C., Inci, G., & Yaldo, K. (2000). Desiccation and cracking behavior of three compacted landfill liner soils. *Engineering Geology*, 57, 105-121.
- Yoshida, S., & adachi, K. (2004). Numerical analysis of crack generation in saturated deformable soil under row-planted vegetation. *Geoderma*, 120, 63-74.
- Yoshida, S., & Adachi, K. (2004). Numerical analysis of crack generation in saturated deformable soil under row-planted vegetation. *Geoderma*, 120, 63-74.
- Yoshimi, Y., & Kishida, T. (1981). A ring torsion apparatus for evaluating friction between soil and metal surfaces. *Geotech. Testing J*, 4(4), 145-152.
- Zhang, B., Li, Q., Yuan, H., & Sun, X. (2015). Tensile Fracture Characteristics of Compacted Soils under Uniaxial Tension. *Journal of Materials in Civil Engineering*, © ASCE, 27(10), -1--1.
- Zhang, Z., Zhou, H., Zhao, Q., Lin, H., & Peng, X. (2014). Characteristics of cracks in two paddy soils and their impacts on preferential flow. *Geoderma*, 228-229, 114-121.
- Zielinski, M., Sánchez, M., Romero, E., & Alvis, A. (2014). Precise observation of soil surface curling. *Geoderma*, 226-227, 85-93.